The Author

Lars Landschreiber, geboren 1978 in Gelnhausen, studierte an der Universität Hamburg Geographie mit den Schwerpunkten allgemeine Bodenkunde und Bodenhydrologie. Während und nach seinem Diplom arbeitete er in zwei Projekten zur Analyse der Auswirkungen des Landschafts- und Landnutzungswandels auf hydrologische und ökologische Systeme in Angola, Botswana und Namibia. Er promovierte am Institut für Bodenkunde der Universität Hamburg im Rahmen des Forschungsprojektes „The Future Okavango“. Schwerpunkte seiner wissenschaftlichen Arbeit sind die Messung und Modellierung bodenhydrologischer Prozesse in natürlichen und in Agrarökosystemen der gemäßigten und subtropischen Klimazonen.

Verein zur Förderung der Bodenkunde Hamburg
c/o Institut für Bodenkunde - Universität Hamburg
https://www.geo.uni-hamburg.de/de/bodenkunde.html

Hamburger Bodenkundliche Arbeiten

2019

L. Landschreiber

Band 93

HBA

Lars Landschreiber

Quantifying the effect of vegetation and land use on soil hydrological functioning along a regional transect in southern Africa

Band 93
2019

ISSN: 0724-6382

Hamburger Bodenkundliche Arbeiten

Quantifying the effect of vegetation and land use on soil hydrological functioning along a regional transect in southern Africa

- Case studies from the Okavango catchment -

Dissertation

with the aim of achieving the doctoral degree in natural sciences

at the Faculty of Mathematics, Informatics and Natural Science

submitted by

Lars Landschreiber

from Gelnhausen

Department of Earth Science

University of Hamburg

Hamburg

2019

Als Dissertation angenommen am Fachbereich Geowissenschaften

Tag der Disputation: 04.07.2018

Erstgutachterin: Prof. Dr. Annette Eschenbach

Zweitgutachterin: Prof. Dr. Eva-Maria Pfeiffer

Vorsitz des Fach-Promotionsausschusses Geowissenschaften: Prof. Dr. Dirk Gajewski

Erschienen als

Hamburger Bodenkundliche Arbeiten, Band 93

Herausgeber: Verein zur Förderung der Bodenkunde Hamburg
Allende-Platz 2, 20146 Hamburg
https://www.geo.uni-hamburg.de/bodenkunde/ueber-das-institut/hba.html
Schriftleitung: Dr. Klaus Berger

»ALLES IST WECHSELWIRKUNG«
Alexander von Humboldt

TO IRMGARD LANDSCHREIBER

Table of content

1. Introduction and aim of this study

Since the pedosphere describes the very part of the earth´s surface where atmosphere, biosphere, hydrosphere, lithosphere and the anthroposphere interact, soils provide crucial functions within terrestrial natural and anthropogenic ecosystems for their development and sustain. This study focuses on a particular part of the pedosphere, where water is the connecting element between the pedosphere and vegetation, ground- and surface water as well as the atmosphere. Fig. 1 gives an overview of the soil hydrological cycle with its compartments, processes and fluxes.

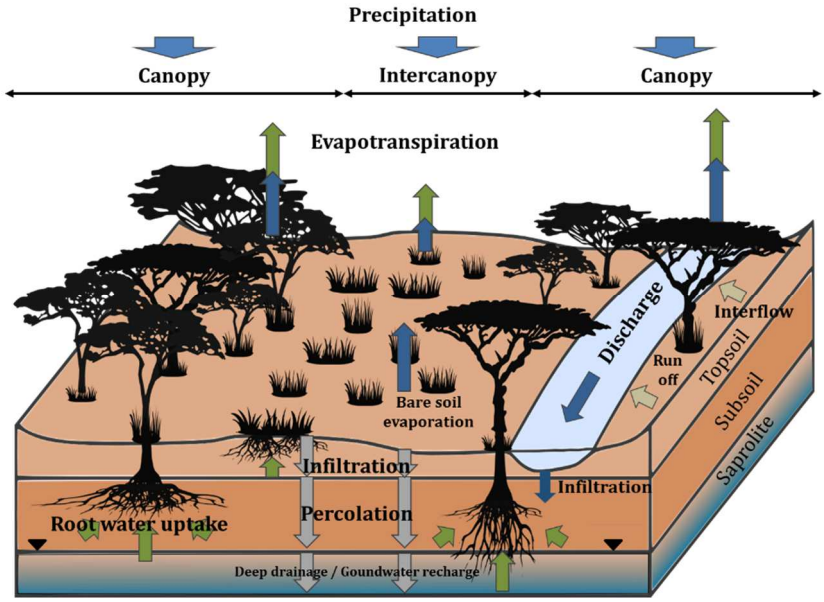

Fig. 1: The hydrological cycle focused on soil hydrological processes

Atmospheric precipitation is reduced by the land surface characteristics due to litter or canopy interception and infiltrates into the topsoil in whole or parts depending on the infiltration capacity of the soil. This capacity is a function of soil water saturation status, soil hydrological properties and surface slope. With infiltration capacity exceeding rainfall intensities, a proportion of the water input is laterally relocated by surface runoff. The infiltrating proportion fills the available void pore space and will be in parts relocated vertically by percolation dynamics and in parts held against gravity due to capillary forces. Whereas deep percolating water supplies groundwater recharge, capillary water supports the transpiration by root water uptake processes and evaporation dynamics on the bare soil parts of the surface due to an atmospheric water vapor demand. An accumulation of soil water in deeper parts of the soil where percolation processes are hampered

by low soil hydraulic conductivities landscapes with sloping topographies may lead to lateral subsurface flows under saturated conditions, the interflow. Saturated lateral surface and subsurface fluxes and high groundwater tables are discharged by stream flow within defined river catchments. In areas, where the groundwater table is not connected to streamlines, for example in allogenic river systems, river water infiltrates into the river bed to supply groundwater recharge. This study focuses on the soil water balances with respect to interception, transpiration, evaporation and bottom fluxes for a set of differing soil-vegetation-atmosphere systems to evaluate appearing flux differences and their consequences for soil hydrology related ecosystem services.

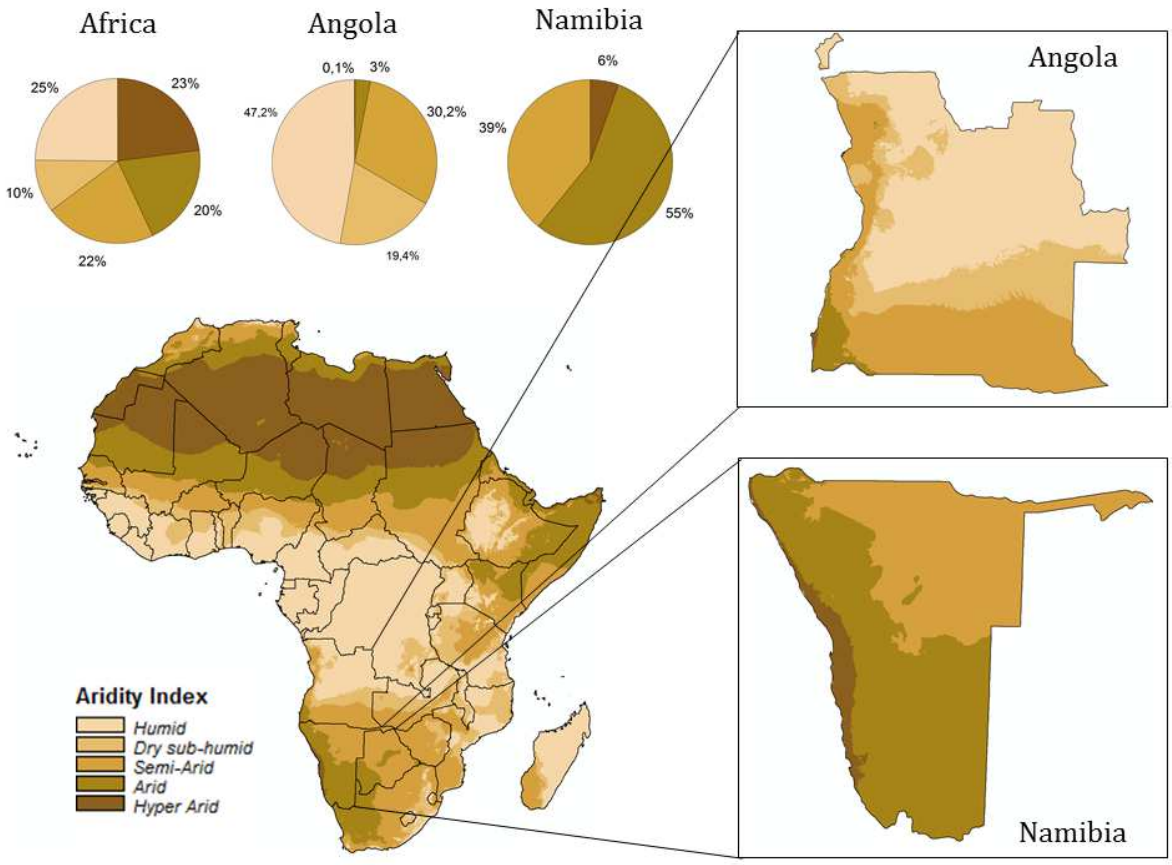

Fig. 2: Spatial distribution and fractions of hydroclimatic regions in Africa, Angola and Namibia. Derived from data from CGIAR (*Trabucco* and *Zomer* 2009)

The regional focus lies on drylands in southern Africa, on areas where water availability is the main driver for any kind of natural vegetation dynamics and human well-being. 75 % of the African landscapes can be characterized as drylands, from hyper-arid to dry sub-humid, by relating the annual sum of the potential evapotranspiration with the mean annual precipitation sums, resulting in the so-called aridity index (AI). Looking at certain

countries in southern Africa, such as the study regions in Angola and Namibia, the relations shift due to their individual location within global and regional climatic circulation systems and their specific geographical settings. 47 % of Angola is humid with a strong north-south oriented gradient over dry sub-humid (19 %) towards semi-arid conditions (30 %) at the transition to Namibia. In contrast, Namibia is divided into three hydroclimatic regions dominated by 55 % arid conditions in the south as well in the western part adjacent to the hyper-arid region (6 %) of the Namib desert. 39 % of the landscapes are semi-arid (Fig. 2) mainly located in the central highlands. Together with a pronounced intra- and interannual precipitation variability, which increases with decreasing precipitation depth as shown in Fig. 3, this combination has an influence on the occurrence, intensity and duration of droughts (*D'Odorico* et al. 2013).

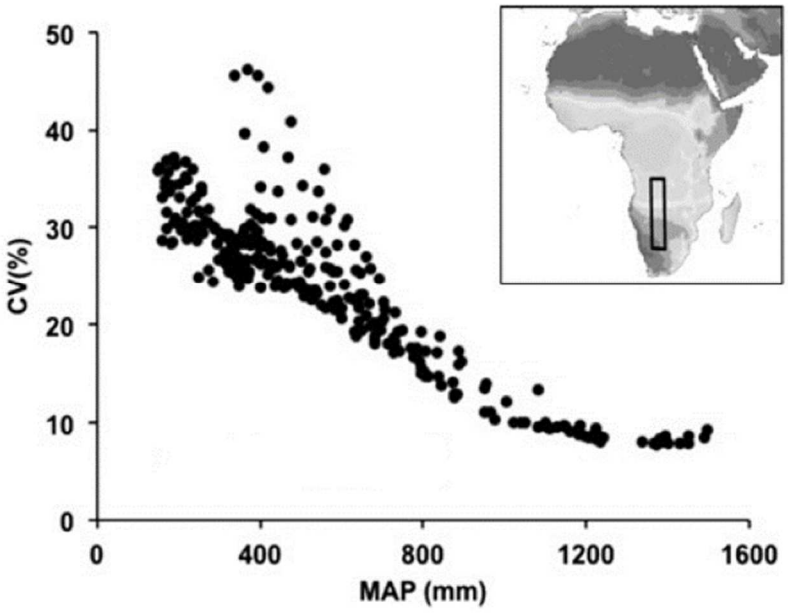

Fig. 3: Coefficient of variation (CV) of precipitation in relation to mean annual precipitation depth (MAP) along the southern African transect (*D'Odorico* et al. 2013).

As all subtropical areas, these two countries are increasingly affected, as described above, by aridification due to the consequences of climate change, which is considered to have a major impact on the precipitation depth and variability (*Chou* et al. 2009; *Huang* et al. 2017; *Maestre* et al. 2012). Additionally, an inadequate land management leads to desertification processes like a vegetation composition change (*Maestre* et al. 2012) and a change in soil properties, both interconnected by feedback loops describing land-atmosphere interaction together with soil-vegetation feedbacks (Fig. 4).

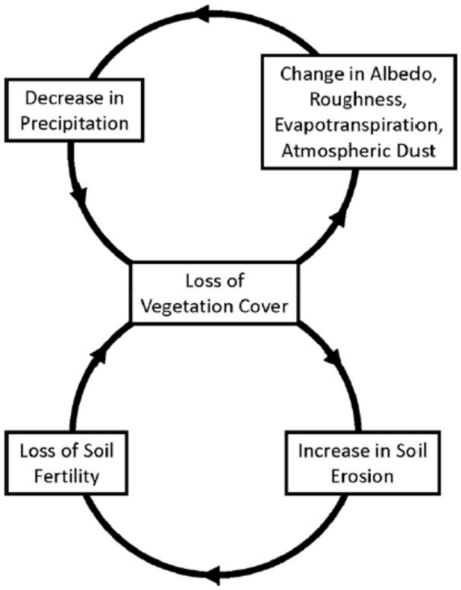

Fig. 4: Feedback loops showing the atmospherical and land degradation consequences of vegetation loss (*D'Odorico* et al. 2013).

An increasing population causes an increased demand for natural goods like timber and firewood as well as an increasing need for cropland for both, industrial and small-scale farming. This dynamic raises the pressure on highly adaptive natural ecosystems, especially on dryland forest (*Bodart* et al. 2013). Once converted into small-scale and rain-fed agricultural ecosystems with a net nutrient export, decreasing yields lead to a shifting cultivation with short rotation spans and expanding deforestation. Secondary plant communities with divergent properties, compared to the pristine status, will replace the pristine vegetation cover. On the other hand, expanding high input irrigation schemes set the pressure on additional sources by using surface or groundwater resources. By using agrochemicals and fertilizer-enriched irrigation water on soils with high drainage properties and low buffer capacities, e.g. Arenosols, there is the risk of leaching nutrients or pesticide and their relevant metabolites into surface or groundwater resources. In contrasting soils with medium to high buffer capacities and good capillary properties, high atmospheric demand together with inappropriate irrigation methods may cause soil salinization. This may also increase desertification processes (*D'Odorico* et al. 2013). In contrast to the previously mentioned active anthropogenic transitions of natural ecosystems into agricultural systems by land clearing, bush encroachment is widely discussed as a passive transition phenomenon thought to be caused by multifactorial impacts. Until now, it is not clearly understood what causes the widely accepted hypothesis of a stable coexisting of

trees and grasses in savannah ecosystems to be imbalanced towards an increased dominance of shrubs and trees. Two major concepts try to explain the so-called "savannah problem". In 1939 WALTER first stated his two-layer hypothesis (*Walter* 1939), where a vertical niche partitioning in the rooting zone stabilize the grasses layer because of their higher water and nutrient use efficiency and intense rooting in subsurface layers, whereas shrubs and trees have access to deeper water sources. This system is in equilibrium until the grass layer is supposed to be overutilized and loses its competitive advantages and trees and shrubs can become dominant (*Klerk* 2004). Although this hypothesis is controversially discussed since it focusses more on interspecific competition while neglecting abiotic factors, it seems to be valid for dry savannah ecosystems (*Ward* et al. 2013; *O'Connor* et al. 2014). To integrate different savannah types and their individual biotic and abiotic conditions the State-and-Transition Model concept (*Scholes* and *Walker* 1993; *Joubert* et al. 2008) focuses on the dynamic nature of savannahs as a highly event depending system based on several determinants. A first attempt to summarize potential factors and theories can be found in (*Klerk* 2004), where a differentiation between primary and secondary determinants is postulated (*Smit* and *Rethman* 2000). As primary determinants the abiotic ecosystem compartments climate and soil properties define basic boundary conditions. Especially the interactions between rainfall and soil water balances are mentioned to have a distinct influence on vegetation structure, composition and ecosystem stability. According to this assumption, a mass tree establishment is benefited by certain long-term precipitation patterns where consecutive rainy seasons with above-average rainfall amounts following pronounced drought events (*Joubert* et al. 2008). The primary determinants are assumed to be flanked by secondary factors like bush fire regime and an altered relation between the numbers of browser and grazer species (game/livestock relation). Therefore, an increased number of livestock in combination with inappropriate management strategies in the semi-arid areas in Namibia can push the savannah ecosystem into a state where bush encroachment gets a serious issue with manifold consequences for ecosystem functions and services. On one hand, widespread areas with dense acacia thickets replace the open character of the former landscape. For game or livestock, it is impossible to enter these areas, which makes these parts uneconomic for grassland pastures unless intensive bush clearing activities together with improved land management will restore the savannah-like pristine state of the grasslands.

On the other hand, bush encroachment is assumed to have negative effects on groundwater resources due to the extensive in-depth as well as lateral rooting of encroacher species (*Klerk* 2004; *Donaldson* 1969). To sustain a sufficient rate of transpiration, encroacher species (e.g. *Acacia mellifera)* utilize two main water resources. On one side, the extensive lateral rooting provides access to a large volume of soil so that even with low volumetric water contents and high soil water pressure heads an adequate amount of soil water is available for transpiration. This may lead to a possible reduction of groundwater recharge due to decreased seepage. On the other side, tap roots allowing access to groundwater sources to support early flouring at the end of the dry season or in times of droughts. Both dynamics will support the establishment of encroacher species by having the advantage of tapping two water sources in contrast to perennial grasses, which rely on soil water resources only. In cases, where groundwater tables are too deep to be tapped by roots, existing bedrock saprolites with a sufficient number of cracks and macropores can serve as a temporal buffer to store percolated water in seasons with high precipitation amounts to allow deep rooting trees to have access to plant available water in times of low rainfall input

This study tries to give insights in small-scale soil hydrological processes to contribute to a better understanding of the interactions between drivers and feedbacks as well as the human impact. Therefore, it focuses on three major topics:

1. How does agricultural land use expansion change soil water balances in a dry subhumid landscape in Angola?

2. How is the influence of different vegetation and agricultural land use characteristics on soil water balances in northern Namibia?

3. How does bush encroachment alter soil water dynamics and potential groundwater recharge in the semi-arid highlands of central Namibia?

By analyzing the impact of vegetation transformation on the soil water dynamics and balances components, consequences for a future land use with respect to water availability are evaluated. To give estimates on the dynamics regarding impacts and drivers, a combination of static and dynamic empirical data sets and model generated balances were used. The empirical data sets consist of time series of volumetric water content and soil water pressure head in combination with lab analyses describing the soil´s hydraulic properties.

The subsequent physically based model application allows predictions of the shift in soil water dynamics and balances according to predefined land use scenarios and vegetation characteristics, driven by weather station data as well as long-term climate model outputs. The evaluation of the simulation results is based on the mean seasonal development of soil water dynamics and balances with a daily resolution.

2. State of the art

Since the geo/hydrosphere or synonymously called the vadose zone was identified to be a crucial compartment to understand water and solute dynamics towards the groundwater, to streams, for vegetation development and climate interactions as well as secondary effects like degradation processes, the analysis of the highly complex interactions between the involved spheres at varying spatial and temporal scales still remains challenging. To improve insights in soil water dynamics, two major concepts are in focus. On one hand, soil water sensing techniques (direct or remote sensed) give the opportunity to obtain empirical datasets with variable resolution in time and space. For a closer look at landscape water dynamics and balances with all its interacting aspects, sensing approaches still remain difficult to implement due to its complexity. On the other hand, to be able to close water balances without having all compartments measured, modeling approaches complement the empirical data acquisition. For a closer look at both approaches and their possibilities and disadvantages, it is referred to two elaborate reviews by *Vereecken* et al. (*Vereecken* et al. 2008; *Vereecken* et al. 2016). This chapter will focus on the state of scientific research by addressing studies with quantitative methods to analyze soil water balances and dynamics in drylands under different assumptions of land use and climate effects than on studies with a more methodical orientation.

2.1. Land use change and its relation to soil water cycling

Subsistence agriculture is an important source of food to improve household food security especially for those with low income but due to inappropriate cropping techniques and the use of low yielding varieties the output is often low and can only be increased by increasing farm area (*Baiphethi* and *Jacobs* 2009). An increasing population growth sets additional pressure on natural ecosystems resulting in increased system conversions from pristine conditions into dry land agriculture areas (*Cabral* et al. 2011; *Schneibel* et al. 2017). In southeast Angola and northern Namibia, the land conversion is concentrated on open to dense woodlands which indicate a higher nutrient status and offers the opportunity to add additional nutrients by ash due to slash and burn agriculture especially at the Angolan part of the Okavango catchment (*Wallenfang* et al. 2015). Previously environmentally adapted ecosystems are replaced by nutrient and water demanding agricultural ecosystems with low plant densities, an increased proportion of bare soil and with time decreasing soil fertility due to residual removal (*Gröngröft* et al. 2013c). A low plant

density and lower rooting depth of crops in comparison to pristine woodlands lead to a shift in soil water balances from transpiration dominated wood- and grasslands to be prone to deep drainage and evaporation under dryland agriculture (*Walker* et al. 2002). The additional loss of water due to deep drainage results in less plant available water for biomass production but is available for river discharge or groundwater recharge. Especially in transnational river system like the Okavango, a balance between groundwater recharge, river discharge and biomass productivity in headwater areas is of crucial interest for riparian states in downstream regions (*Collentine* and *Futter* 2018), since it directly affects water availability for direct human use or for irrigation crop production. Land cover change induced soil hydrological topics are illustrated in more detail in the following sections.

Groundwater recharge is a function of the rainfall input less the lateral and ascending water fluxes induced and influenced by geology, soil properties and water content, topography, rainfall intensity, atmospheric water vapor demand and vegetation characteristics (*Hillel* 2009). Since drylands are defined by a deficient relation between precipitation and evapotranspiration, atmospheric fluxes are the predominant components in the water cycle (*Mainguet* 1999) accounting for up to 90 % of the precipitation input (*Glenn* et al. 2007; *Bennie* and *Hensley* 2001). The active water recycling of precipitation to the atmosphere by transpiration plays thereby an important role because especially deep rooting woodlands extract water from deeper soil areas. These shortcutting process between the pedohydrosphere and the atmosphere is altered by deforestation for agriculture, leading to reduced transpiration, higher evaporation and increased deep drainage (*Peck* and *Williamson* 1987; *Giménez* et al. 2016). Land use change related water balance impacts for xeric to dry-mesic ecosystems showed an increase in groundwater recharge (*Leduc* et al. 2001; *Lal* 1997). Lysimeter experiments under extreme dry desert conditions showed a significant impact of recharge development between bare soil conditions and vegetated surfaces, with 87 mm y^{-1} under bare soil and a complete drop to zero under vegetation (*Scanlon* et al. 2006a; *Wang* et al. 2004). The groundwater recharge regulation by vegetation and the increase in recharge caused by land clearing is directly connected to river runoff generation, in this context *Hough* (1986) discusses the effect of Miombo woodlands on the dry season base flow. A lower groundwater recharge in the rainy season caused by high evapotranspiration fluxes leads to a reduced base flow within the rainy season, whereas in contrary deforestation results in an increase in dry season base flow due to

reduced evapotranspiration rates (*Lal* 1997). Dryland regions with a soil inventory which shows low nutrient buffer capacities and increased drainage fluxes due to land cover change, prone to nutrient leaching (*Dovey* et al. 2014) and a change in surface water quality (*Scanlon* et al. 2005). The trade-off between higher dry season ground and surface water availability and a possible decrease in water quality needs to be addressed in the context of land use or land cover change related compensation measures (*Noorduijn* et al. 2010; *Hatton* and *Nulsen* 1999)

Since rain fed agroecosystems completely rely on precipitation, the effective utilization of the scarce, time and amount variable water input is crucial for a maximized crop production (*Bennie* and *Hensley* 2001). Low input subsistence agriculture often shows low plant densities (*Gröngröft* et al. 2013c) with high evaporation and deep drainage losses which results in low plant available soil water and a less productive water utilization. As a measure of the performance of an agrosystem, the water use efficiency expresses the relation between yield and evapotranspiration fluxes and is strongly related to land and crop management (*Rockström* and *Falkenmark* 2010). To improve the water use efficiency, unproductive water losses need to be reduced in order to support higher transpiration proportions (*Kahinda* et al. 2007; *Kpadonou* et al. 2017). Two major concepts are discussed, amongst others (*Pretty* et al. 2011; *Stroosnijder* et al. 2012), in the context of improving small-scale agricultural output comprising, on one side, techniques to minimize water losses by conservation agriculture practices (*Araya* et al. 2016; *Araya* et al. 2015; *Bayala* et al. 2012)and, on the other hand, measures to store and provide supplemental irrigation water by rain water harvesting techniques (*Schwilch* et al. 2014; *Enfors* and *Gordon* 2008; *Oweis* and *Hachum* 2006). The concept of conservation agriculture is to store water in situ due to adapted tillage practices and soil coverage, whereas rain water harvesting provides a central reservoir which can be combined with a small-scale irrigation infrastructure, often as water efficient drip irrigation schemes (*Sturm* et al. 2009; *Jokisch* et al. 2016). Especially at the beginning of the rainy season, such measures help to enable healthy crop stands once a sufficient rooting depth is established(*Rockström* and *Barron* 2007). These concepts are able to improve yields and water use efficiency (*Thierfelder* and *Wall* 2010) but an implementation needs promoting efforts in the respective regions where often the adaption and adoption of conservation agriculture techniques by the farmers are complex and highly site-specific (*Erenstein* et al. 2012). In this context, *Bouma* and *Montanarella*

(2016) emphasize the role of soil science to promote transdisciplinary research to address the soil and water nexus for sustainable livelihoods.

2.2. Bush encroachment and its potential impact on soil water balances in drylands

Within the last decades, shrub and bush encroachment has been a well-recognized phenomenon in arid and semi-arid environments worldwide, while the drivers of this dynamic, as well as the consequences and their internal interactions, still remain unclear due to their complex feedback mechanisms. While some studies had identified a general decrease in soil related ecosystem functions due to bush encroachment with a special emphasis on Southern Africa (*Klerk* 2004; *Donaldson* 1969), recent analyses assume the need for differentiated consideration of scale-, species- and environment-dependent studies (*Eldridge* and *Soliveres* 2014). A meta-analysis from 2011 (*Eldridge* et al. 2011) summarises outcomes from 244 independent studies dealing with biogeochemical or biogeophysical feedbacks of bush or shrub encroachment with a share of only 40 studies with a regional focus on Africa. Looking at the overall database only 4 % out of the 1175 analyzed cases were focused on soil hydrological issues like soil moisture or infiltration response. Going deeper into the meta-analysis of these particular cases, only 16 % show an increase in soil moisture and infiltration capacities, 9 % show a decline, whereas the majority with 75 % of the cases show no significant alteration of the mentioned soil hydrological parameters. It remains unclear to what extent the parameter soil moisture and infiltration is addressed. To approach this topic in more detail, it seems to be likely to look separately at the hydrological dynamics influencing the state of soil moisture interacting with vegetation characteristics. Three main processes are addressed in the following chapters.

Beside root water uptake, rainfall interception is a major determinant for the modification of soil water balances compared between trees and grass-dominated vegetation compositions, since it returns a certain fraction of the precipitation directly back into the atmosphere as vapor without being turned over within the soil water cycle (*Bulcock* and *Jewitt* 2012). Thus, interception is often subsumed by evaporation losses, because of its unproductive character concerning the increase of biomass (*Honda* and *Durigan* 2016). The process of interception is governed by vegetation characteristics, such as canopy storage capacity as a function of leaf area, crown dimensions and stand density, as well as meteorological parameters like rainfall amounts and intensity together with wind and potential

evaporation depth. The determination of rainfall interception under field condition requires complex setups to measure the amount of through fall and stem flow (*Bulcock* and *Jewitt* 2012; *Llorens* et al. 1997). By recording the actual rainfall above the canopy and balancing it with the amount of through fall and stem flow it is possible to calculate the amount of crown intercepted water. Time series analyses of these components, taking into account the actual canopy wetness at the beginning of a rainfall event, lead to empirical (*Hoyningen-Huene* 1981) or physically based model concepts (*Gash* et al. 1995; *Gash* 1979), to be integrated into hydrological models. An increasing bush encroachment will lead to higher interception water losses and therefore to a change in the water cycle. Focused on the regional scale *Honda* and *Durigan* (2016) conducted a field experiment in the Cerrado savannah in central Brazil where a woody encroachment is recorded due to a decrease in fire frequency (Fig. 5). In relation to tree basal area (TBA) of fourteen fire protected 1000 m^2 plots sampled in 2006 and 2011, it was shown that an increase in TBA leads to a decrease in through fall while stem flow increases (Fig. 6) but with a different ratio. In consequence, the amount of plant available soil water will decrease together with a small increase of soil water content underneath tree canopies.

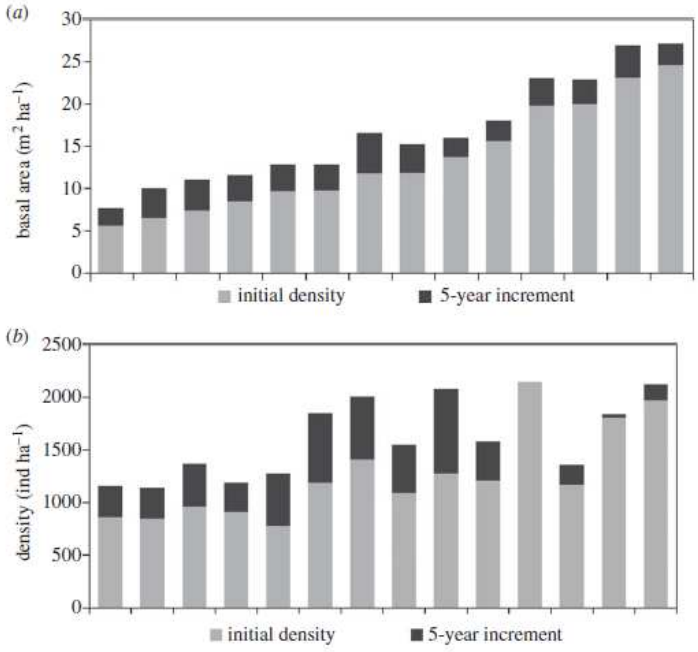

Fig. 5: Changes in tree basal area (a) and tree density (b) over a period of five years and 14 plots in the Cerrado savannah, Brazil (*Honda* and *Durigan* 2016)

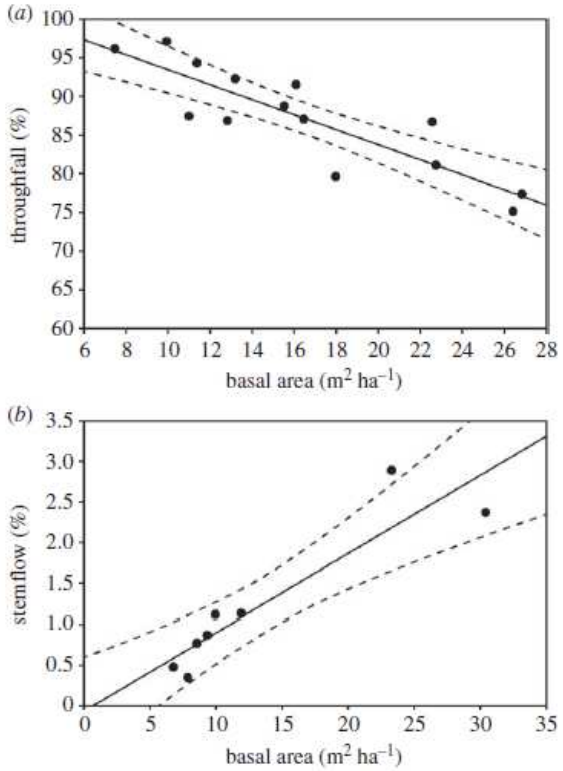

Fig. 6: Changes in through fall and stem flow in relation to tree basal area. Dashed lines represent 95 % confidence interval (Honda and Durigan 2016)

Focusing on the relation between interception of single trees on the point scale and certain rainfall events the data by *Llorens* et al. (1997) show a clear asymptotic trend between rainfall amounts and the quotient of interception and precipitation.

A field-scale infiltration study conducted by *Eldridge* et al. (2015) reveals that a conversion from grassland to shrubland causes a decline of steady-state infiltration by 14 % under ponded conditions, while infiltration rates under tension show no significant differences. This study showed a correlation between infiltration capacity and the distance to stems of encroacher species, suggesting that a certain intensity of bush encroachment alters the spatial variability of infiltrability. Derived infiltration rates from measured time series under rainfall conditions showed that beneath individual canopies the amount of infiltrated water was higher than in intercanopy space (*Bhark* and *Small* 2003). These results are consistent with several studies showing an increased infiltration under tree and shrub canopies due to preferential flow along the tree root system (*Dunkerley* 2002b; *Dunkerley* 2002a, 2000; *Daryanto* et al. 2013; *Johnson* and *Lehmann* 2016; *Scholes* and *Walker* 1993; *Scholes* and *Archer* 1997; *D'Odorico* et al. 2007; *Wilcox* et al. 2003). Taking

into account that unproductive bare soil evaporation is less and nutrient availability is better (*Whitford* et al. 1997) underneath canopies related to open grasslands, the establishment of a dense understory vegetation in these "fertile islands" also increases the infiltration capacity due to intense top soil rooting by annual or perennial herbs. Another canopy-influenced feedback with focus on infiltration is the reduction of precipitation energy due to rainfall interception. High energetic storm events combined with bare soil conditions lead to splash impact with subsequent topsoil sealing effects and reduced infiltrability. Canopy interception lowers the precipitation energy and therefore the risk of soil crusting (*Bhark* and *Small* 2003) to maintain a certain topsoil porosity.

In contrast to measurements of infiltration capacities, the determination of evapotranspiration losses and the interconnection with other hydrological dynamics at various scales is still challenging (*Metzger* et al. 2014). A common way to determine all soil water balance aspects is the use of more or less complex lysimeter. This method is usually applied with crop-related evapotranspiration measurements because of their scalability for uniform land covers, but also in a less complex form to determine bare soil evaporation (*Daamen* et al. 1993). To get insights in natural or pristine ecosystem processes with a high degree of heterogeneity is more demanding since small-scale effects like topographic and vegetation induced wind field modification or shading effects (*Judd* et al. 1996) have a big influence of the gross water balance. These mesoscale climatic effects are also described by *Segal* et al. (1988) and *Leenders* et al. (2007). To cope with highly complex interactions between soil, vegetation and atmosphere recent studies focus on single trees and shrubs for sap flow measurements (*Allen* and *Grime* 1995; *Deans* and *Munro* 2004, 2004; *de Blécourt* et al. 2017) as well as high frequency eddy covariance measurements of climatic variables at different scales to represent ecosystem water and energy exchange as well as under-canopy dynamics. (*Scott* 2003; *Moran* et al. 2009; *Hamerlynck* et al. 2011; *Cavanaugh* et al. 2011). A model-based integration of both concepts supports a better understanding of the partitioning of the actual evapotranspiration into transpiration and evaporation shares (*Dzikiti* et al. 2014).

Tab. 1: Plant physiological characteristics and relative transpiration by grasses and trees or shrubs [mm] (*Klerk* 2004; *Donaldson* 1969)

Woody plant species	Approximate size and foliage spread of plants			Total leaf area (m^2)	Mean relative transpiration per 8-hour day per plant (kg)	Mean daily relative transpiration per 500 woody plants or per 100,000 grass plants (kg)
	Height (m)	Crown diameter (m)	Canopy area (m^2)			
Terminalia sericea	2.8	2.8	6.0	28.55	16.64	8,320
Acacia mellifera	2.5	2.8	6.0	55.68	64.80	32,400
Boscia albitrunca	1.2	1.5	2.0	13.58	13.84	6,920
Grewia flava	1.2	1.9	2.0	8.82	7.68	3,840
Anthephora pubescens	0.28	0.15	0.018	0.141	0.344	34,400
Eragrostis lehmanniana	0.21	0.15	0.018	0.038	0.075	7,500
Schmidtia pappophoroides	0.19	0.15	0.018	0.074	0.116	11,600

An early study of the water consumption by trees shrubs and grasses in savannah ecosystem goes back to *Donaldson* (1969). He balanced the transpiration amounts by different savannah plant species according to their physiological characteristics like growth height, canopy dimensions and total leaf area. As a result, he states that *Acacia mellifera,* the most widespread encroacher species, transpires four times more soil water per plant in relation to the non-encroaching woody plant *Terminalia sericea* while having only the double total leaf area. Compared to a grass species like *Eragrostis lehmanniana* it is almost 900 times more per plant (Tab. 1). *Scholes* and *Walker* (1993) published a regional scale model derived water budget for a broad-leafed type of savannah in South Africa for a 15-year period with a mean annual precipitation of 585.8 mm. The output revealed an evapotranspiration share of 83.8 % of the long-term precipitation input, whereas only 0.8 % account for deep drainage and 15.4 % for interception losses. 47 % of the rainfall input evaporate from soil and 36.7 % is returned to the atmosphere by transpiration in which 21.4 % is the tree fraction and 15.3 % the fraction by grass. An analysis of a spatially distributed hydrological model by *Starr* and *Alam* (2015), conducted in the savannah regions in North Sudan, shows contrasting results, indicating another time the need for a regional precise look at certain scales over time and space. The representation of the vegetation density and transpiration characteristics within the model approach was parameterized according to *Allen* et al. (1998) with a generalized focus on tree density as a proxy for vegetation heterogeneity. The water budgets were calculated for two different soil types, Arenosols and Vertisols (Tab. 2).

Tab. 2: Descriptive output statistic for a Sudanese savannah water budget model. Period 1961 – 1990. 11.5°N, 30.75°E. (*Starr* and *Alam* 2015)

	Rainfall	Temp.	Arenosols (mm)				Vertisols (mm)			
	(mm)	(°C)	*ET*	Runoff	Drainage	*SM*[a]	*ET*	Runoff	Drainage	*SM*
Minimum	339	26.2	297	0	0	1	343	0	0	0
Maximum	970	28.8	509	229	291	34	677	260	139	49
Mean	654	27.3	396	68	189	26	519	89	47	37
Coefficient of variation, %	20	3	13	92	36	23	13	81	77	29

[a]*SM* = end-of-month mean plant-available soil moisture content of upper 1 m soil.

In contrast to *Scholes and Walker* (1993), the model output does not differentiate between plant types and only gives values for evapotranspiration. Nevertheless, these model outputs correspond well to those by *Scholes* and *Walker* (1993), accounting for 75 % - 100% evapotranspiration related to mean annual precipitation for Arenosols and 83 – 100 % for Vertisols respectively. Since groundwater recharge is known to be generally small in drylands with 0.1 % to 5 % of mean annual precipitation (*Scanlon* et al. 2006b) the high variability and fraction in the model output in Tab. 2 are representative for the specific grid cell. According to the authors, the overall groundwater recharge amounts for the whole model domain is within the expected range as found in the literature.

Raz-Yaseef et al. (2012) determined dynamics of evapotranspiration and its partitioning for a semi-arid forest stand with *Pinus halepensis* and sparse understory vegetation in southern Israel with a density of ~ 300 trees ha^{-1}. They combined field measurement techniques to determine soil evaporation (chamber measurements), single tree transpiration (sap flow technique) and statistical upscaling procedures, climatic variables (eddy covariance measurements), soil moisture (time domain reflectometry) with a data-driven multiple linear regression analysis to examine the relation between rainfall and transpiration, evaporation and interception for four consecutive years (Tab. 3). The results for transpiration and evaporation losses expressed as fractions of total evapotranspiration match with previously mentioned studies based on different methods and study sites but similar climatic conditions. 85 % - 100 % of the total precipitation amount is returned to the atmosphere by evapotranspiration with an average share of 49 % transpiration fluxes, 39 % soil evaporation and 12 % interception losses.

Tab. 3: Results of an integrated study for evapotranspiration partitioning in a semi-arid forest in southern Israel (*Raz-Yaseef* et al. 2012).

	P		T_t		E_s		I_P		ET
	mm year^{-1}	P_{30}/P	mm year^{-1}	T_t/ET	mm year^{-1}	E_s/ET	mm year^{-1}	I_P/ET	mm year^{-1}
2003/2004	231	0.56	134	0.57	99	0.42	27	0.11	235
2004/2005	377	0.64	156	0.45	112	0.33	39	0.11	343
2005/2006	224	0.43	111	0.49	93	0.41	26	0.11	227
2006/2007	308	0.55	115	0.44	106	0.40	33	0.13	263
Average	285	0.55	129	0.49	102	39	31	0.12	267
STD	72	0.09	21	0.06	8	0.04	6	0.01	53

These results are valid for a forest stand with 65 % coverage and will change with increasing or decreasing soil cover fraction. Since the LAI of individual trees in this stand was estimated with ~ 1.5 and the relation between transpiration and evaporation is strongly related to that index an increase in LAI will shift the relation towards increased transpiration and decreased evaporation which lead to negative water budgets and drought stress effects (*Raz-Yaseef* et al. 2010)

3. Methodology

3.1. Field data collection

3.1.1. Soil survey and sampling

Prior a first soil sampling campaign, every study site was classified visually on the basis of true color satellite images into landscape and vegetation units based on a 300 x 300 m point grid. According to the share of each derived landscape class, an individual number of soil sampling points within each landscape class was identified. The description of the soil profiles followed the standardized procedures according to the German Soil classification system (*Ad Hoc AG Boden* 2005) as well as the international FAO system (*Food and Agriculture Organization of the United Nations* 2006, 2015). The documented soil parameters included surface characteristics, horizontation, Munsell soil color, bulk density, texture, soil structure, humus content, root density and distribution, rock fragments, lime content and in case of occurrence hydromorphic characteristics and primary and secondary macropores. In addition to the soil related description, the standing vegetation, as well as topographic characteristics, are described. For soil chemical and hydrological laboratory analysis, disturbed mix samples and undisturbed soil cores were taken strata wise.

3.1.2. Soil water content and pressure head measurements

To log time depending changes in the volumetric soil water content and its related matrix pressure heads, representative plots were instrumented with probes in site-specific soil depths according to their horizontation and properties. The soil water content was measured using Theta Probes (ML2x by Delta T-Devices) based on impedance measurements with a 100 MHz sinusoidal signal within an array of four stainless steel rods inserted into the soil. According to the defined dielectric constant of water (~ 81), dry soil (~ 3 - 5) and air (1) the apparent soil water status can be obtained by the impedance of the rod array at the time t_x with a possible maximum of 0,5 m^3 m^{-3}which corresponds to a dielectric constant of 32.In the same depth, as the soil water contents were logged, Watermark (WATERMARK 200S by Irrometer) probes were installed to measure soil matrix pressure heads. The principal bases on resistance measurements by two resistance probes embedded into a granular matrix. Changing water content leads to a change in the resistance of the granular matrix, which is then a measure for the apparent tension logged in centibar (range 0 - 200 cbar). Due to the soil temperature dependency, the obtained tension values

have to be corrected by using empirical functions with measured soil temperature values in corresponding soil depths (*Spaans* and *Baker* 1992; *Thomson* and *Armstrong* 1987). The installation schemes were adopted to the specific research question linked to the individual research area. To focus on different soil water dynamics induced by contrasting vegetation and land use, plots with comparable soil types but different land use and vegetation were selected for measurements.

3.1.3. Meteorological Measurements

To link the obtained soil water dynamics to atmospherical drivers it is mandatory to record influencing climatic parameters by automated weather stations. On one hand, central stations according to WMO standards (*World Meteorological Organization* 2011) were placed in open areas of the specific study site. On the other hand, these station data were complemented by site-specific precipitation measurements to address spatiotemporal variability on the microscale as well as vegetation modified soil water inputs due to interception losses.

3.1.4. Leaf area index measurements

For the soil hydrological model approach conducted in this study, it is crucial to have detailed information about the type and state of the vegetation cover, especially about the soil cover fraction or the leaf area index. Due to short-term field stays time series measurement along the development stages of the vegetation could not be compiled. In order to construct those necessary time series plant with different development stages due to differing sowing dates, here only applicable for crops, were measured. For crops and low grown tree and shrub species in open forest stands the differential insolation measurement device (SunScan© provided by Delta-T Devices) was used. It consists of two radiometers. One measures the direct and diffuse insolation at an open space nearby the vegetated plot. The actual device is a linearly aligned system of 64 radiometer diodes, which is put directly under the plant canopy. Each diode is measuring the transmitted photosynthetically active radiation (PAR) independently to get a representative mean of PAR. On the basis of the relationship between direct, diffuse and PAR together with user estimated leaf angle and light absorption constant, it is possible the calculate the LAI according to the algorithms developed by *John Wood* et al. (2014).

3.2. Laboratory analysis

3.2.1. Soil chemical analysis

The mixed and air-dried soil samples were sieved to 2 mm and analyzed with respect to total nitrogen and total carbon using a Vario MAX element analyzer (Elementar Analysesysteme). To determine the share of the inorganic carbon, it was dissolved in 5 ml phosphoric acid and the released CO_2 was measured by gas chromatography.

Soil pH and electrical conductivity (EC) were determined in a suspension with a soil to H_20 ration of 1:2.5 using multimeter probes. Additionally, soil pH was measured in a suspension with 0.01 M $CaCl_2$ with a ratio of 1:2.5 soil to $CaCl_2$ (*German Institute for Standardization* 1997, 2005).

3.2.2. Grain size distribution

The grain size distribution was analyzed by sieving and sedimentation methods according to German Institute for Standardization (*German Institute for Standardization* 2002), resulting in percentage fractions of clay, coarse, medium and fine silt and coarse, medium and fine sand. In contrast to the international grains size classification, the determined classes have logarithmic boundaries regarding diameter.

3.2.3. Soil water retention

To determine the soil water retention and the related retention function $\theta(\psi)$ undisturbed soil cores were saturated with water from the bottom to the top using capillarity properties. After saturation, the samples were drained stepwise under defined increasing pressure regimes. After reaching a state of equilibrium within each step, the water content is derived by weighing. At the end of each cycle, the matrix pressure heads are assigned to a specific water content (*German Institute for Standardization* 2014a, 2012). The resulting data pairs were used to parameterize soil hydrological retention functions for a subsequent model approach.

3.2.4. Unsaturated hydraulic conductivity

The horizontal wise soil hydrological properties according to the van Genuchten-Mualem (*van Genuchten* 1980) parameterization were derived by using the HYPROP© measure-

ment device (UMS Munich, Germany). The principle behind this setup bases on the evaporation method to estimate soil hydrological conductivity first described by (*Wind* 1969; *German Institute for Standardization* 2014b) and modified by (*Schindler* 1980). This method relates the evaporative water loss of a soil core with the mean gradient of the soil water pressure head at defined time step. Based on the assumption, that the water loss and the pressure head gradient are constant over an interval and that the decrease of the water content within the height of the soil core is linear, this method was positively evaluated for a wide variety of soil textures and inorganic as well as organic substrates (*Schindler* and *Müller* 2006; *Wendroth* et al. 1993).

3.3. Long-term weather data sets

Since site-specific historic weather data for long-term model applications are not available or biased, the model scenario runs are driven by a regional climate model output (*Weber* et al. 2014) based on ERA-INTERIM forcing (*Dee* et al. 2011). The hourly data with a spatial resolution of 25 km x 25 km contain parameter according to Tab. 4.

Tab. 4: ERA-INTERIM forced REMO output parameter as SWAP input for long-term model runs

Variable name	Unit
surface pressure	Pa
2m temperature	K
10m wind speed	m/s
maximum 2m temperature	K
minimum 2m temperature	K
total precipitation	mm
global radiation	W m^{-2}
2m vapor pressure	Pa

Based on this 30-year reanalysis dataset beginning with 1980, long-term soil hydrological system responses to climate variability can be assessed for a variety of land use and land cover scenarios.

3.4. The soil hydrological modeling scheme SWAP

To predict a closed soil hydrological balance for each study site and land use type the open source modeling scheme SWAP ("**S**oil-**W**ater-**A**tmosphere-**P**lant") in version 3.2 provided by Alterra/Wageningen (*Kroes* et al. 2008) was used. This Richards equation based 1D

finite difference field scale model is able to simulate vertical dynamics and balances of water, solutes and heat in the soil in interaction with a dynamic representation of vegetation, climate and groundwater level. Due to a possible integration of lateral soil drainage, SWAP can be defined as a quasi-two-dimensional model. For the purpose of this study lateral soil water movement is seen as negligible and only vertical dynamics were considered. To summarize the model architecture three central compartments are presented in the following chapters. For a description of model parameter and the related model assumptions with its constraints and uncertainties see section 1. All general control parameters concerning geographical settings, timing criteria, crop rotation, climate data input control as well as data handling instructions are defined in the SWP file to initialize a model run. For a detailed description of Fig. 8, it is referred to *Kroes* et al. (2008). SWAP provides different options for meteorological data input to calculate potential evapotranspiration (ETp) according to Penman-Monteith (*Penman* 1948; *Monteith* 1965) and precipitation input. The minimum temporal resolution is set to daily values, whereby subdaily resolutions for precipitation intensities from hours to minutes are optional. In this study, hourly values were used to calculate ETp and as precipitation input. A model run with a daily resolution needs the minimum and maximum Temperature as additional input. Together with the latitude and the height of the given meteorological station or climate model cell SWAP calculates ETp (*Kroes* et al. 2008; *Allen* et al. 1998).

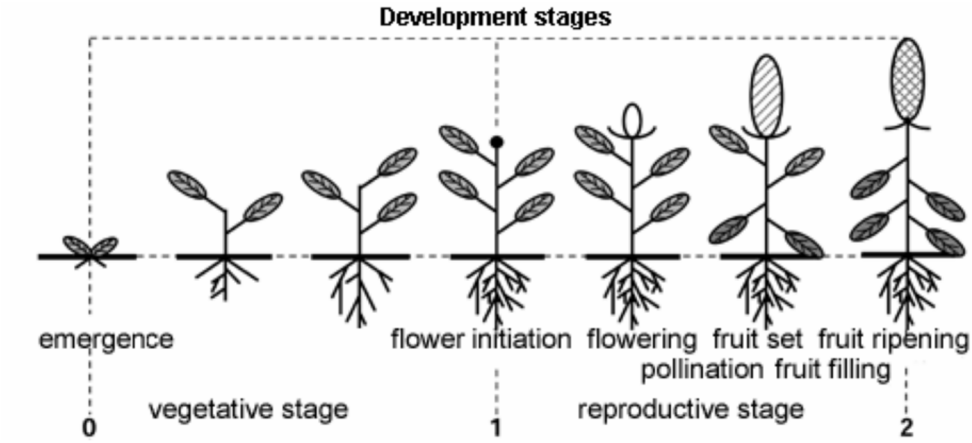

Fig. 7: Description of the specific development stages (DVS) as integrated into SWAP

Beside the main SWP file, vegetation or crop-related parameter are defined in a separate input file (CRP file). Two different types of CRP file exist, where the simple module demands only reduced input parameters addressing only plant and soil water relations

without any feedback dynamics. This module is preferred due to a lack of specific parameter values for natural vegetation. As shown in Fig. 8 the vegetation parameter such as leaf area index, growth height, transpiration factors or rooting depth respective intensities and their development over time is assigned to a specific phenological stage (Fig. 7). The assumed vegetation parameter used in this study can be found in Tab. 5. These dynamic functions control the amount of intercepted precipitation, the relation between bare soil evaporation and transpiration as well as root water extraction in a certain depth. Once defined, all external drivers are linked to the central soil domain. This domain is designed to be a virtual soil column subdivided into horizon representing layer to which soil hydrological parameters according to *van Genuchten* (1980) are assigned. A subsequent refinement of these layers leads to the finale discretization of compartments as the basis for solving the Richards equation (Fig.9).

Tab. 5: Vegetation parameter as included in the model scenarios

Parameter	Unit	DVS	Bare Soil	Grass	Woodland open	Woodland dense	Maize dryland	Maize irrigated	Wheat irrigated	Intercanopy Erichsfelde	Canopy Erichsfelde
Length of vegetation cycle	d		0	366	366	366	125	125	240	366	366
Leaf Area Index	$m^2\ m^{-2}$	0.0	0		0.6	1.2	0.2	0.7	0.8	0.32‡	0.77‡
		0.5	0		2.2		0.7	2.5	2.4	0.45‡	
		1.0	0		3.2	4.9	1.2	4.3	4.0	0.58‡	1.66‡
		1.5	0		3.2		1.2	4.6	4.0	0.50‡	
		2.0	0		0.6	3.0	0.3	1.2	0.8	0.45‡	1.21‡
Soil cover fraction	$m^2\ m^{-2}$	0.0	0	0.8							
		0.5	0	0.9							
		1.0	0	1.0							
		1.5	0	1.0							
		2.0	0	1.0							
Crop factor (k_c)		0.0	0	0.85†			0.3†	0.3†	0.3†	0.50†	1.0
		1.0	0	0.95†			1.2†	1.2†	1.0†	0.97†	1.0
		2.0	0	0.85†			0.3†	0.3†	0.5†	0.72†	1.0
Growth height	cm	0			400	800					
		1.0			400	800					
		2.0			400	800					
Rooting depth	cm	0.0	0	80†	300	300	30†	30†	30†	100	300
		1.0	0	80†	300	300	100†	100†	150†	100	300
		2.0	0	80†	300	300	100†	100†	150†	100	300
Root density	Relative values	Rel depth									
		0.0	0	1.0	1.0	1.0	1.0	1.0	1.0	1.0*	0.0*
		0.1	0	1.0	1.0	1.0	1.0	1.0	1.0	1.0*	0.3*
		0.2	0	0.9	0.9	0.9	0.9	0.9	0.9	0.9*	0.6*
		0.3	0	0.8	0.8	0.8	0.8	0.8	0.8	0.8*	0.9*
		0.4	0	0.7	0.7	0.7	0.7	0.7	0.7	0.7*	1.0*
		0.5	0	0.6	0.6	0.6	0.6	0.6	0.6	0.6*	1.0*
		0.6	0	0.5	0.5	0.5	0.5	0.5	0.5	0.5*	1.0*
		0.7	0	0.4	0.4	0.4	0.4	0.4	0.4	0.4*	0.9*
		0.8	0	0.3	0.3	0.3	0.3	0.3	0.3	0.3*	0.6*
		0.9	0	0.2	0.2	0.2	0.2	0.2	0.2	0.2*	0.3*
		1.0	0	0.1	0.1	0.1	0.1	0.1	0.1	0.05*	0.1*

‡: unpublished data by Oldeland (2006)
†: data modified after Allen et al. (1998)
*: data derived from Scholes and Walker (1993)

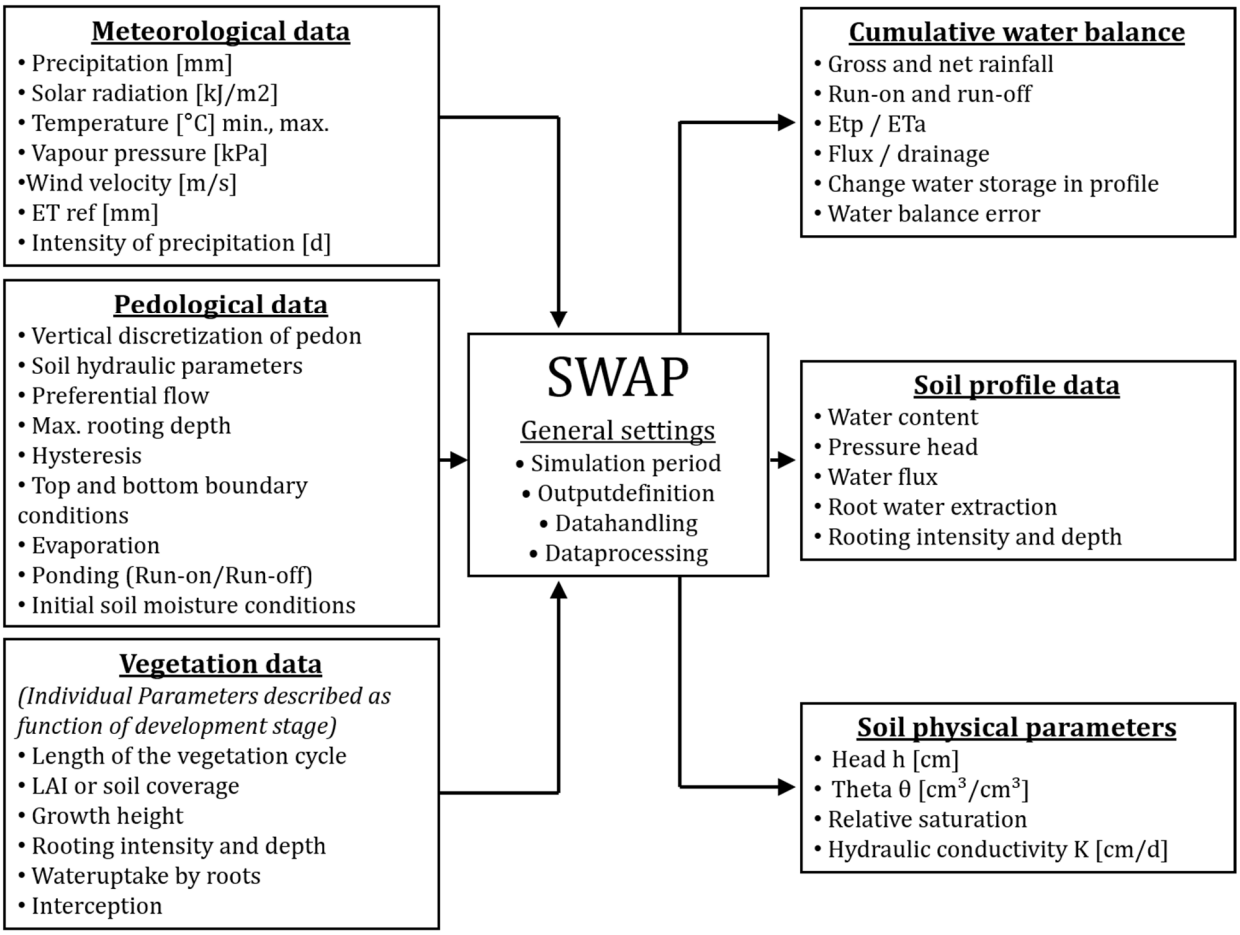

Fig. 8: Model architecture and parameter description for SWAP 3.2

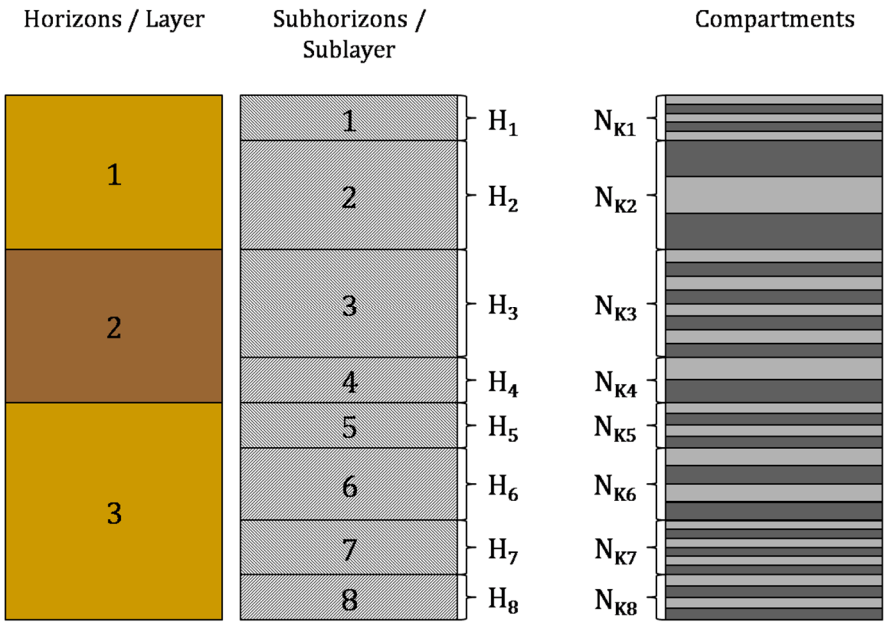

Fig.9: Discretization scheme of a virtual soil column as represented by SWAP (*Landschreiber* 2010)

4. The physical geography of the Okavango catchment – an overview

This section will give a concise overview of selected geographical features within the Okavango basin as well as of the local scaled study sites. For detailed information about the single features mentioned, see (*Oldeland* et al. 2013; *Jürgens* et al. 2010)

4.1. The Okavango basin - a regional overview

The southern African, perennial river system of the Okavango extends over the northern highlands in central Angola via a low undulated midstream region in SE Angola and Namibia towards its inland delta, situated in the north-western part of Botswana. This subdivision into three regions represents the major landscapes of the active catchment which led to the selection of the central study sites.

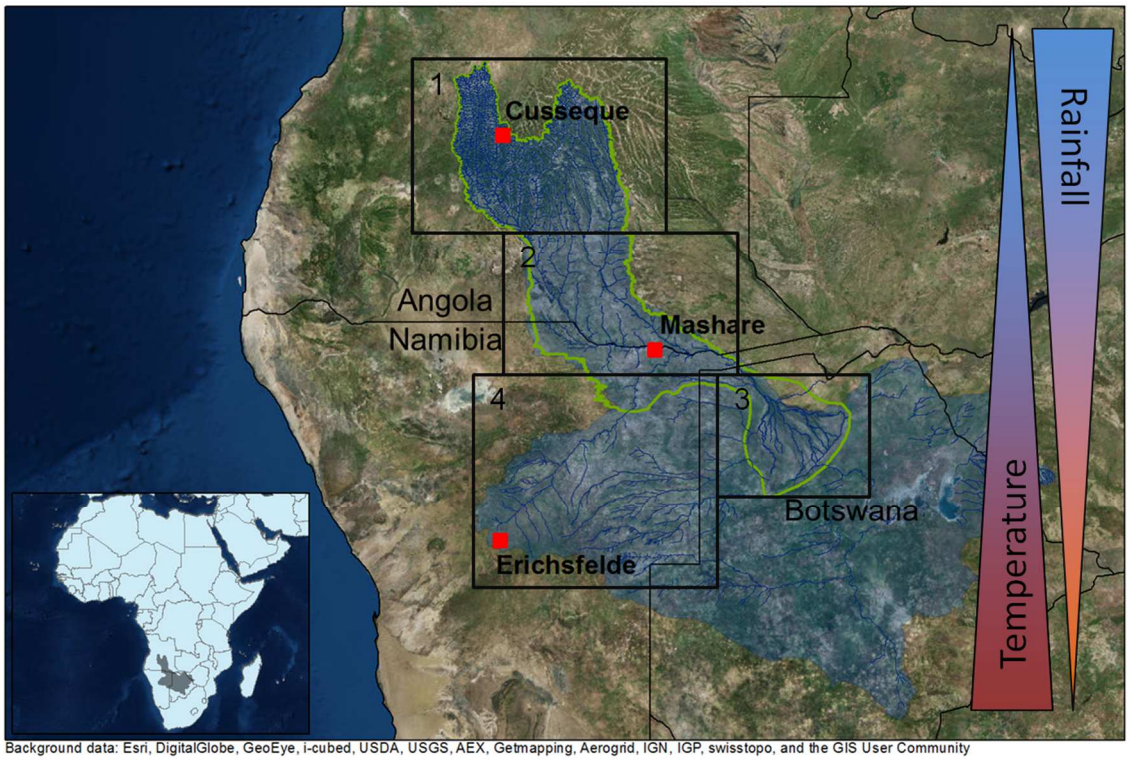

Fig.10: Map of the Okavango catchment hydrologically defined (blue) and the more restricted definition by the TFO project (green outline) with the central study sites of the research

To cover those representative landscapes four study sites with an area of 100 km² each. The headwater region is represented by the "Cusseque" core site going over to the "Caiundo" core site in the midstream region of the Cubango. "Mashare" represents the low-

lands in the Kavango region of northern Namibia whereas the "Seronga" core site is situated on the eastern shore of the so-called "panhandle" as part of the Delta's northern floodplains in Botswana.

The research in hand focuses on the Cusseque and Mashare core sites and, in addition, on a research site by the BIOTA Southern Africa project called "Erichsfelde", about 100 km north of Windhoek/Namibia. This site is not included in the active Okavango catchment and therefore is not a part of the TFO project. Due to its hydrological connection via the ephemeral river Omatako, this tributary defines the southwestern extent of the Okavango mega basin. This extension adds an additional landscape to the regional research area of the TFO project consisting of the thornbush savannah of central Namibia with its typical coexisting of trees and grasses. At the same time, the research area is extended along the climate gradient.

4.1.1. Climate setting

Due to the influence of the seasonal variation of the intertropical convergence zone and the Angolan low-pressure system, the Okavango catchment shows a strong climatic gra-

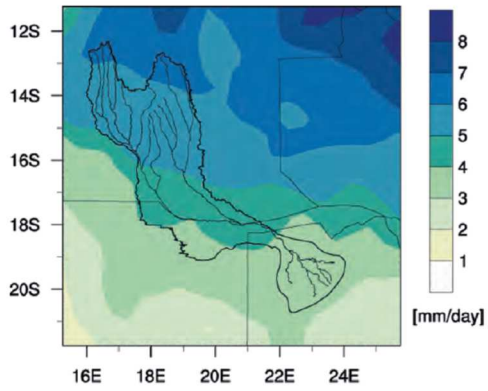

Fig. 11: Mean precipitation intensities from December to February (1971 – 2000) (*Weber* 2013c)

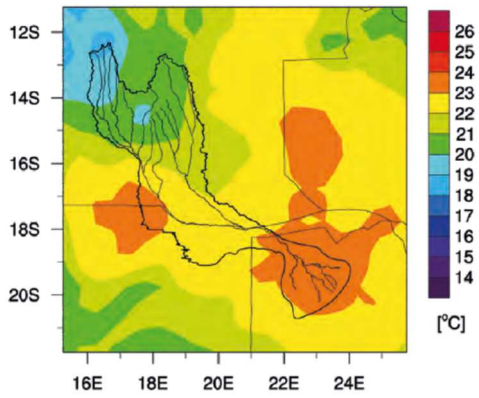

Fig. 12: Mean annual temperature (1971 - 2000) (*Weber* 2013c)

dient going from north to south. The mean precipitation intensities reach 7 mm d^{-1}in the north with mean amounts of about 1000 mm a^{-1} shifting down to 3 mm $d^{-1}$and about 500 mm a^{-1} in the delta region of Botswana ending up with approximately 360 mm a^{-1} in the central highland region of Namibia. The mean annual temperature varies about 6°C with 18°C in the north up to 24°C in the southern regions due to the influence of the Kalahari basin.

4.1.2. The soils in the landscape

Soil types reflect biotic and abiotic soil forming processes being in an interface position between geology, climate, hydrology, vegetation and land use. Looking at the combination of regional landscapes (Fig.10) and soil type distribution (Fig.13), the predominant influence of climate, hydrology and bedrock lead to typical soil landscape delineation. Due to the semi-humid character of the headwater regions (Fig.10 Region 1) tropical soil forming aspects like low pH values and highly weathered bedrock can be observed and is represented by the appearance of Acrisols. Bedrock induced soil types are to appear in form of Arenosols on unconsolidated sediments as well as Plinthisols on weathered granitic bedrock. Histosols occur in areas with year around water saturated conditions along streamlines reflecting special hydrological conditions. The influence of the bedrock is predominant in the Kavango region around Mashare (Fig.10 Region 2). Arenosols appear in areas with deep Kalahari sands whereas Luvi-, Calci- and Fluvisols are to be found in areas with fluviatile sediments along the Okavango and in dry riverbeds. Due to its doleritic saprolites and slightly low pH values the Erichsfelde region (Fig.10 Region 4) is dominated by Luvisols. While being in a transition zone between the influence of the Kalahari sandveld and the consolidated bedrocks of the central highlands also Arenosols and Cambisols appear. Calcisols can be found in areas with a relictic influence of ascending groundwater, typically around the dry riverbeds.

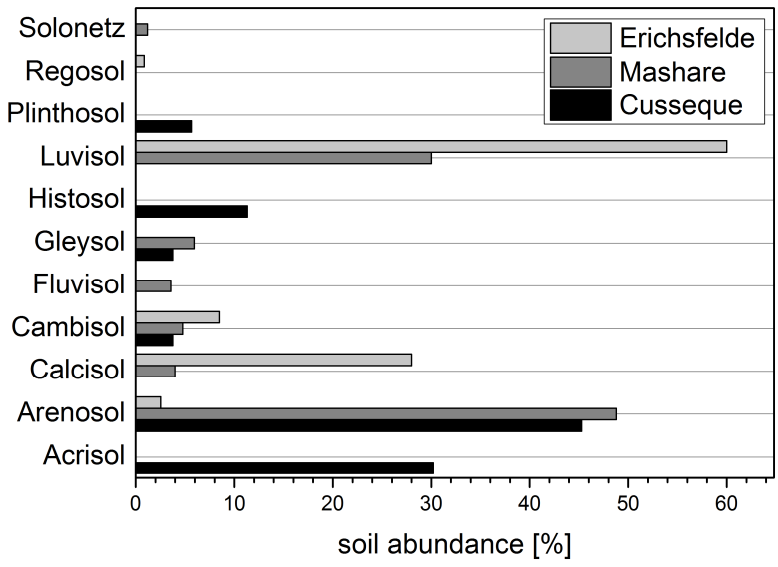

Fig.13: Soil type abundance within the study sites (n = 188)

4.1.3. Natural vegetation and land cover

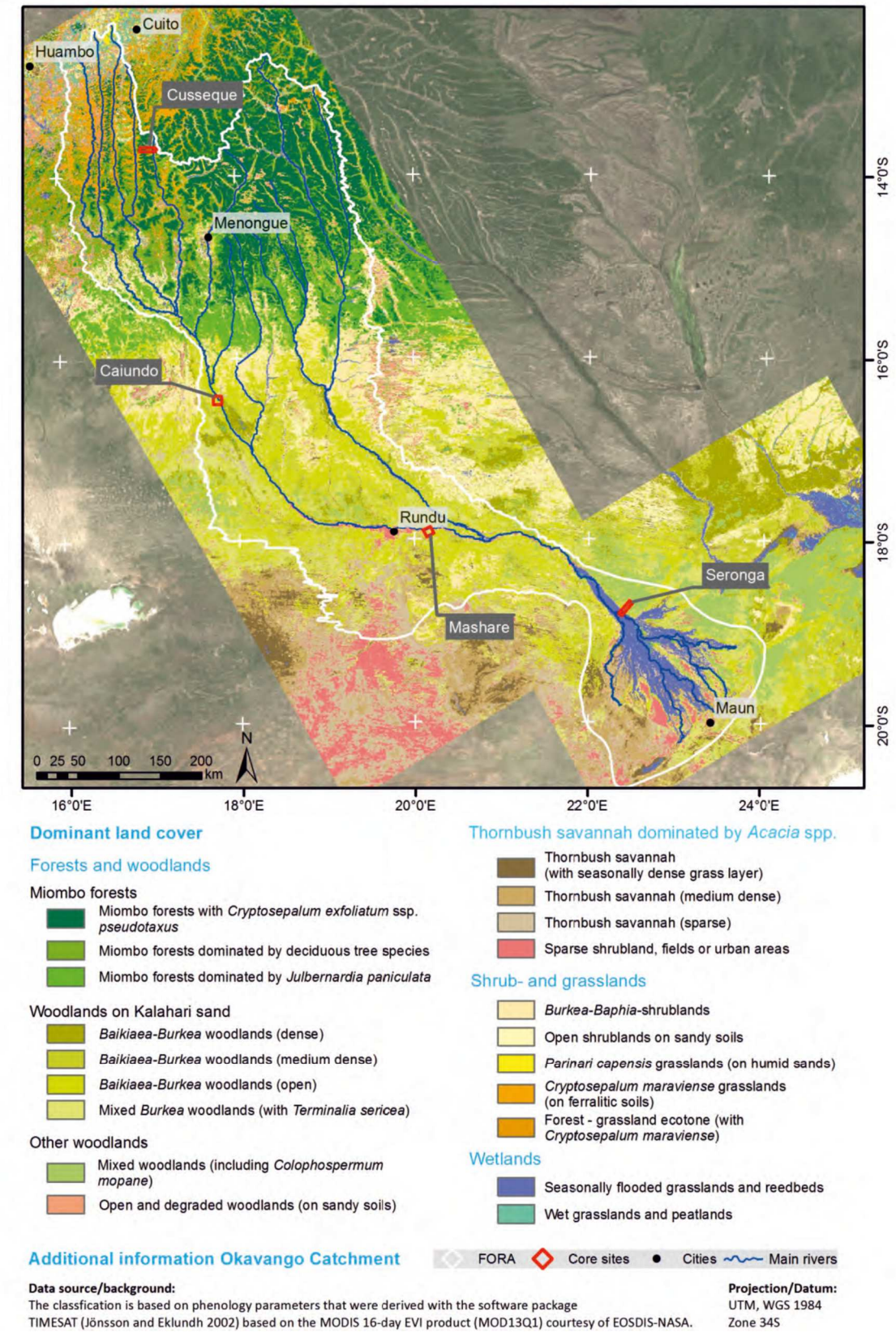

Fig.14: Land cover classes by unsupervised MODIS time series classification (*Stellmes* et al. 2013)

Based on an unsupervised classification of MODIS satellite data, Fig.14 shows the main land cover classes along the river system (*Stellmes* et al. 2013). The northern headwater region of Angola is dominated by broad-leafed savannah type Miombo woodlands with *Cryptosepalum exfoliatum* under a high precipitation regime, whereas the middle reaches with lower precipitation on Kalahari sands show *Baikiea-Burkea* woodlands. Further south to Mashare, in addition, dry forest species such as *Colophospermum mopane* and *Terminalia sericea* are predominant. Leaving the active Okavango catchment to the central-western highlands of Namibia, where the BIOTA observatory is situated, the landscape aspect changes to a typical codominance of grasses and trees in savannahs. Typical woody species are *Acacia mellifera* and *Boscia albitrunca.* The grass layer is dominated by *Stipagrostis* and *Eragrostis* species.

4.2. The study site Cusseque (Angola)

The study site Cusseque is located in the province of Bié, 150 km south of the province capital Kuito (13.69° S, 17.08° E). The defined site has an extent of 5 x 20 km^2 and an east-west orientation. The site was named after the main tributary to the Okavango Cusseque.

4.2.1. Climate

The semi-humid character of this site is defined by a distinct rainy season starting in November and ending in April with a MAP of 987 mm (period 1971 – 2000) while the annual rainfall conditions show a high interannual variability. The annual mean temperature is 20.4°C where October is the hottest (23°C) and July the coldest month (16.1°C) whereas in contrast to the rainfall variability the temperature shows a small inter-annual variation. From May to September an average number of 19 frost days occur (*Weber* 2013c).

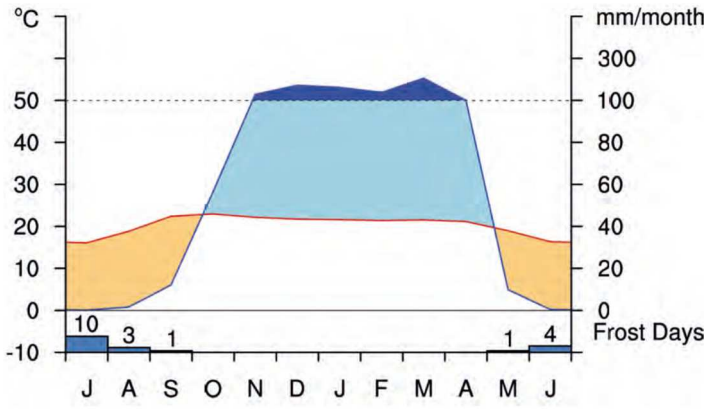

Fig.15: Climate Diagram of the Cusseque study site (*Weber* 2013a)

4.2.2. Landscape structure

The headwater regions landscape in the Angolan highlands is mainly structured by the underlying Precambrian Angolan plateau. Geological weakness zones in combination with fluviatile erosion processes shape the topography of that study site. Thus, a north-south orientated trellis-like river system with first and second order tributaries is noticeable. The landscape of the study site can be structured into three major landscape units with distinct geomorphological, botanical and pedological features (Fig.16).

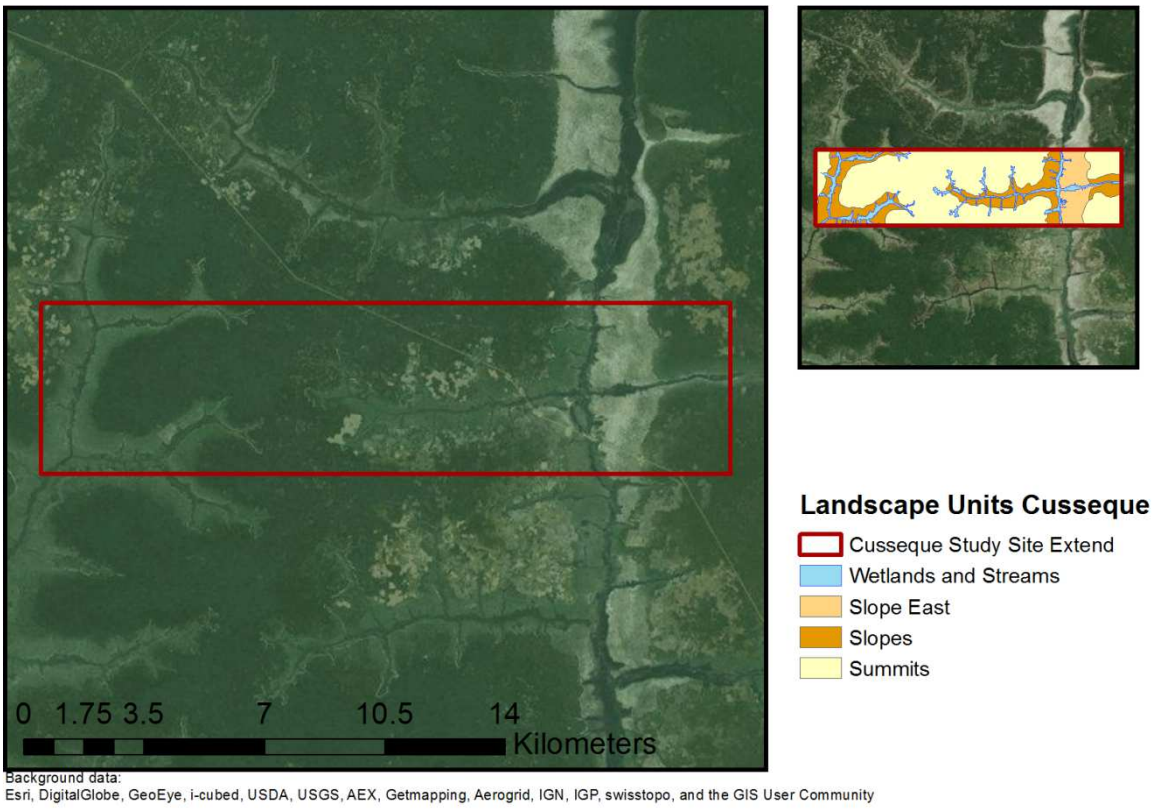

Fig.16: Cusseque study site overview and landscape delineation

The wetlands and streams consist of open water bodies in the valley bottoms flanked by peat bogs with a seasonal water table oscillation. The transition zone between the peat bogs and the midslope areas are framed by bands of white bleached sands indicating a discharge of interflow water. Dissolved organic acids together with pedogenic oxides form metal-organic compounds, which are leaching into to the adjacent waterbodies, resulting in these bleached white sands. The slopes (LSU2) form the transition between the streamlines and the neighboring summit areas. They are subdivided into two subunits to reflect differences in soils and vegetation as well as their individual origin. The western

part of the Cusseque valley slope shows extensive areas with deep fluviatile relocated aeolic sediments by the Kalahari system indicating relictic river terraces while the eastern part of the valley is defined by shallow reddish soils over more or less consolidated oxidic bedrock or saprolites.The summit areas (LSU3) mark the highest points within the relief and rise up to 100 m above the streamlines. The summits are remarkably covered with dense semi-deciduous forests standing on deep weathered reddish soils. Aside from the peat bogs this unit is the preferred area for agricultural activities e.g. slash and burn agriculture and firewood extraction.

4.2.3. Soil inventory and spatial distribution

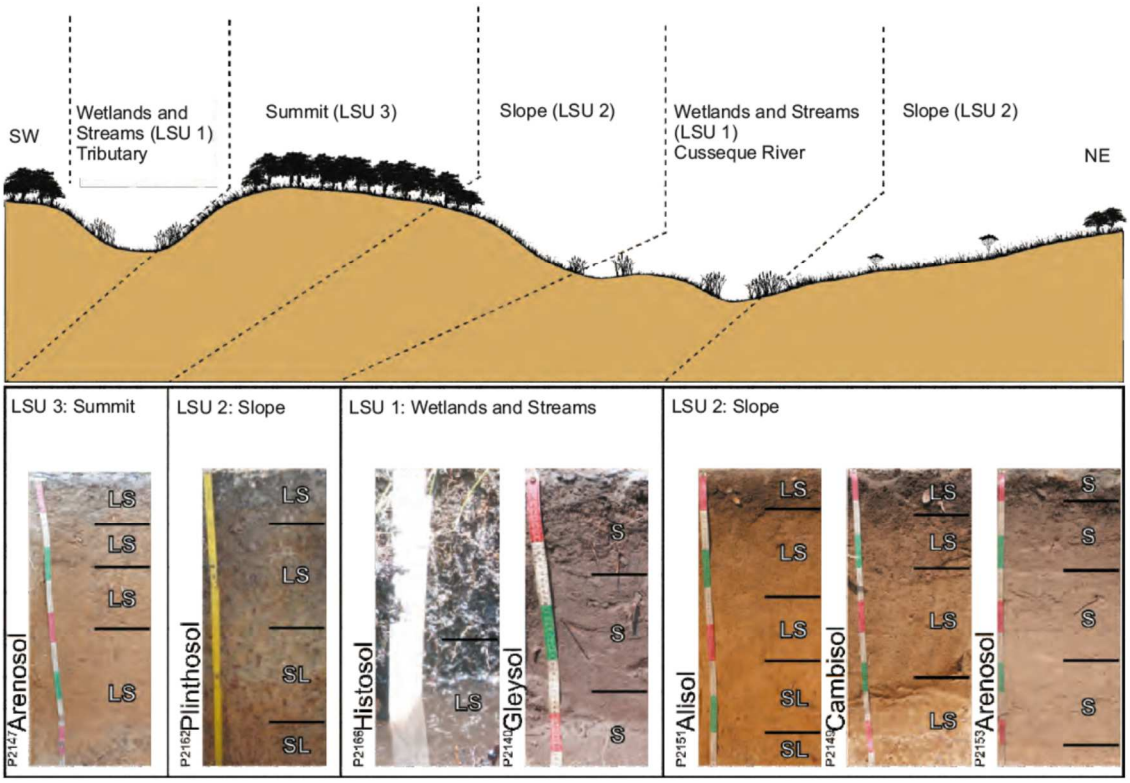

Fig.17: Transect of the Cusseque study site from SW to NE showing the major landscape units and the associated soil types (*Gröngröft* et al. 2013a)

Due to the diverse landscape structure and the semi-humid climate the Cusseque study site shows, in comparison to the other study sites, a high pedodiversity (Fig.17) with highly variable soil properties. In general, leaching processes led to high acidity in all soils but occurs very pronounced in soils of the summits. The wetlands and streams are dominated by groundwater affected mineral or peat soils. Histosols are located in the bog center whereas Gleysols with a layer of bleached white sands are framing the bogs. Acri- and Arenosols are the most frequent soil types to be found in the slope areas especially on the

old river terrace substrate of the eastern Cusseque valley. In addition, Plinthosols appear on the western part of the Cusseque valley where soils have a shallow accumulation of sands over old weathered granitic bedrock. Up in the summit areas deeply developed Arenosols dominate under dense woodlands. Here a slightly loamy soil texture facilitates these parts of the study site for agricultural use due to potentially optimized crop water availability. For detailed soil information see *Gröngröft* et al. (2013a)

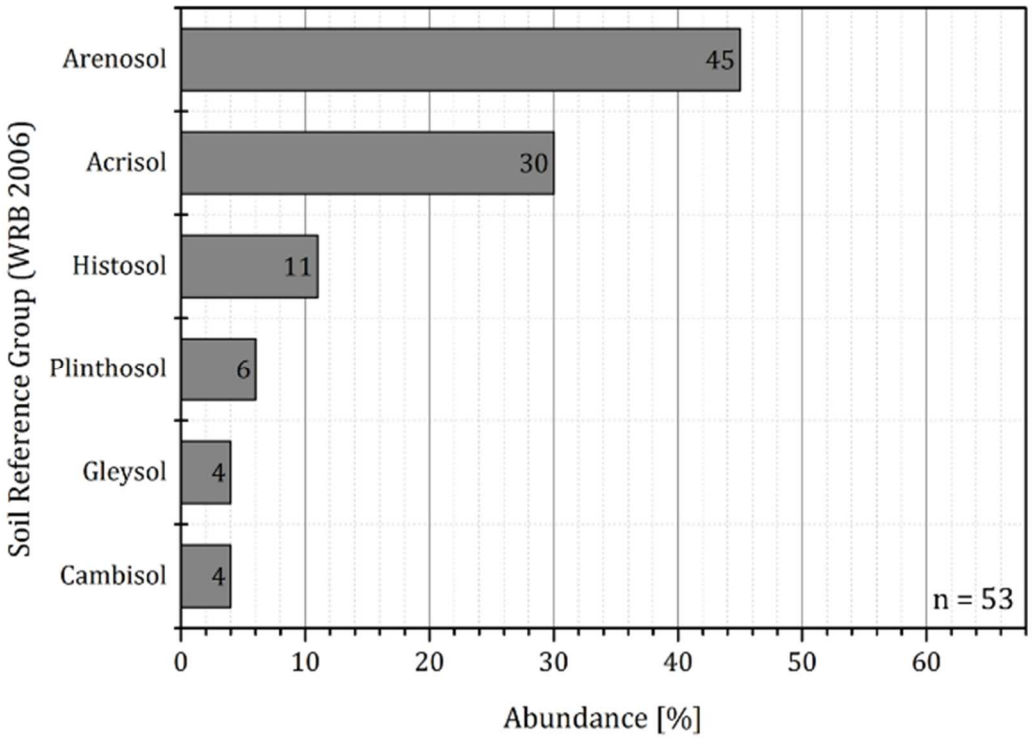

Fig. 18: Soil type abundance of the Cusseque study site

Fig. 18 shows the relative abundance of occurring soil types within the Cusseque study site. Due to the dominance of the sloping river terraces, the major soil type refers to Arenosols followed by Acrisols indicating the influence of long-lasting tropical weathering. The occurrence of Histosols reveals, in addition to tropical soil types, the semi-humid character of that landscape.

4.2.4. Vegetation and land use

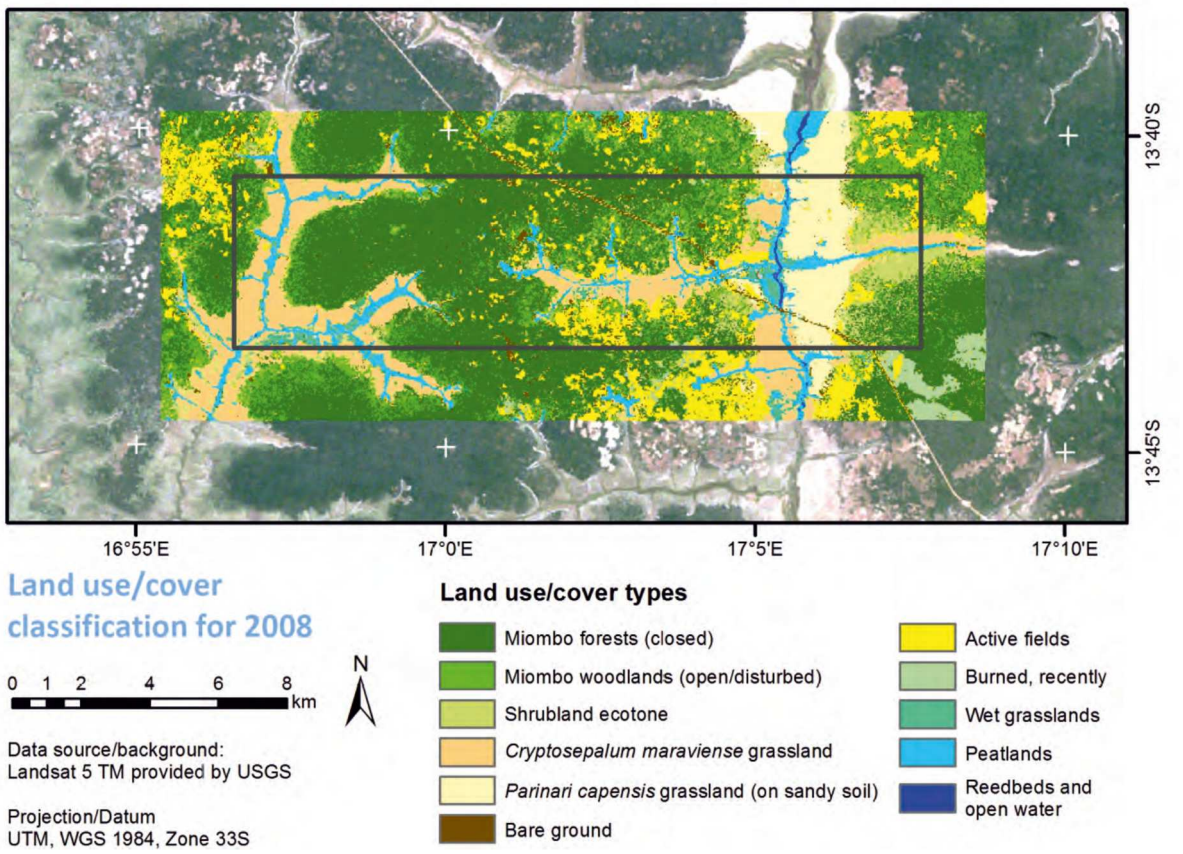

Fig.19: Land use and land cover for Cusseque based on an analysis of Landsat 5 TM imagery for the vegetation period 2008/2009 (*Schneibel* et al. 2013)

The vegetation and its distribution follow the topographical patterns of the study site and reflect the trisection of that area (Fig.19). A large portion of the summit surfaces is covered by dense Miombo woodlands comprising of *Cryptosepalum* species in combination with *Brachystegia spiciformis* and various *Combretum* species.In the transition to the downslope grass- and shrubland ecotones, the woodlands get more open due to a human disturbance which causes higher fire frequency. That transition is characterized by an early regeneration stage but partly suppressed by fern invasion of *Pteridium aquilinum*. Adjacent to the open woodlands the shrubland ecotone stretches over large areas where biotic and abiotic do not support the establishment of more or less dense woodlands anymore. *Combretum* and *Terminalia* species, as well as *Monotes glaber*, are typical tree species in that area. Special vegetation features are the widespread *Cryptosepalum* grasslands of the central western plateau of the valley dominated by *Cryptosepalum maraviense*.

Thick woody rootstocks with enormous extent down to a soil depth of 40 cm are characteristic for these “geoxylic suffrutex” life forms. These species appear to have the best conditions for the establishment in areas with shallow soils.

On deep sandy soils, the *Parinari capensis* grassland is predominant typically in the eastern part of the valley. The vegetation aspect is dominated by tall grasses such as *Monocymbium ceresiiforme* and the appearance of single trees but also geophytes species are to be found as a vegetation live form. Going further down the slope into the wetlands and streams mineral soils of the driftline form a habitat for sedges and tufted grasses whereas the peatlands show a typical vegetation with sedges and *Drosera* species. Reeds dominate the deep-water areas of the streamline.Agri- and horticulture play a dominant role in the regional subsistence in addition to charcoal production, beekeeping and hunting. Fig.19 shows the regional distribution of the active fields in 2008/2009. Preferred areas for slash and burn agriculture are the summit woodlands due to its relatively deep and good plowable soils and a good nutrient supply. The main crops are Maize and Cassava. The peatlands adjacent to the river have good hydrological preconditions as well as a sufficient nutrient provision for horticulture. After drainage potatoes, pumpkin, cucumbers etc. are cultivated in the dry and cold season.Slash and burn agriculture and charcoal production are the major threats to the Miombo woodlands having long regeneration periods while a clearing can also have a significant influence on hydrological processes.

4.3. The study site Mashare (Namibia)

Approximately 50 km east of Rundu the square-shaped Mashare study site is located along the Okavango River within the Kavango region of northern Namibia (17,90° S, 20,16° E). In contrast to the Cusseque site, this site extends over 10 x 10 km^2 to cover all relevant landscape features as well as land use types from subsistence farming to irrigated semi-industrial agriculture.

4.3.1. Climate

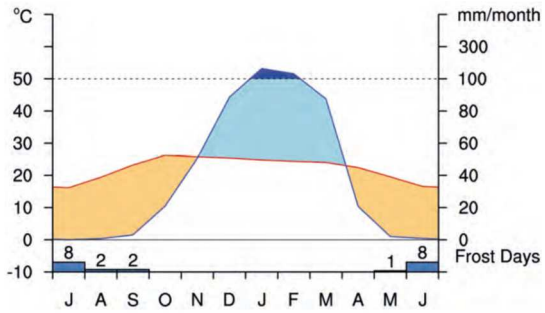

Fig. 20: Climate Diagram of the Mashare study site (*Weber* 2013b)

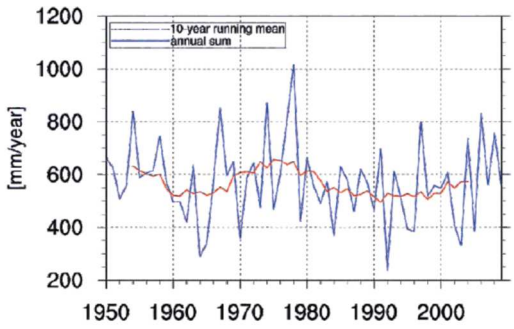

Fig. 21: Rainfall sums from 1950 to 2009 showing high inter-annual rainfall variability (*Weber* 2013b)

Following the north to south going climate gradient, the Mashare study site is characterized by semi-arid conditions with a distinct rainy season from October to April with a mean annual precipitation of 571 mm (Period 1971 – 2000) and high inter-annual rainfall variability. The annual mean temperature is 22.3°C with a mean number of 21 frost days per year occurring within the coldest month of July.

4.3.2. Landscape structure

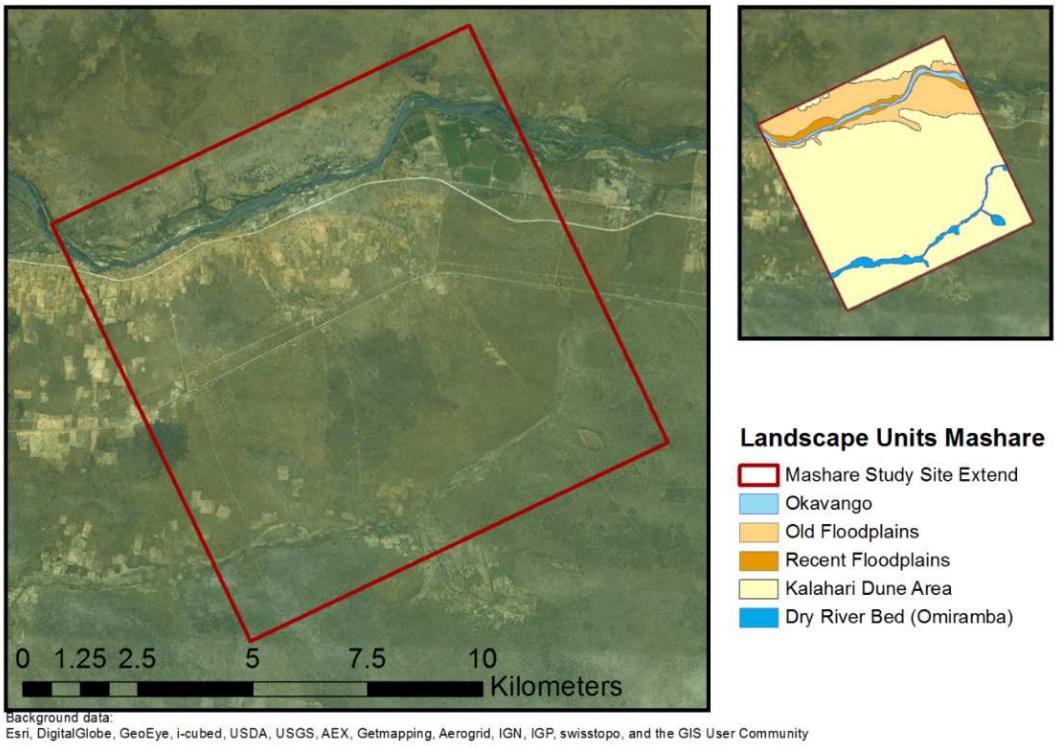

Fig.22: Mashare study site overview and landscape structure

Two dominant landscape features can be identified creating the landscape structure. On one hand, the Okavango River is forming the streamline with its recent (LSU1) and old floodplains (LSU2). Going south, the hinterland is characterized by the widespread Kalahari dune area with its predominant deep sands (LSU3) (Fig.22).

The **recent floodplains (LSU1)** show diverse sub-features created by the meandering river such as sandy textured levees and loamy depressions in periodically to episodically inundated abandoned meanders.

The **old floodplains (LSU2)** consist of former river terraces recently only flooded by extraordinary high water levels. The substrates are comparable to those of the recent floodplains but they had undergone soil development like calcrete formation under the influence of ascending groundwater and former climate regimes with higher water levels. Mound creating termites find an ideal habitat in those carbonate-enriched and slightly clayey areas.

The **Kalahari dune area (LSU3)** has the biggest extend within the study sites landscape units. The remains of leveled parallel dunes, similar to those found yet to be unlevelled in the southern parts of northern Namibia, reflect the former substrates of a dune-interdune system with loamy textures representing the interdune parts and deep sands accumulated in the dune crest regions. In addition to that, a special feature is a dry riverbed located in the southern part of the study site with clay-rich dark black fluviatile sediments in the central parts of the bed and existing pans along the relictic streamline.

4.3.3. Soil inventory and spatial distribution

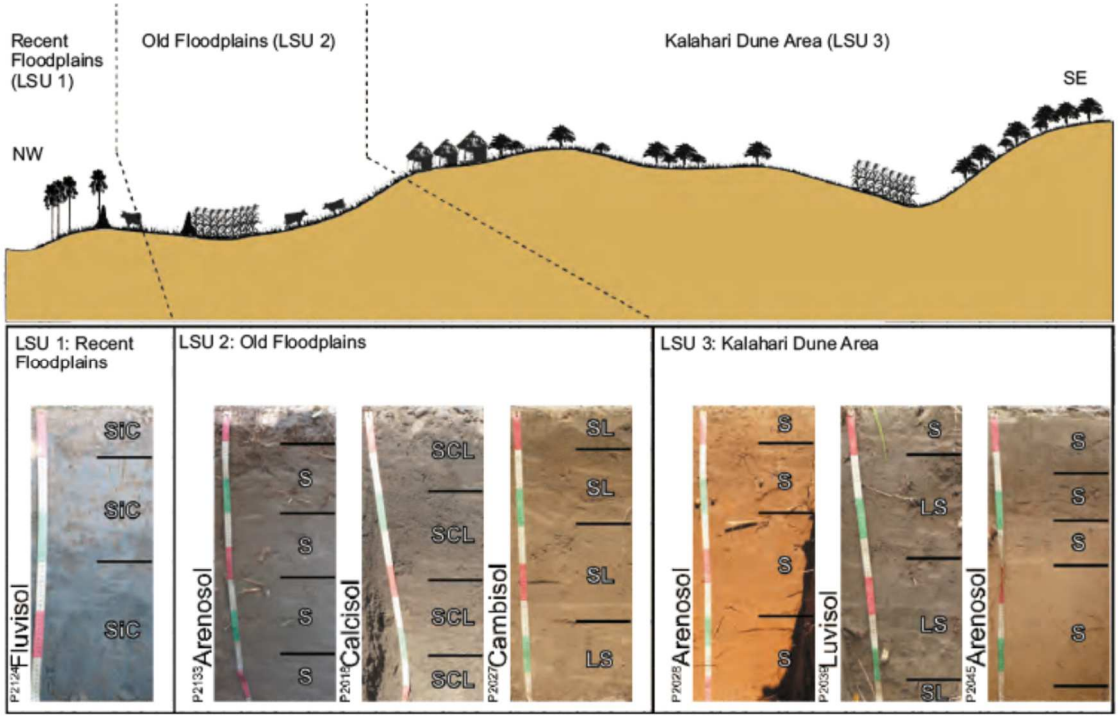

Fig.23: Landscape transect and the landscape units associated soil types of the Mashare study site (*Gröngröft* et al. 2013b)

The distinguished subunits of the **recent floodplains (LSU1)** and their topographic exposition to each other lead to three dominant soil types. Areas, which are periodically enriched with fresh fluviatile sediments are characterized by clayey Fluvisols or arenic Gleysols, whereas higher elevated and less often inundated parts of that unit typically consist of endogleyic Arenosols. Cambisols and Luvisols are representative for the levees and depressions of **old floodplains (LSU2)** while Arenosols dominate the **Kalahari dune area (LSU3)** in the hinterland with its deep Kalahari sands complemented with Luvisols in former interdune areas. In Fig. 24 the influence of Kalahari sands as parent material for soil formation is characterized by the dominance of Arenosols. In contrast to the Cusseque site, the second most abundant soils are Luvisols instead of Acrisols, showing a clear response to a more arid soil-forming environment. Nevertheless, the process of vertical clay migration, which is a diagnostic property for Luvisols, only occurs due to low pH-values with sufficient amount of precipitation.

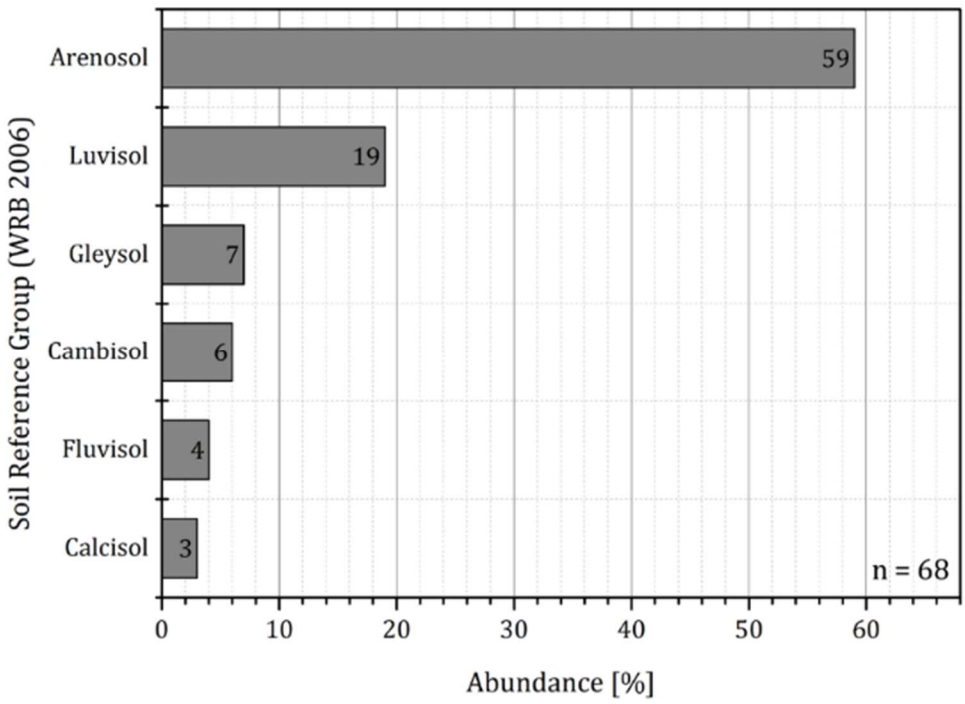

Fig. 24: Soil type abundance of the Mashare study site

4.3.4. Vegetation and land use

The Mashare study site is highly influenced by human activity (Fig.25). Dryland agriculture is starting along the riverside where the most fertile soils can be found. Main crops are Millet, Sorghum and Maize combined with groundnuts and small pumpkin varieties. Due to increasing population the former pristine riparian forest is cleared except a small protected area in the east of the Mashare region with *Acacia nigrescens – Peltophorum africanum* communities. Additionally, the fields have been expanded to the south into the Kalahari sand area, in the last 20 years, the share of fields has been doubled. Life stock keeping is part of the culture, thus grazing cattle and goats can be found from the periodically inundated areas up to the hinterland. An emerging trend in the Kavango region is the politically empowered establishment of large irrigation schemes with center pivots for industrial crop production under intensive use of agrochemical support to utilize the waters of the Okavango. Fires and wood logging have impacted on the natural habitat and vegetation composition of the dry woodlands. *Terminalia sericea*, *Pterocarpus angolensis* and *Combretum* species form the dominant tall trees in that area. Where soil conditions change to better nutrition availabilities in the dry river bed of the southern Omuramba agricultural fields accumulate.

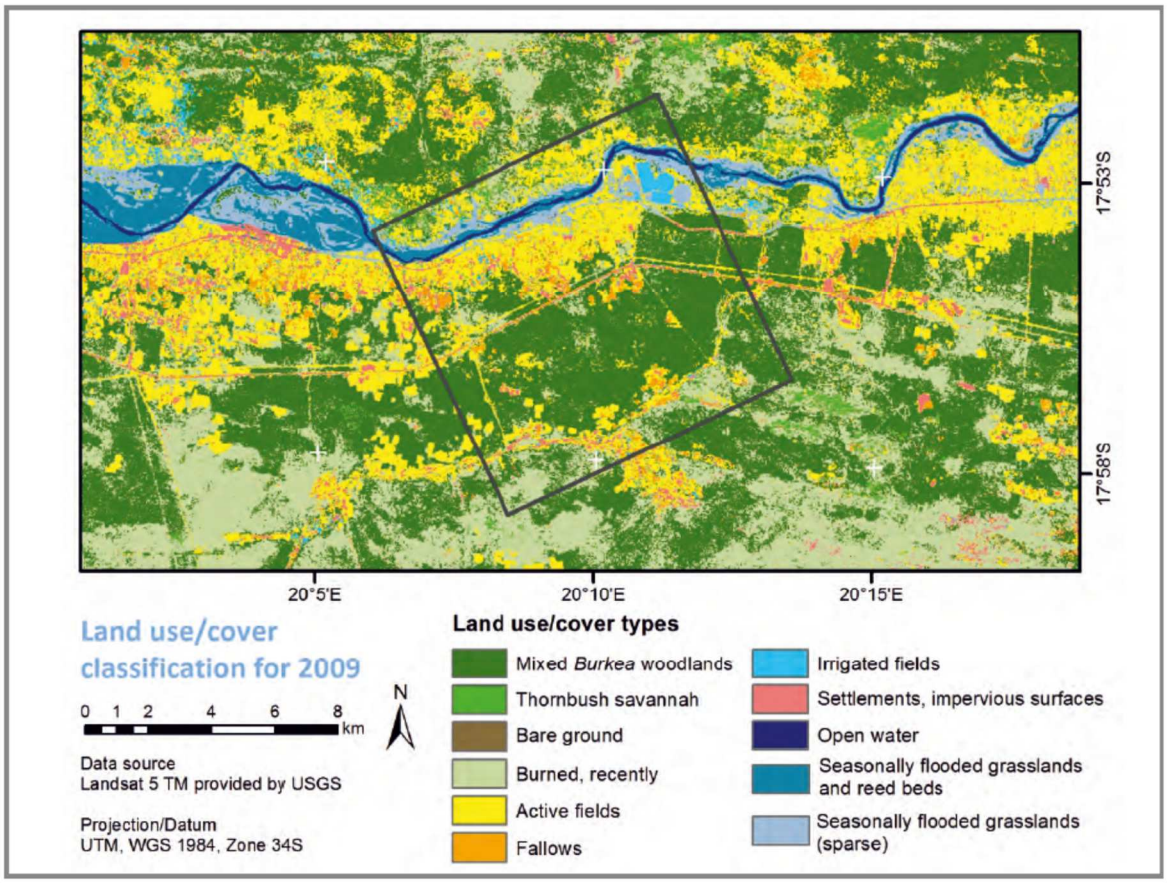

Fig.25: Land use and land cover for Mashare based on an analysis of Landsat 5 TM imagery for 2009 (*Röder* et al. 2013)

4.4. The study site Erichsfelde (Namibia)

The study area is located about 110 km north of Windhoek/Namibia on a commercial cattle farm named Erichsfelde in the thornbush savannah of central Namibia (21,65° S, 16,90° E). Like other farms in the surrounding, the studied farm is used for extensive livestock keeping.

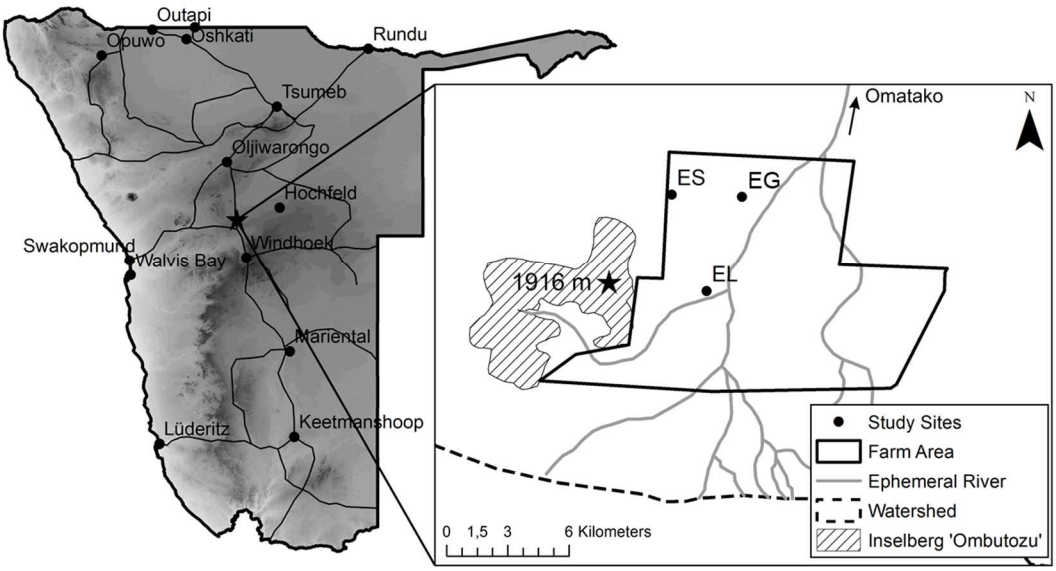

Fig.26: Study site overview Erichsfelde

4.4.1. Climate

The climate in that area is characterized by austral summer rainfalls (predominantly between November and April) with mean annual amounts about 400mm, which vary between 100 and 600 mm a^{-1}. Between 2001 and 2009 at the BIOTA weather station "Toggekry" (25 km northwest of the investigation area) on average 360 mm precipitation were measured whereas within the period of 2010 to 2015 the SASSCAL weather station at Erichsfelde measured 447 mm. The mean monthly values are given in Fig.27. Typical for this savannah landscapes are pulsed rain events often in combination with heavy thunderstorms. The monthly mean air temperature shifts between 13 °C (June) and 25 °C (December) with a mean value of 20 °C. The potential evaporation rate of 1,800 to 2,000 mm a^{-1} causes a strong climatic water deficit of 1500 to 1700 mm a^{-1} (*Mendelsohn* 2009) leading to a semi-arid climate.

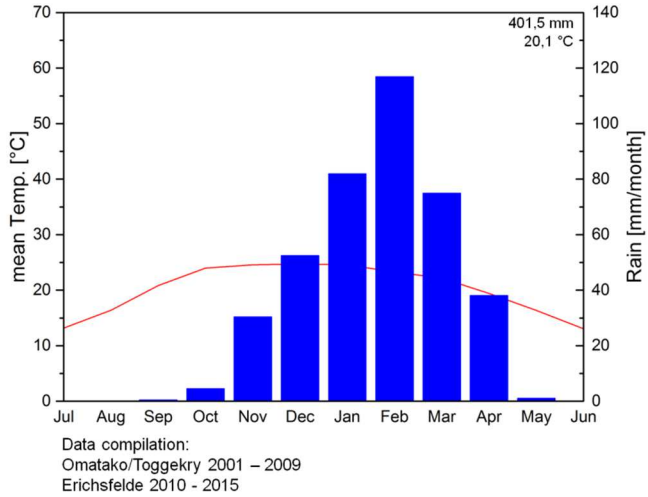

Fig.27: Regional Climate compiled of the weather station Omatako/Toggekry and Erichsfelde

4.4.2. Landscape

The topography of the farm is almost flat with an altitude about 1500 m a.s.l. The inselberg 'Ombutozu' with an altitude of 1916 m a.s.l. is located at the western farm border. The landscape surface is plain with weak relief energy. The ephemeral river systems (riviers) drain into the Omatako ephemeral river going in north-eastern direction to conjunct with the Okavango at Shitemo, about 40 km east of Mashare. In the rainy season, the run-off water is retained in dams and swales along this riviers. Feldspar rich doleritic-granitic bedrocks form the lithology of the study site. Adjacent to the inselberg Ombutozu several gullies accumulate clay-rich sediments in pans with distinct swelling and shrinking properties. In areas with mica schist and marble, due to its fine-grained weathering resulting in high capillarity, consolidated carbonate crusts can be found in depths up to 30 cm under the soil surface. The rivier lines consist of medium to coarse sand with high hydraulic permeability.

4.4.3. Soil inventory and spatial distribution

Mendelssohn et al. (2009) indicate a soilscape formed by Chromic Cambisols. However, detailed investigations reveal a wider spectrum of soil units (*Petersen* 2008) such as Calcisols on calcrete dominated plateaus, Vertisols in pans and depressions and Arenosols alongside the riviers (Fig.13). On a part of the farm area with a size of 1 km^2, Petersen (2008) found seven different soil units (WRB 2006, 1st qualifier level) with the haplic Luvisol and the epipetric Calcisol as the dominant soils. The overview of occurring soil types within the Erichsfelde study site shows the dominance of consolidated soil parent

material and the absence of Kalahari Sands. Where Arenosols were the dominating soil type in the more northern parts of the transect, the area of the central highlands of Namibia is characterized by typical semi-arid soil forming processes on consolidated rock parent material like clay migration and calcrete forming dynamics due to ascending groundwater.

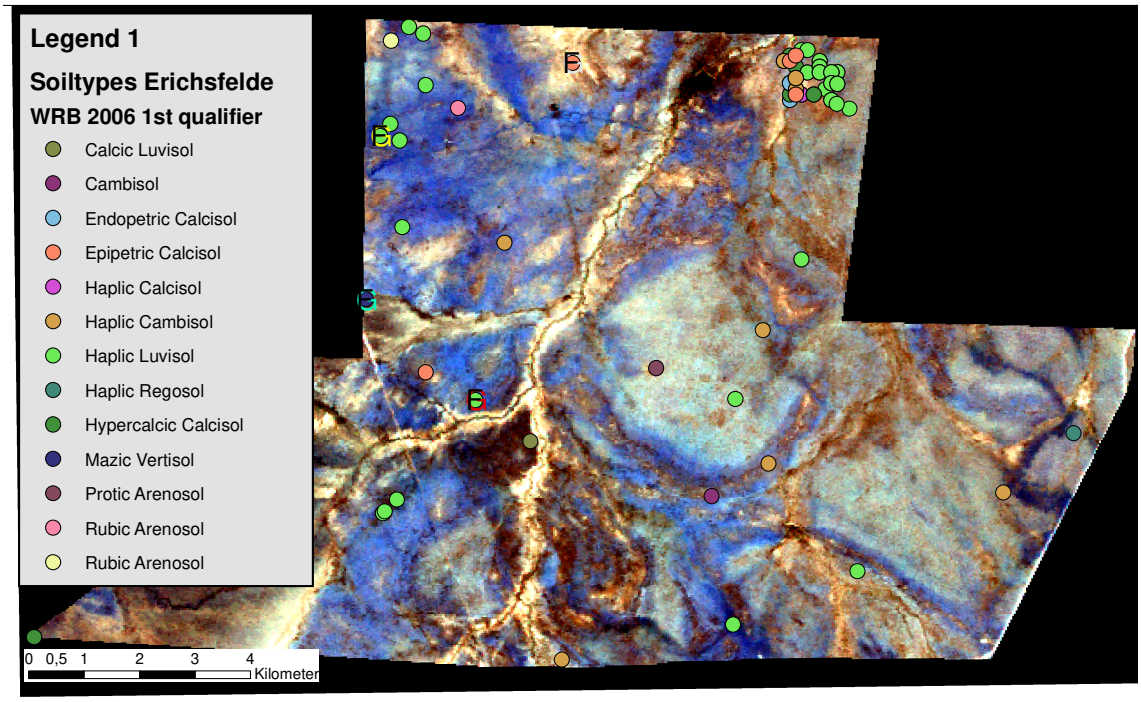

Fig.28: Distribution of soil types according to WRB 2006 (1st qualifier level) (*Petersen* 2008)

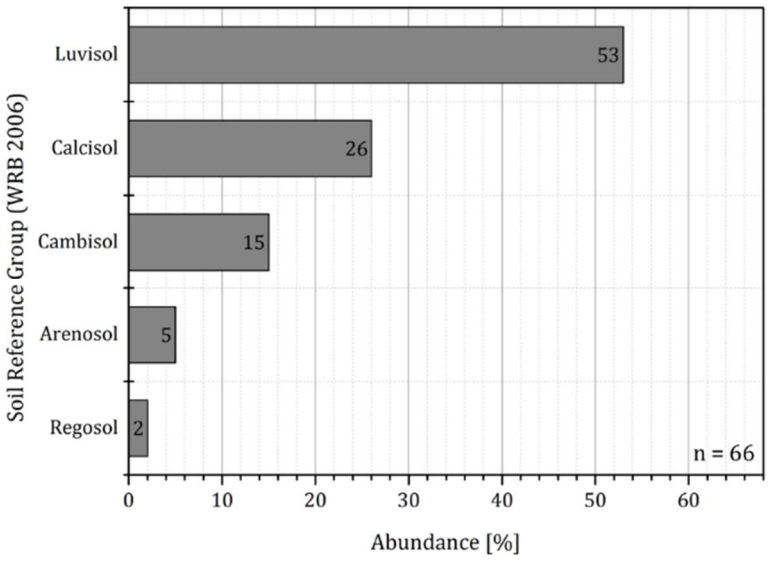

Fig. 29: Soil type abundance of the Erichsfelde study site

4.4.4. Vegetation and land use

The region of the study area belongs to the thornbush savannah and the vegetation is characterized by open grass patches with scattered trees (e.g. Acacias) (*Jürgens* et al. 2010). Furthermore, dense tree or shrub cohorts who consist mainly of bush encroachers like *Acacia mellifera* appear in the landscape. In between these vegetation patterns it mixes with any kind of composition of grasses, herbs, shrubs and trees occur in this region. In Tab. 22 and Tab. 23 the dominant plant species which are observed 2009 at the BIOTA observatory "Otjiamongombe" on the farm area of Erichsfelde (*Jürgens* et al. 2010) are listed. Trees species are predominantly characterized by Acacias like *Acacia mellifera*, which is the most important encroacher species, or *Acacia erioloba.* As perennial shrub *Lycium oxycarpum* and *Monechma genestifolium* are frequently observed where grasses like *Stipagrostis uniplumis* and *Eragrostis jeffreysii.*

The farm extends over approximately 13000 ha and is stocked with 900 pieces of cattle which are driven between fenced grazing areas to manage vegetation biomass production by controlling the grazing pressure. In some parts of the farm area, dense shrub thicket hinder the cattle getting access to this area which is a loss of grazing potential. In addition, the composition of fodder grasses changes towards more annual species with lower fodder value or inedible kinds. An improved vegetation management with debushing measures and a subsequent sowing of blue buffel grass (*Cenchrus ciliaris)* is seen to improve the fodder grass production and therefore to sustain or even raise the livestock carrying capacity of the farmland.

Fig. 30: Debushed area in Erichsfelde

Fig. 31: Blue buffel grass (*Cenchrus ciliaris*)

5. How does agricultural land use expansion change soil water balances in a dry sub-humid landscape in Angola?

5.1. Case study introduction

To predict the influence of expanded and intensified agricultural land use on soil hydrological dynamics and balances at first field monitoring data of two sites with contrasting vegetation however low land-use intensity are compared. Here, the key question is to analyze the role of woodlands in comparison to open grasslands under similar soil and climatic conditions. In a modeling approach for both sites contrasting possible future land use scenario are compared. Land use units comprise bare soil, rain-fed maize cropping, grasslands and woodlands. Aiming to produce results of general importance, the modeling was done with constructed 30-years weather data and the profile discretization was based on the assumption of a 3 m pedon with free drainage at the bottom. The key questions are:

- How is the feedback to the atmosphere divided in interception, evaporation and transpiration to evaluate the possibilities of biomass production?
- What is the amount and temporal distribution of deep drainage to discuss the role of land use on the hydrological system within the upper catchment of the Okavango?

5.2. Soil hydrological modeling plots

Although the extent of the study site Cusseque is 20 km in east-western direction, the actual soil survey concentrated on the eastern part of the site because of the topological reference to the Cusseque river catchment. The overall soil survey consists of 74 soil profiles and topsoil samples as a basis for the definition of locations for the soil water monitoring.

Two distinct locations were identified by fulfilling the specification needs. In the following, it will be focused on these two locations which are showing contrasting environmental and vegetation settings, different soil properties and therefore assumed contrasting soil water dynamics.

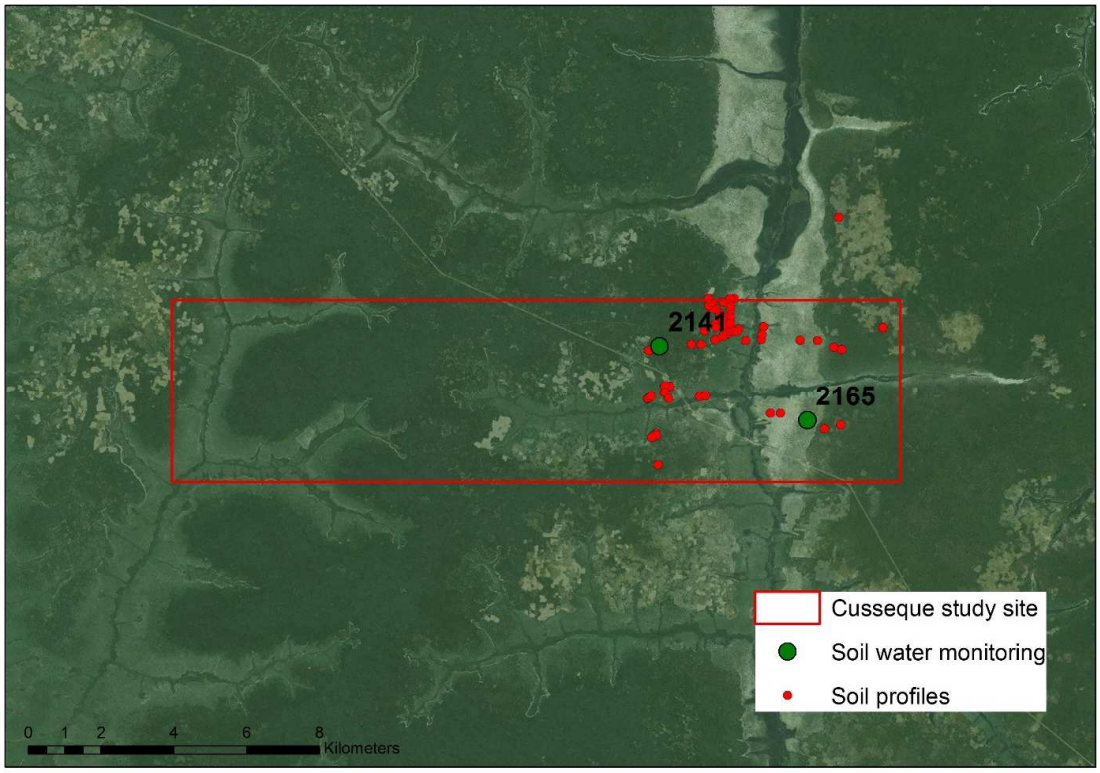

Fig. 32: Map showing the soil survey points and the locations of the soil water monitoring stations within the Cusseque study site

5.2.1. Plot and soil profile descriptions

Fig. 33: Environmental aspect and site impression of profile 2141

The profile described as Rubic Arenosol in Fig. 34 represents a typical soil of the summit woodland areas within the Cusseque study site. It is characterized by a homogenous brown reddish soil color and slightly loamy texture with depth, with up to 75 % Sand and no rock fragments. A low aggregation status leads to a light subangular structure. The presence of clay coated secondary macropores showing bioturbation and clay migration dynamics. The soil reaction ranges from very acidic (pH 4.1) in the upper 10 cm, due to the accumulation of organic acids, to more medium acidic reaction (pH 5.2) in deeper horizons. The depth related EC-values correspond to the soil reaction development but on a very low level, indicating low-level nutrient content (Fig. 35). Within 120 cm there are no redoximorphic features visible as a sign for good drainage properties. Nearly 50 % of the determined roots can be found in the upper 10 cm. The soil surface is covered with fresh litter and mosses and there are signs of anthropogenic activities like logging, as shown in Fig. 33.

Profile 2141	Lat: -13,68961°	Long 17,06607°	1585 m h.s.l.	Loc.: Cusseque / Angola

Topography:	Slope:	Exposition:	Curvature:	Landscape unit:	Land use unit:	Vegetation / Crop:
Upper slope	0°	/	plain	Summit area	Woodland (W)	Dense woodland, mosses

Remarks: Cusseque, wood harvest, fresh litter (shredded), no recent fire

Ah	**Grain Size:** light clayey sand St2 (KA5)/LS (WRB); light subangular structure; **Munsell Colour**: moist 7,5 YR 3/3, dry 7,5 YR 5/4; **Roots:** 38 roots dm^{-2};
10 cm Bw1	**Grain Size:** light clayey sand St2 (KA5)/LS (WRB); light subangular structure; **Munsell Colour**: moist 5 YR 4/4, dry 5 YR 5/6; **Roots:** 20 roots dm^{-2};
35 cm Bw2	**Grain Size:** light clayey sand St2 (KA5)/LS (WRB); light subangular structure; **Munsell Colour**: moist 5 YR 4/6, dry 5 YR 5/7; **Roots:** 12 roots dm^{-2};
50 cm Bw3	**Grain Size:** light clayey sand St2 (KA5)/LS (WRB); light subangular structure; **Munsell Colour**: moist 2,5 YR 4/6, dry 2,5 YR 5/8; **Roots:** 3 roots dm^{-2};
75 cm Bw4 120 cm	**Grain Size:** light clayey sand St2 (KA5)/LS (WRB); light subangular structure; **Munsell Colour**: moist 5 YR 4/6, dry 5 YR 5/7; **Roots:** 5 roots dm^{-2};

Fig. 34: Description of profile 2141

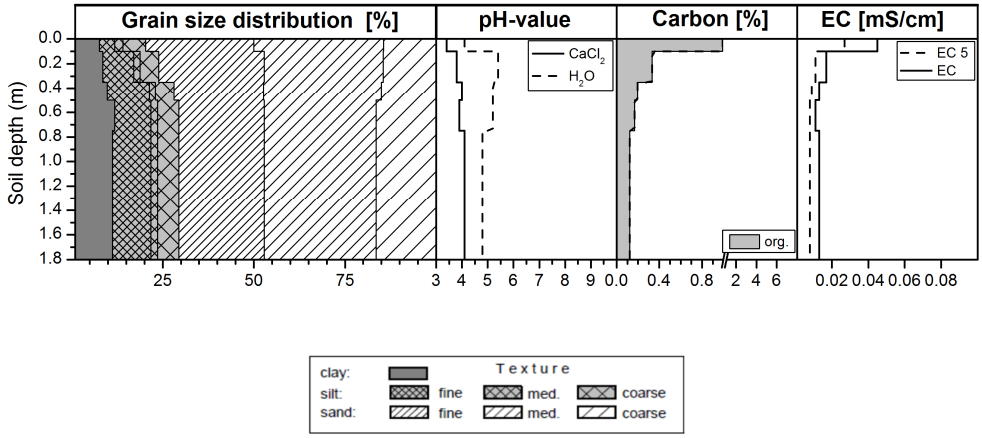

Fig. 35: Soil texture and chemical properties of profile 2141

Fig. 36: Environmental aspect and site impression of profile 2165

Profile 2165 is located on the eastern slope of the Cusseque valley, where an open grassland with geophytes and single trees is the characteristic aspect (Fig. 36). It is classified, similar to profile 2141, as Rubic Arenosol, due to its weak pedogenic development and its sandy texture (Fig. 37) with single grain structure. In contrast to profile 2141, the soil texture is dominated by medium and fine sand with very little silt and increasing clay content with depth to a maximum of 9 % in 170 cm (Fig. 38). The soil color changes from greyish brown in the upper parts to ochre-reddish colored horizons with red mottling in deeper areas. A light to medium acidic soil reaction decreases with depth from pH 4.8 in 10 cm to pH 5.7 in 170 cm. Intense rooting occurs in the topsoil area with nearly 75 % of the total profile root numbers. Redoximorphic features like red mottling can be found beginning in 60 cm with a depth increasing intensity. Other profiles along a downslope transect heading towards the river valley showing increasing reduction features with depth due to episodic to periodic water-saturated conditions. It can be assumed that this indicates a potential interflow dynamic towards the Cusseque River.

Profile 2165	Lat: -13,70787°	Long 17,10374°	1537 m h.s.l.	Loc.: Cusseque / Angola

Topography:	Slope:	Exposition:	Curvature:	Landscape unit:	Land use unit:	Vegetation / Crop:
Plateau	0°	/	plain	Slope east	Geophyte, woody	Woody geophytes, sporadic grass bunches

Remarks: Cusseque, burned

Ah	**Grain Size:** fine to medium sand mSfs (KA5)/S (WRB); single grain structure; **Munsell Colour**: moist 10 YR 4/1, dry 10 YR 5/2; **Roots:** 150 roots dm^{-2};
10 cm Bw1	**Grain Size:** fine to medium mSfs (KA5)/S (WRB); single grain structure; **Munsell Colour**: moist 10 YR 4/3, dry 10 YR 6/3; **Roots:** 18 roots dm^{-2};
30 cm Bw2	**Grain Size:** medium to fine sand fSms (KA5)/S (WRB); very light subangular structure; **Munsell Colour**: moist 10 YR 5/5, dry 10 YR 7/4; **Roots:** 11 roots dm^{-2};
60 cm Bw3	**Grain Size:** medium to fine sand fSms (KA5)/S (WRB); single grain structure; **Munsell Colour**: moist 10 YR 5/5, dry 10 YR 7/4; **Roots:** 8 roots dm^{-2}; light oxidic coloured mootling
85 cm Bw4 85+ cm	**Grain Size:** medium to fine sand fSms (KA5)/S (WRB); single grain structure; **Munsell Colour**: moist 10 YR 5/6, dry 10 YR 7/6; **Roots:** 7 roots dm^{-2}; oxidic red coloured mottling

Fig. 37: Description of profile 2165

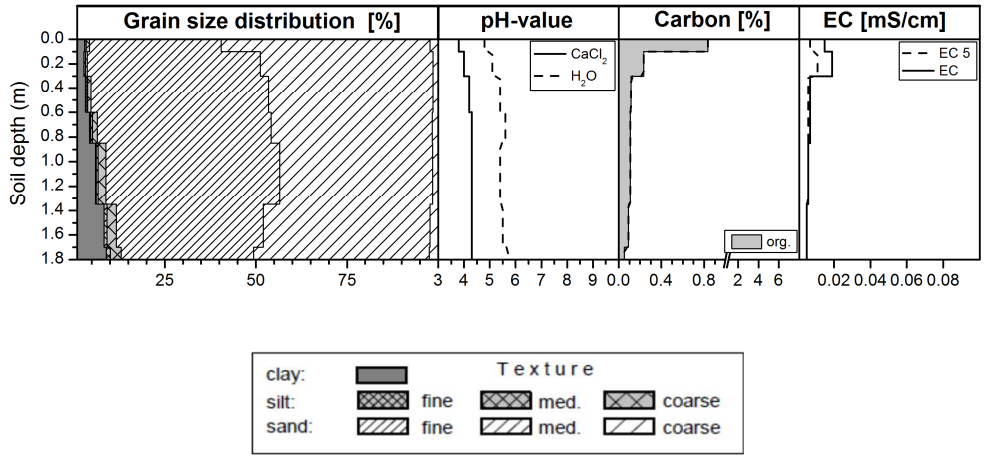

Fig. 38: Soil texture and chemical properties of profile 2165

5.2.2. Soil hydrological properties

The soil hydraulic properties of the profiles and the derived van Genuchten-Mualem parameter for a subsequent simulation, based on the results of the soil physical lab analysis, are presented in this section. As shown in the previous section the two sampled profile

differ with respect to the grain size distribution where the profile summit shows a sandy-loamy texture with an apparent amount of silt and clay which account together for one-third of the bulk texture at depths of 40 cm downwards. In contrast, the eastern slope profile is characterized by a sandy texture with a slight depth-increasing amount of clay. Fig. 39 shows the correspondent soil water retention curves for the sampled depth. The total pore volumes (θ_s) decrease with depth as a result of the increasing bulk density at both profiles having 0.53 $cm^3\ cm^{-3}$ in the topsoil of profile 2141 (summit site) and 0.45 $cm^3\ cm^{-3}$ in 30 cm depth in profile 2165 (eastern slope profile). Comparative statements between the topsoil properties cannot be made since no samples were taken in the upper horizons of the eastern slope profile. At a comparative depth of 25 – 60 cm θ_s is nearly identical at both sites but with slightly higher water contents at the permanent wilting point (PWP), as shown in Tab. 6. Higher water contents at field capacity (FC) in profile 2165 and lower contents at PWP result in slightly higher water contents of the usable field capacity in comparison to the summit profile 2141.

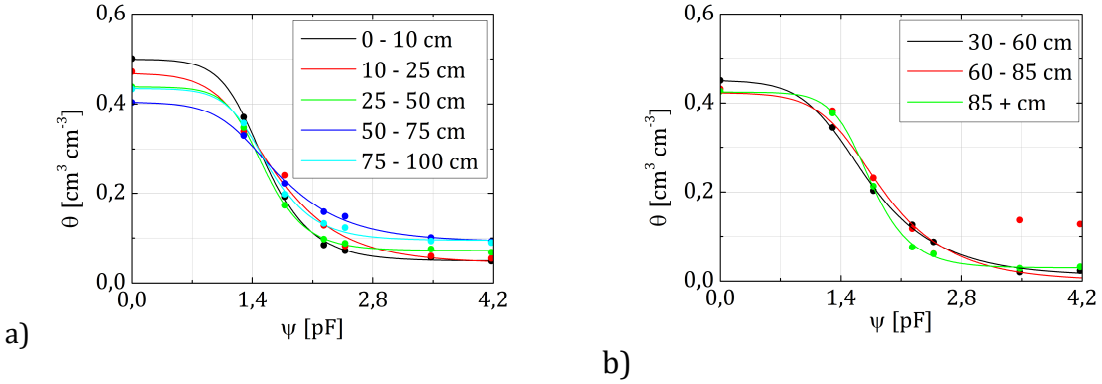

Fig. 39: Water retention curves for profiles (a) 2141 and (b) 2165

The steepness of the retention curves of both profiles reflects their sand dominated textures whereby the presence of silt and clay in 2141 is recognizable due to higher PWP values. Altogether, both profiles show only slight differences with respect to the soil water retention. A combined fitting of the soil water retention values and the soil hydraulic conductivity measurements to the van Genuchten-Mualem functions result in the corresponding parameters in Tab. 7. Since no saturated conductivity measurements were done the respective parameter was adopted by standard values according to *Renger* et al. (2014).

Tab. 6: Soil hydrological characteristics of the studied horizons at the Cusseque site.

Horizon	Upper [cm]	Lower [cm]	θ_s [$cm^3\ cm^{-3}$]	PWP [$cm^3\ cm^{-3}$]	FC [$cm^3\ cm^{-3}$]	uFC [$cm^3\ cm^{-3}$]
2141_1	0	10	0.53	0.05	0.21	0.16
2141_2	10	25	0.47	0.06	0.19	0.13
2141_3	25	50	0.47	0.04	0.14	0.10
2141_4	50	75	0.45	0.06	0.18	0.12
2141_5	75	100	0.46	0.06	0.18	0.12
2165_2	30	60	0.45	0.02	0.20	0.18
2165_3	60	85	0.43	0.12*	0.23	0.11*
2165_4	85	+	0.43	0.03	0.21	0.18

* measurement failure

Because of the similarities between the soil´s hydraulic parameter of the horizons only on set for each profile was identified to be parameterized as simulation input. The resulting sets and the corresponding functions are presented in Tab. 7 and Fig. 40.

Tab. 7: Derived van Genuchten-Mualem parameter for the eastern slope and the summit areas in Cusseque

Plot	θ_r [$cm^3\ cm^{-3}$]	θ_s [$cm^3\ cm^{-3}$]	α	n	K_s [$cm\ d^{-1}$]	l
Cse	0.0300	0.4240	0.0171	1.5730	712.00	5.6670
Csu	0.0950	0.4347	0.0413	2.1648	350.00	3.8800

Due to the combined fitting of the van Genuchten-Mualem parameter to the retention and conductivity measurements, the final set of hydraulic functions is slightly different compared to the underlying measurements by preserving the tendency of original characteristics. The eastern slope soil water retention now is characterized by a θ_s of 0.4240 $cm^3\ cm^{-3}$ with a PWP of 0.04 $cm^3\ cm^{-3}$. The fitted function results in a 0.33 $cm^3\ cm^{-3}$ at FC which leads to an uFC of 0.29 $cm^3\ cm^{-3}$. Looking at the unsaturated hydraulic conductivity as a function of soil water pressure head ($k(\psi)$) it shows 712.00 cm d^{-1} under saturated conditions, according to standard values, with a significant decrease to 7.73 cm d^{-1} at the lower boundary of the field capacity at pF 1.8 and $2.12 \cdot 10^{-3}$ cm d^{-1} at pF 2.5. In comparison, the summit profile functions show a different characteristic with a similar θ_s of 0.4347 $cm^3\ cm^{-3}$ but a lower FC with 0.21 $cm^3\ cm^{-3}$ and a higher PWP of about 0.095 $cm^3\ cm^{-3}$. The uFC is therefore only 0.115 $cm^3\ cm^{-3}$. The $k(\psi)$ function begins with 350 cm d^{-1} , at water saturation, to decrease to a lower conductivity, compared to Cse of $2.05 \cdot 10^{-2}$

cm d^{-1} at pF 1.8 and $2.12 \cdot 10^{-8}$ cm d^{-1} at pF 2.5. Summarized, the evaluation of both parameter sets show that the eastern slope soil reallocates with significantly higher rates pore water under field capacity conditions than the summit area soil. This results in higher downward directed fluxes at times when percolating processes occur, whereas the summit area soil shows a more pronounced ability to hold water against gravity due to lower unsaturated conductivities at field capacity. This results, under certain gradient conditions, in more upward orientated fluxes due to capillary rise.

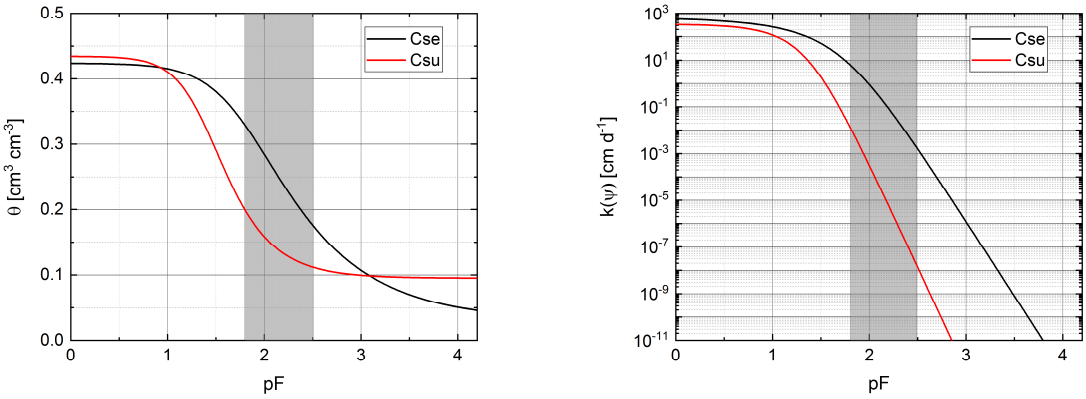

a) b)

Fig. 40: Diagram of the resulting soil hydrological retention (a) and conductivity functions (b) according to the fitted van Genuchten-Mualem parameters for the eastern slope (Cse) and the summit (Csu) profiles in Cusseque.

5.2.3. Soil hydrological measurements

The time series of the soil water measurements include the rainy season 2011/2012 and 2012/2013 at both profiles in Cusseque. While the measurements in profile 2141 consist of volumetric water contents and soil hydraulic heads a description of the appearing soil water dynamics in profile 2165 refer only the soil matrix potentials since the TDR measurement set up was destroyed. The probes were installed in depth of 10 cm. 20 cm, 40 cm, 80 cm and 160 cm and the logging interval was eight hours. To obtain precipitation input data a tipping bucket rain gauge was installed at both sites but only the device at profile 2165 delivered plausible results. The following descriptions and evaluations help to understand the soil hydrological dynamics on these to plots and serve to evaluate the subsequent modeling approach. A detailed model validation by comparing measured and simulated soil water contents and hydraulic heads cannot be done because of missing weather station data as model forcing for the measurement period. Nevertheless, the apparent spatiotemporal variations of measured soil water contents can be consulted to

conduct a qualitative model evaluation. The measurement period is divided into two rainy seasons whereby the second season in 2012/2013 is not fully covered. The first season starts in October 2011 and ends at the end of June in 2012. The second season follows until the end of the measurements in March 2013. Within the first season, a total precipitation of 610 mm was measured whereas the second season shows a total rainfall of 760 mm which is 61 % respectively 77 % of the long years mean of seasonal precipitation sums with 987 mm for this region. The precipitation dynamic shows a bimodal distribution with an intermediate absence or reduction of rainfall in February 2012 and January 2013. The rainfall characteristics show a mean intensity of 3.2 mm d^{-1} and rain event with a maximum of 23.9 mm in the first rainy season whereas the second season shows a mean of 5.8 mm d^{-1} and rain event and a seasonal maximum of 45.4 mm d^{-1}.

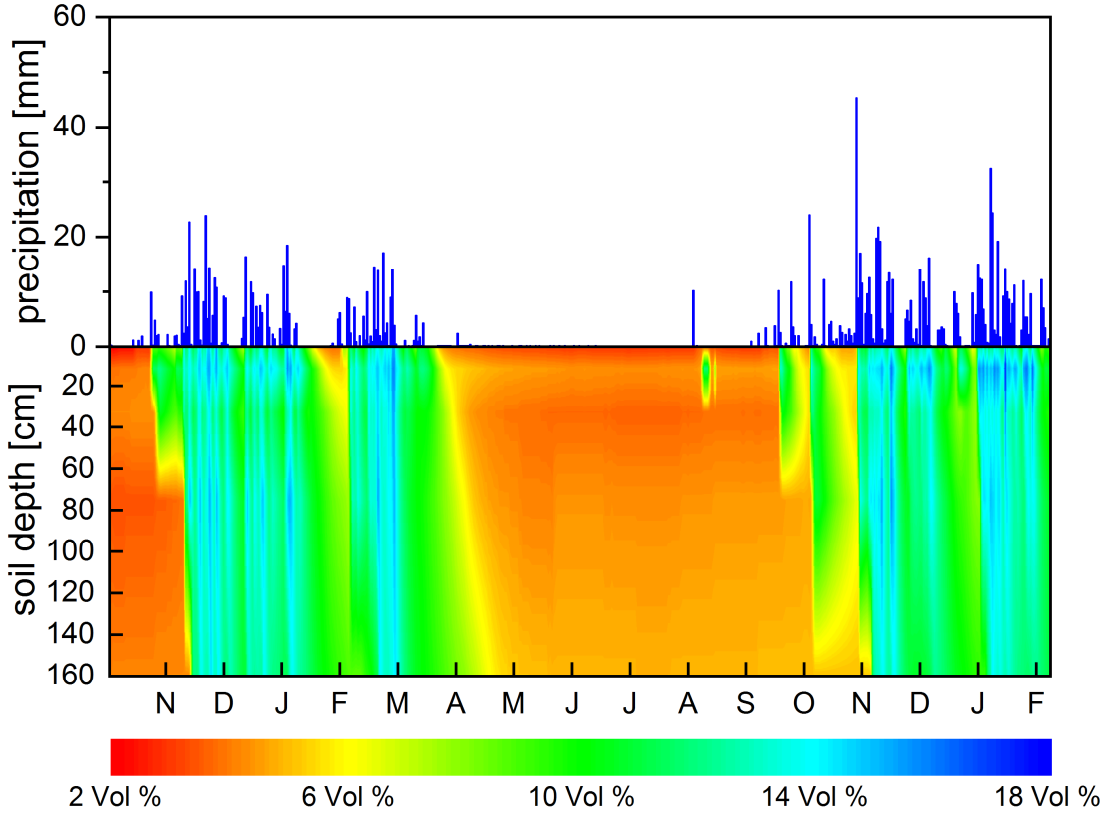

Fig. 41: Time series of measured water content and precipitation for profile 2141 from October 2011 to February 2013

Fig. 41 shows the soil hydrological response of the summit area profile to the incoming precipitation and the intermediate drying characteristics in the dry season expressed in volumetric water contents. The soil water dynamic shows an immediate increase in water

contents to precipitation inputs > 10 mm d^{-1} to a depth of 30 cm in times with low preceding soil moisture in the topsoil. Successive inputs even with lower intensities are able to form proceeding wetting fronts which increase water contents down to the bottom of the measurement profile within two days which indicates high unsaturated conductivities or a bypass flow through macropores. To compare incoming rainfall amounts with the bulk soil water increase amount as a first balance approach is shown in Fig. 42. It correlates the cumulated rainfall amounts over both seasons to the cumulated bulk soil profile water increases on a daily basis. The linear regression shows a significant correlation between these parameter, whereas the slope reveals that a share of 84 % of the precipitation input infiltrates into the soil over the considered period, respectively 16 % of the input is not captured by the TDR probes within the first 10 cm or is directly turned back to the atmosphere by litter or canopy interception evaporation.

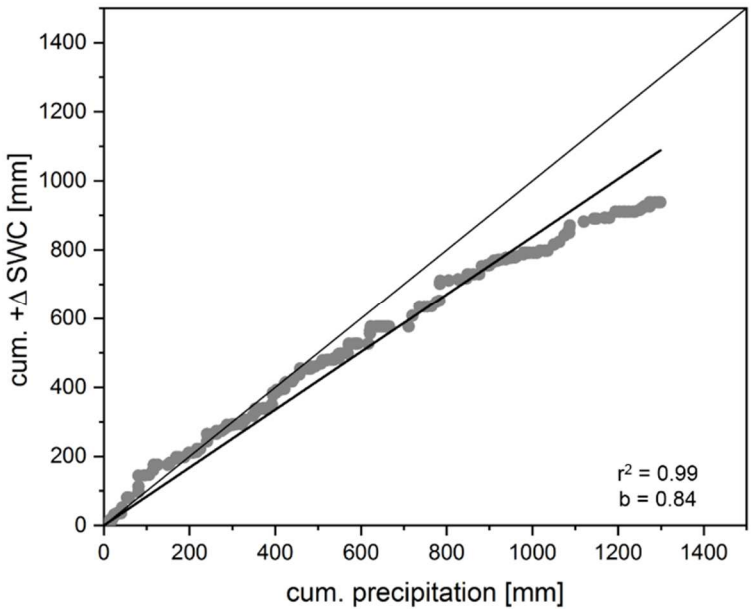

Fig. 42: Scatterplot and linear regression between cumulated rainfall amounts and cumulated profile water increase events

Looking at the course of the soil water dynamics throughout the dry season, the soil water buffer, formed within the rainy season, is depleted by evapotranspiration fluxes within one month to the maximum depth of the measurement profile with a constant on moving drying front.

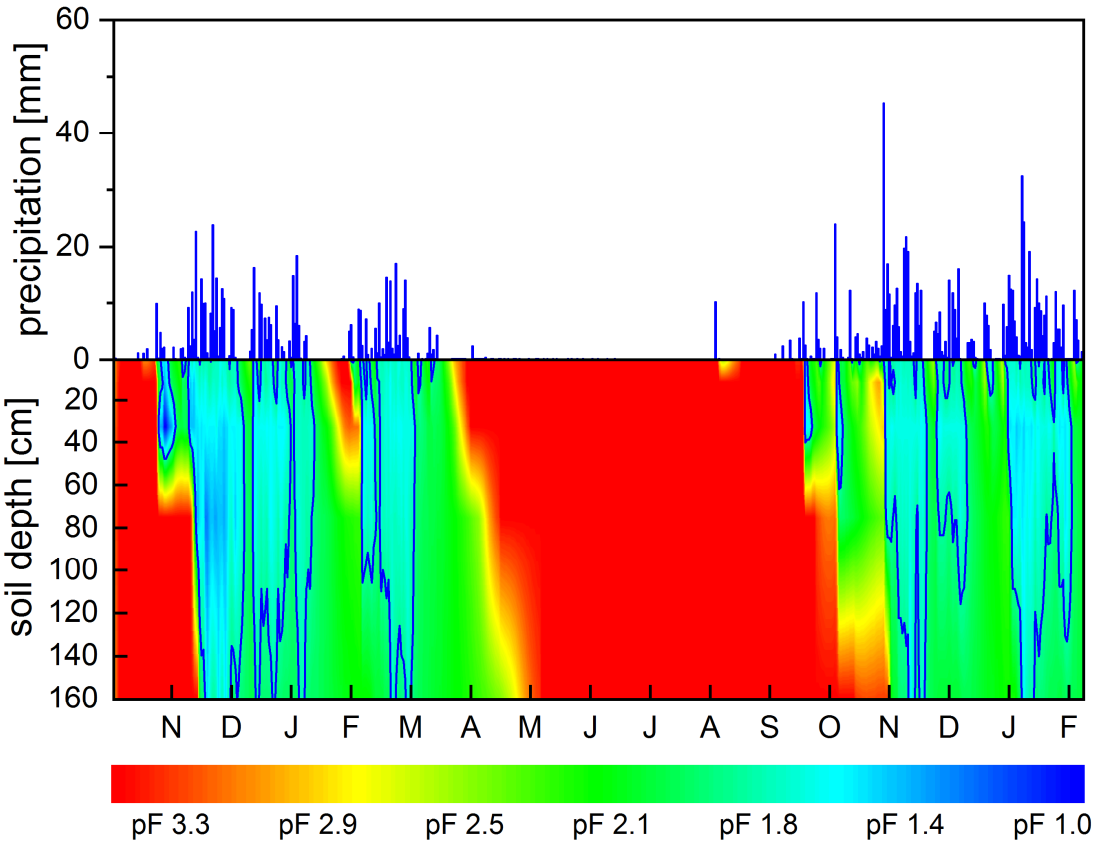

Fig. 43: Time series of measured soil water pressure head and precipitation for profile 2141 from October 2011 to February 2013

To describe potential deep drainage processes the measurements of the soil hydraulic heads in the defined depth are shown in Fig. 43 as the logarithm of the matrix potentials. The blue lines include soil areas in times where the soil hydraulic head is below pF 1.8 and gravitational soil water translocation occurs. As already described with respect to soil water contents, the immediate reaction of the matrix potentials to infiltrating water lowers matric potentials to areas where percolation processes begin even in depth of 160 cm. As a result, on 51 % of the measured days, the soil water potentials are equal to or lower than pF 2.5 at the bottom of the monitoring profile. On 6 % of the days the potentials are equal to or lower pF 1.8 so it can be concluded that this specific soil-vegetation-atmosphere system yields a certain amount of deep percolation water which contributes to a potential groundwater recharge.

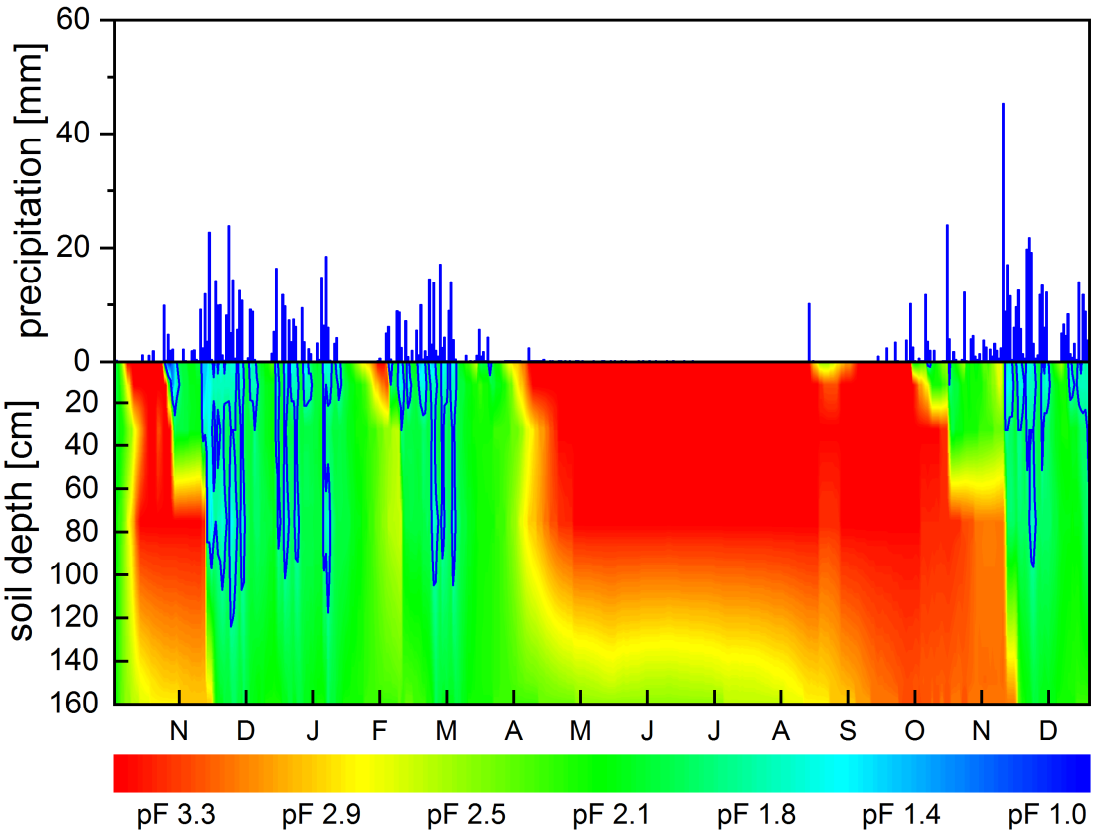

Fig. 44: Time series of measured soil water pressure heads and precipitation for profile 2165 from October 2011 to December 2013

The grassland plot on the eastern slope of the Cusseque study sites shows a less dynamic response of the soil water pressure heads (Fig. 44) on precipitation input compared to the summit profile. With the onset of the rainy season 2011/2012, the incoming rain rewets the profile down to a depth of about 60 cm with resulting soil water potentials of about pF 2.5 with even lower of < pF 1.8 in the first 20 cm. This wetting front is stable until the following rains increase the water contents down to 160 cm depth. In comparison to profile 2141 the wetting front with potentials < pF 1.8 stays in medium profile depth without reaching the bottom of the measurement profile. After a short intermediate drying cycle, then again increasing rainfalls start to rewet the profile but again without leading to low pF ranges in the maximum soil depth. After the rainy season, a drying front moves from top to bottom and is stabilized at a depth of 120 cm over a period of nearly four months. Within that period the soil water potentials are at pF 2.5 at the bottom of the profile whereas the overlying horizons are at pF 3.4 and above. In September the subsoil potentials increase to pF 3.4 or higher which may be an effect of the new beginning phenological cycle of the grassland vegetation. As the profile description in section 5.2.1 showed, roots

are still present in depth down to 85 cm and beyond so that a transpiration withdrawal of deep buffered soil water seems plausible. Taking the phenological development dynamics of the wood- and grassland into account, the difference in soil water depletion over the dry season between these vegetation types can be explained by the differing amplitude of the enhanced vegetation index (EVI) shown in Fig. 45.

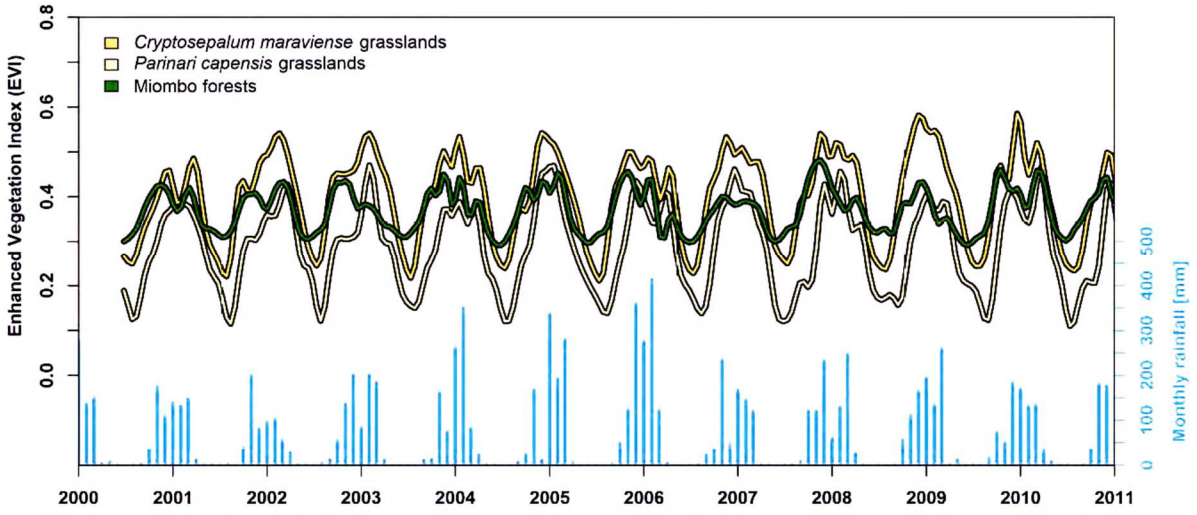

Fig. 45: MODIS EVI profiles for *Parinari capensis* grasslands, Miombo forests and *Cryptosepalum maraviense* grasslands (*Schneibel* et al. 2013).

While the *Parinari capensis* grassland shows a strong seasonal dynamic, the woodlands have lower amplitudes with only a minor interannual variability (*Schneibel* et al. 2013). In combination with the deep rooting characteristics, the woodlands may utilize the plant available soil water in total whereas the grassland vegetation with its shallow to medium root distribution and the pronounced phenology is not able to utilize buffered soil water in deeper areas at the end of the phenological cycle due to reduced transpiration rates. With the beginning of the following phenological cycle in September to October, these soil water resources can then be utilized.

To summarize and conclude, the findings of the soil water measurement analysis show that 84 % of the precipitation input is turned over in the woodland dominated soil-vegetation-atmosphere system within a period of six months with 6 % of the observed time showing potential groundwater recharge dynamics. The respective soil water turnover time in the grassland system is prolonged by 5 months due to reduced root water extraction as a consequence of the highly dynamical phenology and less deep rooting characteristics. At no time within the measurement period, soil water potentials are at a range for

potential groundwater recharge in a depth of 160 cm. Statements about the infiltrating fraction of precipitation cannot be made since soil volumetric water content measurements are missing.

5.2.4. Weather forcing data

Fig. 46 shows the weather input data for the 30-years simulation as long year monthly sums for radiation and precipitation as well as monthly means for temperature and humidity. With 944 ± 164 mm annual precipitation and a mean annual potential evaporation of 1840.9 ± 49.2 mm the dataset shows a dry sub-humid characteristic with an aridity index of 0.51 and a climatic water deficit of -896.1 mm. The rainfall variability, described by the relation between standard deviation and the 30 years mean, is 17 %.

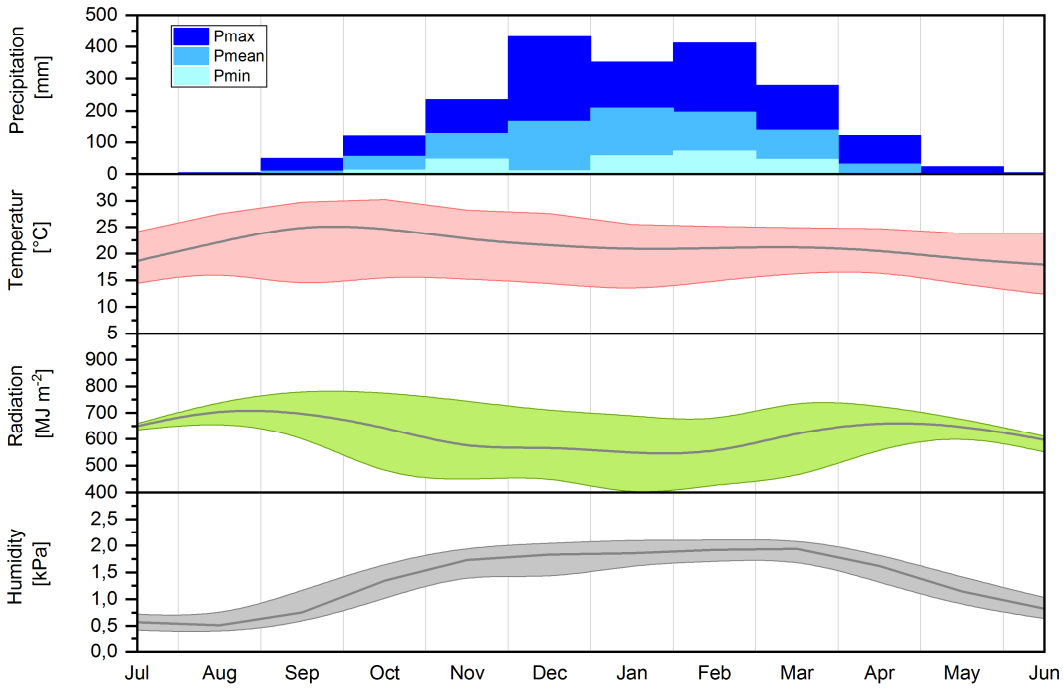

Fig. 46: Diagram showing the 30year ERA-INTERM Dataset for the study site Cusseque as monthly means for temperature and humidity as well as monthly sums for radiation and precipitation (with minimum and maximum).

5.3. Model results

5.3.1. Scenario description

In this section, a short overview of the assumptions made for the different model parameterizations is given. For a closer and more detailed insight into parameter settings, it is referred to the Appendix, where all in- and output files together with all necessary SWAP control files can be found. To predict the influence of land use change on soil hydrological dynamics and balances, six different model settings, three per plot, were parameterized according to its actual state and the potential conversion from pristine conditions to dryland agricultural use. On the basis of 30-years mean daily water contents for equidistant layers with 20 cm vertical resolution the soil water dynamics are evaluated. Balances and fluxes are evaluated through seasonal and monthly means of the respective balance components.

The profile discretization based on the assumption of a 300 cm pedon with free drainage at the bottom and no integrated hysteresis or macropore flow while rooting is possible throughout the whole profile without any restrictions or barriers. The initial soil moisture conditions were set to -300 hPa at the first 100 cm and to -3000 hPa onto the lower boundary of the pedon in 300 cm depth. Runoff as well as run on dynamics are not considered because of missing parameter inputs.

Tab. 8: Scenario overview Cusseque

Plot	Land use/vegetation	Simulation period	Abbreviation
Cusseque slope east (Cse)	Bare soil (B)	1980 - 2010	CseB
	Grass (Gr)		CseGr
	Dryland maize (Ma)		CseMa
Cusseque Summit (Csu)	Bare soil (B)		CsuB
	Woodland dense (Wd)		CsuWd
	Dryland maize (Ma)		CsuMa

5.3.2. Scenario-based soil water dynamics at Cusseque slope east (Cse)

Fig. 47 compares simulated water contents of three different land cover classes as 30 years daily means for one hydrological year from July to June. As a reference to evaluate the impact of certain vegetation types on soil water dynamics and balances the bare soil variant shows the specific soil hydrological response to atmospheric drivers with respect to evaporation and precipitation input. At the onset of the rainy season in October the

topsoil in 20 cm depth reaches mean minimum water content of 18 Vol% (pF 2.5; ku = $2.12 \cdot 10^{-3}$ cm d^{-1}) with depth increasing contents up to 22 Vol% (pF 2.2; ku = $7{,}98 \cdot 10^{-2}$ cm d^{-1}) in subsoil regions at 300 cm. Due to its hydrological properties with very high near saturation conductivities with about 700 cm d^{-1} and a rapid decrease to about 7 cm d^{-1} at field capacity, capillary rise is limited and water is kept over the dry season in subsoil regions from 180 cm depth on downwards. In return, wetting events will instantly increase the conductivity due to the high initial water contents, which results in fast percolation rates into deeper subsoil layer. In the middle of the rainy season, the whole profile

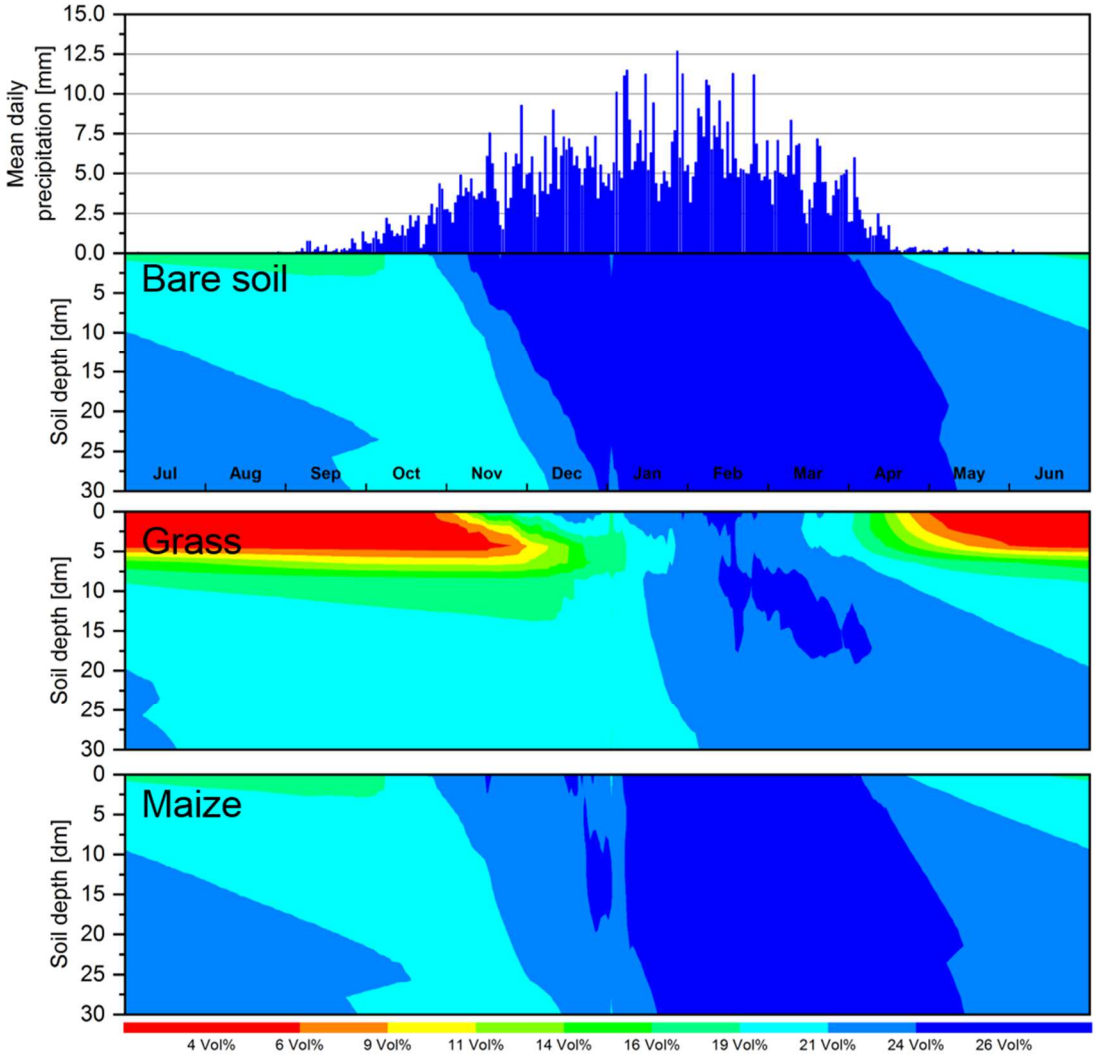

Fig. 47: Mean daily water content for a period from July to June based on a 30-year model run and three different land cover scenarios on the eastern slope of the Cusseque study site

is at its maximum water content of about 28 Vol%. With the last rains in April, the drying front again starts to enter deeper layers to re-establish the mean water content gradient of about 4 Vol%. Fig. 48a illustrates this low dynamic range of water contents throughout

the rainy season, with a slightly more pronounced range in the upper 20 cm and decreasing variabilities with depth.

Compared to the bare soil scenario the grassland assumption leads to an increase in soil water dynamics to a depth of 80 cm which is the lower boundary of the assumed rooting zone (Fig. 47). The additional transpiration lowers to water contents to 4 – 8 Vol% close to the permanent wilting point (PWP) at the onset of the rainy season. The resulting upward orientated gradient forces water from beneath the rooting zone to rise up, the influence of root water extraction is noticeable in Layers beneath as to be seen in Fig. 48b. The within the dry season established and kept upward orientated soil water gradient prevents the promotion of the wetting front in subsoil areas until the middle of the rainy season when cumulative rainfall amounts exceed the cumulated evapotranspiration and interceptive losses. At that time percolation is possible, due to downward orientated gradients at reasonable hydraulic conductivities, down to the lowest soil layer with mean water contents of 22 – 24 Vol %. At the end of the rainy season, the vegetation utilizes the available water to sustain transpiration until the PWP is reached onto a depth of 80 cm and transpiration losses go to nearly zero. Now, the state as it is before the onset of the rainy season is re-established.

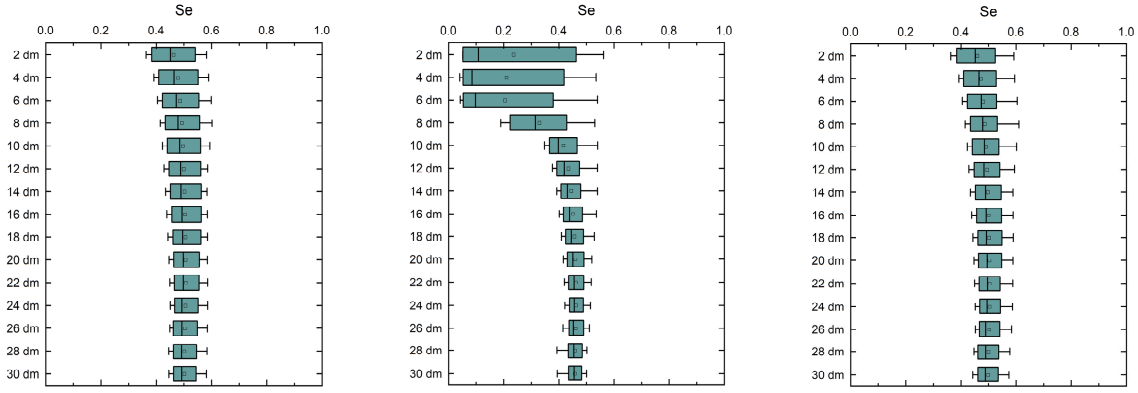

Fig. 48: Boxplots showing the long year simulated effective saturation (Se) at 20 cm soil layer resolution down to 300 cm for the Cusseque slope east site. a) Bare soil, b) Grass, c) Dryland Maize. Whisker showing mean minimum and maximum water contents.

The third scenario describes the soil hydrological conditions under dryland cropping of maize with a low plant density of about 1-3 maize plants per square meter. The resulting low LAI of 1.2 in maximum combined with a short cropping season of 125 days starting

with the onset of the rainy season account for the similarity in soil water dynamics between the bare soil scenario and the maize cropping conditions. Within the cropping season, small differences are visible which reflects the additional transpiration losses and the slightly decreased evaporation so that the maximum water contents as simulated under bare soil conditions reach their maximum one month delayed.

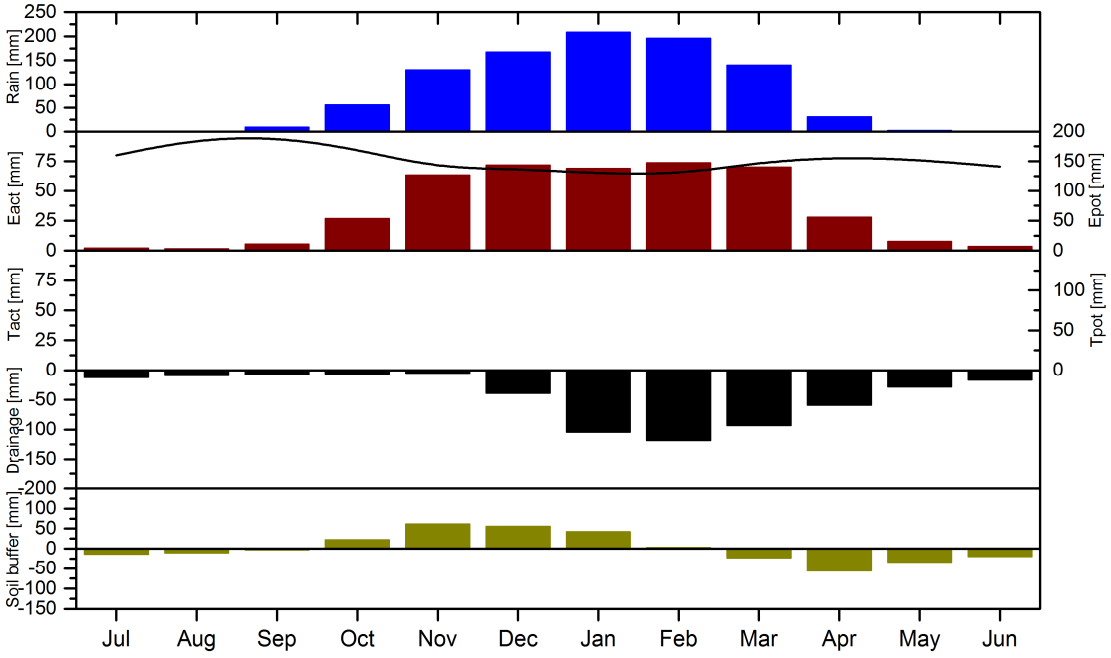

Fig. 49: Monthly mean soil water balance components for the bare soil scenario at the eastern slope of the Cusseque study site. The lines represent the monthly course of Epot and Tpot

Fig. 49 shows the monthly means of the soil water balance components under bare soil conditions. Since these conditions have no vegetation, potential and actual transpiration, as well as interception, does not occur, the only loss of water, by neglecting interflow and runoff, is due to deep percolation and evaporation withdrawal. The course of the actual evaporation follows the precipitation trend and reaches its maximum of 71 mm with about have of the potential values in November to December when the soil pedon reaches its maximum positive change to sustain upward water delivery. Due to the high water contents in the middle of the rainy season percolation and low vertical gradients within the profile, deep drainage leads to a significant amount of outflow at the bottom of the profile with a maximum in February. The establishment of upward orientated gradients with decreasing rains but constantly high Epot rates diminish the soil buffer to fulfill atmospheric water vapor demand and deep percolation processes. The water balances of

the 30 years simulation shown in Tab. 9 indicate that evaporation and deep drainage processes are almost evenly distributed. The relation between the only two sinks in this scenario (bottom flux and evaporation) as a proxy for the ability of the soil to hold water against gravity or to deliver sufficient amounts to the surface for evaporation is in this case 1.8. This means for every evaporated millimeter of soil water 1.2 mm are drained at the bottom.

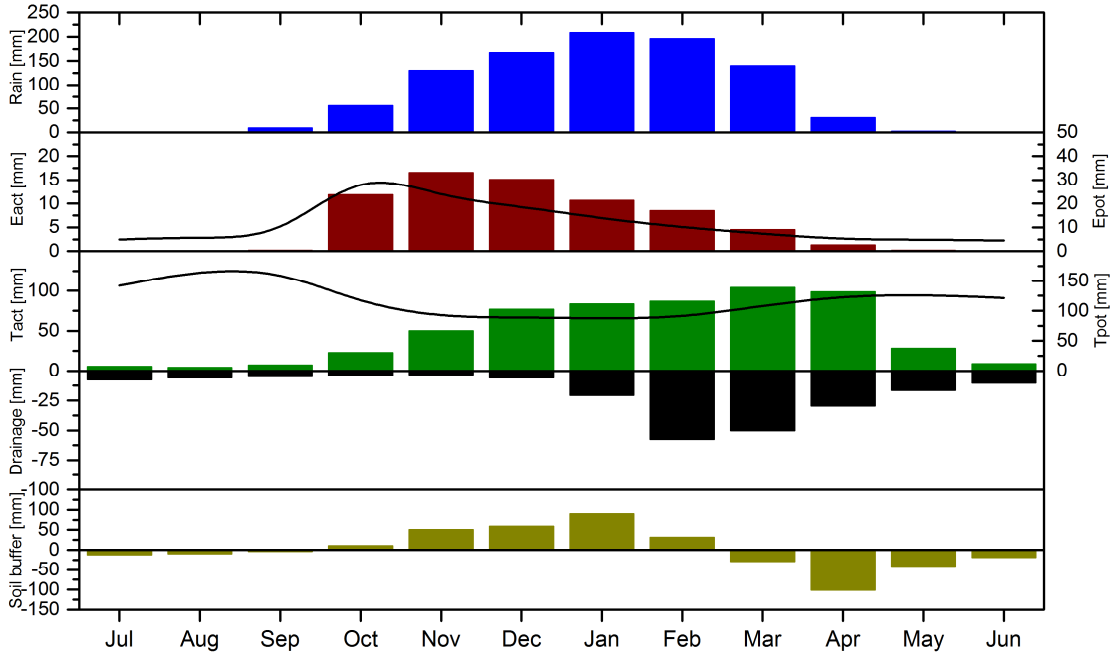

Fig. 50: Monthly mean soil water balance components for the grassland scenario at the eastern slope of the Cusseque study site. The lines represent the monthly course of Epot and Tpot

As a consequence of the additional vegetation dynamic included in the grassland simulation a significant shift of the water balances is obvious (Fig. 50). The actual evaporation rates reach their maximum in November with 17 mm with a slight decrease in the following month. The monthly course of the transpiration is therefore anti-cyclic with an increase starting in October to its maximum in March with 104 mm. This development reflects the phenology of the grass, where the developing soil coverage increases transpiration rates and diminishes evaporation dynamics. In relation to bare soil conditions, the lower potential evaporation rates and the withdrawal of soil water by transpiration, concentrated to the first 80 cm, leads to a higher increase of water in the soil buffer in January below 80 cm. Due to capillary rise, this water is available for transpiration at the end of the rainy season in April where transpiration is still high with 98 mm but evaporation is low at 1 mm. When water contents drop to near PWP in the rooting zone and no water is

delivered from deeper layers, the actual transpiration drops to its minimum. The long year means (Tab. 9) show clearly that the transpiration and interceptive losses reduce evaporative losses by 87 % and deep drainage amounts by 60 % in relation to bare soil conditions.

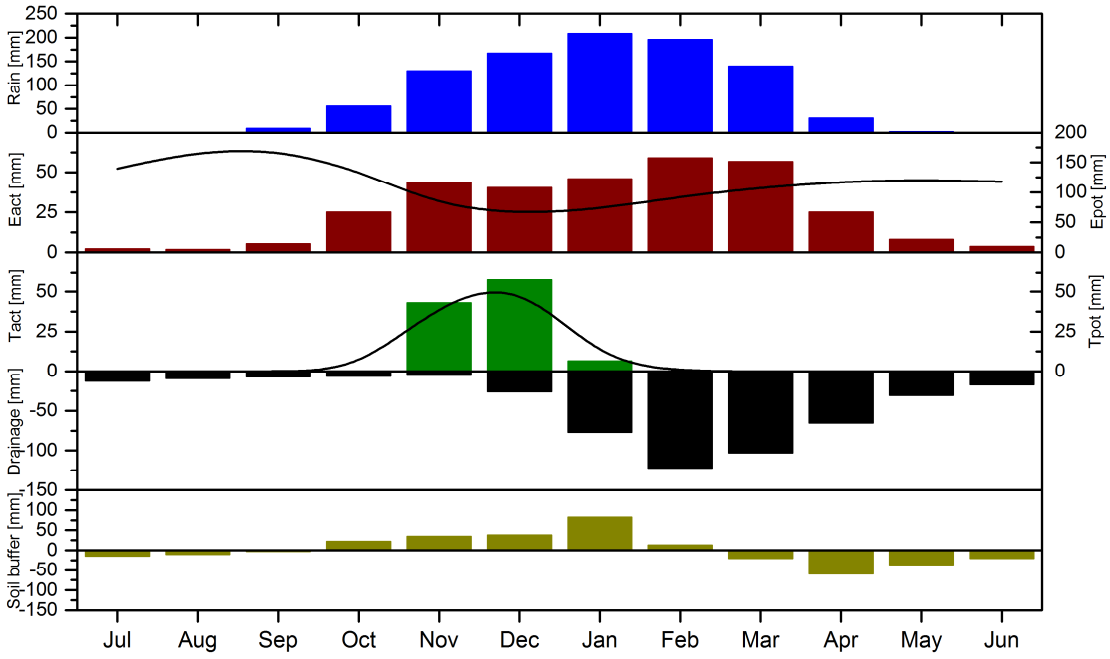

Fig. 51: Monthly mean soil water balance components for the maize cropping scenario at the eastern slope of the Cusseque study site. The lines represent the monthly course of Epot and Tpot

The similarities of bare soil conditions and the cropping scenario shown in section 5.3.2 can be found again looking at the comparison of the soil water balances of maize (Fig. 51) and the bare soil conditions. Before the emergence of the plants, Eact rates of the maize scenario correspond to those with bare soil. With the start of the cropping season, the soil cover increases together with transpiration rates having its maximum in December with 57 mm whereas evaporation is only 63 mm and therefore only half of the amount compared to bare soil. After the harvest in January evaporation rates start to increase again but without reaching rates as high as those compared to the bare soil scenario which indicates a decreased water delivery due to decreased conductivities as a consequence of top soil water losses by transpiration. The short period of cropping has, therefore, the greatest influence on evaporative losses which are reduced compared to the bare soil by 112 mm or 25 % whereas the influence on the shift of bottom flux from 509,3 mm to 486,6 mm or 4 % relatively small.

Tab. 9: Long year means of water balance components for the Cse scenarios

Scenario	Precipitation [mm a^{-1}]	Interception [mm a^{-1}]	Transpiration [mm a^{-1}]	Evaporation [mm a^{-1}]	Bottom flux [mm a^{-1}]
Bare soil	944.0	0.0	0.0	435.6	509.3
Grassland	944.0	67.1	614.1	57.6	205.0
Maize	944.0	18.0	116.2	324.1	486.6

5.3.3. Scenario-based soil water dynamics at Cusseque summit areas (Csu)

Three different land cover scenarios were parameterized to reflect on one hand the actual pristine conditions and on the other hand a possible scenario with agricultural use. In contrast to the slope east areas, the pristine conditions at the summit of the study site are dominated by woodland (section 5.2.1). The remaining others are with respect to vegetation parameterization and weather input identical.

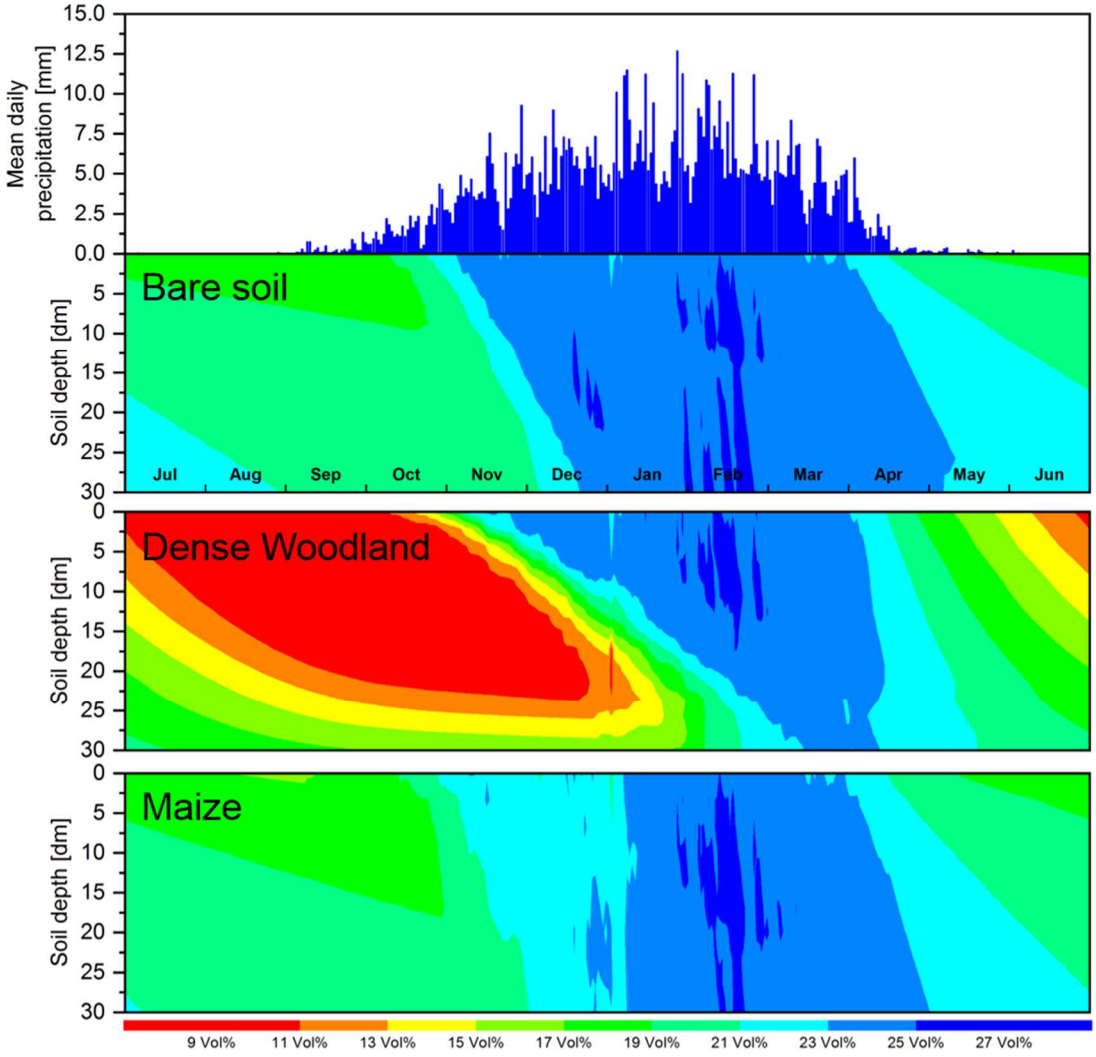

Fig. 52: Mean daily water content for a period from July to June based on a 30-year model run and three different land cover scenarios on the summit areas of the Cusseque site

The reference bare soil simulation (matrix 1 in Fig. 52) for the summit areas reveals a pattern of soil water dynamics similar to the bare soil simulation of the slope east area throughout the hydrological year from July to June. Despite this correspondence, there are slight differences looking at the volumetric water contents. The total amount of available soil water for evapotranspiration and deep drainage is reduced by a higher residual water content but nearly the same amount of the saturated status. This results in a more pronounced dynamic with respect to minimum and maximum water contents over a hydrological year. At the onset of the rainy season the soil water distribution shows a mean content of 19 Vol% (pF 1.8; ku =6.7 · 10^{-3} cm d^{-1}) in the topsoil with a slight increase with depth to 21 Vol% (pF 1.7; ku =3.1 · 10^{-2} cm d^{-1}) at the bottom of the profile. After the first

rain events the infiltrated water reaches the bottom of the profile within 30 days and increase the water content to 27 Vol% (pF 1.5; ku =8.4 · 10^{-1} cm d^{-1}). In the middle of the rainy season, the water content reaches its maximum of 29 Vol%. Since the corresponding soil hydraulic heads are at or under field capacity and the emerging upward gradients are small, infiltrated water will be redistributed relatively quickly to deeper areas where it remains uninfluenced by evaporation. Due to the low unsaturated conductivities even at field capacity capillary rise from shallow depths to the surface is reduced. Similar to the slope east site the overall dynamic of the bare soil profile shows no significant differences in variance in soil water dynamics with respect to the depth of soil layers as shown in Fig. 53a.

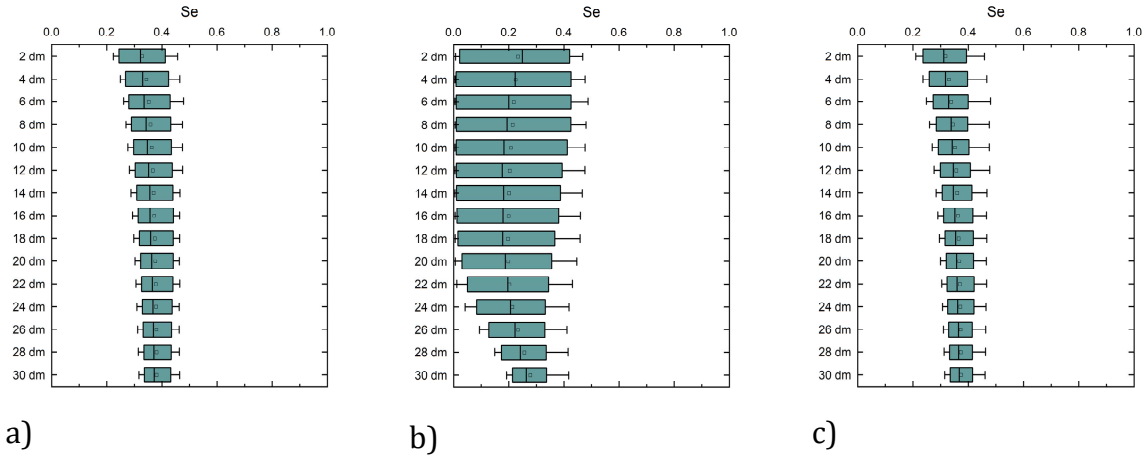

Fig. 53: Boxplots showing the long year simulated effective saturation (Se) at 20 cm soil layer resolution down to 300 cm for the summit area. a) Bare soil, b) Woodland, c) Dryland Maize

The dynamic integration of woodlands as vegetation alters the soil water dynamics significantly. With a permanent rooting depth of 300 cm and a phenological cycle of 365 days available soil water is utilized the whole year through. Coming from the dry season, the water content in all depth is near to the PWP at 9 Vol% only the lowest part of the profile stays unaffected within the dry season. With the beginning of the rainy season a wetting front with a stable soil water gradient forms around 9 Vol% in depth and 25 Vol% in upper layers. This moves constantly with time towards greater soil depths to reach the bottom of the profile by the last third of the season. From there the soil water contents remain similar to those of the bare soil reference but diminish more quickly at the end of the last rains where a broad drying front establishes which leads to the overall low water content

towards the next rainy season. Compared to the soil water dynamics of the bar soil reference the variability of volumetric water contents in certain depths is highly pronounced due to the inclusion of woodland vegetation (Fig. 53b). Down to a depth of 180 cm, all available soil water is utilized by vegetation down to near the PWP. Only in greater depth, from 200 cm to 300 cm, a residual amount of water remains unutilized.

Referring to the cropping scenario on the eastern slope site, the influence of maize on the soil water dynamics at the summit site is comparable but with the specific characteristics of the soil hydraulic properties. Within the cropping period at the first third of the rainy season, the water content is slightly lower compared to the reference bare soil. After harvest, the soil water dynamic develops to be the same as the reference. The similarity is proven by the long year means of the effective saturation (Se) for 20 cm layers shown in Fig. 53c.

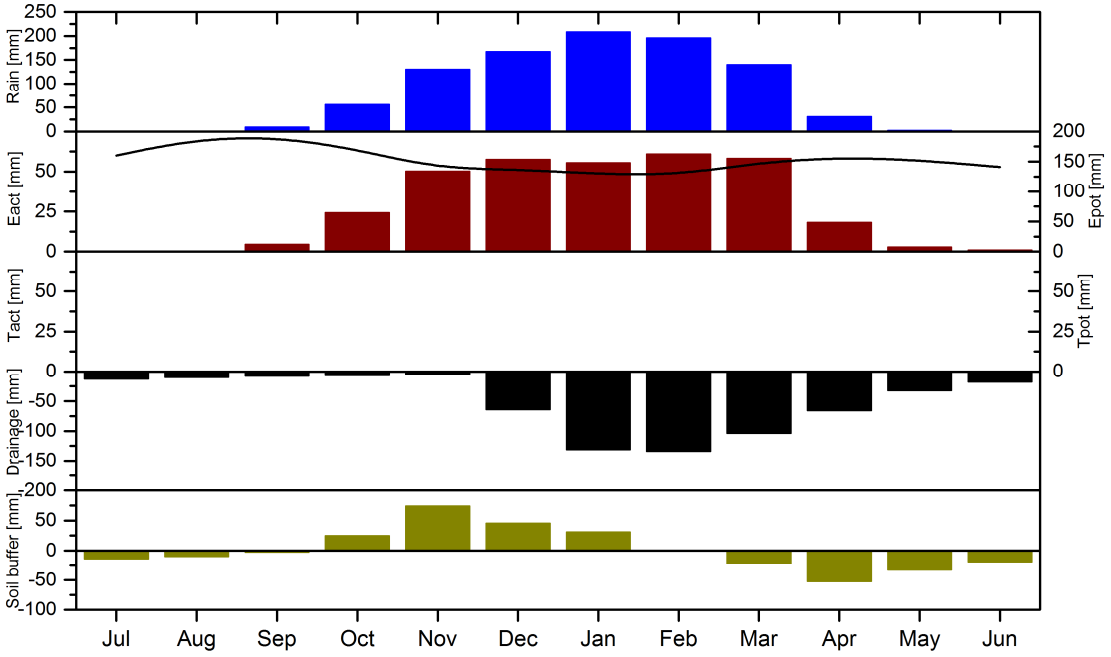

Fig. 54: Monthly mean soil water balance components for the bare soil reference scenario at the summit areas of the Cusseque study site. The lines represent the monthly course of Epot and Tpot

According to the description of the bare soil results of the eastern slope, the monthly course of the evaporation follows the trend of the precipitation with constantly high Eact values from December to March of 58 mm month-1 or 43 % of the potential evaporation (Fig. 54). The amount of bottom flux increases significantly in December after the soil buffer reaches its positive maximum level in November. Percolated water remains in

deeper layers in December and January which increases the amount of water in the soil buffer until the bottom flux reaches its maximum in February with 134 mm. At that point, the positive dynamic reverses with decreasing precipitation amounts, and the evaporation drops from March with 58 mm to 18 mm in April whereas the bottom flux slowly decreases as a function of soil water content. The bottom flux-evaporation relation, in this case, is 1.8 (see Tab. 10) and therefore higher than in the bare soil reference of the slope east simulation, indicating that this soil has a trend towards higher yield with respect to groundwater recharge under bare soil conditions.

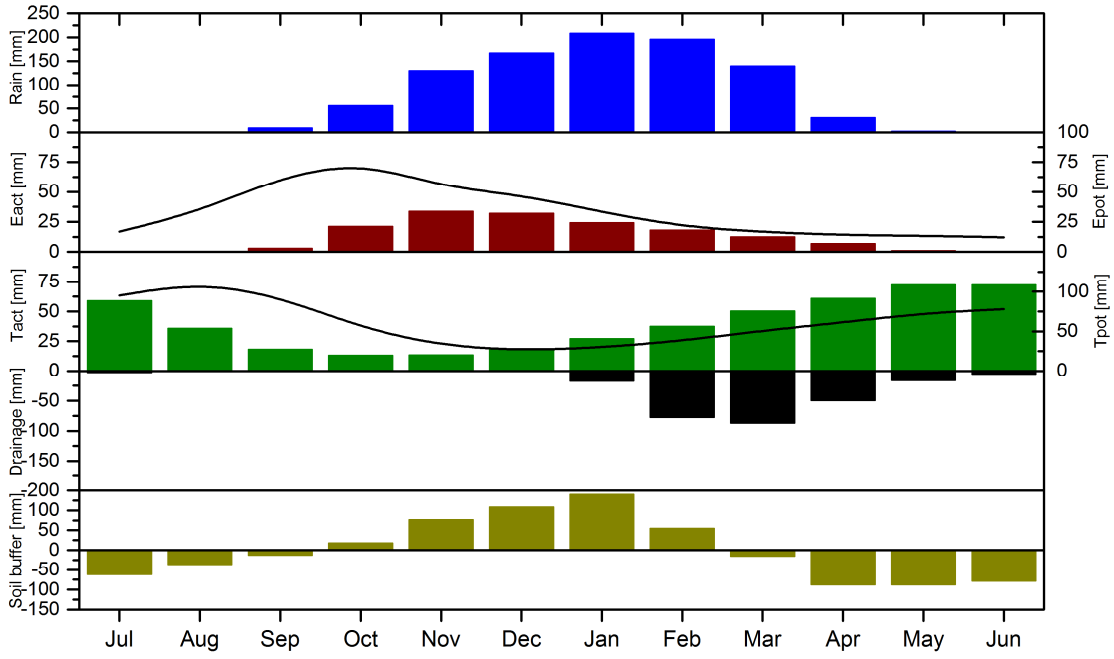

Fig. 55: Monthly mean soil water balance components for the woodland scenario at the summit areas of the Cusseque study site. The lines represent the monthly course of Epot and Tpot

As already mentioned in section 5.3.3 the integration of woodland vegetation has a significant influence on soil water dynamics and in consequence on soil water balances, too. Deep rooting properties in combination with high LAI values transpiration is the dominant sink in this simulation with simultaneous lowering of actual evaporation rates due to shading effects and low topsoil water contents. Fig. 55 illustrates this modification. Due to the assumption, that the phenological cycle of the woodland starts in October with low LAI values the transpiration rates increase continuously over time to reach their maximum with 72 mm in May and June or 100% of the potential transpiration. The actual evaporation rates develop from September to a maximum in November with 34 mm and decrease again due to the increasing soil coverage. As a consequence, from September to

November the evaporation exceeds the transpiration rates while in the remaining months the relation is reversed. The water extraction by roots throughout the whole profile lowers the bulk soil water content which has also consequences for the bottom flux. The soil buffer reaches its highest level in January where transpiration is still at nearly 50% of its maximum and evaporation rates decrease. In this time the soil buffer contributes to deep drainage while in the following month this buffer is utilized for transpiration to sustain high transpiration amount without any precipitation input. In relation to the bare soil reference, the bottom flux is reduced by 50 % (Tab. 10).

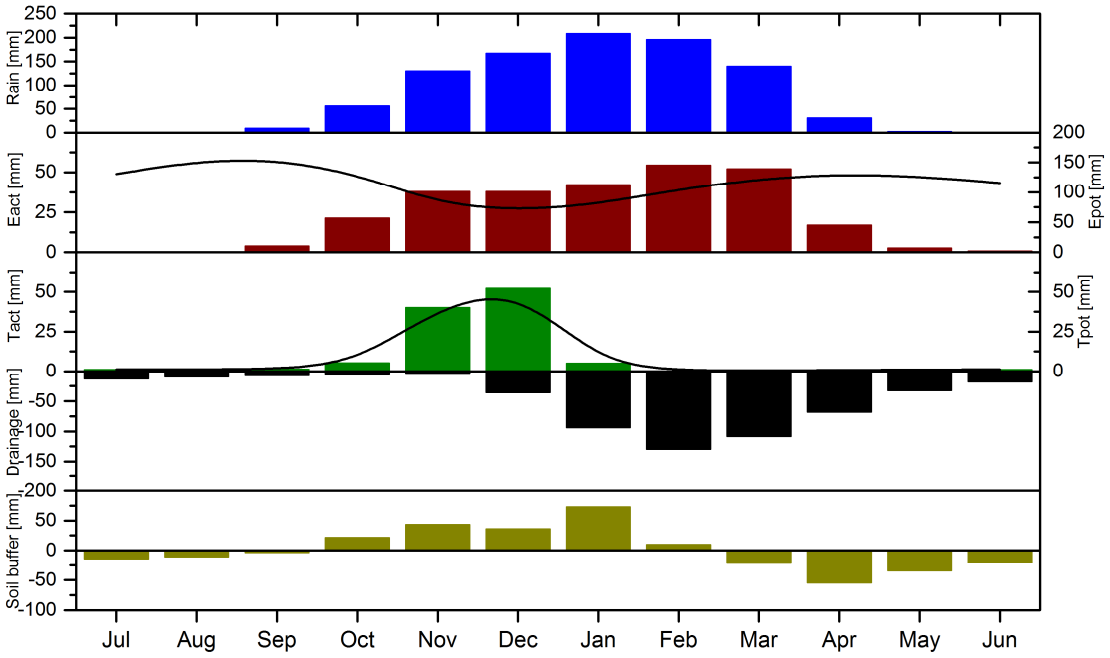

Fig. 56: Monthly mean soil water balance components for the cropping scenario with maize at the summit areas of the Cusseque study site. The lines represent the monthly course of Epot and Tpot

The temporal development of the monthly mean soil water balance components (as shown in Fig. 56) is similar to the simulation of the cropping scenario on the eastern slope with slightly different amounts due to the different soil characteristics. Because of the relatively small influence on the soil water dynamics in relation to the bare soil reference the additional transpiration sink and the soil coverage lowers the evaporation amounts. The surplus of soil water is not fully utilized by the vegetation and is partially added to the drainage fraction or remains within the soil buffer. This is the reason, why the bottom flux of the maize scenario exceeds the bottom flux of the bare soil reference (Tab. 10).

Tab. 10: Long year means of water balance components for the Csu scenarios

Scenario	Precipitation [mm a^{-1}]	Interception [mm a^{-1}]	Transpiration [mm a^{-1}]	Evaporation [mm a^{-1}]	Bottom flux [mm a^{-1}]
Bare soil	944.0	0.0	0.0	341.1	603.8
Woodland	944.0	38.7	503.6	150.2	251.3
Maize	944.0	18.0	119.0	274.9	533.8

5.4. Discussion

5.4.1. Characterisation of atmospherical demand driven fluxes under different land use

A closer look at the soil water balance components as relative input fractions presented in Fig. 57 shows the tendency of the simulated soil-atmosphere system on both sites to support bottom flux processes with a share of 54 % of input under bare soil conditions on the eastern slope part whereas 64 % of the rainfall is drained at the bottom in the summit areas. Under agricultural conditions, the transpiration withdraws 12 % of the precipitation on both sites.

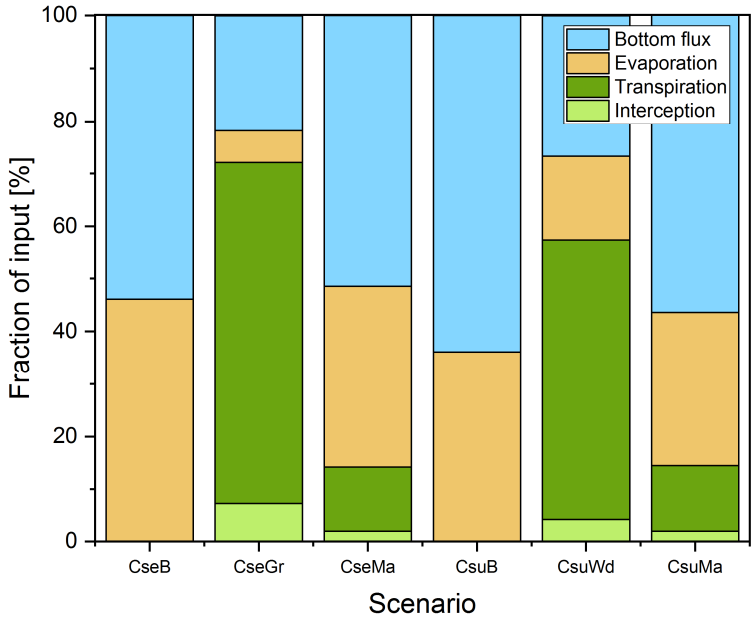

Fig. 57: 30-years mean proportion of modeled fluxes related to precipitation of input

While the interception losses are the same due to the identical vegetation coverage, the reduction of the evaporation and bottom flux share in relation to the bare soil reference is different on both sites. On the contrary, the evaporation reduction due the leaf soil coverage effects and root water extraction is reversed. The eastern slope shows a higher evaporation reduction to 34.4 % whereas the summit area evaporation reduction shows

a lower impact with still 29.1 % of the input compared to 36.1 % under bare soil conditions. The grassland scenario transpiration at the eastern slope accounts for 65 % of total input and diminishes evaporation withdrawals to only 6 %. The woodland scenario effect appears to be little less pronounced with 53 % transpiration share while evaporation withdraw is at 16 % of the total input. The interception losses account for 7 % for the grasslands and 4 % for the woodland scenario.

The following explanations refer all to a comparison between bare soil conditions and assumed vegetation scenarios to identify causes and consequences of different vegetation impacts on soil water balances and dynamics. A comparative assessment between the bare soil and the extensive agriculture scenario on the eastern slope and the summits shows that the different effects of identical vegetation characteristics on soil water balances are caused by the differences in soil hydrological properties. Since evapotranspiration processes are mainly controlled by the capillary properties of the soils coarse to medium pore system, the area of interest within the soil hydraulic functions lies above the area of field capacity between pF 1.8 and pF 2.5. The area below field capacity needs to be considered too because gravitational water flows withdraws water from areas where primary evapotranspiration fluxes. Going back to Fig. 40, the illustrated hydraulic functions show divergent characteristics which result in the previously mentioned tendencies of the two sites to either support percolation or evapotranspiration. Coming from saturated conditions the eastern slope soil can potentially redistribute 9 Vol% under the influence of gravity before reaching the lower boundary of the field capacity whereas the summit soil can percolate 23 Vol%. In other words, the eastern slope soils show a relative saturation of 77 % at field capacity while the summit soil has a much lower relative saturation of only 32 %. At field capacity, the gravitational water redistribution is reversed to an upward capillary force driven dynamic. Being already at a low saturation level the summit soils showing conductivities of $2 \cdot 10^{-2}$ cm d^{-1} and therefore much lower rates than the eastern slope soil with still 7.7 cm d^{-1}. In consequence, the summit soil tends to support percolation processes whereas the eastern slope can hold more water against gravity and is able to transfer this by capillary rise at high conductivities back to the atmosphere.

Amidst these considerations, the bare soil-atmosphere system is supplemented with an additional water extraction by roots and a shading effect of emerging leaves by integrating

the dryland agriculture scenario. Since the relative balances show no significant differences of transpiration fluxes between both sites and the relationship between actual and potential transpiration is at optimum. Hence, a good water supply for the vegetation is indicated over the whole cropping period. Since the potential evaporation is reduced by the same amount at both sites as a result of the same leaf area index, the differences in bottom fluxes and evaporation changes from the bare soil to the dryland agriculture scenario can only be explained by the different soil physical reaction towards soil water reduction by root water extraction. The highest impact on evaporation fluxes is shown on the eastern slope site where evaporation under bare soil conditions is the highest of both sites. The additional water flux reduces the water content within the root zone to a level, where lower unsaturated conductivities decrease the upward water fluxes to the soil surface to evaporate. The evaporation reduction of 111.5 mm is nearly equal to the transpiration amount. The reduction of evaporation due to lower water contents and conductivities is therefore compensated to a certain degree by the active process of transpiration. In contrast, the evaporation reduction at the summit site is overcompensated with 55 % of the transpiration which indicates, that, in reverse, the remaining 45 % need to be compensated by other balance components, which will be explained later on.

The following consideration for pristine conditions cannot be compared directly as it is possible with the agricultural scenario because of the individual combinations of site and vegetation scenario. The grassland scenario of the eastern slope site shows a severe reduction of evaporation fluxes due to the high soil cover fraction. Based on the assumption in this scenario, the actual evaporation is reduced by 87 % reflecting a high leaf shading effect and high transpiration fluxes which overcompensates the evaporation reduction. The decrease in evaporation is 1.6 times overcompensated by transpiration and has to be complemented by other sources. As described in section 5.3.2 the grassland scenario reduces the plant available water almost completely within the root zone over the dry season. Only the capillary supply of water from below the rooting zone enables the vegetation to sustain low transpiration rates. The incoming rainfalls less the appearing interception losses, at the beginning of the rainy seasons, need to rewet the dry root zone first and contribute almost to 100 % to transpiration unless the transpiration demand is less than the incoming precipitation sums. The rainfall excess now contributes to a small proportion of evaporation and bottom fluxes since the vegetation only has access to plant available water within the first meter. On the other side, the evaporation and transpiration

characteristics of the deep rooting woodland scenario at the summit area shows a completely different dynamic with a less steep decrease in evaporation. Based on the assumptions of a not fully covered soil evaporation processes are possible. Nevertheless, the reduction in evaporation accounts only for 38 % of the transpiration increase compared to the bare soil scenario which is a 2.6 times overcompensation of the evaporation reduction. Where the dry layer at the grassland is only 100 cm in extend, nearly the whole plant available water of the profile is utilized by the woodland throughout the dry season the upcoming rainy season needs one month to rewet the soil surface to a point on which the unsaturated conductivities and water contents can contribute to evaporation processes. Once the medium to upper soil layers are at a saturation status comparable to the bare soil conditions the occurring capillarity starts to supply evaporation fluxes.

5.4.2. Transpiration fluxes and possible consequences for plant production

In the previous sections, the considerations based on the long year means to assess dominant trends and patterns in soil water dynamics as well as in balances as a function of vegetation. This section goes more into details of the interannual variability of precipitation to consider the influences and possible impacts on transpiration and to lead over to the next section.

In the following section, the term “effectiveness” is used to describe the ability of a given soil-vegetation-atmosphere system to turn over plant available soil water by transpiration. Since the term “efficiency” is already used to describe the carbon fixation rate in relation the transpiration (*Bacon* 2009) it is necessary to differentiate between these two terms to prevent any misleading interpretations.

As a basis for the evaluation, the annual sum of evaporation amounts, bottom fluxes and interception losses (blue water) are related to transpiration fluxes (green water) (adapted after *Cosgrove* and *Rijsberman* 2000). The ratio between these two values is used an index to describe the effectiveness of soil water utilization with respect to plant productivity. It has to be mentioned, that since no coupled vegetation module with feedback loops between soil water status and phenological development is used, the transpiration is only governed by the fixed vegetation development dynamics and therefore it is

not possible to make any assumptions regarding a potential plant productivity. Nevertheless, this analysis gives a clue about whether a certain vegetation scenario already exhausts possible soil water sources or if there is still some potential.

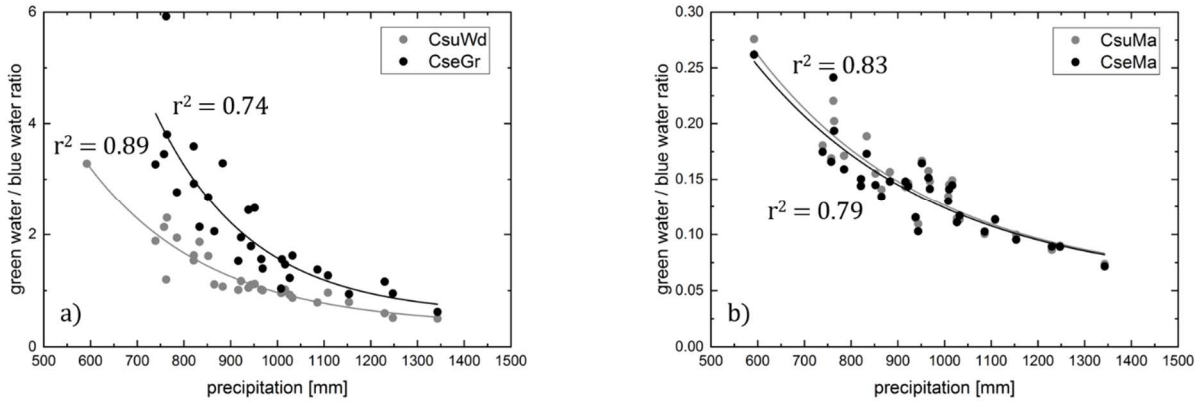

Fig. 58: Green water to blue water ratio as a function of annual precipitation for a) pristine conditions and b) under dryland agricultural use

The water use effectiveness as function of the precipitation amount shown in Fig. 58 illustrate the high water use effectiveness of assumed pristine vegetation due to its high soil cover fraction as measure of the transpiration potentials. On the other hand, the long phenological cycles in combination with deep and intensive rooting allow an optimal utilization of plant available soil water over time and space. But still, more water does not mean more transpiration. As Fig. 58 clearly shows, the water utilization by plants in relation to the remaining unproductive fluxes is already at a high index with low rainfall amounts to decline asymptotically with increasing precipitation. The decline does not mean a decrease in transpiration, moreover, the transpiration remains at a high level the surplus in soil water is then transferred to other soil water fluxes such as evaporation and bottom fluxes. As described earlier, with increasing soil coverage and transpiration withdrawals the evaporation fluxes decrease while bottom fluxes increase. The decrease in the green to blue water ration (GB ratio) is therefore not a decrease in transpiration but an increase in unproductive fluxes. The grassland vegetation shows to be highly effective in soil water consumption by suppressing evaporation fluxes and an instant uptake of plant available water to sustain a maximum of transpiration, especially over the dry season. In result, the GB ratio is the highest among the pristine vegetation with, in maximum, four to six times more transpiration than unproductive fluxes. Since the major period for maximized transpiration is limited to the dry season, the soil buffer remains the only source for plant available water over the dry season which is in turn depleted by the vegetation at the end

of the rainy season, in consequence, the GB ratio shows a seasonal dynamic. In times with high precipitation, the GB ratio of the grasslands drops only slightly below one, which shows, that still 50 % of the all-over fluxes account for transpiration dynamics, which is, considering an actual rooting zone of 100 cm highly effective. The analysis of all simulated seasons reflects this tendency with a mean GB ration of 2.18. In contrast, the woodland scenario shows lower GB ratios due to the lower soil coverage based on a pronounced phenology. As described above, evaporation rates and bottom fluxes are higher which reduces the mean GB ratio to 1.26 although the woodlands have a deeper developed root system and are therefore able to explore more plant available water and able to reduce bottom fluxes (*Walker* et al. 2002). In parts, the phenological cycle is responsible for the relatively low ration since in times with a good water supply the actual transpiration rates are lower due to early development stages. Nevertheless, with a maximum GB ration of 3.2 in the dry season with the least precipitations the effectiveness is still reasonable to support biomass production. In contrary, the dryland agriculture scenario, with its low plant density and soil cover fraction as well as with a short growing period, shows the lowest effectiveness in soil water utilization and no significant differences between the two sites.

With a maximum ratio of 0.27 areas under dryland agriculture show four times more unproductive water fluxes than plant production supporting transpiration. A comparison with the grassland scenario, which has approximately similar vegetation characteristic with respect to rooting depth, suggests that the available soil water can be used far more effective. Focusing on the months where the crop shows the highest transpiration rates reveal a difference of 75 % to 50 % less effective soil water consumption. A higher plant density could adjust the GB ratio to increasingly effective water utilization but it needs to be considered whether the soil nutrition status of the respective soils supports higher plant densities or if it is necessary to apply additional manure or fertilizer to increase yields. The soil chemical analysis shows that a combination of low pH values resulting in a low nutrient buffer capacity with all-over low plant available nutrients is more likely to have a greater effect on crop yield than the plant available water content. Another aspect that has to be considered in the context of plant water consumption is the highly variable precipitation dynamic in the headwater region of the Okavango. Even if yearly precipitation sums are sufficient to sustain dense wood- and grasslands, an agricultural use de-

pends on regular rainfall patterns, especially if Maize is the primary crop. Low water effective cropping systems need to compensate unproductive losses by periodic rain events, to keep the soil water content of the rooting zone on a level within the usable field capacity and not to risk yield declines. The precipitation dynamic in the central highlands of Angola with its episodically appearing intermittent dry season bears the risk of dry spells. With a depleted soil water buffer by high evaporative losses in times prior the arising of dry spells, the crops show only little resilience against drought stress. Depending on the manifestation of the dry spells it seems to be possible to overcome drought stress by adjusting the right plant density to ensure a sufficient soil coverage on one hand without over-utilizing buffered soil water. An additional soil surface coverage with plant residuals also can reduce evaporative losses in times when rainfall is scarce. By changing the subject from bottom flux induced river runoff and groundwater recharge to plant water use and biomass production, the reference scale changes from the (sub-) catchment scale to the field scale. The converted fields around Chitembo experience an increase in bottom flux to about 54 % of the precipitation input which is equal to 509 mm a^{-1} whereas before the conversion under pristine conditions the fields yield only 228 mm a^{-1} ergo a change of additional 281 mm bottom flux. As already mentioned, this significant increase in percolating water is likely to have consequences for the specific fields. While the pristine vegetation is highly adapted to a short circuit type of nutrient cycle where short-term litter decomposition sustains a distinct input of plant available nutrients, an unsustainable agricultural practice withdraws soil nutrients mostly by crop residual removal which causes a constant decline in plant available nutrients. The additional high bottom fluxes further decrease buffered nutrients in soils with a tendency of leaching, as observed in that area by the field soil survey. It can be expected, that under the assumed simulation parameterization the plant productivity will decrease within a certain period without additional nutrient input. Taking the pristine scenarios as references for the soil hydrological elasticity (Fig. 59) of a soil-vegetation-atmosphere system with respect to bottom fluxes some of the mentioned trade-offs and negative consequences can, to some extent, be compensated by applying a site adapted agricultural management. The grassland scenario shows very low BA ratios due to the highly effective plant water uptake, therefore an increased plant density beyond the point of the evaporation loss compensation by transpiration seems a plausible way to reduce bottom fluxes over the cropping period. With respect to the wood-

land conversion and the related measures for bottom flux reduction, it needs to be considered, that the elasticity of this pristine system is defined by differing boundary conditions like extended rooting depth and growth height.

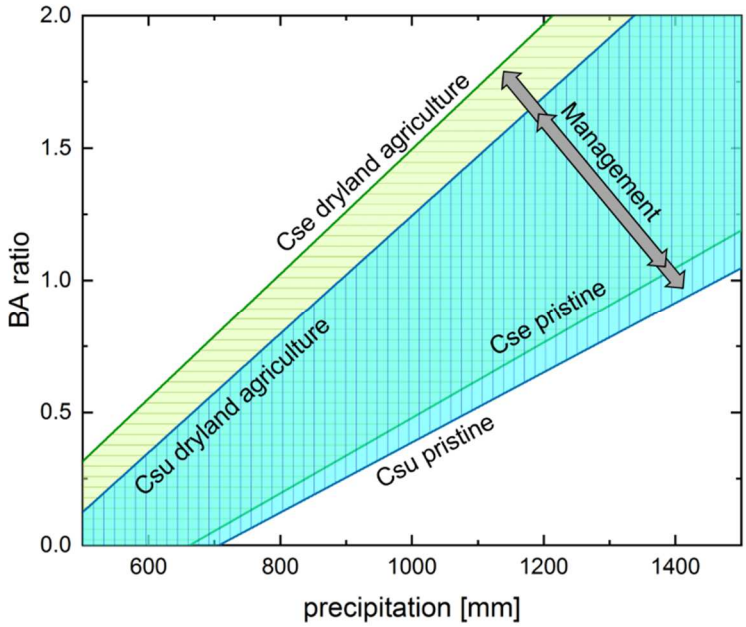

Fig. 59: BA ratio range between pristine and dryland agriculture scenario for Cse and Csu study site as a proxy for soil hydrological ecosystem elasticity referring to bottom fluxes

But a transfer of the grassland results to the summit soils can be an orientation to which degree an increase of plant density can reduce bottom fluxes. These more theoretical reflections only take soil hydrological relation into account. Whereas the Cusseque study area has sufficient precipitation input to sustain dense woody ecosystems, the increase in crop density is restricted by nutrient pool limitations in acidic soil. Therefore, a high increase in crop density will result in yield losses not because of water limitation but by nutrient depletion.

To focus on the plant water use effectiveness of a cropping system and a possible improvement, many of the previous considerations regarding bottom flux reduction are transferable to the following evaluation. The loss of soil water by bottom flux as well as by evaporation leads to low effective plant water utilization. As it was already discussed, a reduction of bottom fluxes by an adapted crop management is only possible within narrow boundaries limited by plant available nutrients.

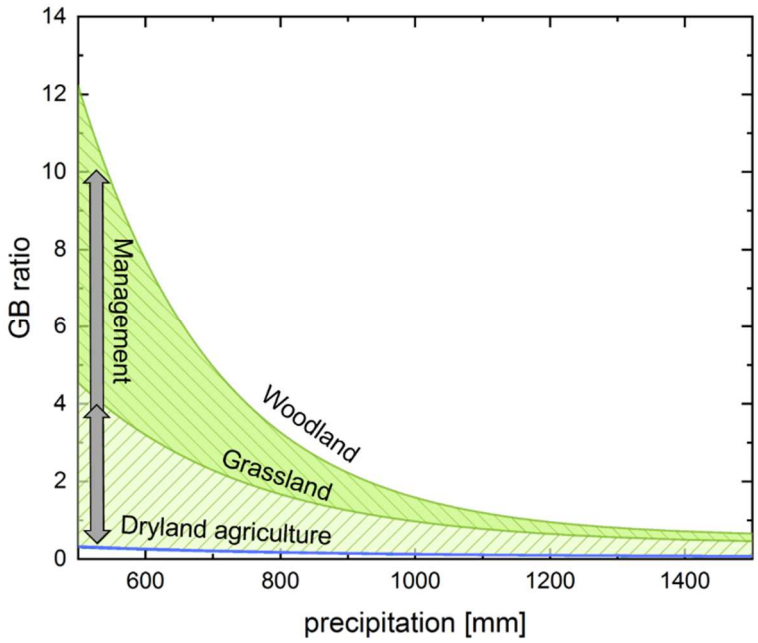

Fig. 60: BA ratio range between pristine and dryland agriculture scenario for Cse and Csu study site as a proxy for soil hydrological ecosystem elasticity referring to plant water use effectiveness

Nevertheless, the soil hydrological ecosystem elasticity can support high crop densities at minimum to the density which is the basis for the grassland scenario (Fig. 60).

5.4.3. The development of deep drainage and its relation to vegetation influences

The importance of deep drainage balancing in relation to vegetation characteristics and land use change becomes apparent since the headwater regions of the Okavango basin play a significant role in the discharge generation and are therefore of supra-regional and even supra-national relevance for providing freshwater in downstream regions with lower precipitation availability. On the regional scale, deep drainage is an important driver for the stability of certain ecosystems that rely on high water tables such as stream-line accompanying wetlands. The provisioning of potable water is of high importance for human use, but the situation in the dry sub-humid area of the Cusseque site with its highly weathered soils bears an indirect trade-off between deep drainage and soil nutrient availability for biomass production. As already mentioned, the mainly acidic soils with low nutrient buffer capacities prone to leaching processes by deep draining percolation water which participate to a large extent on runoff formation of the Okavango. Hence, an overarching assessment of deep drainage fluxes needs to consider occurring trade-offs on the regional as well as on a supra-regional scale with a focus on possible net ecosystem nutri-

ent withdrawals in headwater regions and river discharge formation for water provisioning in downstream areas. With these introductory considerations, the following section leads back to the study site scale with its individual characteristics and the scenario-based simulation results which form the fundament for a later data-based evaluation with respect to the mentioned ecosystem functions and services.

In the previous sections, the vegetation depended relation between transpiration and evaporation showed that high transpiration rates cannot be fully compensated by the reduction of evaporation fluxes. Therefore, the necessary subsidy has to be provided by a change of the deep drainage or soil water buffer component. Because of a water turnover time of one hydrological year, the soil water buffer plays a role for the inter-seasonal dynamic of the deep drainage rates but shows no compensation function considering seasonal balances. Similar to the GB ratio method the analyses of the vegetation impact on deep drainage processes is based on the reversed ratio where the bottom fluxes are related to the remaining soil water balance components driven by atmospheric demands, in the following named BA ratio.

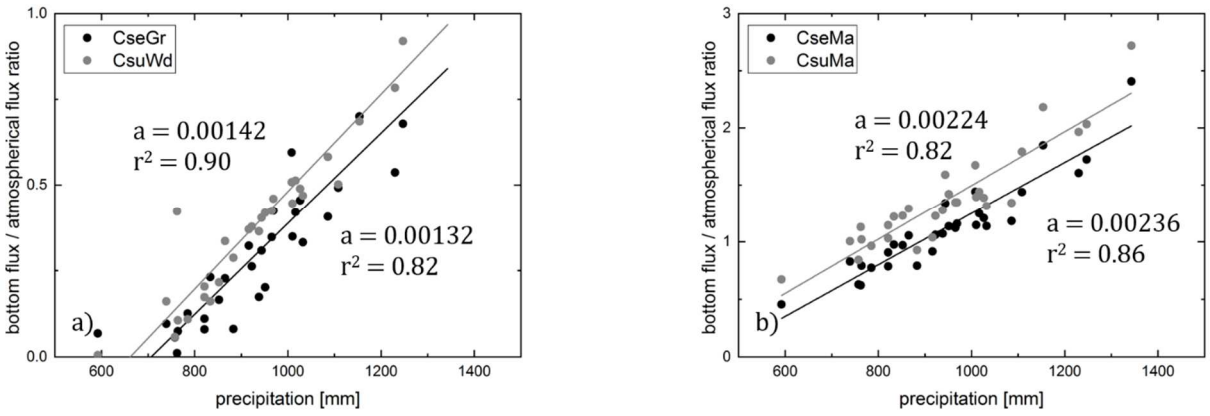

Fig. 61: Bottom flux to atmospherical flux ratio (BA ratio) as a function of precipitation for a) pristine conditions and b) under dryland agricultural use

Fig. 61 illustrates the BA ratios for pristine conditions and under agricultural land use as a function of the seasonal precipitation input. The existing linear relationship is expressed in a regression with significant correlations and explained variations between 82 % and 90 %. Under pristine conditions show mean BA ratios of 0.31 for the grassland scenario and 0.40 for the woodlands which reflects the already mentioned tendency of the woodlands to yield more bottom fluxes as a consequence of the site-specific soil hydrological properties. The maximum ratios of 1.11 at the grassland site and 1.12 at the woodlands

occur in times with exceptional high seasonal precipitation sums of 1342 mm. These conditions are contrasted by the dryland agriculture scenarios which showed no or only a little overcompensation effects of the transpiration increase in relation to the evaporation reduction. In consequence, these scenarios show 3.4 to 3.6 times higher mean BA ratios compared to the pristine conditions. The maximum ratios of 2.41 at the eastern slope site and 2.72 at the summits at times with high input is clearly orientated to higher bottom fluxes at the summits where again the site-specific soil hydrological are visible due to the higher ratios while having identical vegetation characteristics.

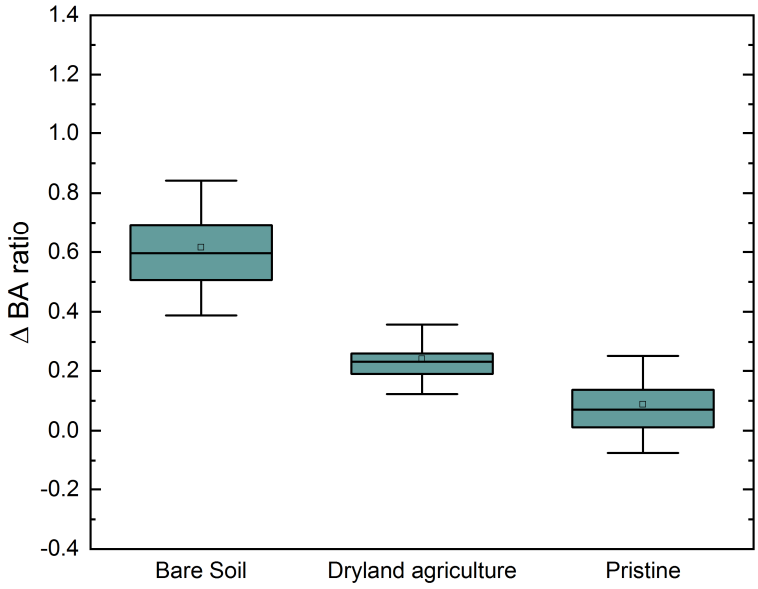

Fig. 62: Differences in BA ratios between the summit site and the eastern slope for three scenario classes

To characterize the effect of the soil hydraulic relations on one hand and to determine the impact of land use on these relations on the other hand deviation between the summit areas and the eastern slope is shown in Fig. 62. Under bare soil assumptions, the difference between the two sites is the highest with 0.61 whereas with increasing vegetation densities the purely physical effects get superimposed by transpiration and shading effects towards only small differences between the pristine scenarios. Overall, the scenario evaluation regarding the impact of vegetation on bottom fluxes shows, that with increasing vegetation rooting depth the impact on the relationship between the bottom and atmospherical fluxes decreases due to the compensation by transpiration fluxes. The compensation is the highest under pristine condition, with lower bottom fluxes compared to the dryland agriculture scenario where bottom fluxes only compensate a small proportion of the transpiration increase.

A pristine vegetation is seen to be highly adapted to the present environmental conditions and the resulting soil hydrological fluxes reflecting a system in balance. A system changed by increasing human activity results in changed fluxes and balances with consequences for the system balance which will be re-established with different boundary conditions. The concluding considerations of the Cusseque simulation scenarios focus on two main issues comprising the effect of land use change on the soil hydrology related fluxes and pools with respect to groundwater provisioning for human use and runoff generation on one side and the agricultural land use potentials from a hydrological point of view with possible nutrient leaching implications and freshwater quality on the other side.

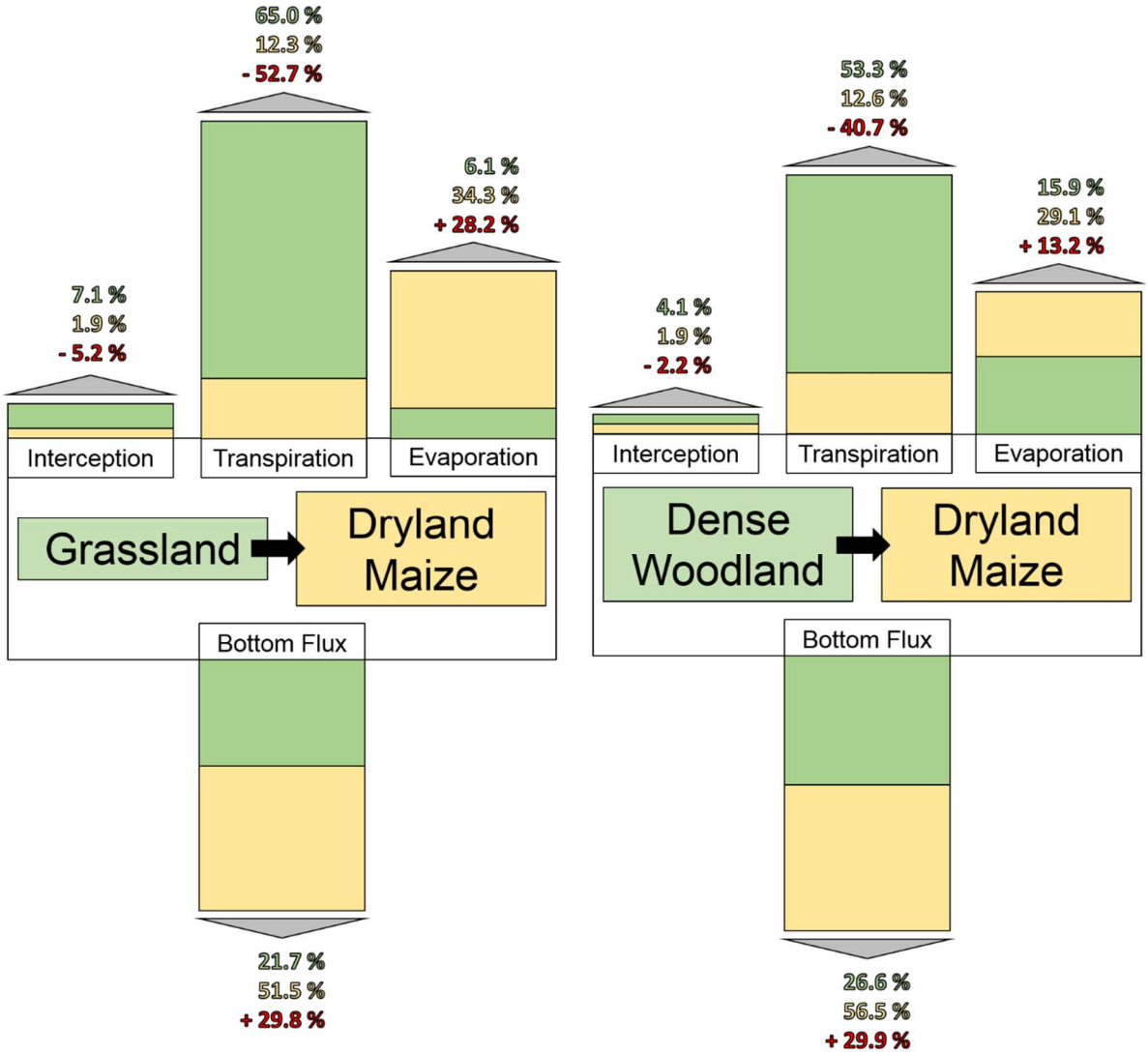

Fig. 63: Balance shifts from pristine conditions to dryland agricultural use in a) eastern slope area and b) the summit sites of the Cusseque study site

In Fig. 63 the impact of land use conversion from a pristine to an agricultural system is expressed as soil water balance shift as a fraction of input. Whereas the impact on interception losses is relatively small, the change of transpiration and bottom fluxes are significant, followed by the effect on evaporation. Both conversion scenarios show an increase in bottom fluxes by more than double with respect to the pristine state. Assuming, that these fluxes contribute to groundwater recharge a proportion of this additional groundwater is affecting the flow regime of the Cusseque river. As shown in section 5.3 the main bottom flux change occurs within the rainy season due to high percolation rates with as a consequence of high rainfall input. Only a small amount of water is buffered in the soil to be released constantly during the dry season. A possible system response to the changed land cover characteristic is a higher peak of the discharge hydrograph with an increase in base flow volumes resulting in a greater runoff amplitude. Due to the delayed release of groundwater to river runoff, the increased volume of groundwater supports human consumption while the higher runoff peak limits the areas for agricultural use in the by flood-affected parts of the Cusseque catchment. The effective magnitude of this impact is related to the intensity of land use change. A remote sensed land cover conversion study by *Schneibel* et al. (2017) shows that the conversion rate to agriculture within the last 15 years of a 20 km buffer around the city of Chitembo was 0.6 % a^{-1} to 1.5 % a^{-1}. Assuming a mean conversion rate of 1.1 % a^{-1}, additional 16.5 % are under agricultural use compared to 2003. Relating this increase to the mean bottom flux change from pristine conditions to agricultural use, a total increase of 5 % in bottom flux can be predicted for that area under the assumptions made within the simulations. Depending on the topology of the fields towards a river system this increase is likely to have no to little effects with respect to hydrograph changes (*Warburton* et al. 2012) whereas the additional groundwater may be an improvement for direct human use. Since the land use change analysis was done for an area around a larger city the conversation rates may be lower in remote areas with a lower population density and the increase in bottom fluxes therefore, too.

6. How is the influence of different vegetation and agricultural land use characteristics on soil water balances in northern Namibia?

6.1. Case study introduction

Characterized by irregular amounts of growing season rainfalls and low-fertility soils (*Gröngröft* et al. 2013b), the majority of land-users are confronted with challenging conditions for sufficient crop production. Beside soil fertility problems, the current and future land-use potential is linked to the question how to use the restricted amount of rain-, river- and groundwater for productive crop production. Currently, on small areas with high-intensity of agricultural inputs river water is irrigated for two crop cycles per year, predominantly maize and wheat. In contrast, the majority of the fields are used for rain-fed subsistence agriculture of local smallholders (*Gröngröft* et al. 2013d). The analysis of the impact of land-use including irrigation on soil water balances focuses on the following key questions:

- Under the climatic and pedological conditions, which soil water balance modifications are typical for different land use and vegetation characteristics?
- What is the resulting water use effectiveness of the different scenarios with respect to biomass production and ecosystem elasticity and
- which consequences have an increase of commercial irrigation on river water withdrawals?

6.2. Soil hydrological modeling plots

Based on 102 profiles and topsoil samples 5 different locations were identified for a detailed soil sampling to analyze hydrological properties as well as to install soil water monitoring stations. Due to a subsequent redefinition of the study site extend by the project, most of these locations are not within the actual study site. This fact has no consequences for this specific work in hand.

The following considerations and observations will concentrate on the sites where soil water monitoring stations were installed but the respective time series are not included in this work due to measurement devices failures and bushfire impact.

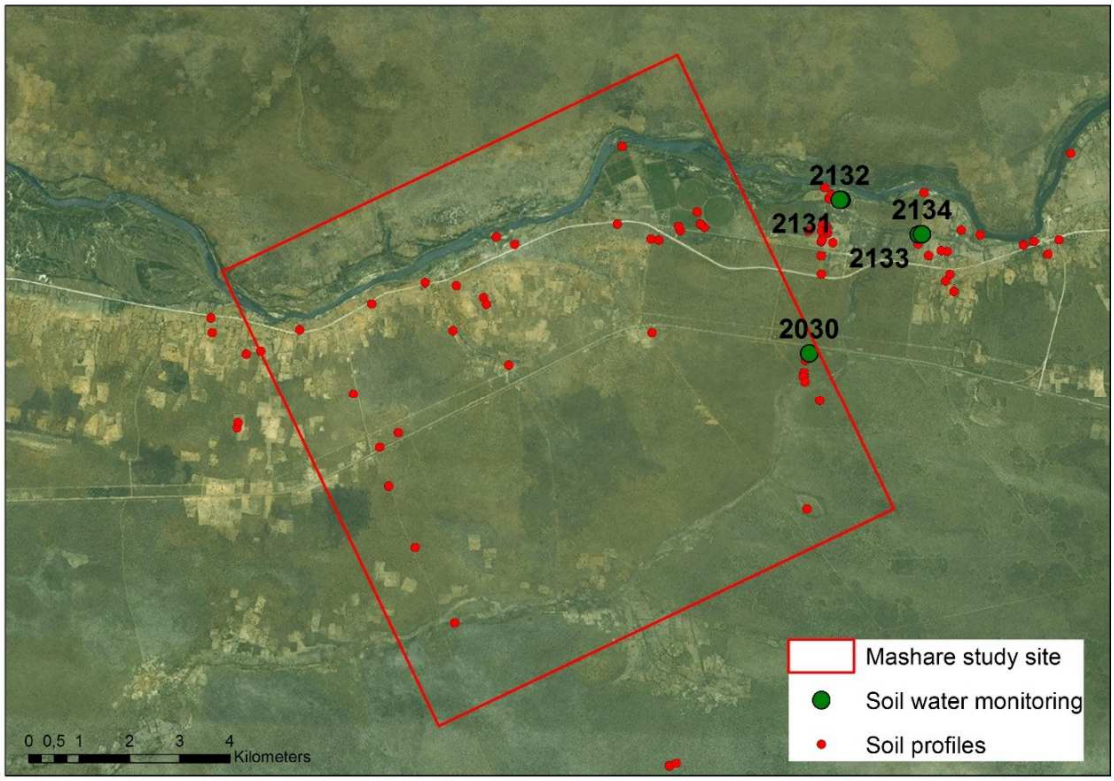

Fig. 64: Map showing the soil survey points and the locations of the soil water monitoring stations within the Mashare study site

6.2.1. Plot and soil profile descriptions

Fig. 65: Environmental aspect and site impression of profile 2131

Profile 2131 (Fig. 66) is located at the bush encroached margins of a field within an agricultural training center situated on a former levee within the old floodplains of the Okavango river. A thicket of *Terminalia sericea* covering 80 % of the surface (see Fig. 65). The soil surface is covered with litter from more than one vegetation period. Because of the presence of calcium carbonate throughout the profile together with depth-increasing clay contents and calcrete fragments in 75 cm, the soil is defined as a Petric Luvic Calcisol. Within the WRB texture class "loamy Sand (LS)", which is attributed to all horizons, the clay content changes with depth from 10 % to 20 %, with little silt (ca. 5%) and a dominating fine sand subfraction with more than 50 % of the sand fraction. An irregular layer of silicatic rock fragments can be found in depth of 75 cm. The soil reaction decreases with depth because of the increasing carbonate concentration starting with pH 6.1 in 10 cm to light alkaline conditions at pH 7.5 in 75 cm. 57 % of the total root number can be found within the first 50 cm where light acidic conditions favor nutrient uptake and a non-restricted, well-formed root system can be developed.

Profile 2131	Lat: -17,88670°	Long: 20,21305°	1032 m h.s.l.	Loc.: Mashare / Namibia

Topography:	Slope:	Exposition:	Curvature:	Landscape unit:	Land use unit:	Vegetation / Crop:
Former levee	1°		Double convex	Old Floodplain	Bushveld (B)	Terminalia (cover ca. 80%)

Remarks: Mashare Development Institute (MADI), dryland agriculture field in 15 m distance, termite mound in ca. 10 m distance N, grazing

Ah	**Grain Size:** light clayey sand St2 (KA5)/LS (WRB); subangular structure; **Munsell Colour**: moist 7,5 YR 5/4, dry 7,5 YR 2,5/3; **Roots:** 14 roots dm^{-2};
10 cm Bw1	**Grain Size:** light clayey sand St2 (KA5)/LS (WRB); subangular structure; **Munsell Colour**: moist 7,5 YR 4/6, dry 7,5 YR 2,5/3; **Roots:** 30 roots dm^{-2}
30 cm Bw2	**Grain Size:** light clayey sand St2 (KA5)/LS (WRB); subangular structure; **Munsell Colour**: moist 7,5 YR 4/6, dry 7,5 YR 3/3; **Roots:** 25 roots dm^{-2}
50 cm Bwkc	**Grain Size:** light clayey sand St2 (KA5)/LS (WRB); subangular structure; **Munsell Colour**: moist 7,5 YR 5/6, dry 7,5 YR 4/4; **Roots:** 20 roots dm^{-2}
65 cm Bwkc	**Grain Size:** light clayey sand St2 (KA5)/LS (WRB); subangular structure; **Munsell Colour**: moist 7,5 YR 4/6, dry 7,5 YR 3/3; **Roots:** 15 roots dm^{-2};
75 cm Bwkm	**Grain Size:** light clayey sand St2 (KA5)/LS (WRB); subangular structure; **Munsell Colour**: moist 7,5 YR 4/6, dry 7,5 YR 3/3; **Roots:** 15 roots dm^{-2}; calcrete fragments +/- consolidated

Fig. 66: Description of profile 2131

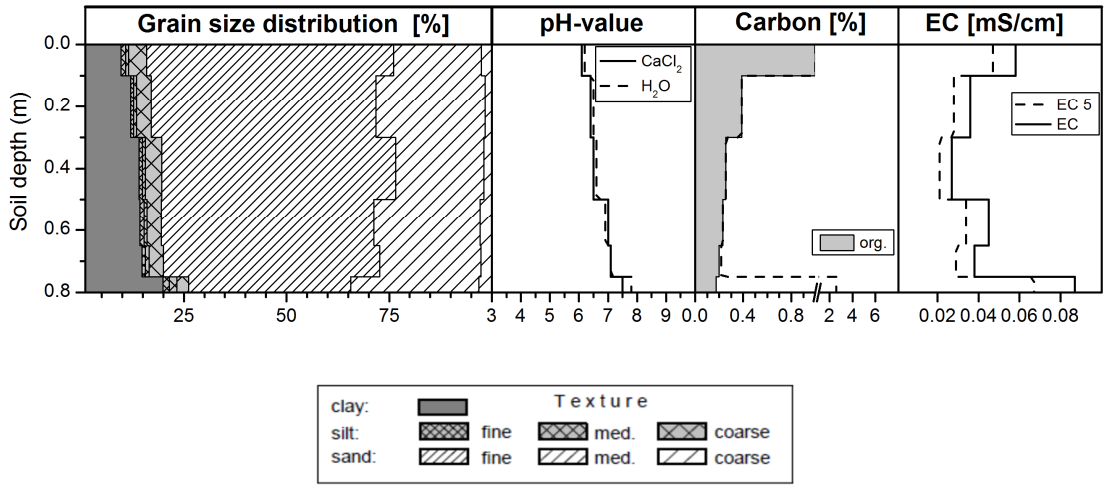

Fig. 67: Soil texture and chemical properties of profile 2131

Fig. 68: Environmental aspect and site impression of profile 2132

Profile 2132 is located only 30 m western from 2131 on an extensively managed field (Fig. 68). These two profiles exemplary show how soil properties can change within small distances. In contrast to the carbonate-rich profile 2131, profile 2132 is described as a Rubic Arenosol (Fig. 69), typically dominated by sand with fine sand as a major fraction and a slight increase of clay with depth from 6% to 9%. It is brownish colored in the upper 30 cm with a smooth transition to more yellowish-reddish in the lower parts indicating a weakly developed plow horizon. The soil reaction is light acidic throughout the whole profile. The carbon content is with 0.5 % on a low level in the upper 30 cm dropping to 0.2 % underneath (Fig. 70). Due to its bare condition at the time of surveying only single dead and dry roots were visible. The soil surface was dry without any crusting due to grazing and trampling impact by cattle.

Profile 2132	Lat: -17,88673°	Long: 20,21276°	1057 m h.s.l.	Loc.: Mashare / Namibia

Topography:	Slope:	Exposition:	Curvature:	Landscape unit:	Land use unit:	Crop:
Former levee	0°	/	plain	Old Floodplain	Dryland agriculture (D)	Maize

Remarks: Mashare Development Institute (MADI), off season, worked with hoe, no machining but ploughed and ribbed before, grazing impact

Ah	**Grain Size:** light clayey sand St2 (KA5)/S (WRB); single grain structure; **Munsell Colour**: moist 7,5 YR 4/4, dry 7,5 YR 5/6; **Roots:** 0 roots dm^{-2};
10 cm Bw1	**Grain Size:** light clayey sand St2 (KA5)/LS (WRB); light subangular structure; **Munsell Colour**: moist 7,5 YR 4/4, dry 7,5 YR 5/6; **Roots:** 10 roots dm^{-2};
30 cm Bw2	**Grain Size:** light clayey sand St2 (KA5)/LS (WRB); light subangular structure; **Munsell Colour**: moist 5 YR 4/4, dry 5 YR 5/6; **Roots:** 9 roots dm^{-2};
50 cm Bw3	**Grain Size:** light clayey sand St2 (KA5)/LS (WRB); light subangular structure; **Munsell Colour**: moist 5 YR 4/6, dry 5 YR 5/8; **Roots:** 5 roots dm^{-2};
70 cm Bw4 100 cm	**Grain Size:** light clayey sand St2 (KA5)/LS (WRB); light subangular structure; **Munsell Colour**: moist 5 YR 4/6, dry 5 YR 5/8; **Roots:** 6 roots dm^{-2};

Fig. 69: Description of profile 2132

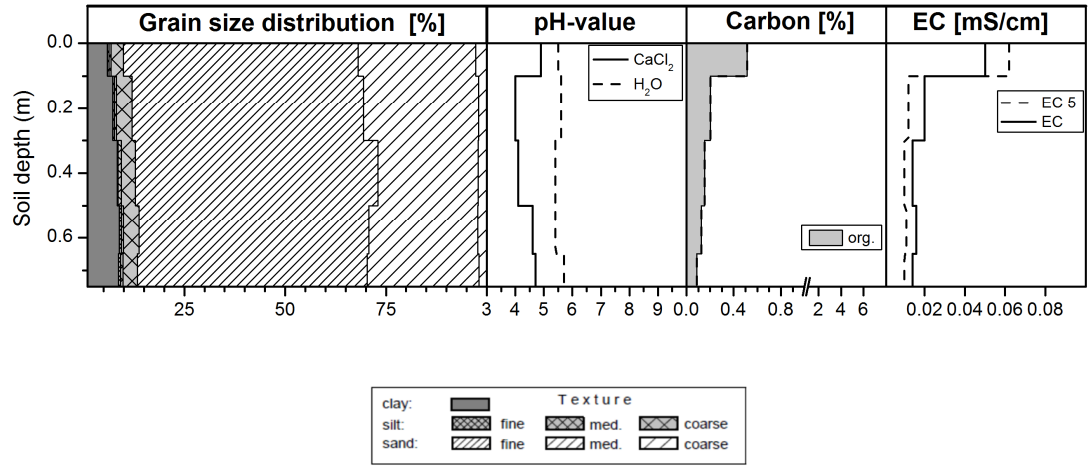

Fig. 70: Soil texture and chemical properties of profile 2132

Fig. 71: Environmental aspect and site impression of profile 2133

The homogeneous dark grey colored soil of profile 2133 is characteristic for soils developed out of fluvial parent material in the Kavango region. It is located in a former riverbed or a former depression where water was retained over time of flooding events. The soil is sparsely covered with litter over dry and loose bleached sand on the surface. The soil texture is fine and middle sand dominated loam with > 85 % Sand and depth increasing amounts of clay. The soil reaction is nearly neutral to weak acidic with high electric conductivity values in the top layer, which corresponds to the high amount of organic carbon with 3.6 %. More than 70 % of the total roots are concentrated in the upper 30 cm with the second horizon as the main root horizon.

Profile 2133	Lat: -17,89251°	Long: 20,22772°	1058 m h.s.l.	Loc.: Mashare / Namibia

Topography:	Slope:	Exposition:	Curvature:	Landscape unit:	Land use unit:	Vegetation:
Middle slope of former ephemeral riverbed	2°	S	plain	Old floodplain	Bushveld, grazing	shrubs

Remarks: Mashare Development Institute (MADI) grazing camp

Ah	**Grain Size:** light silty fine to middle grained sand (KA5)(field); single grain structure; **Munsell Colour**: moist 10 YR 4/1, dry 10 YR 5/2; **Roots:** 28 roots dm^{-2};
10 cm Bw1	**Grain Size:** light clayey sand St2 (KA5)/LS (WRB); light subangular structure; **Munsell Colour**: moist 10 YR 4/1, dry 10 YR 5/2; **Roots:** 50 roots dm^{-2};
30 cm Bw2	**Grain Size:** light clayey sand St2 (KA5)/LS (WRB); light subangular structure; **Munsell Colour**: moist 10 YR 4/1, dry 10 YR 5/2; **Roots:** 15 roots dm^{-2};
50 cm Bw3	**Grain Size:** light clayey sand St2 (KA5)/LS (WRB); light subangular structure; **Munsell Colour**: moist 10 YR 4/1, dry 10 YR 5/2; **Roots:** 7 roots dm^{-2};
75 cm Bw4 110 cm	**Grain Size:** light clayey sand St2 (KA5)/LS (WRB); light subangular structure; **Munsell Colour**: moist 10 YR 4/1, dry 10 YR 5/2; **Roots:** 3 roots dm^{-2};

Fig. 72: Description of profile 2133

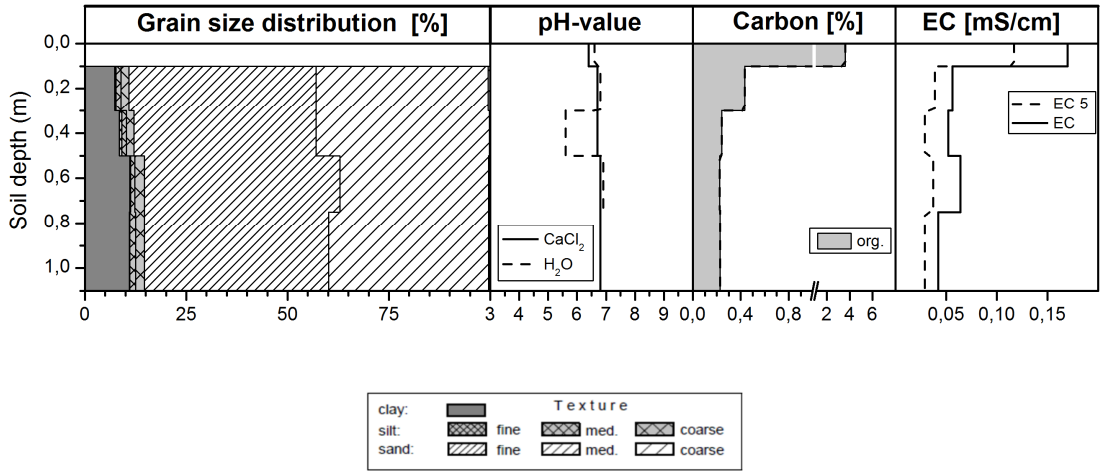

Fig. 73: Soil texture and chemical properties of profile 2133

Fig. 74: Environmental aspect and site impression of profile 2030

The profile 2030 represents a typical soil of the Kalahari dune area with light reddish brown soil color in upper profile areas and red brownish coloring in deeper areas (Fig. 75). According to the WRB taxonomy, it is classified as a Rubic Arenosol. The soil texture is homogenously sandy with negligible little amounts of clay and silt. The soil reaction is moderately acidic with a low organic carbon concentration in the topsoil (Fig. 76). Although this site is extensively used for grazing the vegetation is fairly thick with bushes and shrubs and only little understory vegetation (Fig. 74). The main rooting area is focused on a depth to 40 cm with singular main roots in areas below. The appearance of charcoal, in major proportions within the first 40 cm of the profile, indicates a periodical to episodic fire regime.

Profile 2030	Lat: -17,91439°	Long: 20,20790°	1088 m h.s.l.	Loc.: Mashare / Namibia

Topography:	Slope:	Exposition:	Curvature:	Landscape unit:	Land use unit:	Vegetation / Crop:
	1°	ENE	undulated	Kalahari dune area	Grazing (G)	Acacia, bushes

Remarks: Mashare grazing camp beside Road

	Grain Size: fine to medium sand S (KA5)/S (WRB); single grain structure; **Munsell Colour**: moist 7,5 YR 2,5/3, dry 7,5 YR 4/4; **Roots:** 22 roots dm^{-2};
10 cm	**Grain Size:** fine to medium sand S (KA5)/S (WRB); single grain structure; **Munsell Colour**: moist 7,5 YR 2,5/3, dry 7,5 YR 4/4; **Roots:** 32 roots dm^{-2};
40 cm	**Grain Size:** fine to medium sand S (KA5)/S (WRB); single grain structure; **Munsell Colour**: moist 5 YR 4/4, dry 5 YR 4/6; **Roots:** 3 roots dm^{-2};
70 cm	**Grain Size:** fine to medium sand S (KA5)/S (WRB); single grain structure; **Munsell Colour**: moist 5 YR 4/4, dry 5 YR 4/6; **Roots:** 2 roots dm^{-2};
150 cm	

Fig. 75: Description of profile 2030

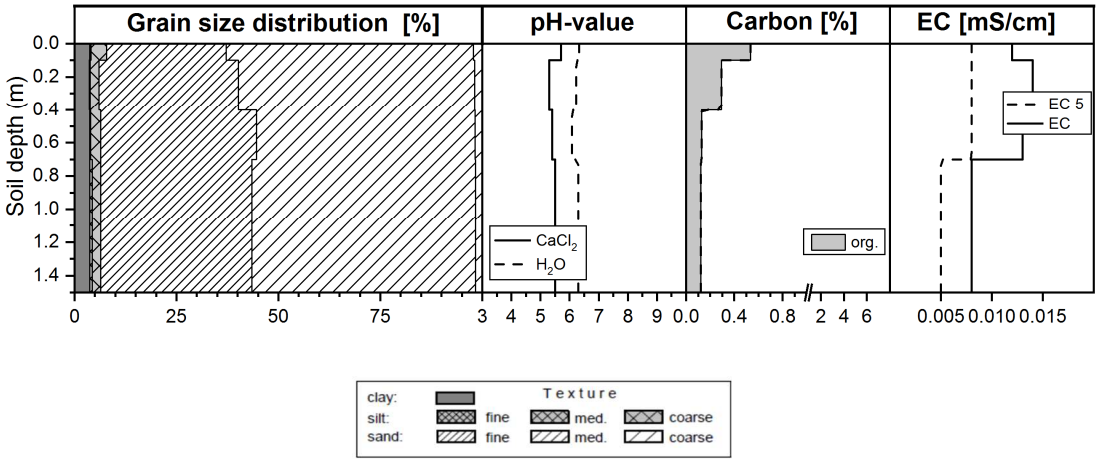

Fig. 76: Soil texture and chemical properties of profile 2030

6.2.2. Soil hydrological properties

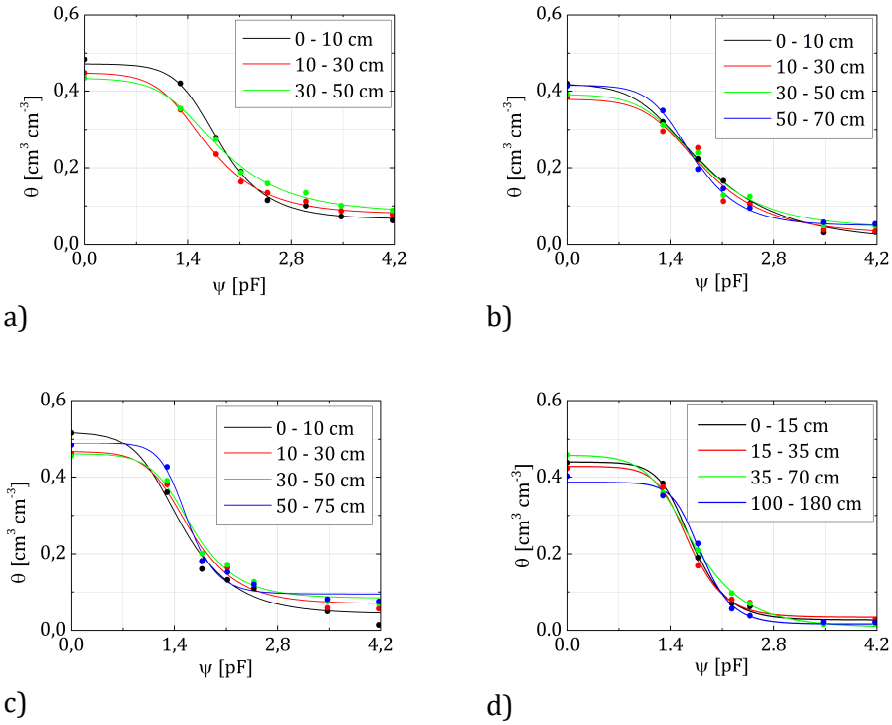

Fig. 77: Water retention curves for profiles (a) 2131, (b) 2132, (c) 2133 and (d) 2030

Four profiles were analyzed with respect to their soil hydraulic properties representing the soils of the Kalahari dune area and the old floodplains of the Mashare study site. The, in general, more loamy texture of the old floodplain soils is reflected by the soil water retention characteristics (Tab. 11). With an increase in bulk densities with depth, θ_s decreases from maximum water contents of 0.52 $cm^3\ cm^{-3}$ in the first horizon of profile 2133 to a minimum of 0.41 $cm^3\ cm^{-3}$ in the bottom-most layer in profile 2132. The retention curve shapes (Fig. 77) of the old floodplain profiles (2131 – 2133) are further on almost similar going into higher soil water pressure heads, only profile 2133 shows a sandier type of retention. The water contents at field capacity range from 0.16 $cm^3\ cm^{-3}$ in the topsoil of profile 2133 to 0.28 $cm^3\ cm^{-3}$ in the respective depth of profile 2131. Due to the amount of clay, the PWP is increased (besides 2133) at volumes of 0.03 $cm^3\ cm^{-3}$ in the first horizon of 2132 to 0.09 $cm^3\ cm^{-3}$ in the deepest horizon of 2131. In result, the uFC volumes range between 0.10 $cm^3\ cm^{-3}$ and 0.22 $cm^3\ cm^{-3}$ according to texture and bulk densities.

By looking at the retention characteristics of the Kalahari dune area profile 2030, the sandy texture of that soil is represented by the retention with a low PWP and medium uFC

values. Due to the near absence of clay, the PWP is at 0.02 $cm^3\ cm^{-3}$ and the field capacity ranges between 0.17 $cm^3\ cm^{-3}$ in the second horizon and 0.23 $cm^3\ cm^{-3}$ in 100 cm depth. In general, the retention curve in Fig. 77 shows a steep development with increasing pressure heads, which is typical for sandy texture. It is in parts comparable to the retention of profile 2133 but with lower PWP due to the lack of clay impact.

Tab. 11: Soil hydrological characteristics of the studied horizons at the Mashare site.

Horizon	Upper [cm]	Lower [cm]	θ_s [$cm^3\ cm^{-3}$]	PWP [$cm^3\ cm^{-3}$]	FC [$cm^3\ cm^{-3}$]	uFC [$cm^3\ cm^{-3}$]
2131_1	0	10	0.48	0.06	0.28	0.22
2131_2	10	30	0.45	0.08	0.24	0.16
2131_3	30	50	0.43	0.09	0.28	0.19
2132_1	0	10	0.42	0.03	0.22	0.19
2132_2	10	30	0.38	0.03	0.25	0.22
2132_3	30	50	0.39	0.04	0.24	0.20
2132_4	50	70	0.41	0.05	0.20	0.15
2133_1	0	10	0.52	0.01	0.16	0.15
2133_2	10	30	0.46	0.06	0.18	0.12
2133_3	30	50	0.45	0.07	0.20	0.13
2133_4	50	75	0.48	0.08	0.18	0.10
2030_1	0	15	0.44	0.02	0.19	0.17
2030_2	15	35	0.42	0.02	0.17	0.15
2030_3	35	70	0.46	0.02	0.21	0.19
2030_4	100	180	0.40	0.02	0.23	021

According to the procedure of the derivation of the representative simulation input parameter carried out in section 5.2.2, a combined fitting of van Genuchten-Mualem retention and conductivity parameter result in two parameter sets, representing the Kalahari dune area (Mkda) and old floodplains (Mofp), shown in Tab. 12. The associated diagrams in Fig. 78 illustrate the differences in retention and conductivity development with changing hydraulic heads.

Tab. 12: Derived van Genuchten-Mualem parameter for the Kalahari dune areas and the old floodplain soils of Mashare

Plot	θ_r [$cm^3\ cm^{-3}$]	θ_s [$cm^3\ cm^{-3}$]	α	n	K_s [$cm\ d^{-1}$]	l
Mkda	0.027	0.439	0.0260	2.918	712.8	2.808
Mofp	0.083	0.433	0.0284	1.587	350.2	1.540

While θ_s volumes are nearly the same in both parameter-sets the PWP volumes differ, with 0.027 $cm^3\ cm^{-3}$ in the Mkda set and 0.093 $cm^3\ cm^{-3}$ in the old floodplain. At field capacity the difference in slope steepness is obvious. Where the old floodplain soil still has 0.31 $cm^3\ cm^{-3}$ the Kalahari parameter sets reveals a volume of only nearly the half with 0.18 $cm^3\ cm^{-3}$. At pF 2.5 the sandy texture is already near the volume of the PWP whereas the loamy set of the old floodplains still shows a water content of 0.18 $cm^3\ cm^{-3}$.

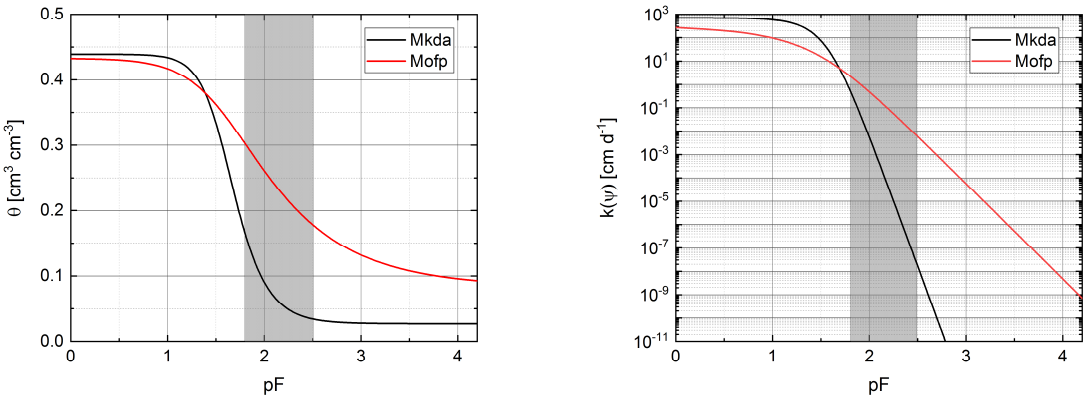

a) b)

Fig. 78: Diagram of the resulting soil hydrological retention (a) and conductivity functions (b) according to the fitted van Genuchten-Mualem parameters for the Kalahari dune area (Mkda) and the old floodplain (Mofp) profiles in Mashare.

This significant difference in retention has a considerable impact on soil water redistribution processes and dynamics, which can be explained by taking the conductivity function in Fig. 78b into account. While the old floodplain conductivity shows a slight decrease in unsaturated conductivities with increasing pressure heads, the decrease is very pronounced within the Kalahari dune area relation after passing the air entry point. Both curve progressions meet at a certain point where conductivities are the same to diverge again with increasing pressure heads. At pF 1.8, the Kalahari set shows an unsaturated conductivity of $8.97 \cdot 10^{-1}$ cm d^{-1}, whereas the old floodplains reveal higher rates with 2.76 cm d^{-1}. In consequence, the old floodplain soil can translocate higher amounts in times with higher water contents near or below field capacity, whereas the Kalahari sand redistributes only in near saturation conditions, at higher pressure heads a lack of pore water together with low conductivities prevents percolation processes. The loamy old floodplain soils show higher unsaturated conductivities in pF ranges > 2.5 where capillary

forces compensate gravitation which results in a pronounced support of evaporation fluxes whereas these fluxes are reduced in the sandy substrates of the Kalahari dune area.

6.2.3. Weather forcing data

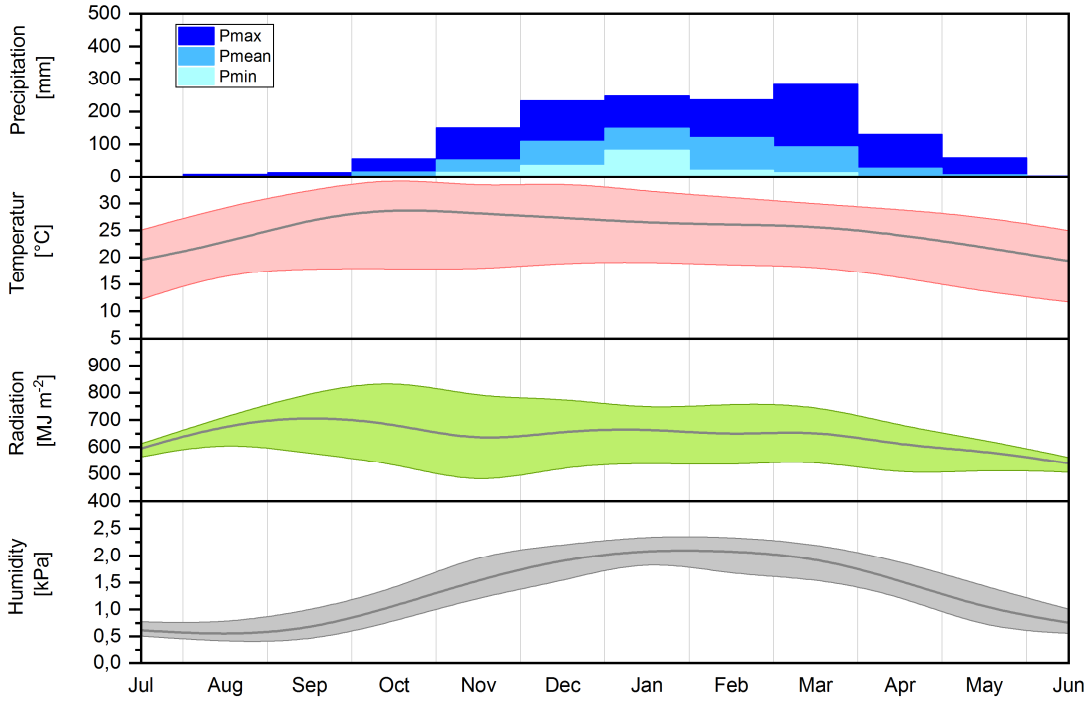

Fig. 79: Diagram showing the 30year ERA-INTERM Dataset for the study site Mashare as monthly means for temperature and humidity as well as monthly sums for radiation and precipitation (with minimum and maximum). The grey lines represent mean values whereas the colored areas showing the span between minimum and maximum.

Fig. 79 shows the weather input data for Mashare as long year monthly sums for radiation and precipitation as well as monthly means for temperature and humidity. With 580.6 ± 106.5 mm annual precipitation and a mean annual potential evaporation of 2127.9 ± 60.3 mm the dataset shows a clear semi-arid character with an aridity index of 0.27 and a climatic water deficit of -1547.3 mm. The rainfall variability, described by the relation between standard deviation and the 30 years mean, is 18 %.

6.3. Land-use impact on modeled soil water dynamics

6.3.1. Scenario description

In contrast to the Cusseque simulations, the Mashare land use scenarios are extended by two additional conditions. The pristine conditions are extended by a less dense scenario

representing open bushvelds whereas the land use scenarios are supplemented by a commercialized irrigation agriculture scenario with a crop rotation of winter Wheat over the dry season and Maize over the rainy season. In Tab. 13 a scenario overview is given including simulation periods and abbreviations used in the following sections. In result, six different land use and vegetation scenarios on two different soils built the basis for a subsequent evaluation of the land use and vegetation induced impacts on water resources and of the effectiveness of vegetation water consumption in relation to the gross atmospherical water supply by precipitation.

Tab. 13: Scenario overview Mashare

Plot	Land use/vegetation	Simulation period	Abbreviation
Mashare Kalahari dune area (Mkda)	Bare soil (B)	1980 - 2010	MkdaB
	Grass (Gr)		MkdaGr
	Open woodland (Wo)		MkdaWo
	Dense woodland (Wd)		MkdaWd
	Dryland agriculture Maize (Ma)		MkdaMa
	Irrigated crop rotation Wheat/Maize (MaWi)		MkdaMaWi
Mashare old floodplains (Mofp)	Bare soil (B)	1980 - 2010	MofpB
	Grass (Gr)		MofpGr
	Open woodland (Wo)		MofpWo
	Dense woodland (Wd)		MofpWd
	Dryland agriculture Maize (Ma)		MofpMa
	Irrigated crop rotation Wheat/Maize (MaWi)		MofpMaWi

6.3.2. Land-use on Arenosols of the Kalahari dune areas in Mashare

Fig. 80 illustrates the differences in soil water dynamics according to the assumed scenarios with respect to pristine vegetation and identical soil parameter and weather data input. With these assumptions, the bare soil scenario shows, as a reference for the later evaluation of vegetation influences, the unaffected state of dynamics throughout the rainy season with its onset in September and the last rains in April. Since the atmospherical water vapor demand is fairly high at the beginning of the rainy season the first infiltrated water appears in the upper soil layers with a lag of one month when the cumulative infiltration depth exceeds the cumulative actual bare soil evaporation. From that point onwards, the whole profile increases its water content from 7 Vol% in the topsoil regions

and 10 Vol% in the subsoil to its mean maximum water content of 15 Vol% onto a depth of 300 cm by the middle of the rainy season. With decreasing precipitation amounts the appearing drying front moves from top to the bottom of the profile until the initial soil

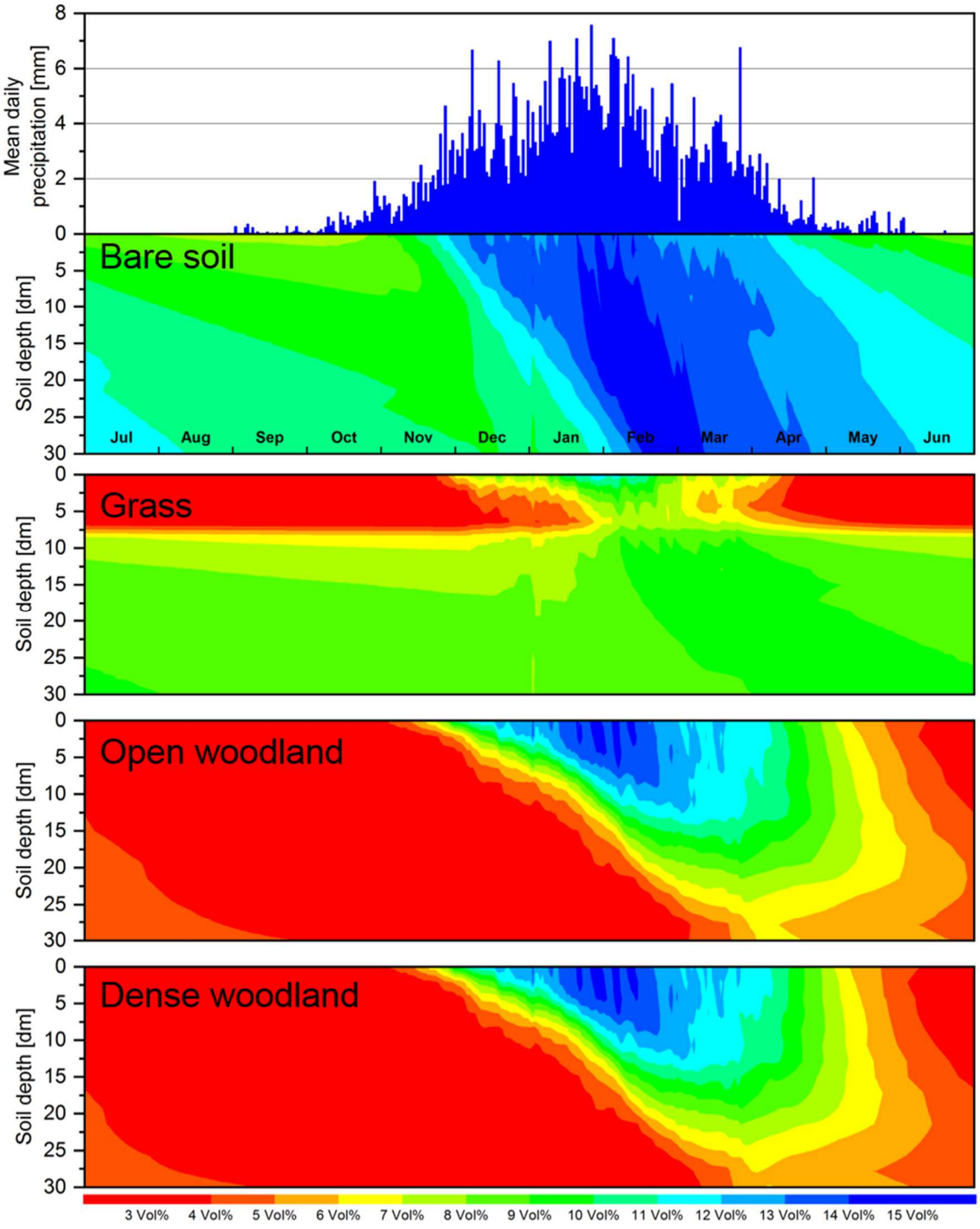

Fig. 80: Mean daily water content for a period from July to June based on a 30-year model run for bare soil conditions and three different pristine land cover scenarios in the Kalahari dune area of the Mashare study site

water conditions at the onset of the next rainy season are re-established. The observable mean soil water difference at the beginning of the rainy season spans over 9 Vol% in 300 cm depth to 7 Vol% in the topsoil. This difference reverses and has a maximum in the first third of the rainy season with 10 Vol% at the bottom to 14 Vol% in the topsoil to be reversed again at the outgoing season with 12 Vol% in the subsoil and 9 Vol% in the topsoil.

The assumed grassland cover modifies the reference scenario due to the additional root water extraction onto a depth 80 cm and slightly beyond. In September the mean soil water difference between subsoil and topsoil is 6 Vol%. Due to the soil coverage and the additional transpiration sink, the first infiltrated water encloses dryer layers between 50 cm and the bottom of the by roots affected layers in 125 cm depth. In the middle of the season cumulative precipitations are able to almost level out the soil profile water contents to a mean maximum of 12 Vol% in the topsoil and 9 Vol% to 10 Vol% in the subsoil layers. With decreasing rains, transpiration processes start to form layers with lower water content in areas between 25 cm to 80 cm while water still infiltrates into the topsoil. From that point on, with the absence of rain, the soil water content in the topsoil drops to the level of the PWP to a depth of 80 cm. In contrast to the bare soil reference the soil dynamic of the deepest layer is not affected by either percolated water or capillary rise due to evapotranspiration processes at mean water contents of 8 Vol% to 9Vol%.

Both woodland scenarios show a completely different pattern of drying and wetting cycles within the profile. It is similar the pattern of the woodland scenario in Cusseque but with a more pronounced dynamic. At the beginning of the hydrological year, the whole profile is dry onto the bottom at 3 Vol%. With the onset of the rainy season, the bottom of the profile remains dry until the middle of the season. Before the first infiltrated water reaches the bottom the difference between topsoil and subsoil increases to 12 Vol%. Compared to the bare soil reference soil water contents at the bottom do not exceed the amount of 7 Vol% in the middle of the season while topsoil water contents rise to 15 Vol%. With decreasing rains, the whole profile dries out almost uniformly to the PWP due to the root water extraction onto the bottom, hence the turn over time of infiltrated water matches one hydrological year.

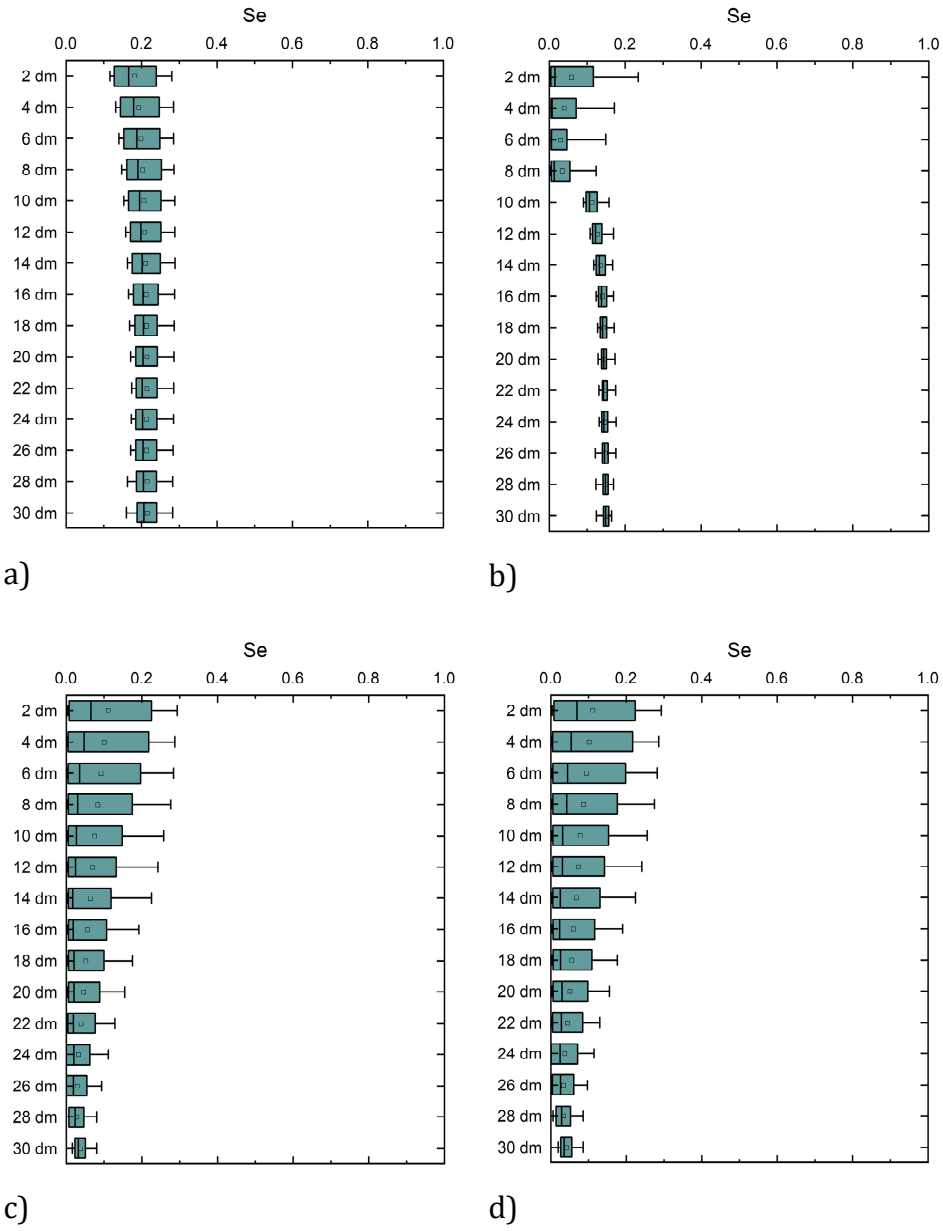

Fig. 81: Boxplots showing the long year simulated effective saturation (Se) at 20 cm soil layer resolution down to 300 cm for pristine conditions of the Kalahari dune area in Mashare. a) Bare soil, b) Grass, c) Dense woodland, d) Open woodland

Fig. 81a-d compare, in a condensed way, the already mentioned differences in soil water dynamics of the pristine vegetation scenarios and the bare soil reference. The bare soil scenario shows almost equally distributed soil water dynamics with respect to depth with slightly higher variabilities in the topsoil layers. However, the grass scenario evolves a higher variability of soil water contents in the root zone to 80 cm depth and lowers compared to the bare soil scenario the subsoil variability together with decreased mean water contents. The influence of deep rooting trees in both woodland scenarios showing its effect on the deepest areas of the simulated profile. While the bare soil and grass scenario

keeps a certain amount of unutilized water in the subsoil, the woodland scenario turns over almost all. Additionally, the overall dynamic of this scenario is the highest among all and shows a decrease with profile depth with lower mean effective saturation at the same time.

To focus on the consequences of the described soil water dynamics in section 6.4 this paragraph describes the resulting water balances of the pristine scenarios. As expected Fig. 82 shows that the actual evaporation amounts of the bare soil reference follow the course of the rainfall development with a maximum of 69 mm or 38 % of the potential evaporation in January and a slight asymptotic decrease until the end of the hydrological year in June. Deep drainage occurs the whole year around fed by the remaining water which is stored in deeper layers and not supplied to evaporation. The maximum rate of drainage appears related to the maximum precipitation input two months later in March after the soil buffer reaches its turn-over point from an increase to a decrease. The relation of the seasonal evaporation and the bottom flux sums is 1.03 (see Tab. 14) indicating a well-balanced relation between these two components.

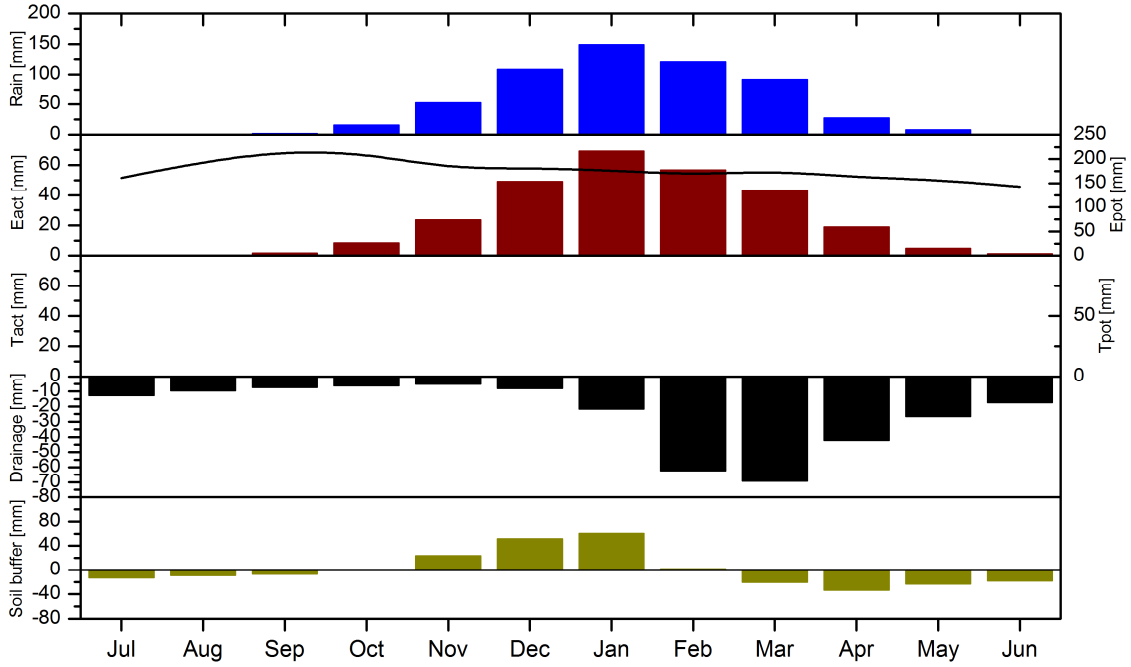

Fig. 82: Monthly mean soil water balance components for the bare soil scenario at the Kalahari dune areas of Mashare. The lines represent the monthly course of Epot and Tpot

Due to the parametrization of the grassland scenario, the seasonal course of the transpiration is governed by the amount of plant available water within the rooting zone (Fig.

83). As shown, grass utilizes all the available water in the root zone at the end of the rainy season. Subsequently, transpiration rates go to zero, which marks the initial condition for the following rainy season. Having this in mind the development of the transpiration rates starts with 0 mm and increases with increasing available soil water due to precipitation input. In February the transpiration reaches its maximum with 94 mm or 78 % of the potential transpiration. The lag of one month between precipitation maximum and transpiration maximum can also be explained by the lagged soil buffer level rise to support maximum transpiration rates. After this maximum, the rates go down again until the available root zone water content is depleted. The highest level of soil water buffering in January indicates the time of the season, where the water contents throughout the soil profile are nearly leveled and percolation into deeper soil layers can occur. As a consequence, bottom fluxes start to increase but on a very low level with a maximum of 11 mm compared to the bare soil reference. Nearly two-thirds of the buffered soil water is supplied to the evapotranspiration, consequently, only one-third yields deep drainage. The seasonal budget in Tab. 14 show that vegetation induced losses by interception and transpiration account for nearly five times the amount of the seasonal sum of evaporation and bottom flux together. Which is to be found due to low evaporation losses by shading effects of the vegetation.

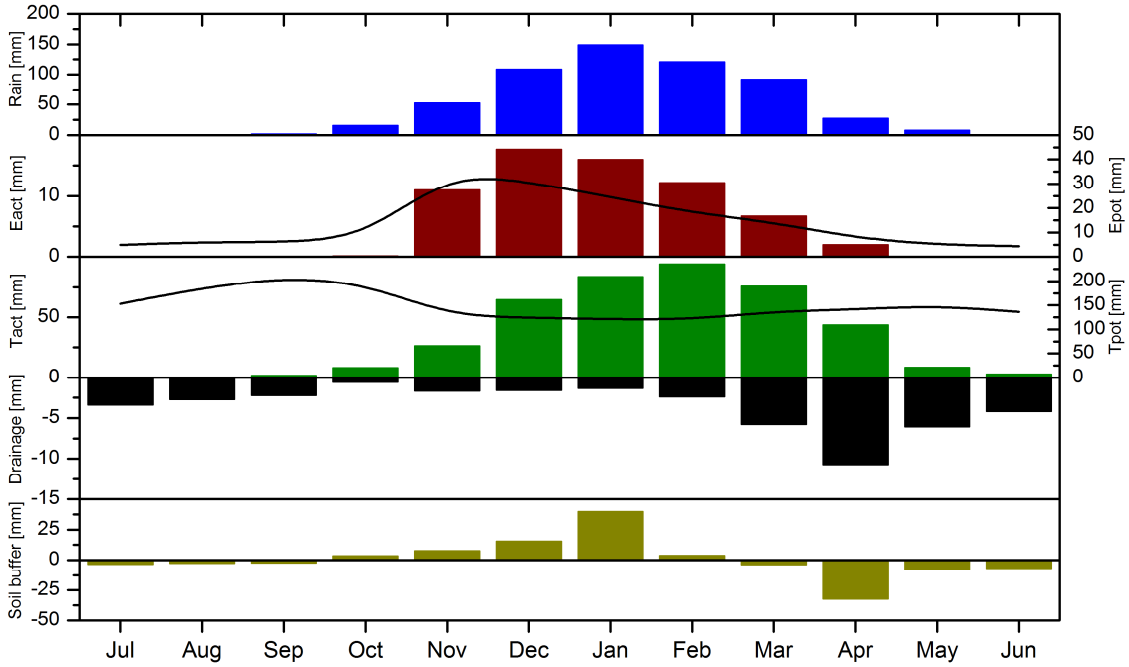

Fig. 83: Monthly mean soil water balance components for the grassland scenario at the Kalahari dune areas of Mashare. The lines represent the monthly course of Epot and Tpot

Similar to the parametrization of the grassland vegetation the transpiration course of the woodland scenarios, dense and open as well, is controlled by the plant available soil water within the root zone. Since the maximum rooting depth of the woodland scenarios is set to 300 cm the potential amount of available soil water is 3.75 times higher compared to grasslands. With the phenological development of the woody vegetation with a more pronounced dynamic as it is parameterized for the grasslands, the maximum transpiration is reached at a time where LAI and soil water availability is at optimum in April, with 62 mm for open woodland conditions and 73 mm for dense equals 88 % of the potential transpiration (Fig. 84 and Fig. 85).

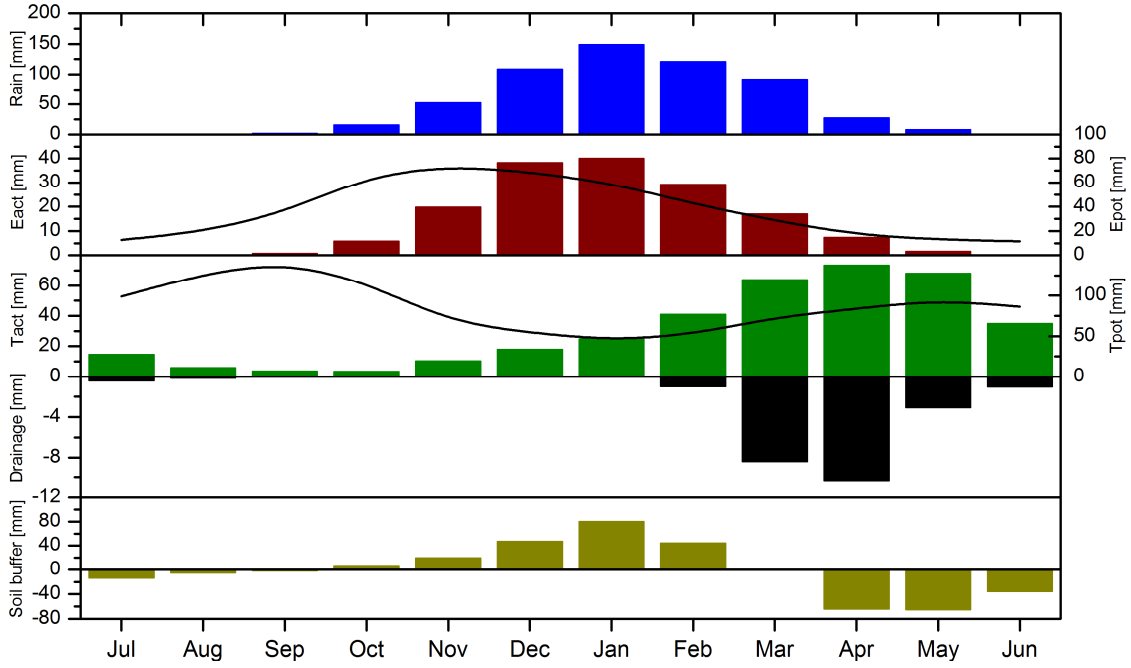

Fig. 84: Monthly mean soil water balance components for the dense woodland scenario at the Kalahari dune areas of Mashare. The lines represent the monthly course of Epot and Tpot

The soil buffer sustains transpiration processes at a high to a medium level even with little or no more precipitation input at the end of the hydrological year. At the beginning of the following year woodlands still can utilize soil water and maintain low transpiration rates until the onset of the next rainy season. As a result of the periodically variable soil coverage due to the phenological leaf development, evaporation rates are higher than in the grassland scenario where the soil coverage was assumed to be between 80% and 100%. The maximum of about 40 mm evaporation correlates with the maximum precipitation input in January but the seasonal evaporation sum is reduced by shading effects in relation to the bare soil reference by 44 %.

Tab. 14: Long year means of water balance components for the pristine condition scenarios in the Kalahari dune areas of Mashare

Scenario	Interception [mm a^{-1}]	Transpiration [mm a^{-1}]	Evaporation [mm a^{-1}]	Bottom flux [mm a^{-1}]
MkdaB	0.0	0.0	285.6	294.9
MkdaGr	52.8	427.9	60.4	42.4
MkdaWd	26.1	374.5	158.5	21.5
MkdaWo	38.3	356.5	162.0	23.8

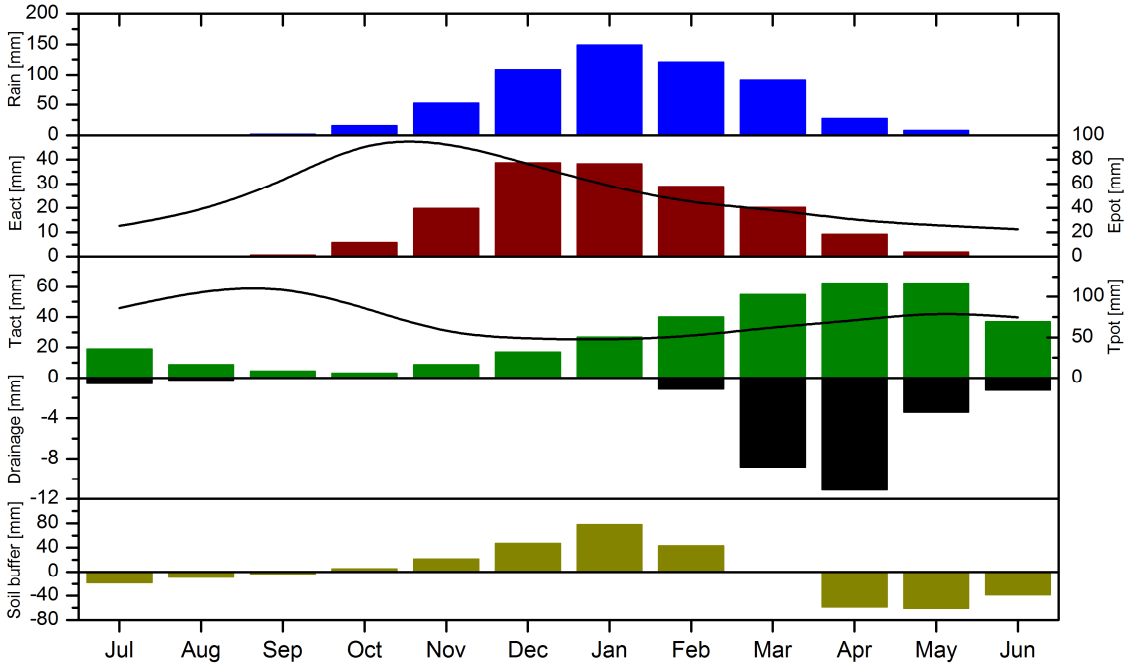

Fig. 85: Monthly mean soil water balance components for the open woodland scenario at the Kalahari dune areas of Mashare. The lines represent the monthly course of Epot and Tpot

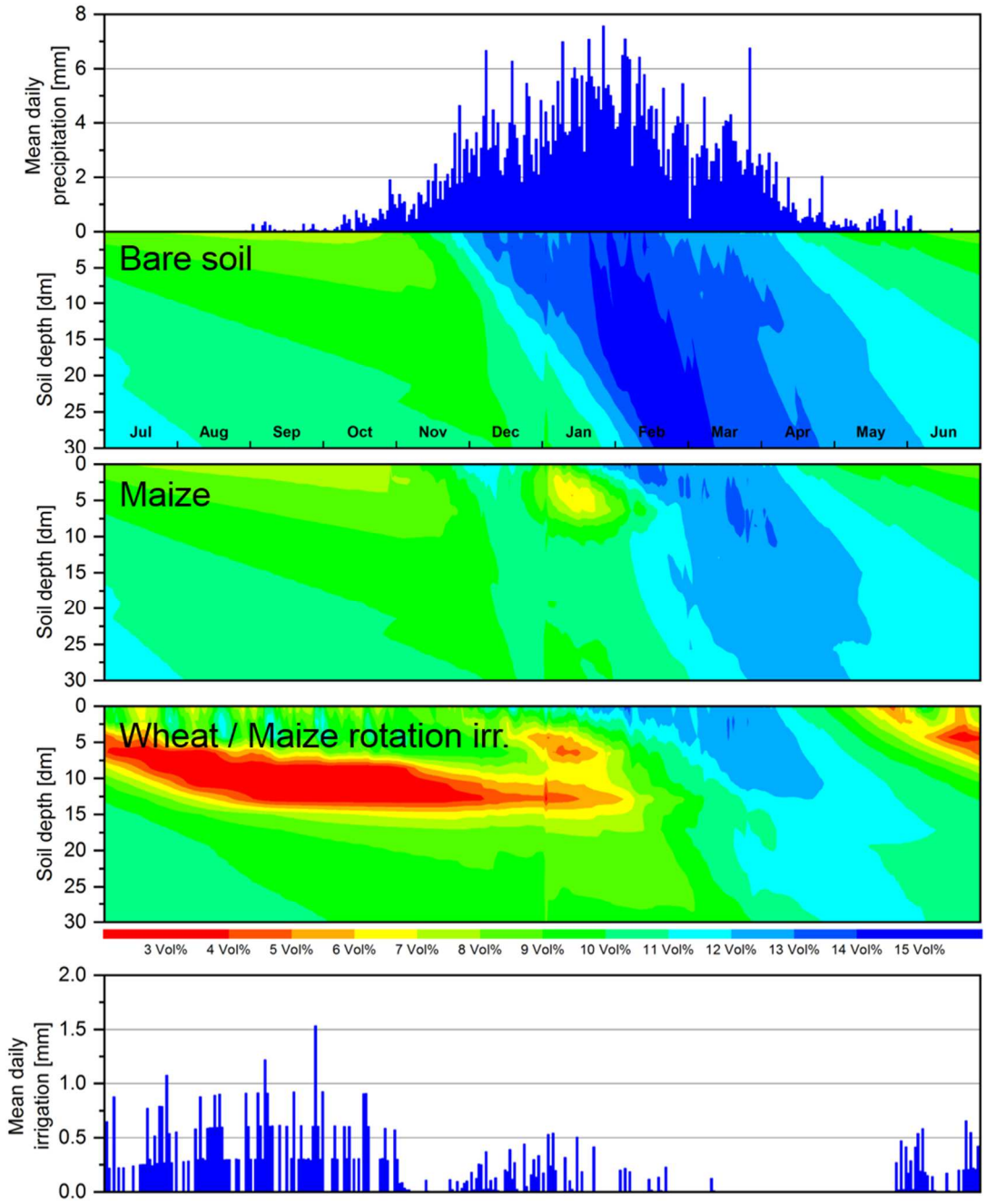

Fig. 86: Mean daily water content for a period from July to June based on a 30-year model run for bare soil conditions and two different cropping scenarios in the Kalahari dune area of the Mashare study site.

Compared to the pristine conditions the cropping scenarios in Fig. 86 show divergent soil water patterns according to the changed rooting characteristics, phenological development and transpiration reduction functions. The irrigation scenario represents a special case, where an additional water input in combination with a two-staged cropping rotation includes the dry season and therefore artificially modifies the soil water dynamics.

Looking at the Maize scenario, the beginning of the hydrological year in July shows no significant difference compared to the bare soil scenario. With the emergence of the first Maize shoots in November with an initial shallow rooting depth and low soil coverage, the soil water content gets diminished only in a small proportion. At the beginning of December, the water contents are even a little higher in the topsoil due to the lowering effects on the evaporation rates by leaf shading which are at the same time not compensated by transpiration. With the ongoing cropping season, the rooting depth and the soil coverage increases until the crop reaches its mature stage in January with a maximum rooting depth of 100 cm and an LAI of 1.2. At that time the soil water content of the first 100 cm is diminished significantly to a level of about 7 Vol% whereas the areas underneath the root zone receive only little to no percolation input. After the harvest in March infiltrating precipitation can increase the water contents to a level of 12 Vol% down to the bottom of the profile but without reaching the amounts as simulated in the bare soil scenario. At the end of the hydrological year in June, the water contents reach the amounts of the reference scenario.

The industrial type of agricultural practice under irrigation, as assumed in the second cropping scenarios, is characterized by a much higher plant density and a second crop type in rotation with maize. The additional irrigation input as it is set in the irrigation scheme of the model reacts to a defined threshold of soil hydraulic heads in a depth of 30 cm. When this -1000 hPa threshold is reached, the input is calculated according to the necessary amount of irrigation water to rewet the reference layer in 30 cm back to field capacity.

Starting the rotation with Maize in November, the initial vertical soil water distribution, formed by the outgoing wheat period, shows a vertical sequence of fairly moist topsoil conditions followed by a dry layer between 75 cm and 150 cm with a minimum water content near the PWP. Going deeper the contents increase again to amounts comparable to those in the topsoil. Because of the incoming precipitation, the topsoil stays at a moisture level above the irrigation threshold where no additional water input is needed. With the ongoing phenological development of Maize, the rooting zone and the LAI increases together with the transpiration water demand and the irrigation scheme reacts with additional inputs. While the still present dry layer shrinks in expansion due to a downward moving wetting front and capillary rise from the bottom, a second dry layer forms, as a

reaction of root water extraction, from 30 cm to 75 cm depth. By arriving in the middle of the rainy season in January the crop reaches its mature state where the rooting depth and the LAI is at maximum and the incoming precipitation is sufficient to keep the topsoil above the irrigation threshold. In the following two months the crop dries out and the transpiration demand drops to zero. The incoming rains now infiltrate and percolating water reaches greater depths to increase the water content in 300 cm to 12 Vol%. At the end of the Maize period, the vertical soil water distribution shows a downward orientated increase of moisture with 9 Vol% in the topsoil and 12 Vol% in 300 cm depths.

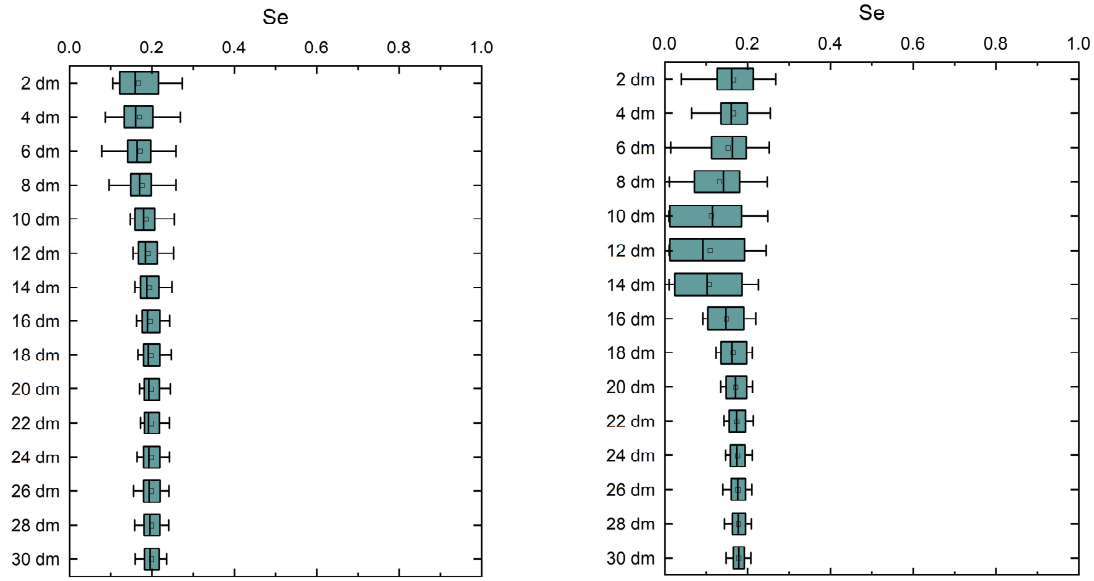

a) b)

Fig. 87: Boxplots showing the long year simulated effective saturation (Se) at 20 cm soil layer resolution down to 300 cm for cropping conditions of the Kalahari dune area in Mashare. a) Maize, b) Wheat-Maize rotation under irrigation

This marks the initial soil water conditions at the beginning of the Wheat period in April. Since the transpiration demand by the young plants in April is still low, the root water uptake does not lead to a rapid diminution of water in the topsoil and the incoming precipitation is sufficient enough to contribute to transpiration. When the crop reaches the next phenological stage the transpiration demand increases and the irrigation sets in at the end of May. This pulsed irrigation input introduces a wetting front which cannot enter the soil deep enough to form a uniform wetting regime. In contrary, continued root water uptake and reduced evaporation dynamics due to leaf shading begin to form the previous mentioned dry layers in 30 cm at the end of the hydrological year in June. The ongoing

root growth explores more and more of the deeper laying soil areas until the rooting system is fully developed at the end of August with its maximum depth of 150 cm. While precipitation is missing in the middle of the dry season in July, it has to be substituted by irrigation input to sustain a sufficient amount of transpirable amount of soil water. In this situation, the dry layer with minimum water contents appears to be a barrier for down-moving wetting fronts introduced by irrigation. It is stable in dimension until the Wheat is harvested in October and the sowing of Maize begins in November, where precipitation can infiltrate and transpiration is on a low level.

In Fig. 87b the mentioned dry layer is indicated by the highly variable long year means of the effective saturation in depth of 80 cm to 140 cm. Even though with the additional irrigation input of 600 mm, compared to the dryland agricultural simulation of Maize, there are no significant differences visible beneath the depth 180 cm. The mean values of the irrigation simulation are a little lower but with a similar variability which reflects that no irrigation water penetrates the dry layer and increase the water contents down to the bottom.

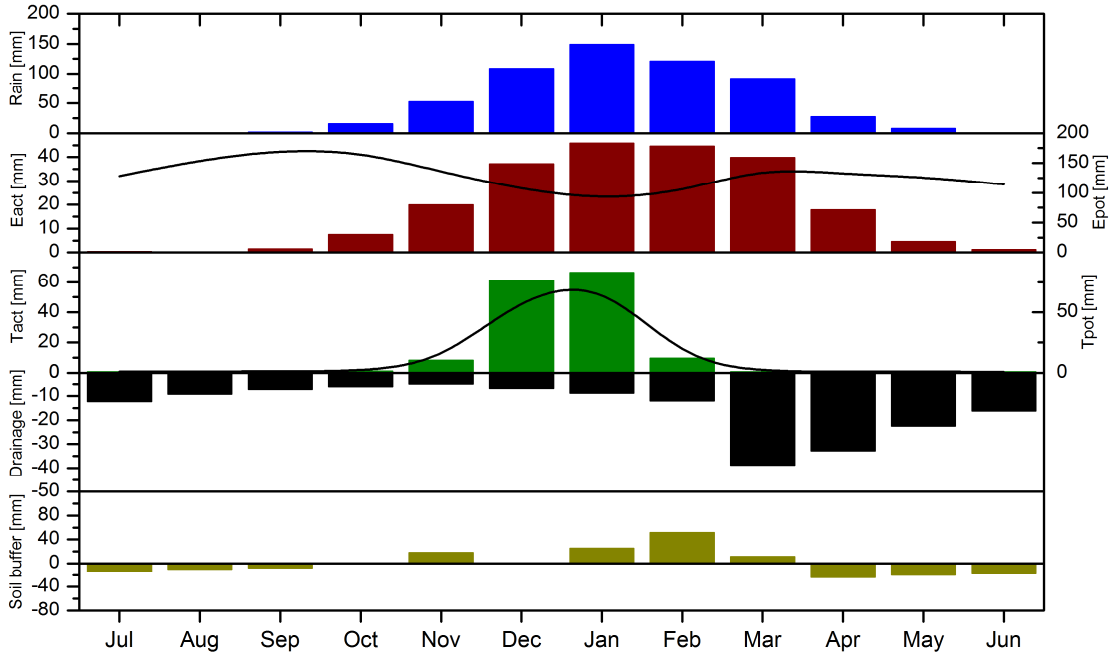

Fig. 88: Monthly mean soil water balance components for the maize scenario at the Kalahari dune areas of Mashare. The lines represent the monthly course of Epot and Tpot

Fig. 88 shows that at the beginning of the hydrological year, the sink components deep drainage and evaporation get their input from the still available soil water, concentrated

in deeper layers of the profile. Therefore, the deep drainage processes outweigh the evaporation rates. This dynamic continues until the first rains set in September where simultaneously the soil buffer leveling is nearly balanced. The relation between deep drainage and evaporation gets reversed with increasing evaporation rates due to infiltrated water in the topsoil regions. With the beginning of the phenological cycle of Maize transpiration rates increase starting in November with a maximum of 66 mm in January where the relationship between the actual transpiration and the potential is 0.88. The evaporation rates increase at that time to a level of 45 mm which indicates the high level of atmospheric demand. Looking at the relationship between actual and potential evaporation it reveals the low potential of the soil to deliver soil moister, due to its limited capillarity, to the atmosphere. Deep drainage still occurs in times with high transpiration rates due to relatively high percolation rates into the subsoil. With the end of the phenological cycle towards the harvest, transpiration rates drop at the times of crop drying. Without leaf shading effects and transpiration together with decreasing evaporation rates, deep percolation processes lead to an increase in bottom flux rates in March with the all year maximum of 38 mm. The ongoing decrease of rain input in the following month lead to a subsequent decrease of both, evaporation and deep drainage. This dynamic continues with respect to bottom flux rates until the onset of the following rainy season. While evaporation rates drop to zero, drainage can be sustained at a mean dry season level of about 11 mm.

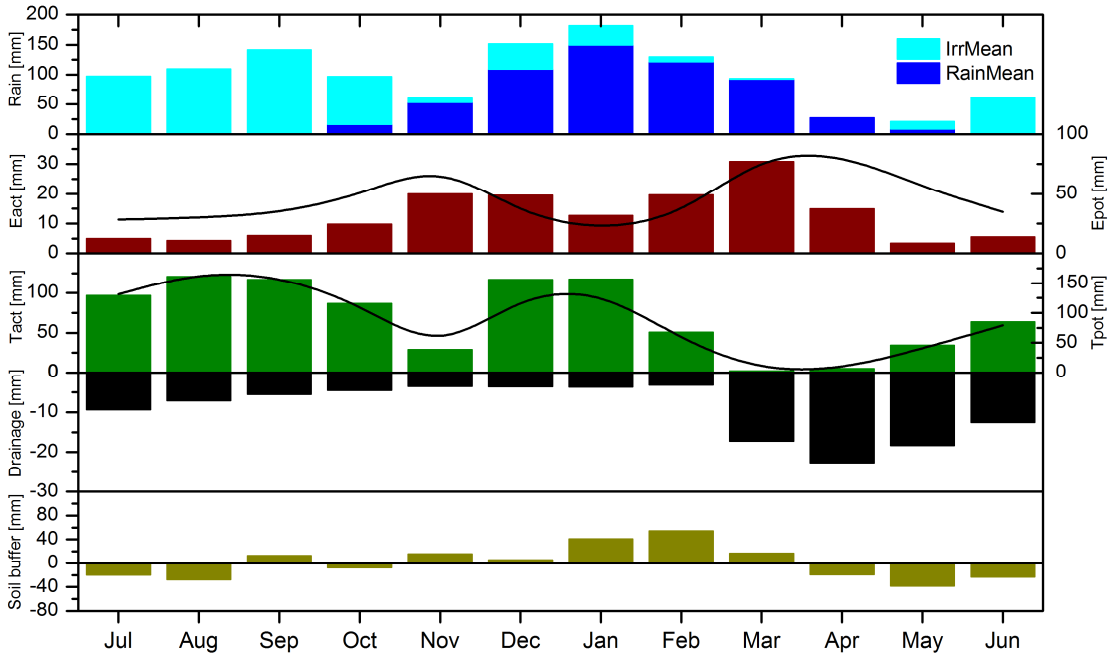

Fig. 89: Monthly mean soil water balance components for the wheat-maize crop rotation scenario under irrigation at the Kalahari dune areas of Mashare. The lines represent the monthly course of Epot and Tpot

The consequences of the additional water input by irrigation and a two-stage crop rotation for soil water balance dynamics is shown in Fig. 89. Since the irrigation input is governed by the soil water status in 30 cm depths, the timing and the required amount of additional water is defined by boundary conditions. The course of the irrigation application is therefore linked to the phenological development of the respective crops with their developing transpiration demand and the seasonal development of the precipitation input. The description of the seasonal cycle begins with the Maize period in November one month after the onset of the rainy season. As described the actual rooting depth and the leaf development of the crop phenological stage is still at a low level. The topsoil water content is at relatively high level due to the remaining irrigation water infiltrated at the end of the previous wheat period. In combination with the low phenological development of Maize, the relation of actual and potential transpiration is 0.93 which shows, that nearly an optimal amount of soil water is available for transpiration. This relation stays at a high level as the phenological development goes on but decreases to 0.84 and 117 mm when the roots grow deeper in layers where infiltrated rain and additional irrigation water cannot percolate. With increasing rainfalls towards the middle of the rainy season, the relation gets reversed to nearly 100 % as layers at the bottom of the rooting now receive additional percolated water and the transpiration demand is lowered because of the near end of the phenological cycle. The following Wheat period begins in April with sufficient

top soil water contents to contribute to transpiration indicated by 99 % of its potential. In the following month, the relation is lowered to 72 % because the water uptake by the developing root system produce the mentioned dry laver from which roots cannot extract any water. The remaining source of plant available water is, therefore, the by irrigation periodically rewetted topsoil. It has to mentioned, that, in contrast to the dryland scenario with Maize, the LAI and plant density in the irrigation scenario is significantly higher which results in a much higher absolute transpiration amount, even without additional irrigation water (see upcoming sections). As the phenological development of Wheat goes on and when it comes to later stages the LAI governed transpiration decreases again but with a still deep expanded root system. After the Wheat harvest, the rotation starts again with Maize. Focusing on the seasonal evaporation development influenced by leaf shading and topsoil water reduction by root extraction, the relatively low absolute amounts, compared to the bare soil scenario, throughout the year are noticeable. Only in phases where the leaf area is low and rainfall can infiltrate and percolate into medium soil depths, hence only at the beginning of each crop period, the evaporation rates rise significantly. This is the case in the months of November to December and in April with 20 mm and 30 mm. Where the seasonal course of the evaporation in the bare soil scenario has a unimodal dynamic correlated with the precipitation development, the dynamic of the evaporation within the irrigation scenario shows a bimodal distribution which is inversely linked to the phenological development of the two-stage crop rotation. The seasonal course of the deep drainage amounts under irrigation application reacts with respect to its peak with a time lag of one month compared to the bare soil scenario. This peak occurs at the end of the rainy season where water is able to percolate deeper into the soil. Within the dry season, even with noticeable amounts of irrigation input, no significant drainage increase is simulated as a result of the percolation-blocking effect of the dry layer. Remaining subsoil water transferred into this area at the last half of the rainy season contributes to a monthly decreasing amount of bottom fluxes starting with its peak in April to remain stable but on a low level with about 3.7 mm in the months of November to February.

6.3.3. Land-use on Luvisols of the old floodplains in Mashare

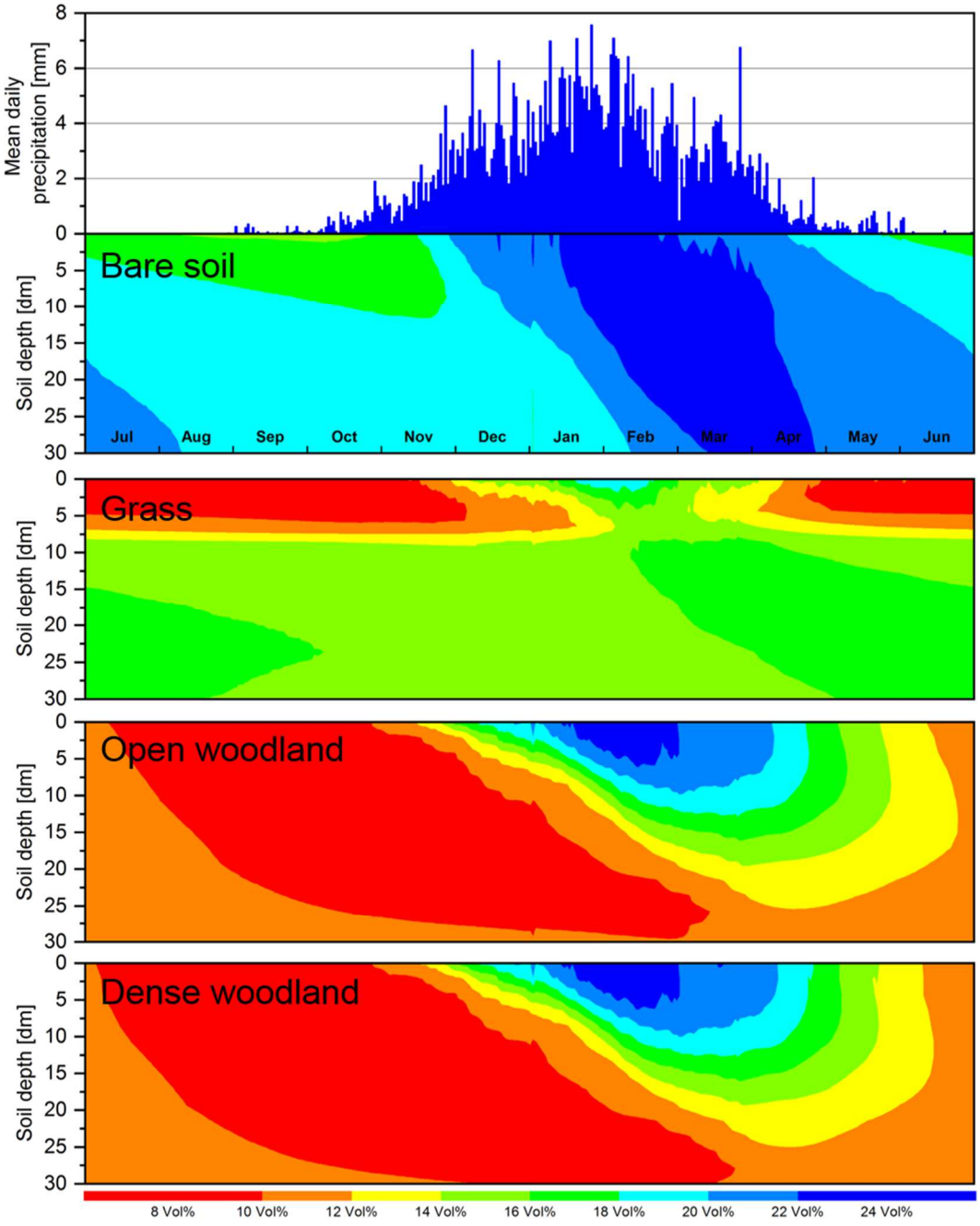

Fig. 90: Mean daily water content for a period from July to June based on a 30-year model run for bare soil conditions and three different pristine land cover scenarios in the old floodplains of the Mashare study site

With changing soil characteristics, from the sandier conditions of the Kalahari dune are to the loamy-clayey conditions in the old floodplains, the residual water content θ_r increases from about 3 Vol% to 9 Vol% along with the retention functions and the saturated and unsaturated hydraulic conductivity properties. The seasonal development pattern of the soil water contents in the bare soil scenario is comparable to the Kalahari dune area

scenario. A wetting front forms at the onset of the rainy season with an increase in water contents down to the bottom of the profile in the middle of the season in February followed by a drying cycle with decreasing rainfall inputs in April. The apparent differences in the absolute water contents, as well as the wetting and drying dynamics, are due to the different soil hydrological properties of this scenario site (see section 6.2.2). In comparison to the sandy site of the Kalahari Dune area, the old floodplain soil is characterized by a less steep decrease of the retention function as well as a much lower decrease of the unsaturated hydraulic conductivity with increasing soil water potentials. This results in a higher water holding capacity as well as a better capillary rise of pore water from areas with high potentials in medium layers of the soil to areas with lower potentials in the topsoil regions. Especially at the end of the rainy season, this ability takes effect on the dry front formation. The mean soil water difference between top- and subsoil is greater at the Kalahari dune area with about 4 Vol% whereas this difference is only 2 Vol% in the old floodplains. These circumstances will be discussed later on with a look at the soil water balances. The different dynamics between the Kalahari site and the old floodplains can also be realized by taking a comparing look at Fig. 91a and Fig. 81a. The absolute effective saturation values in 20 cm depth differ with a mean of 0.3 in the old floodplains and 0.18 in the Kalahari dune area indicating higher soil water contents in the topsoil regions in the loamy areas of the study site. Looking at the water potentials at the end of the rainy season in relation to soil water contents, the old floodplain soil is with a mean level of 22 Vol% already at a mean pF of 2.3 where only little to no gravitational water relocation occurs with simultaneous formation of upward oriented potential gradients. At the same time, the sandy Kalahari soils have, with a mean water content of 10 Vol%, a hydraulic potential of pF 1.8 where percolation can occur.

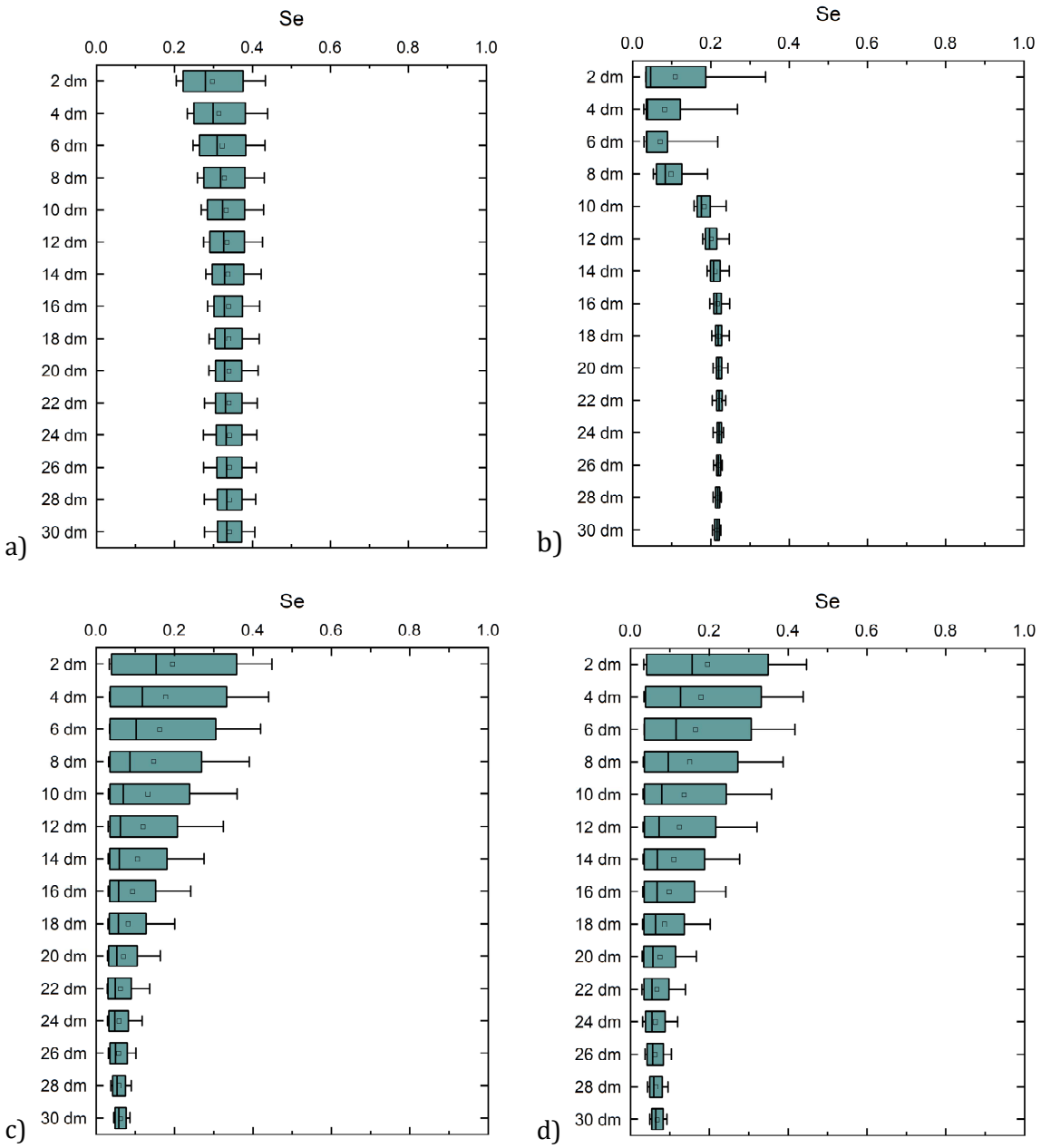

Fig. 91: Boxplots showing the long year simulated effective saturation (Se) at 20 cm soil layer resolution down to 300 cm for pristine conditions of the old floodplains in Mashare. a) Bare soil, b) Grass, c) Dense woodland, d) Open woodland

The grass scenario of the old floodplain site simulation shows no significant pattern differences compared to the Kalahari grass scenario, despite the fact, that absolute soil water contents differ as a consequence of the retention characteristics. With the beginning of the hydrological year in July, the vegetation has transpired all available soil water left by the previous rainy season down to a rooting depth of 50 cm whereas soil water contents start to increase again slightly down to the maximum rooting depth of 80 cm due to an additional supply of capillary risen water from beneath the rooting zone. There, the soil

is still moist at a yearly mean level of about 16 Vol% to 18 Vol% down to the bottom of the profile. With a sufficient precipitation input at the beginning of December a wetting front forms, which reaches a depth of 30 cm and forms the already described wet-dry - wet sequence until the on-moving wetting front has rewetted the dry layer in February. The profile reaches its middle of the season state with a wet topsoil at 20 Vol% and depth decreasing contents down to 14 Vol% to 16 Vol% in 300 cm. With decreasing rainfalls, the ongoing rainy season is characterized by a decrease of soil water contents starting at the bottom of the root zone where root water extraction is higher than the infiltrating water amounts. This results in the re-establishment formation of a wet-dry-wet sequence until the precipitation is not sufficient anymore to partially sustain transpiration. From that point onwards, the vegetation fully depletes the available soil water of the root zone to near PWP until the next rains appear in the upcoming hydrological year.

The seasonal pattern of the soil water dynamics, modified by the woodland scenarios, is similar to the development described in the woodland scenario of the Kalahari dune area site. The vegetation utilizes all available soil water buffered in deeper soil areas to maintain transpiration at a low level even beyond the rainy season. This leads to a depletion of the available soil water throughout the whole profile until the onset of the rainy season, where a wetting front forms to move forward in depth until it reaches the bottom of the profile in April. The main differences to the woodland scenarios appear from that point on. Where the Kalahari soil is wetted from 3 Vol% to 6 Vol% the wetting front of according scenarios of the old floodplains shows a lower amplitude unable to increase the subsoil areas significantly. This refers again to the higher water holding capacity of the old floodplain soil in comparison to the Kalahari soil. After the peak of the rainy season, the drying cycle begins. The wetting front enters the old floodplain soil, compared to the Kalahari dune area, relatively low speed. In June, the difference of the topsoil to subsoil contents is quasi zero whereas the mean maximum difference at the Kalahari site is 3 Vol% with higher subsoil water. Where the sandy texture of that site still relocates water downwards, the loamy old floodplain soil holds it against gravity. These appearing processes will be described from the balances point of view to characterize the consequences of the different soil hydraulic properties of the two sites simulated. Fig. 91a-c shows the differences expressed as effective soil water saturation as a function of the soil depth. It is clearly visible, that due to the rooting characteristics of the assumed scenarios, the soil

water dynamics get more pronounced with depth with a complete depletion of the available soil water by deep rooting trees.

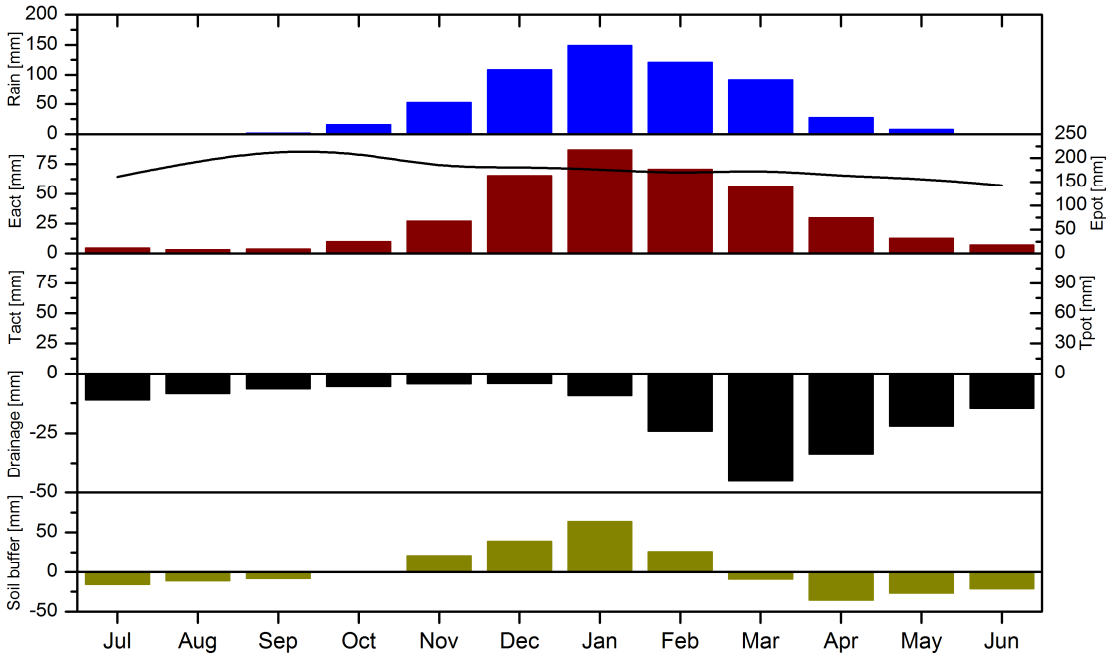

Fig. 92: Monthly mean soil water balance components for the bare soil scenario at the old floodplains of Mashare. The lines represent the monthly course of Epot and Tpot

The development of the evaporation rates over the hydrological year for the bare soil reference (Fig. 92) follows the rainfall dynamic and reaches its maximum with 87 mm together with the highest precipitation amounts in January. With the outgoing rainy season, the evaporation amounts start to decrease again almost linearly with -17 mm per month. The evaporation stays on a low level with a mean of 4.5 mm from June to September even throughout the dry season. This indicates that the soil hydraulic properties lead to a certain capillarity for partially satisfying the atmospheric water vapor demand, whereas the Kalahari soil evaporation drops to 1 mm within that period. Focusing on the bottom fluxes the still recognizable but slowly increasing amounts at the beginning of the year get their input by the buffered soil water until the soil buffer dynamic gets reversed by the incoming precipitation in October. The input at that time exceeds the output driven by deep drainage and evaporation and the soil buffer gets constantly filled again whereas bottom fluxes still decrease. After reaching the maximum storage within the profile, bottom fluxes start to increase again in January to their maximum in March with 45 mm where the soil

buffer dynamic gets reversed again. The resulting relation between evaporative and bottom fluxes of 0.5 shows clearly that this soil has a relatively strong capillarity which leads in tendency to two times higher evaporation rates than deep drainage amounts.

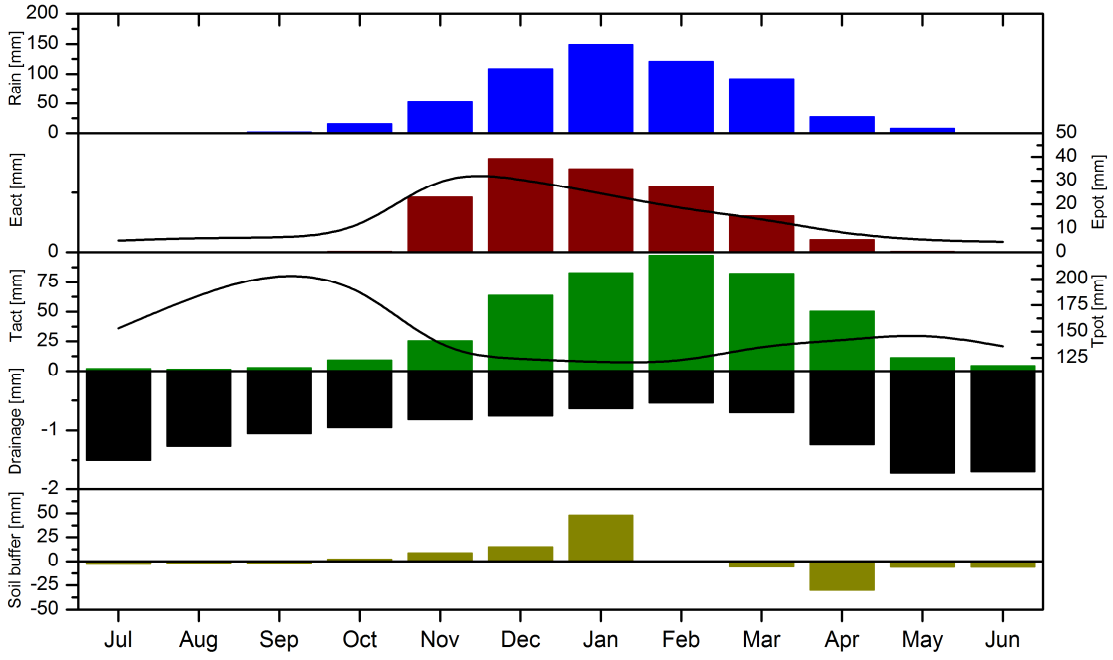

Fig. 93: Monthly mean soil water balance components for the grassland scenario at the old floodplains of Mashare. The lines represent the monthly course of Epot and Tpot

Fig. 93 shows the seasonal course of monthly means of the water balance components with the integration of grassland vegetation. The phenological development suppresses evaporation rates due to leaf shading by 80 % of the total evaporation. Simultaneously the timing of maximum evaporation rate, in this case of 19 mm, is shifted from January to December where the leaf development has not reached its climax state and the mentioned wet-dry-wet sequence is formed to contribute to evaporation due to high topsoil water contents. The evaporation rates decrease again because of the increasing soil coverage and the increasing root water extraction to zero in May to stay at that level until the onset of the next rainy season. Transpiration fluxes are governed mainly by the precipitation inputs since the grassland vegetation can, because of a maximum rooting depth of 80 cm, can only utilize a small proportion of the potentially available soil water supplied by the profile. The transpiration dynamic follows a sinusoidal development according to the phenological development and reaches its maximum February with 97 mm and 80 % of its potential when the available root zone soil water content is at maximum too. In the following month, the transpiration rates decrease again because of decreasing precipitation

input and the initializing depletion of the root zone soil water. After the nearly complete depletion transpiration rates are reduced to mean amounts of 4 mm in the dry season. This transpiration rate is based on the capillary supply of soil water from beneath the root zone. Looking at the bottom fluxes, only 6 % of the yearly reference amount under bare soil condition is simulated integrating grassland vegetation (Tab. 15). This significant reduction is based on the impermeable dry layer with reduced conductivities and simultaneously high water extraction by roots. The only source of percolation water lies within the month of January to March, where the deeper soil layers receive a sufficient amount of water, which is the later source of bottom fluxes.

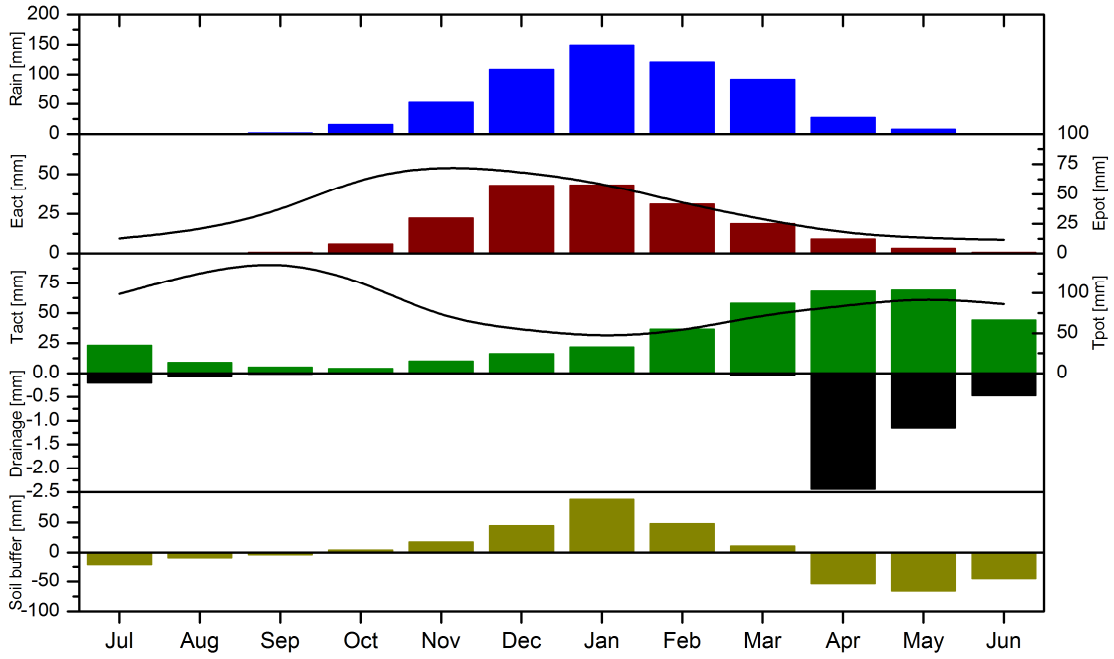

Fig. 94: Monthly mean soil water balance components for the dense woodland scenario at the old floodplains of Mashare. The lines represent the monthly course of Epot and Tpot

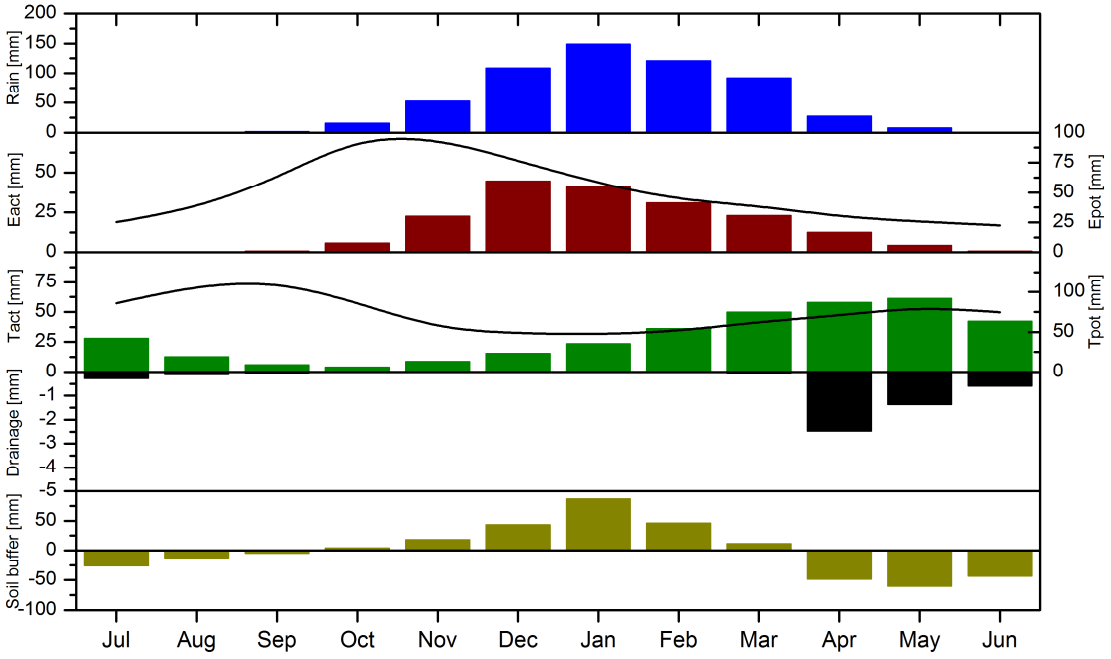

Fig. 95: Monthly mean soil water balance components for the open woodland scenario at the old floodplains of Mashare. The lines represent the monthly course of Epot and Tpot

Fig. 94 and Fig. 95 illustrate the woodland vegetation effects on soil water balances. Since the rooting of the assumed scenario parameter enables the woodlands to explore 300 cm of available soil water the monthly course of the transpiration is not only governed by the phenology but also by the available soil water in deeper layers, which cannot be explored by grassland vegetation. The course of the potential transpiration has its maximum in September. Due to the lack of plant available water and the first low phenological stage at beginning of the hydrological year, the actual transpiration rates are at a minimum. With the ongoing precipitation input, the difference between potential and actual transpiration gets smaller to its minimum in the month of February to April with an absolute transpiration peak of 69 mm in May under dense conditions and 61 mm for open conditions. Because of the rooting properties and the buffered soil water, the vegetation can maintain its transpiration in the dry season from June to October on a mean level of 18.7 mm per month.

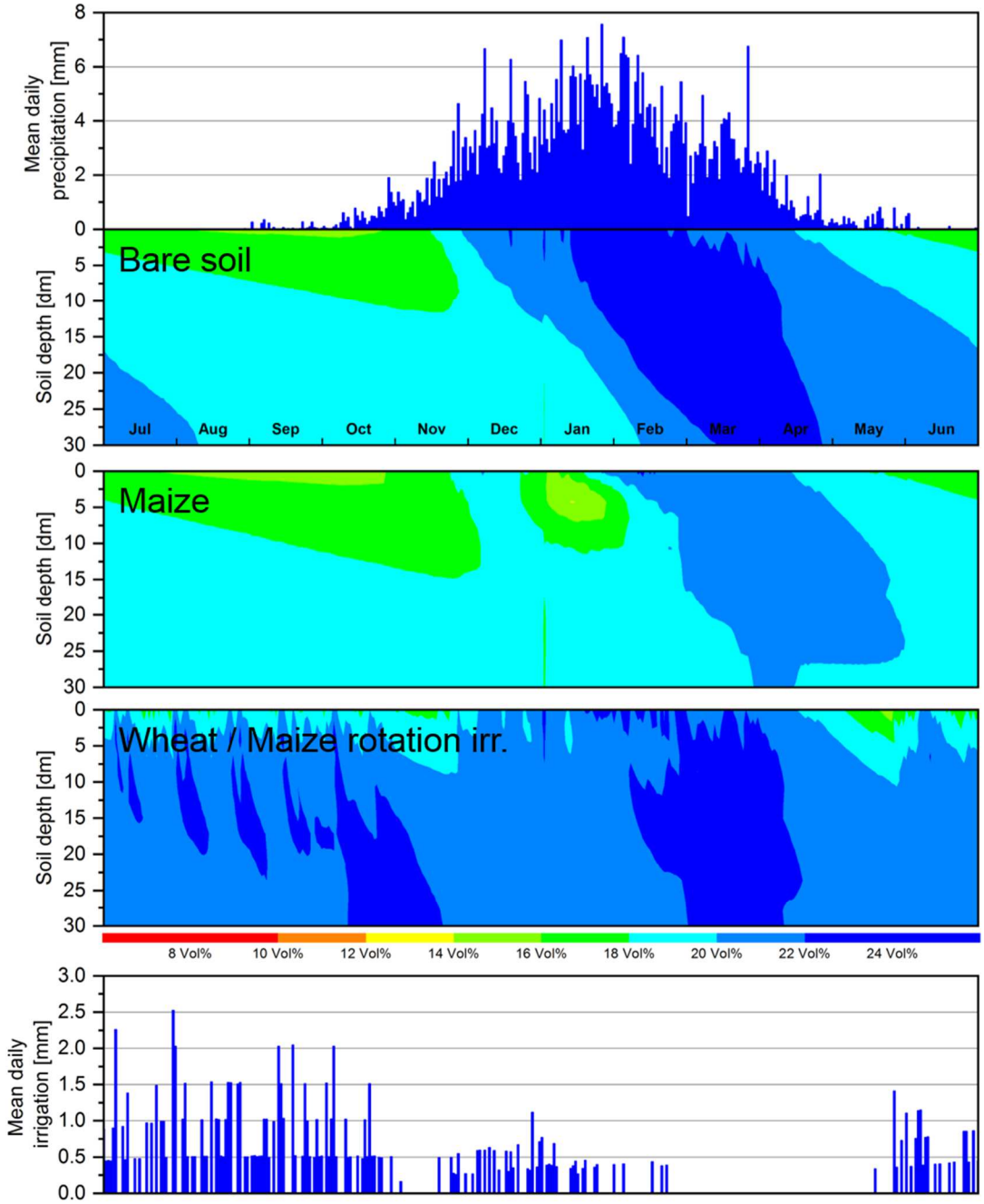

Fig. 96: Mean daily water content for a period from July to June based on a 30-year model run for bare soil conditions and two different cropping scenarios in the old floodplains of the Mashare study site.

Fig. 96 illustrates the modification of the reference bare soil scenario by the integration of Maize under dryland agricultural conditions and the application of irrigation with a two-stage crop ration with Wheat and Maize like it was integrated into the simulation for the Kalahari dune area settings. Compared to the bare soil conditions, the seasonal development of the soil water contents follows the pattern of the Maize scenario at the Kalahari dune area site. With the onset of the rainy season in October, the mean soil water contents

show a decrease with depth with 14 Vol% in the topsoil over 16 Vol% to 18 Vol% in medium range depths to 20 Vol% on the bottom of the profile. The vegetation is still in an initial stage of its phenological development so that leaf shading and root water extraction does not hamper in a significant way the infiltration and percolation of incoming precipitation input. In December the profile is rewetted onto a level of 20 Vol% throughout the whole depths. As the phenological development moves on, the root extraction and leaf shading effects the decrease of soil water contents down to a depth of the maximum root zone in 100 cm onto a level of the period before the onset of the rainy season. In the middle of January, the increasing rainfalls form a wetting front which compensates water losses by the vegetation in its mature stage which results in outbalanced water content with deep percolation processes and high water contents of 22 Vol% in 300 cm depth in April. Since the absolute water contents are in a lower range compared to the bare soil scenario, the following drying cycle has a lower dynamic with respect to the speed of the moving drying front. The ongoing evaporation processes diminish high to medium range soil depths water content until the next rainy season begins. Fig. 97a shows the increased dynamic in soil water contents in relation to Fig. 91a especially within the root zone from 20cm to 100 cm with its highest range in 60 cm. The absolute range of the mean effective saturation is within a range of 0.27 in topsoil regions with a slight increase with depth to have a mean saturation of about 0.31 in 300 cm depth.

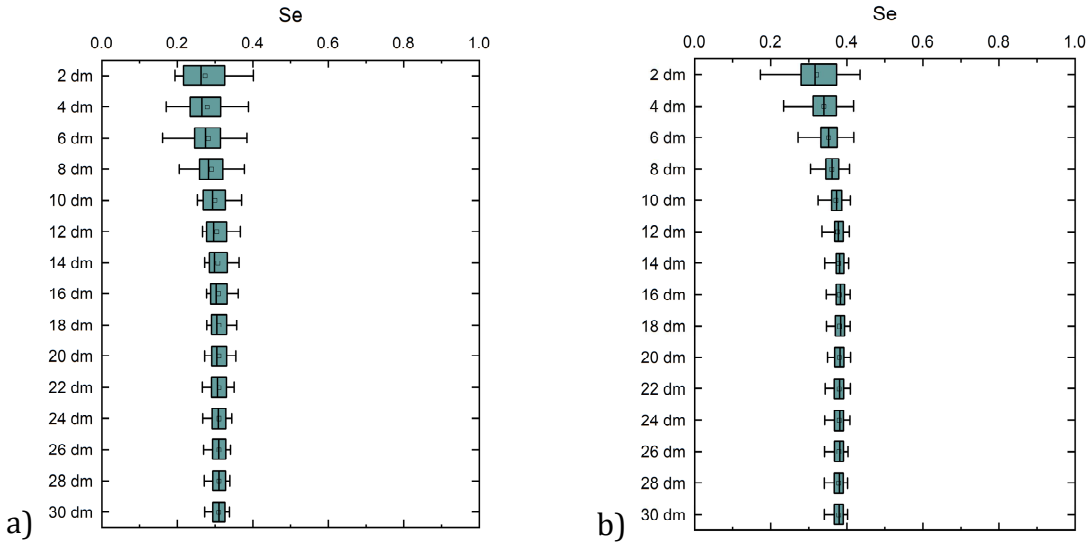

Fig. 97: Boxplots showing the long year simulated effective saturation (Se) at 20 cm soil layer resolution down to 300 cm for agricultural conditions of the old floodplains in Mashare. a) Maize under dryland condition, b) irrigated Wheat-Maize crop ration

The irrigated crop rotation scenario on the loamy soil of the old floodplains results in highly modified soil water conditions throughout time and soil depths. Beginning the description again with the Maize period in November. The water content at the beginning of this period is compared to the dryland scenario with 18 Vol% to 22 Vol % in maximum 10 % points higher. Especially medium to deep range soil layers have significantly higher water contents with the remains of the previous irrigation input over the Wheat period in the dry season. The low outgoing phenology of Wheat together with the initial low stage of Maize in November the available soil water content is sufficient to maintain transpiration and the threshold of -1000 hPa for irrigation application is not reached. Due to the low rainfall input and the missing irrigation soil water, contents decrease within the first 100 cm due to evapotranspiration processes until the irrigation threshold leads to an additional water input which rises the topsoil water content to a level of pF 1.8 or 22 Vol% and the whole profile is, for a short time levelled out. Now, a sequence of drying and wetting begins where the irrigation supplements rainfall inputs to sustain a soil water level between pF 3 and pF 1.8 until the rainfall amount are able to stabilize these conditions without supplementation in the months of March and April. Since the beginning of the irrigation application, the whole profile is at a high soil water status and the drying-wetting sequences only affect the first 80 cm only in short intervals. With the ongoing rainy season and higher phenological stages of maize, the active root system explores soil water onto a depth of 100 cm with subsequently lower LAI and transpiration demand due to the drying phase of the plants. In March the Maize comes to its final stage short before harvest and the soil water content is at a high level similar to the state of the bare soil scenario at that time. With the emergence of the first Wheat shoots in April, the second rotation period begins again with low rooting depths and leaf area development. The soil water contents decrease from the top of the profile onto a depth of 100 cm at the end of May where again irrigation sets in to increase the water contents to a level of pF 1.8. at the end of the hydrological year in June. The previously mentioned sequences of drying and rewetting of the first soil layers onto a depth of 50cm to 75 cm are now, with the absence of additional precipitation input, more pronounced and more periodic. The medium to deep range soil areas are still at a high saturation level of 22 Vol% but increase periodically to < 24 Vol% after the onset of an irrigation period with increasing depth, due to the increasing transpiration demand of Wheat in mature development stages with a fully developed root system. In the month of October, the infiltrating irrigation water is able to increase

water contents down to the bottom of the profile due to less interception losses and less evapotranspiration fluxes in the topsoil. At that stage, the initial conditions at the beginning of the Maize period are re-established. Fig. 97b shows the modified soil water dynamics with respect to absolute effective saturation and its variability over time ad depths as a consequence of the additional irrigation input. The mean effective saturation is increased to 0.32 in the topsoil and 0.39 at the bottom of the profile with depths decreasing variability as an effect of the topsoil wetting-drying sequences. Compared to the bare soil scenario as shown in Fig. 91a, the all over variability is increased with respect to minima and maxima saturation but decreased looking at the upper and lower quartiles which indicates lower drying and wetting dynamics induced by the irrigation application.

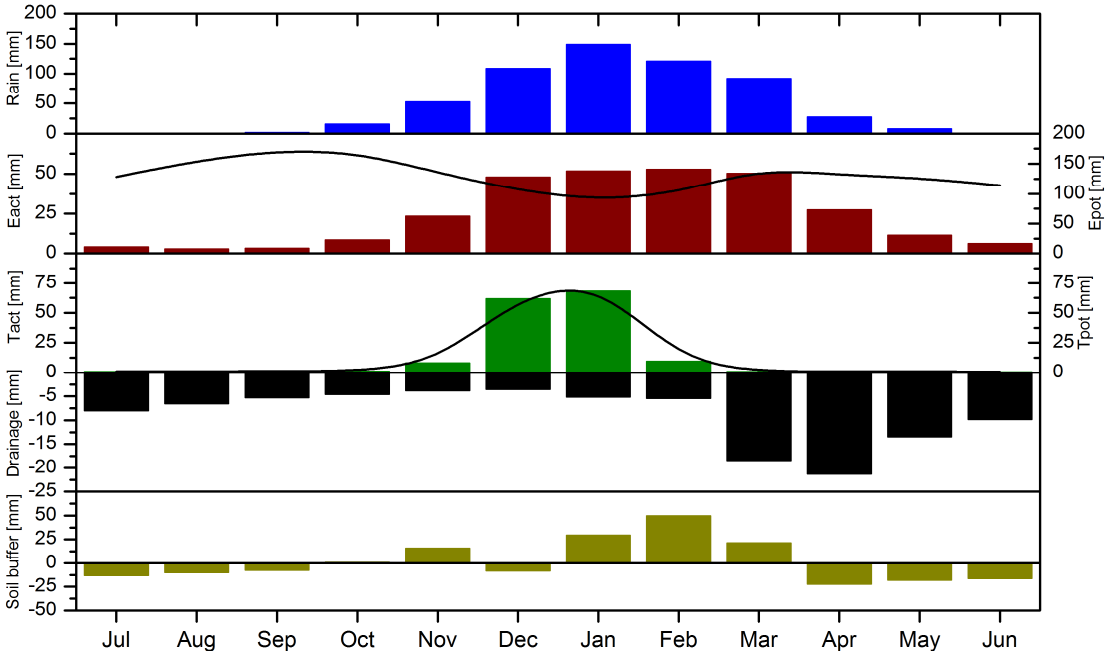

Fig. 98: Monthly mean soil water balance components for the maize scenario at the old floodplains of Mashare. The lines represent the monthly course of Epot and Tpot

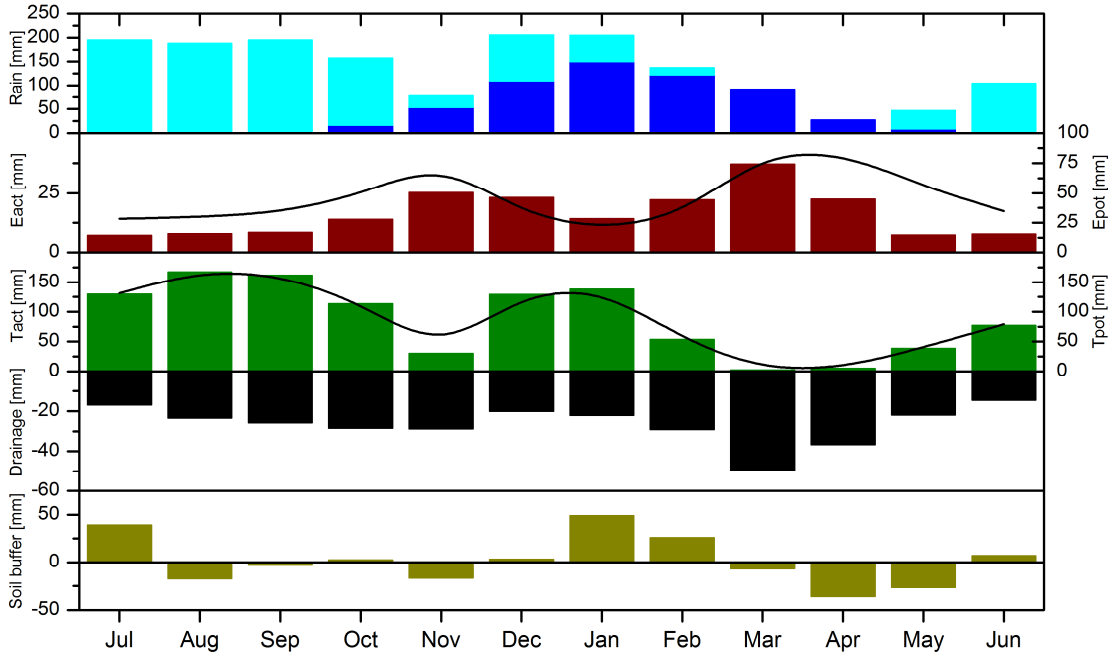

Fig. 99: Monthly mean soil water balance components for the wheat-maize scenario under irrigation at the old floodplains of Mashare. The lines represent the monthly course of Epot and Tpot

Fig. 98 shows the soil water balances for the Maize scenario under dryland conditions. The specific soil water retention of the loamy soil of the old floodplain conditions favors an optimal water supply for transpiration purposes. The seasonal development of the transpiration rates shows, like the Kalahari site simulation does, a phenology-governed course with a peak at the mature state in January. Including the relation between actual and potential transpiration, the analysis show, that in nearly all month where transpiration occurs, this relation is over 90 %. Only in January, the relation is at 86 % where the depletion of available soil water within the rooting zone by evaporation, transpiration and percolation reduces actual transpiration rates but having its seasonal peak with 69 mm. The increasing phenological development decreases the transpiration demand by simultaneously increasing input, which sets the relation back to 96 % in the month of the harvest. Due to the low leaf-based soil coverage of the Maize scenario, the seasonal course of the evaporation follows again the development of the rainfall inputs over the rainy season. The amplitude is lowered, compared to the bare soil scenario based on the reduced topsoil water contents in January and the additional soil coverage at the mature state of the vegetation. There is no significant peak visible but a stable rate of about 50 mm in the months of January to March with a subsequent decrease to about 4 mm per month in the dry season from June to September. The bottom fluxes peak in March to April one month

later compared to the bare soil reference due to impact of the modified topsoil water contents with reduced amounts of percolating water. Only after the harvest rainfall inputs can percolate effectively to increase bottom flux rates to a maximum of 26 mm in April. After that peak, the soil buffer sustains a steadily decreasing drainage of the profile over the dry season.

The irrigation scenario shows with respect to the relation between actual and potential rates a nearly optimal soil water availability overall two periods of Maize and Wheat. Due to the high unsaturated conductivities and the specific retention curve, the root of the crop is at all times saturated to a degree, where transpiration is supported on a very good level. Beginning in Maize the initial actual transpiration rate is 30 mm to increase rapidly to 138 mm according to the mature state in January. From that point on it drops again towards the time of harvest to 2 mm in March. With the development of the Wheat period, the increase of the transpiration rates is lower compared to Maize because of the slow phenological development of leaves and roots. In the mature state in August Wheat has its transpiration peak with 168 mm, about 18 % higher than Maize, due to its physiological adaptation and the deeper development root system. The transpiration rates start to decrease again getting to the end of the phenological cycle towards the time of harvest in October. Similar to the seasonal course of the evaporation rates of the Kalahari dune areas scenario, the two-stage rotation scheme shows a bimodal dynamic based on the two crop phenological developments per hydrological year. The peaks of the evaporation rates are to be found in the month between crop change with low leaf area development and little transpiration fluxes at rates of 25 mm in November and 37 mm in March. The course of the bottom fluxes is aligned to the dynamic of the evaporation. In the transition Maize and Wheat, where evaporation rates peak, the incoming precipitation together with the initial soil water status, percolation occurs and together with the already percolated water, which accumulated in the middle of the rainy season lead to a significant increase of the soil conductivity resulting in an increase of bottom fluxes to 50 mm in maximum with a consecutive steep decrease towards the end of the year. At the beginning of the next year, the bottom fluxes start to slightly increasing again by the additional irrigation which is transferred to a certain proportion to deeper profile areas where it stays unaffected by root water extraction and contributes to deep drainage with a second maximum in November of about 29 mm.

6.4. Discussion

6.4.1. A comparative evaluation of the vegetation induced soil water balance modifications

In section 6.3, the different model scenarios showed that the contrasting land use and pristine vegetation assumptions lead to an intra-site specific variation of soil water dynamics as well as an, based on differing soil hydrological properties, inter-site specific variability. The following section summarises these modifications to evaluate regional soil water balances.

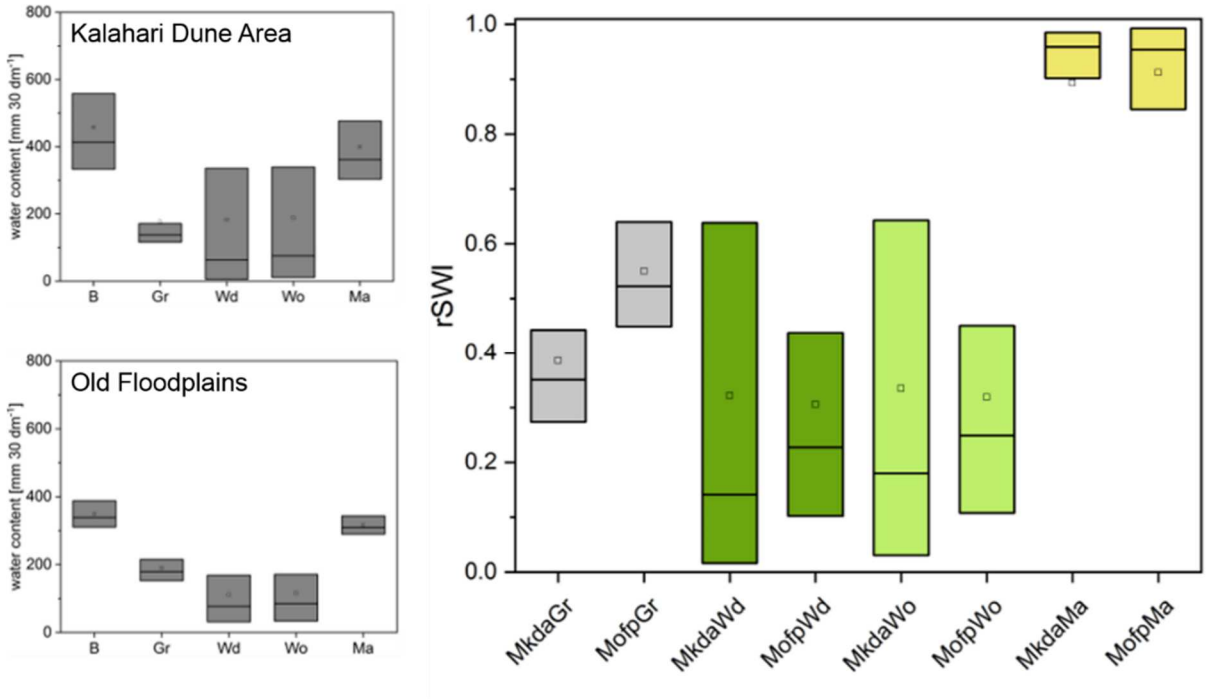

Fig. 100: Comparison of the intra- und inter-site-specific variabilities of the summed-up profile water contents (left) and the relative soil water index (rSWI) showing the relative reduction of soil water contents in relation to the bare soil scenario (right)

The two boxplot diagrams on the left side in Fig. 100 show the absolute profile water contents based on the 30-year simulation for both sites with additional vegetation scenarios. The upper and lower boundaries of the boxes represent the third and first quartile whereas the point shows the mean and the line the median values. The boxplot on the right side compares the impact of vegetation scenarios on the bare soil reference water contents as an index value between 0 and 1 referring to the relation between the vegetation scenario water content and bare soil water content as relative reduction of the bare soil reference.

The bare soil scenario of the Kalahari dune area shows a pronounced seasonality of the total profile water contents with a mean of 458 mm and an interquartile distance of 225 mm. This high dynamic range is reflected by the mean seasonal bottom flux of 294.9 mm and 285.6 mm evaporation as shown in Tab. 15. The relatively quick soil water redistribution from medium to lower profile areas where it contributes to the bottom fluxes withdraws a significant amount of water in a short period, whereas the transfer to the surface by capillary rise is much lower and keeps the temporal dynamic of the upper part of the profile on a low level. In contrast, the old floodplain soil responses to atmospheric drivers with a lower total mean amount of 349 mm and an interquartile distance of 78 mm indicating lower seasonal variability. This low variability appears to be because of the high capillary properties to hold water against gravity and to transfer these waters to the soil surface to evaporate or is available for transpiration. With only 189.3 mm mean seasonal bottom flux and 391.3 mm evaporation at the same time, the relation between these two components shows that the water redistribution is driven by atmospheric demand and therefore with a low dynamic in comparison to the quick downward oriented dynamics in the sandy Kalahari substrates.

Tab. 15: Long year means of water balance components for the Mashare scenarios

Scenario	Input [mm]	Interception [mm a^{-1}]	Transpiration [mm a^{-1}]	Evaporation [mm a^{-1}]	Bottom flux [mm a^{-1}]
MkdaB	580.6	0.0	0.0	285.6	294.9
MkdaGr		52.8	427.9	60.4	42.4
MkdaWd		26.1	374.5	158.5	21.5
MkdaWo		38.3	356.5	162.0	23.8
MkdaMa		16.3	166.0	224.1	174.2
MkdaMaWi	580.6+619.5	61.5	873.1	148.8	113.4
MofpB	580.6	0.0	0.0	391.3	189.3
MofpGr		52.8	449.4	65.6	12.8
MofpWd		26.1	374.5	175.9	4.1
MofpWo		38.3	353.6	184.0	4.6
MofpMa		16.3	168.4	295.5	100.4
MofpMaWi	580.6+1092.6	60.3	1086.2	505.6	327.7

The grass scenario diminishes the profile water content on all two sites nearly at the same amount by transpiring 427.9 mm on the Kalahari dune areas and 449.4 mm in the old floodplain scenario together with an interception caused reduction of the mean seasonal

input of 52.8 mm. Bottom fluxes are reduced to 42.4 mm (by 86 %) at the Kalahari site and to 12.8 mm (by 94 %) in the old floodplains. The evaporation is reduced to 60.4 mm (by 79 %) in the Kalahari dune area and to 65.6 mm (by 84 %) in the old floodplains. The high transpiration flux in these scenarios nearly equalize the apparent profile water differences of the bare soil scenarios whereas the impact of the grass scenario on the Kalahari site is higher than on the old floodplains. The rSWI in Fig. 100, which represents the likeliness of a scenario to its bare soil reference, emphasize this higher impact by showing a lower index compared to the old floodplain. While the mean sums of the soil profile water content are reduced by 61 % in the Kalahari dune area, the reduction in the old floodplains is only by 45 %. As a measure of the increase of soil water variability, the interquartile distance of 0.16 in the Kalahari dune area and 0.19 in the old floodplains reveals only small differences but an increase of 16 % in dynamic in relation to the bare soil reference. The impact of the woodland scenarios is the highest showing a bottom flux reduction of about 93 % to 98 % as a result of the nearly complete utilization of soil water, even in deeper soil layers, whereas the sum of transpiration and evaporation losses is 1.8 times higher in the Kalahari dune area and 1.4 times in the old floodplains, relative to their bare soil references. The comparison of the rSWI between the woodland scenarios of both sites showing a clear vegetation impact on the underlying soil water dynamics with a 67% to 68 % reduction of the mean soil water content. While this reduction appears to be only slightly lower in the old floodplains, the interquartile distances reveal a significant difference between the soil water dynamic modifications. While the woodlands in the old floodplains increase the soil water dynamics by 34 % the water dynamic impact at the Kalahari site is with 61 % nearly twice as high.

Focusing on the Maize scenario under dryland agriculture conditions the impact with respect to water balances and soil water contents is the lowest of all scenarios because of the short cropping period and the low soil cover fraction. Mean seasonal transpiration losses account for 166 mm in the Kalahari dune area and 168 mm in the old floodplains. The evaporation is reduced by 22 % in the Kalahari dune area and by 25 % in the old floodplains, whereas the reduction of bottom flux is slightly lower in Kalahari dune area with 41 % compared to the old floodplains with 47 %. The cropping impact of the mean profile water content shows a soil water reduction by 11 % on the Kalahari site as well as by 9 % in the old floodplain where the soil water dynamic is slightly higher compared to the Kalahari site.

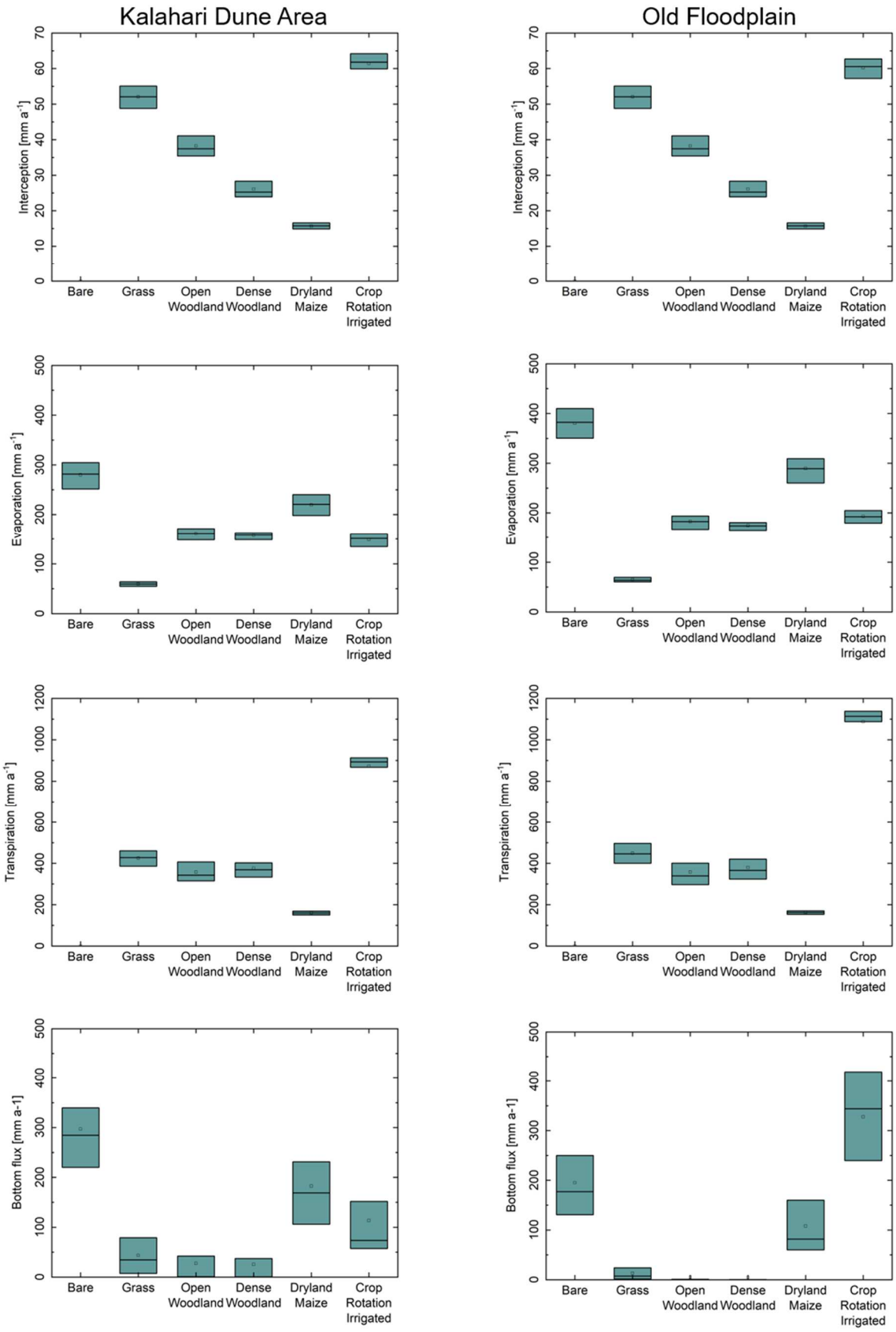

Fig. 101: Boxplots showing the impact of vegetation on soil water balance components.

Fig. 101 together with Tab. 15 presents the individual soil water balance components according to the integrated vegetation scenario. The seasonal sums of interception losses are governed by the LAI development together with rain intensities. Therefore, there is no inter-site difference between the respective vegetation scenarios due to identical vegetation characteristics. An exception is presented by the crop rotation scenario because of the different irrigation inputs at the simulated sites. Since the grass vegetation has the highest soil cover fraction the interception loss is the highest followed by the open woodland scenario. Even if the LAI of this condition is slightly lower compared to the dense woodlands the interception is higher because of the timing and function of the phenological development over the rainy season. When the leaf area in times with low rain intensities is a little higher than in the dense woodland scenario, as it is at the onset and the end of the rainy season, the seasonal interception sums are somewhat higher. The lowest interception losses appear within the Maize scenario where the soil cover fraction is, even at high phenological stages, low and concentrated to a three-month period with increasing rain intensities.

As to be assumed, the mean seasonal evaporation sums decrease with increasing soil cover fractions. The bare soil reference has the highest fluxes followed by the dryland agriculture scenario with its low plant density and short soil cover period. The open woodland scenario shows, compared to the dense scenario, slightly higher evaporative fluxes due to its lower leaf coverage whereas the grassland scenario reduces these fluxes to the minimum of 60 mm to 65 mm.

In contrary, the transpiration fluxes are determined by the leaf area and rooting depth development together with the amount of plant available water. With 428 mm and 449 mm, the grass scenario shows the highest transpiration fluxes. The woodlands transpire 374 mm per season and under dryland agriculture conditions the transpiration losses are the lowest with 166 mm to 168 mm per season.

Starting with the highest bottom fluxes the bare soil scenario shows the highest amounts with 294 and 189 mm followed by the dryland agriculture scenario with 174 mm and 100 mm since its conditions result in the most comparable soil water dynamics as shown in Fig. 100. The third most seasonal mean bottom fluxes appear with the grassland scenario simulation with 60 mm and 66 mm due to the reduced evaporation fluxes and the root

water extraction only to a depth of 80 cm, whereas the woodland scenarios show the lowest bottom fluxes with 22 mm – 24 mm in the Kalahari dune area and 4 mm in the old floodplains due to deep root water depletion.

By comparing the vegetation induced modifications of the soil water balances with the focus of the contrasting sites and their differing soil hydrological properties, evaporation and bottom fluxes show remarkable differences. While the old floodplains have a pronounced tendency to support evaporation processes the relation between evaporation and bottom flux in the Kalahari dune area is nearly 1:1 at bare soil conditions.

Tab. 16: Differences in evaporation amounts between the old floodplains and the Kalahari dune area in relation to vegetation and land use

Δ [mm]	Scenario	Relation between Mkda & Mofp
105.7	Bare soil	72 %
71.4	Dryland agriculture	75 %
22.0	Open woodlands	88 %
17.4	Dense Woodlands	90 %
5.2	Grass	92 %

Evaporation fluxes are governed by the development of the soil cover fraction of leaves and the soil water content of the topsoil. While interception losses as a function of the leaf area reduce the incoming precipitation amounts and therefore the topsoil rewetting the leaf shading effect reduces the evaporation dynamics by creating microclimatic conditions with a lowered atmospheric water demand. On the other hand, root water uptake within the topsoil reduces water contents which leads to a reduction of the evaporation since evaporation is seen to be a function of soil saturation status. Having this in mind Tab. 16 shows the dependency of evaporation fluxes on vegetation expressed by the relation between the old floodplain fluxes and the Kalahari dune area evaporation. Under bare soil conditions, the Kalahari dune area shows only 72 % of the old floodplain evaporation amount with an absolute difference of 105.7 mm. As the soil coverage increases with different land cover scenarios the evaporation amount increases but the relative and absolute differences decrease to have only 5.2 mm absolute difference or 92 % of the old floodplain evaporation. The analysis shows, that the higher the vegetation effect is on evaporation dynamics, the lower will be the pure soil physics driven effect.

In contrary, Tab. 17 expresses the dependency of bottom fluxes as relational and absolute differences between the two sites. Since the Kalahari dune areas yield more bottom flux in relation to the old floodplains, under bare soil conditions the old floodplains produce only 64 % or 105.6 mm fewer bottom fluxes as the Kalahari dune area followed by the dryland agriculture scenario with 73.8 mm less bottom flux or 58 % of the Kalahari dune area.

Tab. 17: Differences in bottom fluxes between the Kalahari dune area and the old floodplains in relation to vegetation and land use

Δ [mm]	Scenario	Relation between Mofp & Mkda
105.6	Bare soil	64 %
73.8	Dryland agriculture	58 %
29.6	Grassland	30 %
18.8	Open Woodlands	19 %
17.4	Dense Woodlands	19 %

Comparing both scenarios with no or just a little vegetation influence in Tab. 16 and Tab. 17, it is striking that the absolute differences in evaporation and bottom fluxes are the same. Hence, that amount of water which evaporates in the old floodplain scenarios leads to bottom fluxes in the Kalahari dune area. The next scenario which shows an absolute bottom flux difference of 29.6 mm is, instead of the open woodland in Tab. 16, the grassland scenario where one-third of the Kalahari dune area fluxes get drained at the bottom of the old floodplain profile. It can be shown, that with along with the decreasing absolute differences in bottom flux the relative relation between two sites increases, too. As the main driver for this process, the transpiration utilizes increasing amounts of soil water as a function of increasing rooting depth, length of vegetation cycles and leaf area. While only topsoil influences by the vegetation are responsible for the evaporation reduction the transpiration demand has the highest impact on bottom fluxes, especially when the soil physical properties of the respective soil support transpiration due to its retention characteristics. Tab. 17 clearly shows this relationship. Whereas the more sandy substrates of the Kalahari dune area bear still a certain amount of bottom fluxes, the higher capillarity of the old floodplain soil supports higher evapotranspiration amounts as to seen in Tab. 15 and Fig. 101. Because of the additional input due to irrigation application the comparison between the soil water balance components is done separately for the crop rotation

scenario. To allow a two-staged crop rotation including the dry season the additional input for the irrigation scenarios is 619.5 mm in the Kalahari dune area and 1092.6 mm in the old floodplains. Because of the hydraulic head driven irrigation application the different amount of input is based on the different soil water dynamic reaction in 30 cm depth at both sites as described in section 6.3. Regarding the impact on the balance components, a shift of the relation between the two sites appear. Tab. 18 shows this shift by comparing the relative deviation of the old floodplain and Kalahari balances as vegetation scenario aggregated indices with the respective relations of the irrigation scenario.

Tab. 18: Relative deviation of the soil water balance components comparing the old floodplains and the Kalahari dune area for all rainfall scenarios with vegetation as means with standard deviations and the irrigation application.

Scenarios	Interception	Transpiration	Evaporation	Bottom flux
With rainfall	1.00	1.01 ± 0.02	1.16 ± 0.09	0.32 ± 0.16
With additional irrigation	0.98	1.24	3.40	2.89

The vegetation scenarios with rainfall as the only input show nearly no differences between the simulation sites with respect to interception and transpiration whereas the evaporation is 1.16 times higher at the old floodplains. Regarding the bottom fluxes, only one third is drained at the bottom of the profile in the old floodplains with a high standard deviation indicating the vegetation induced variability. Compared to these relations, the irrigation scenarios show little higher interceptions at the Kalahari site. Regarding transpiration, evaporation and bottom fluxes, the irrigation scenario changes all component relations with the effect of an increase of already existing tendencies to even a reversion. The transpiration difference increases from almost none to 24 % more and the evaporation difference increases from 16 % to 3.4 times more in the old floodplains. Looking at the bottom fluxes, the old floodplains yield only one-third of the bottom flux amounts of the Kalahari dune area under natural rainfall conditions but 2.89 times more under irrigation application. This shift can be explained by the wet-dry-wet sequence appearance within the Kalahari irrigation. Due to the insufficient irrigation input to rewet the dry layer, this stabilized layer prevents any percolation processes to deeper soil layers which results in a significantly low amount of bottom fluxes. Because of the low capillarity of the Kalahari soil, the irrigation water accumulates in the first soil layers, where it contributes to evaporation and transpiration. The absence of a dry layer in the old floodplain scenario

in combination with high unsaturated conductivities at field capacity leads to increased bottom fluxes. These percolation processes together with higher transpiration rates due to higher amounts of plant available water require higher irrigation amounts to keep the topsoil between the irrigation scheme thresholds of pF 1.8 and pF 3.0. With 327.7 mm bottom flux, this scenario shows the highest drainage amounts among all simulated vegetation scenarios.

To summarize these details for a condensed comparison of the vegetation caused differences Fig. 102a and Fig. 102b show the proportion of the soil water balance components as fraction of input for all respective scenarios and simulation sites. The interceptive losses stay the same at both sites because of the identical assumptions for the vegetation scenario parameterizations. The bare soil scenario emphasizes again the already mentioned leveled relation between evaporation and bottom flux in the Kalahari dune area whereas in the old flood plain the relation is clearly shifted to a trend towards a higher proportion of evaporation fluxes. The grass scenario shows higher bottom fluxes in the Kalahari dune area which are reduced in the old floodplains by higher proportions of evaporation fluxes while transpiration fluxes are only slightly higher. The bottom fluxes of the woodland scenarios in the Kalahari dune area still present with a fraction share of 3.7 to 4.1 %, whereas only 0.7 to 0.8 % of the input is drained in the old floodplains again compensated by the higher proportion of evaporation fluxes.

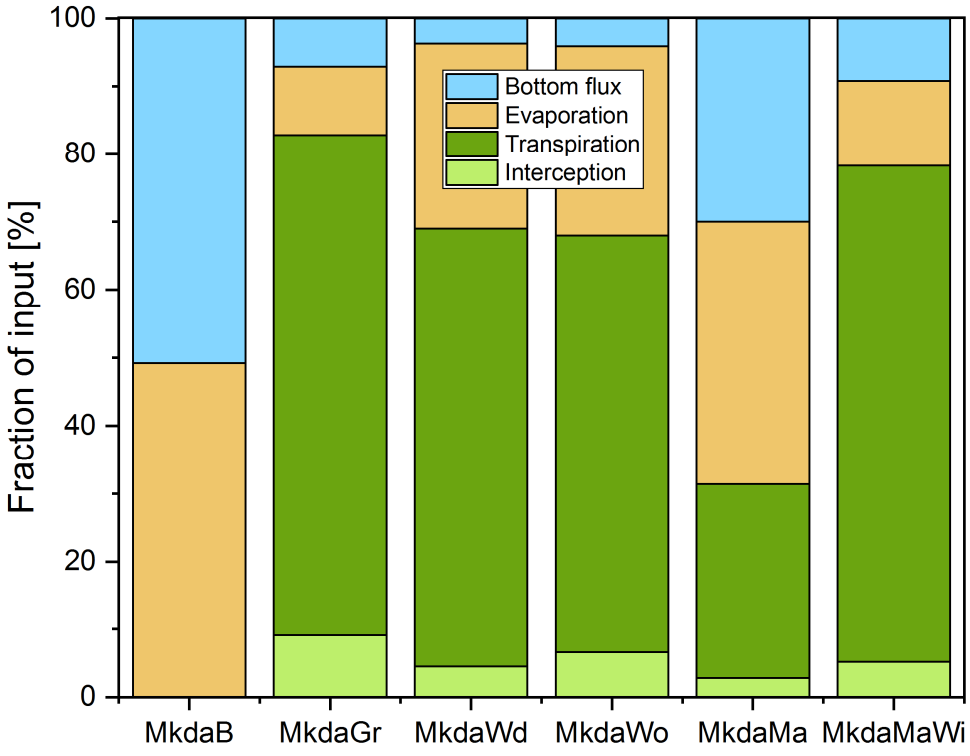

a)

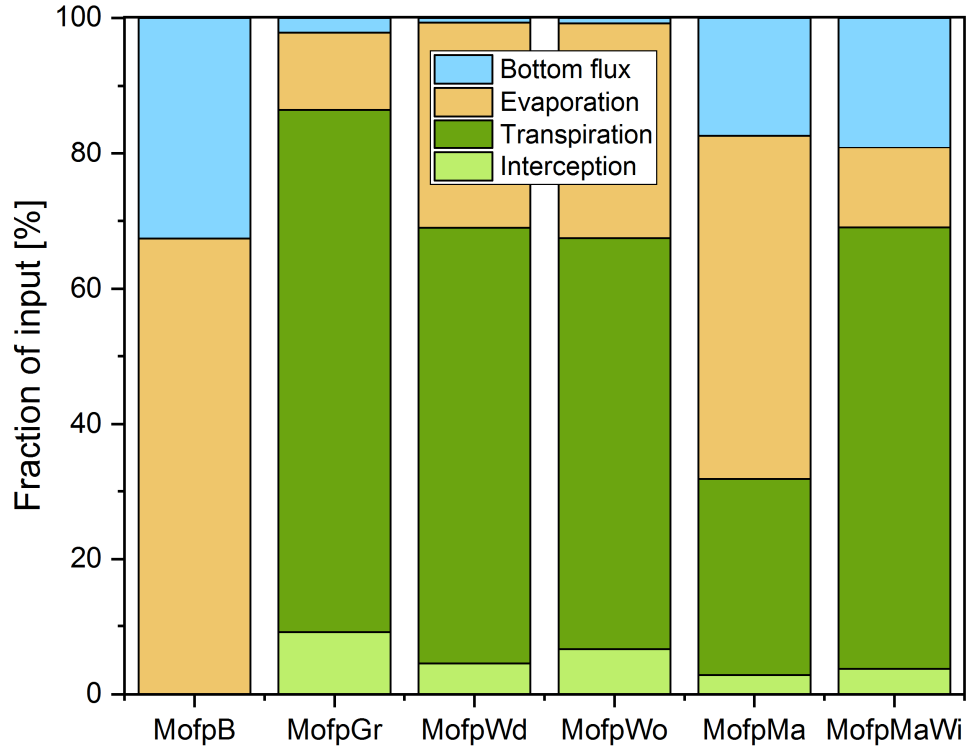

b)

Fig. 102: Bar charts showing the relative proportions of the soil water balances as fraction of the input for a) the Kalahari dune area and b) for the old floodplain scenarios

Under dryland agriculture conditions with low plant densities, the bottom fluxes have a share of 30 % of the input in the Kalahari dune area and 17.3% in the old floodplains, again compensated solely by higher evaporation fluxes. Under irrigation, the trend is reversed to higher bottom fluxes with a share of 19.1 % at the old floodplains. As a consequence of the combination of irrigation timing and depth, crop rotation scheme, phenological characteristics and the specific soil hydrological properties at the Kalahari dune area site, the bottom flux fraction is only 9.2 % of the input. Since the transpiration fluxes of the related scenarios do not differ between the two study sites, the soil physical properties seem to have no major influence on these fluxes, therefore, the appearing balance differences can only be explained by soil hydrological processes which lead to a trade-off between evaporation and bottom fluxes, as one of these always compensate the other, comparing both study sites. The comparison of the different vegetation scenarios to the bare soil reference shows that the pristine conditions with their seasonal phenological cycles, their high soil cover fraction as well as their partially deep root system extract significant amounts of soil water. This water contributes to primary production, whilst ensuring at the same time a reduction of unproductive water losses due to evaporation or bottom fluxes. In the following section, the relation between productive and unproductive water turnover will be addressed in detail by the adaption of the green to blue water relation concept.

6.4.2. What is the effectiveness of productive soil water consumption by the different vegetation scenarios?

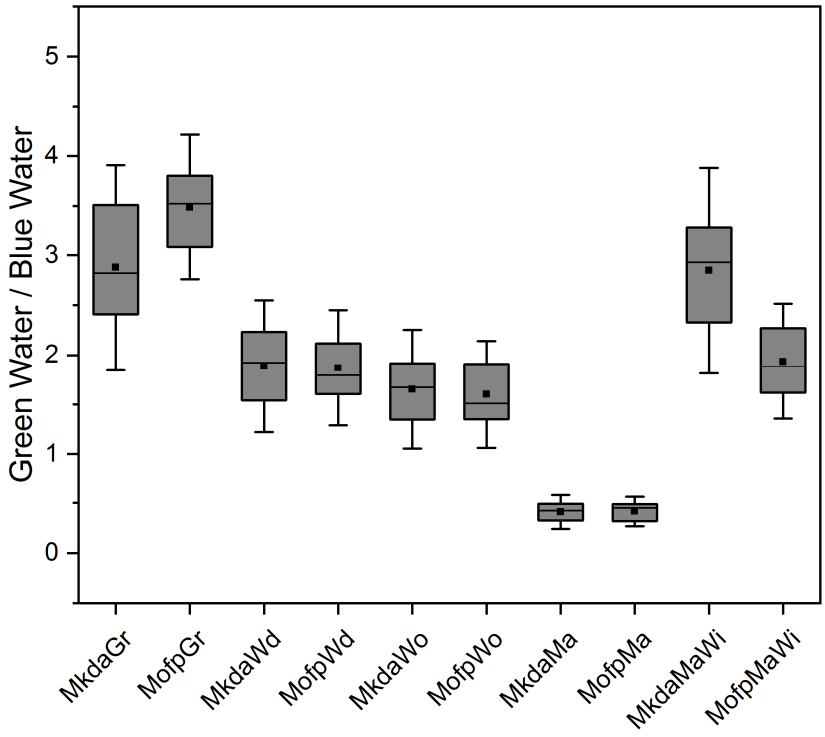

Fig. 103: Boxplots showing the green to blue water ratio of the simulation results with differing land use and vegetation cover

Fig. 103 illustrates the green to blue water relation for individual vegetation scenarios on both sites on the basis of the seasonal flux sums of the 30-year simulations. The boxes represent the lower and upper quartile, the whiskers show the minimum and maximum ratio whereas the point represents the medium relation together with the line showing the median. With a mean ratio of 2.9 and 3.5, the grassland scenarios show the highest effectiveness in soil water consumption with a higher relation on the old floodplain site. Since the Kalahari dune areas tend to produces higher bottom fluxes the amount of plant available soil water within the root zone is reduced due to deep percolation processes. In contrast, the different water retention function of the old floodplain soils provides higher amounts of soil water within the root zone for transpiration which explains the higher ratio. The dense woodland scenarios show mean ratios of 1.9 at both sites, and therefore lower compared to the grasslands. Because of the pronounced phenological development, increased unproductive water losses occur in times with low leaf development in which evaporation rates and bottom fluxes get addressed while transpiration fluxes are on a low

level. Even if the woodland is able to explore the total soil volume of the profile, the periods of low transpiration in combination with on- or offsetting rainfalls diminish the green to blue water ratio. The in total lower soil cover fraction but identical phenology and rooting characteristics of the open woodlands shows its effect on the ratio with again lower means of 1.7 on the Kalahari site and 1.6 in the old floodplains. The in comparison to the dense scenario small increase in evaporation and bottom flux lowers the ratio by 0.2 to 0.3. The Maize scenario with the highest seasonal blue fluxes shows the lowest green to blue ration because of the high impact of the crop-free period. The ratio of 0.4 is the lowest among all scenarios. By relating the ratio only to the cropping period where transpiration occurs, the ratio increases to 0.76 in the old floodplains and 0.8 at the Kalahari site and is therefore nearly doubled but still in a very low range. Responsible for these low ratios is the low plant density which supports high evaporative and drainage losses due to low leaf shading and occurring deep percolation caused by high water contents in the middle of the profile. As a special case, the irrigated crop rotation scenario reveals mean ratios ranging between 2.8 in the Kalahari dune area and 1.9 at the old floodplain site. Due to the increased input by additional irrigation water and the two-staged cropping rotation the total transpiration fluxes exceeds all other scenarios but without having higher ratios. As Fig. 102a shows the fluxes as fraction of input are similar between grassland and irrigation scenario which consequently results in a nearly identical green to blue water ratio at the Kalahari site, since a major proportion of the additional input, especially in the dry season within the Wheat period, is transpired by the vegetation while bottom fluxes and evaporative losses are only slightly higher due to the hampered percolation and the high leaf shading effects. In contrary, the different ratios between the grasslands with 3.5 and the irrigation scenario with 1.9 at the old floodplain site are explained by the increased bottom fluxes induced by the additional input which increases mid profile water conductivities and reallocates water beneath the root zone. To summarize the analysis of the previous sections, under the assumed conditions with respect to soil, weather, vegetation and irrigating settings, the grasslands show the best effectiveness focused on soil water utilization by vegetation followed by the woodlands and at least by the dryland agricultural scenario. Taking the grassland as a reference according to their transpiration characteristics and rooting properties which are in parts comparable to those of the Maize properties, the dryland scenario results reveal a high potential in soil water utilization since a major proportion of the soil water is lost by unproductive fluxes. By increasing the

plant density evaporative fluxes could be reduced while having an increased plant available soil water content in the root zone. The trade-off between higher soil cover fraction and interception losses accounts in this case only for a small proportion since it represents in maximum only up to 10 % of the rainfall input. Another measure to reduce unproductive losses may also be to hamper evaporation by covering the soil in times with low leaf development at the beginning of the cropping period. This measure shows its biggest effect with sites having a pronounced capillarity such as the old floodplain soils.

To evaluate the irrigation scenario regarding its effectiveness it is important to understand that this good ratio, as shown in Fig. 103, is only possible by supplement a significant amount of water input which can lead to a highly effective system but needs technical infrastructure, energy and water sources to sustain. The simulation results showed, that according to the combination of soil hydraulic conditions and vegetation properties the irrigation scheme must be adjusted individually to minimize trade-offs like increased bottom fluxes or the appearance of unevenly saturated layers within the root zone which both can lead to a reduced effectiveness. Increased bottom fluxes can also result in increased nutrient leaching processes especially under low pH conditions and low buffer capacities together with a deep relocation of in industrial agriculture commonly used fertilizer or pesticides.

6.4.3. What is the impact of land use change from pristine conditions to subsistence farming on the soil water balances?

Since a strong positive population growth sets pressure on natural resources in northern Namibia, a shift from pristine ecosystems into agricultural systems under dryland conditions has a major impact on soil water balances. The consequences of this transformations depend first of all on the initial state with its soil and vegetation conditions and on the condition after the transformation process. This section focuses on the transformation of wood- and grassland into a dryland agricultural system, since this transformation process is seen to be the most immanent dynamic in the Kavango region in Namibia.

The impact evaluation of the transition considers two soil hydraulic ecosystem services provided by functions directed connected to the water balance. On one hand the provisioning of groundwater for human use as well as the support of transpiration processes

for agricultural production or natural goods. As indicators for the impact on these services the bottom flux and the evapotranspiration are used to describe appearing changes.

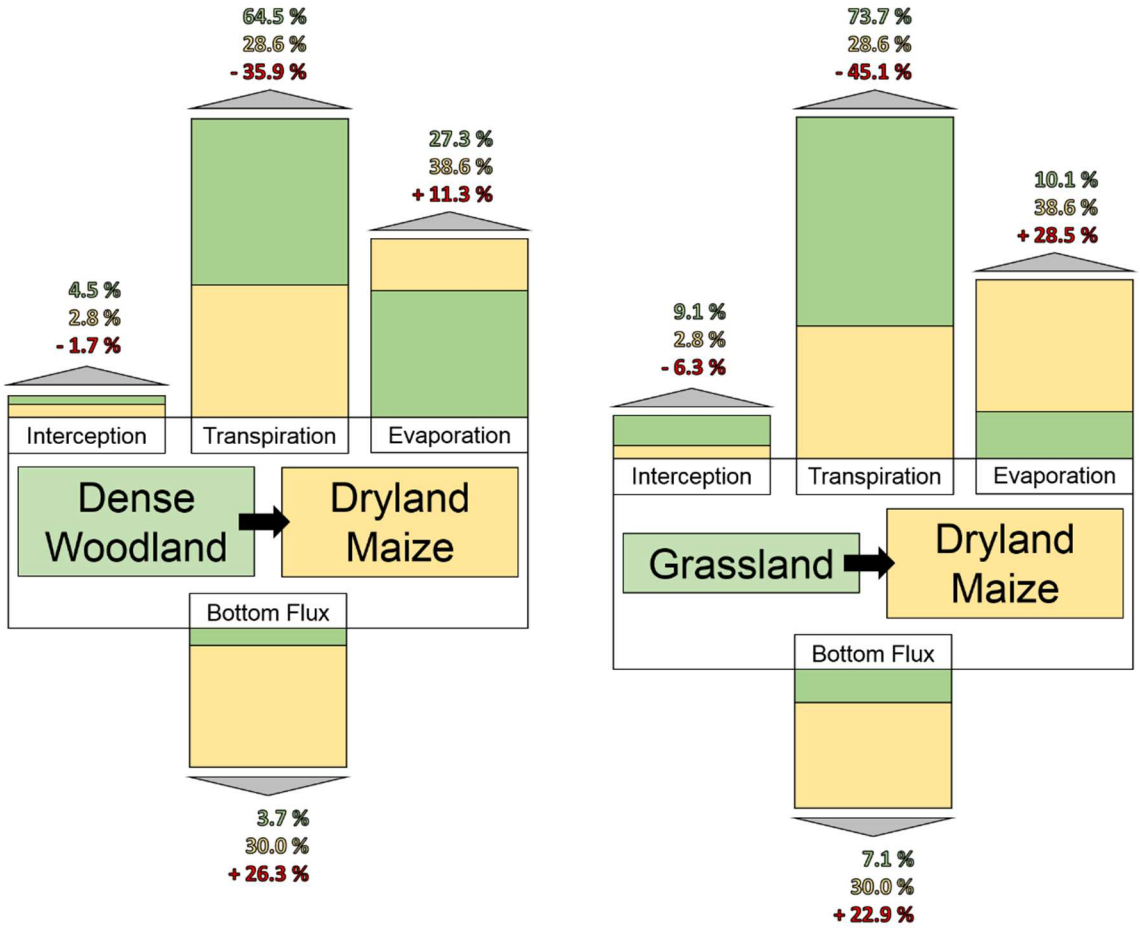

Fig. 104: Balance shifts from pristine conditions to dryland agricultural use in the Kalahari dune area.

Fig. 104 shows the water balance components as fractions of input for the transition from woodland and grassland to dryland agricultural cropping of Maize for the Kalahari site. The green bars represent the pristine conditions whereas the yellow bars show the dryland agriculture scenario, the red numbers show the differences between the scenarios. The all over trend shows an increase in potential groundwater recharge accompanied by an increase of evaporation while the transpiration fluxes increase significantly. The changes based on the woodland state are less pronounced compared to the grassland transformation except for bottom fluxes with an absolute change +26.3 %. On one hand, this surplus of potential groundwater recharge contributes to the provisioning of water for human use but is thwarted by the disproportional reduction of transpiration by absolute 35.9 %. On the other hand, the unproductive evaporation fluxes increase by absolute 11.3 %. The grassland transformation reveals a more distinct change with 6.3 % more

input due to fewer interception losses, which contributes to an increased amount of plant available water. On the other side, this positive change is outweighed by the 45.1 % reduction of transpiration which leads to an absolute 28.5 % increase in evaporation together with an increase of 22.9 % in potential groundwater recharge. Similar to the woodland transformation the surplus of potential groundwater is outweighed by the strong reduction of plant productive water use together with an increased unproductive water loss due to evaporation. In comparison, the grassland transformation shows a higher impact on human used soil water sources and balances as the woodland transformation.

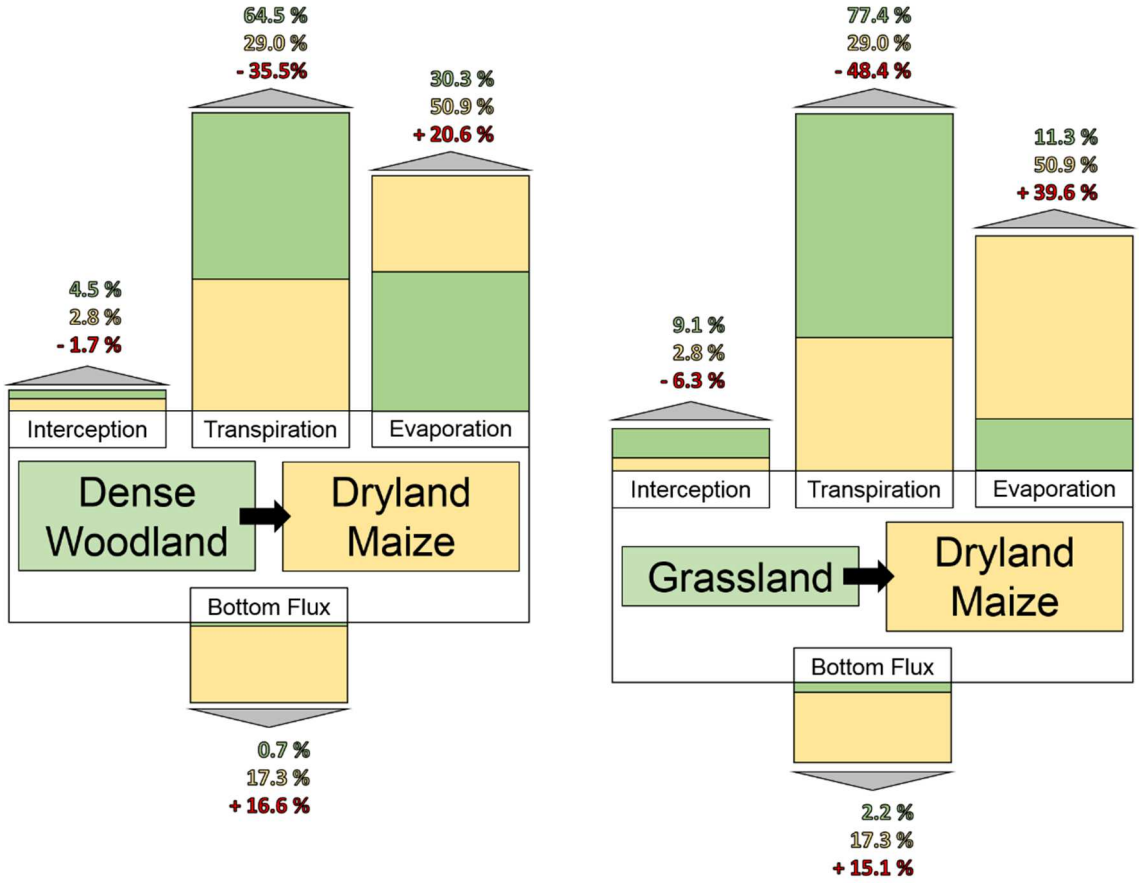

Fig. 105: Balance shifts from pristine conditions to dryland agricultural use in the old floodplains.

Fig. 105 shows the balance shifts for the old floodplain site. Since this site has the tendency to yield more evaporation the impact of land use change on this component is more pronounced than at the Kalahari site. In contrary, the bottom flux changes are smaller. The same overall tendency in changes, as realized in the Kalahari dune area, can be recognized in at that site. Looking at the woodland transformation changes the transpiration loses 35.9 % while the evaporation increases by absolute 20.6 % whereas the potential groundwater recharge increases to 17.3 % which is an absolute change of 16.6 %. According to

the differences between the transformation scenarios at the Kalahari site, the difference between the woodland and the grassland transformation is more distinct with a reduction of transpiration by absolute 48.4 % and additional 39.6% to the evaporation fluxes, whereas the increase of the potential groundwater recharge with additional 15.1 % is lower than in the woodland transformation scenario. The sum of the balance changes for the usable components bottom flux, as a measure for potential groundwater recharge and the transpiration, as a proxy for primary production reveals the total impact of a land use conversion from pristine to dry land agricultural conditions as shown in Tab. 19.

Tab. 19: Absolute change of the by human's utilizable soil water components, bottom flux and transpiration, expressed as fractions of the input

Simulation site	Transformation scenario	Δ Transpiration	Δ Bottom flux	total change
Kalahari dune area	Woodland to Dry-land agriculture	-35.9 %	26.3 %	-9.6 %
	Grassland to Dryland agriculture	-45.1 %	22.9 %	-22.2 %
Old floodplains	Woodland to Dry-land agriculture	-35.5 %	16.6 %	-18.9 %
	Grassland to Dryland agriculture	-48.4 %	15.1 %	-33.3 %

Through a conversion from woodland to dryland agriculture at the Kalahari site 9.6 % less of the incoming rainfall is usable, whether by plant production or groundwater extraction. This net change increases when grassland is transformed to dryland agriculture to 22.2 % less. At the old floodplain site, the change is even more severe with 18.9 % less rainfall utilization due to a conversion from woodland to dryland agriculture and 33.3 % less productive turnover by the transformation from grassland to dryland agriculture.

6.4.4. Consequences of increasing commercial agriculture areas under irrigation for river water and groundwater resources

The geographic conditions of the Kavango region make it a favorable area for industrialized commercial agriculture including irrigation application to enable crop rotation. The perennial but seasonally high variable river flow of the Okavango is in this context the primary source of water, which is already utilized for irrigation purposes on large scale green schemes. The simulation results are transferred to an existing green scheme expansion in Mashare to illustrate the impact of this small-scale development. Later on, based

on a technical report by the permanent Okavango river basin commission (OKACOM) (*Liebenberg* 2009), the modeled irrigation scenarios are evaluated, embedded in the assumptions and calculations presented in this publication. It presents several development scenarios with respect to the areal extent and cropping routines and evaluates water abstraction rates from the Okavango based on the necessary needs derived by atmospherical demand approach referring to the FAO reference evapotranspiration (see *Allen* et al. (1998)). The simulated irrigation demands of the SWAP model run are compared to the impacts presented in the report regarding the assumed abstractions rates and the connected flow consequences to the Okavango.

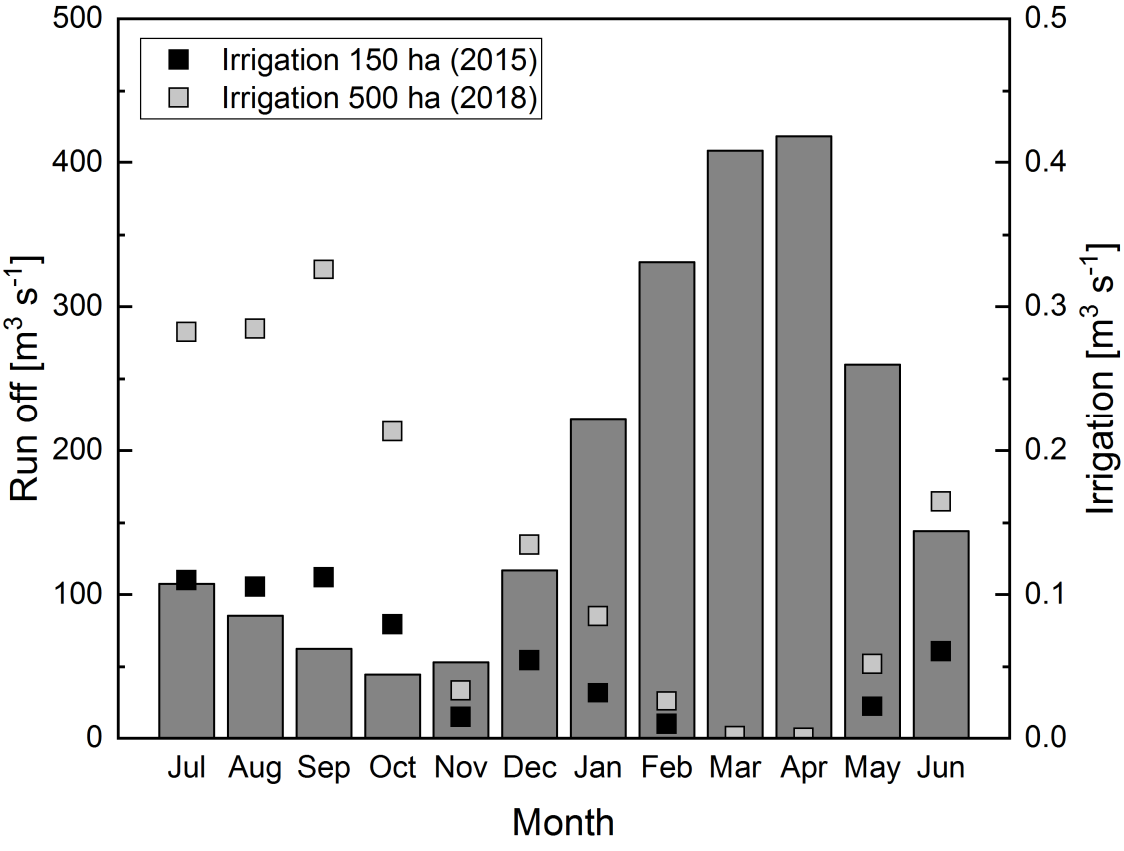

Fig. 106: Modelled monthly mean river runoff (*Steudel* et al. 2013a) and simulation-based river water withdrawal for irrigation need for two different development conditions of a green scheme in Mashare

As described in the previous sections the irrigation demand under the set timing and depth thresholds in combination with the crop rotation assumptions show a distinct seasonal pattern with high irrigation input over the dry season. The modeled monthly mean discharge for the river gauging station in Rundu, in the upstream part of the Okavango prior the conjunction with the Cuito River, show a seasonality with a low flow pattern in

the month of July to November (see Fig. 106). In this time the irrigation demand is particularly high due to high atmospheric demand and the lack of precipitation input. The green scheme in Mashare, situated in the old floodplains near the Okavango, operated two center pivot irrigation schemes together with five rectangular sprinkler fields to a total extent of about 150 ha in 2015. Recently, the farm receives additional cleared land for cultivation to a total extent of about 500 ha also including areas in the Kalahari dune area. The simulation results for irrigation water abstractions rate for both conditions, at 2015 and after the extension, are shown in Fig. 106. The course of the water abstraction is anticyclical to the river hydrograph the highest irrigation demand in low flow periods. The mean abstraction rate under the 2015 condition is 0.04 $m^3\ s^{-1}$ with a maximum in September of 0.11 $m^3\ s^{-1}$. After the extension, the mean abstraction rate in $m^3\ s^{-1}$ is tripled according to the three times higher area. Together the mean extraction rate is 0.03% to 0.07% of the mean monthly river discharge. The mean seasonal amount of water for irrigation is for the 2015 state $1.05735 \cdot 10^5\ m^3\ ha^{-1}\ a^{-1}$ and $8.4860 \cdot 10^5\ m^3\ ha^{-1}\ a^{-1}$. The differences are based on the different share of soils within the development between 2015 and 2018. Only focusing on this example the impact of water extraction on stream flow dynamics seem little but since the agricultural policy intend to intensify irrigation agricultural practice in the Kavango region the already mentioned assessment by *Liebenberg* envisages three different development scenarios divided into low, medium and high impact of water withdrawals connected to the size of the expansions planned (Tab. 20).

Tab. 20: Simulated irrigation water abstraction for three different development scenarios of the sections of the Okavango comparing SWAP model results with assumptions made by *Liebenberg* (2009)

Scenario		OKACOM (*Liebenberg* 2009)	SWAP MkdaMaWi	SWAP MofpMaWi
Cuito upstream				
Low increase 2461 ha	Water abstraction [$Mm^3\ a^{-1}$]	36.92	14.75	26.02
	Share of mean discharge [%]	0.71 %	0.28 %	0.50 %
	Share of min. discharge [%]	1.63 %	0.65 %	1.15 %
Medium increase 3600 ha	Water abstraction [$Mm^3\ a^{-1}$]	54.00	21.58	38.06
	Share of mean discharge [%]	1.04 %	0.41 %	0.73 %
	Share of min. discharge [%]	2.39 %	0.96 %	1.68 %
High increase 4545 ha	Water abstraction [$Mm^3\ a^{-1}$]	68.18	27.25	48.06
	Share of mean discharge [%]	1.31 %	0.52 %	0.92 %
	Share of min. discharge [%]	3.02 %	1.21 %	2.13 %
Cuito downstream				
Low increase 4394 ha	Water abstraction [$Mm^3\ a^{-1}$]	65.91	26.34	46.46
	Share of mean discharge [%]	0.71 %	0.28 %	0.50 %
	Share of min. discharge [%]	1.17 %	0.47 %	0.82 %
Medium increase 9000 ha	Water abstraction [$Mm^3\ a^{-1}$]	135.00	53.96	95.16
	Share of mean discharge [%]	1.44 %	0.58 %	1.02 %
	Share of min. discharge [%]	2.40 %	0.96 %	1.69 %
High increase 15659 ha	Water abstraction [$Mm^3\ a^{-1}$]	234.89	93.88	165.57
	Share of mean discharge [%]	2.51 %	1.00 %	1.77 %
	Share of min. discharge [%]	4.17 %	1.67 %	2.94 %

The assessment published by the OKACOM based on an assumed irrigation demand of 15000 $m^3\ ha^{-1}\ a^{-1}$ for a crop rotation of Wheat and Maize with a peak demand of 10 mm d^{-1}. For the calculation of the relative water withdrawal compared to the river discharge the share of the Okavango in the Kavango region is divided into two parts reflecting the different flow regimes with its individual discharge volumes. The upstream areas prior the conjunction of the Cuito River are characterized by a minimum discharge of 2260 $Mm^3\ a^{-1}$ and an average of 5200 $Mm^3\ a^{-1}$. After the conjunction of the Cuito, the discharge increases to a minimum of 5635 $Mm^3\ a^{-1}$ and an average rate of 9350 $Mm^3\ a^{-1}$. The increase

in discharge in downstream areas of the Kavango region is reflected by the high development scenario assumptions due to the improved conditions for irrigation water abstraction. The atmospheric demand calculation does not include soil hydrological relations and is therefore only oriented on the potential crop water demand. After *Liebenberg*, the possible irrigation water abstraction is equal to 1.63 % to 3.02 % of the minimum discharge for the upstream regions prior the conjunction and a share of 0.71% to 1.31 % for average discharge conditions. Since the development scenarios show higher extents in the downstream regions with a maximum of total 15659 ha assumed development potential, the total extraction rates increase to 65.91 Mm^3 a^{-1} for the lowest scenario up to 234.89 Mm^3 a^{-1} for the highest. This is equal to 0.71 % and 2.51 % of the average discharge and in low flow periods up to 1.17 % to 4.17 %. With the integration of soil hydrological dynamics and a soil hydraulic head-controlled irrigation management in the SWAP simulations the mean irrigation demand for the individual soil types in Mashare is 10573 m^3 ha^{-1} a^{-1} under old floodplain soil conditions and 5995 m^3 ha^{-1} a^{-1} in the Kalahari dune areas. With these assumptions, the abstractions rates of all defined OKACOM scenarios are consequently lower with 0.28 % to 0.52 % of the average discharge in the Kalahari dune area of the upstream regions and 0.50 % and 0.92 % on old floodplain soils. For the downstream region, the mean discharge extraction is equal to 0.28 % to 1.00 % of for irrigation on Kalahari dune area soils and 0.50 % up to 1.77 % for the highest development scenario in the old floodplains. The highest calculated impact shows the old floodplain irrigation in the downstream region in low flow times with a share of 2.94 %. Taking the effect of irrigation on soil water balances into account, the irrigation application results, especially in the old floodplains, show a secondary impact on groundwater resources (Tab. 21). The high water inputs result in, depending on soil texture and crops used, 9.6 % to 20.0 % bottom fluxes as fractions of the input amount. Under the soil hydraulic head-controlled irrigation management scenario and the derived irrigation demand annual bottom fluxes of 113.4 mm to 327.7 mm occur. Transferred to the assumed irrigation demand of the OKACOM report approximately 199.9 mm to 416.3 mm can be expected to drain and contribute potentially to groundwater recharge.

Tab. 21: Bottom fluxes calculated by the scenario simulation and transferred bottom flux input related to the irrigation demand defined by OKACOM

Site	Precipitation [mm a-1]	Irrigation demand SWAP [mm a-1]	Irrigation demand OKACOM [mm a-1]	Bottom flux SWAP [% input]	Bottom fluxes SWAP [mm a-1]	Calc. bottom fluxes OKACOM [mm a-1]
MofP	580.6	1057.3	1500	9.60	113.4	199.92
Mkda		599.5	1500	20.00	327.7	416.25

An exact determination is only possible by calculating model-based fluxes due not represented soil physical and vegetation interactions. Nevertheless, the higher estimated irrigation demand of the OKACOM calculation is likely to produce higher drainage amounts. Since a certain amount of drainage in irrigation agriculture is intended to prevent soil salinization a negative consequence for groundwater quality is likely to appear due to leaching processes and the reallocation of dissolved fertilizers which are applied with the irrigation water. Depending on the topology of the fields and the streamline of the Okavango a solute input in saturated areas of the soil or even in shallow groundwater table reach the Okavango over a base flow and is likely to increase the nutrient concentrations of the river water.

It needs to be mentioned that these results are only valid for the assumed soil hydrological relations and the specific model setting with regard to irrigation timing and depth. Nevertheless, this exemplary comparison showed, that a soil hydrology-controlled irrigation management can increase the efficiency of irrigation water use and helps to optimize water abstraction for a more sustainable river water use, which lowers subsequently the impact for the downstream situated regions with respect to water availability and interannual river flow dynamics. Because the impact of water abstraction is the highest in low discharge periods the water abstraction impact needs to be minimized for these times.

7. How does bush encroachment alter soil water dynamics and potential groundwater recharge in the semi-arid highlands of central Namibia?

Bush encroachment is seen to be a major driver of soil aridification processes in the semi-arid regions in central Namibia with implications for groundwater recharge as one source for potable water for human use or livestock. On the other hand, an increased bush encroachment is known to have negative consequences on the amount of plant available water. Systematic assessments of the effects and causes of bush encroachment are dominated by studies localized in the Americas but only little numbers of studies focus on the southern African area (*O'Connor* et al. 2014). Since studies about the influence of bush encroachment on soil water balances and subsequent processes like groundwater recharge for southern African regions are scarce, some assumptions that are repeatedly cited going back to the 1960s and whereas newer publications refer mostly to ecohydrological aspects. To contribute to an improved understanding of the hydrological consequences of a thornbush savannah under change following questions are:

- What kind of soil water dynamic modifications are related to increasing shrub densities?
- How are the interactions between individual soil water balance components and
- what is a possible impact of bush encroachment on deep drainage fluxes as a source for groundwater recharge?

To answer these questions empirical data evaluations of soil water measurements are combined with modeling approaches reflecting canopy scenarios as a proxy for a high bush encroachment dynamic and intercanopy conditions for the typical open character of a savannah landscape. Where empirical data analysis describes the tendency of the individual site characteristic statistically, the model approach is able to illustrate the time depending development of soil-vegetation- atmosphere fluxes and feedbacks, as far as they are considered within the model application.

7.1. Soil hydrological modeling plots

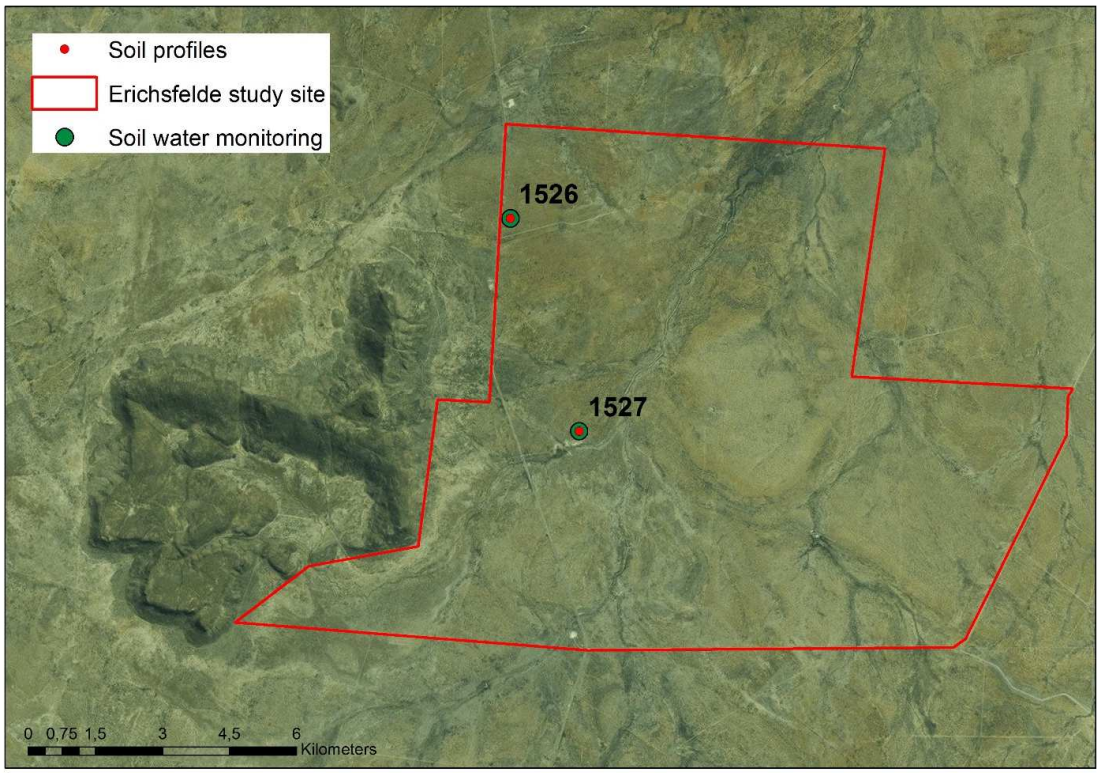

Fig. 107: Map showing the soil survey points and the locations of the soil water monitoring stations within the Erichsfelde study site

To study the influence of increasing bush encroachment dynamics on soil water balances, two different soil water monitoring points with differing vegetation composition were selected. Therefore, it was focused on two main decision criteria were, on one hand, the soil properties have to be comparable, to ensure minimum influence by the soil itself. On the other hand, the number of encroacher individuals must be significantly different (low versus high) to get pronounced signals, caused by encroaching trees or shrubs. The profile plot 1526 is characterized by a low bush encroachment with a dominating grass vegetation covering 50 % of that area where only 1 % is covered by the encroacher species *Acacia mellifera* (see Tab. 22). The soil coverage is in total 54 % with nearly one have of bare soil patches in between. The second profile plot 1527 has a lower total coverage of 31 % but with an absolute higher encroacher density of 15 %. Beside the Acacia species, perennial shrubs are the second dominating vegetation form followed by grasses with only 4 % coverage (Tab. 23).

Tab. 22: Vegetation composition at profile 1526

Specie	Cover [%]	Remarks
Stipagrostis uniplumis	50	Perennial grass
Lycium oxycarpum	2	Perennial shrub
Acacia mellifera	1	Shrub/tree
Geigeria ornativa	1	Annual herb
Total cover	54	

Tab. 23: Vegetation composition at profile 1527

Specie	Cover [%]	Remarks
Acacia mellifera	15	Shrub/tree
Monechma genestifo-lium	5	Perennial shrub
Acacia tortilis	5	Shrub / tree
Stipagrostis uniplumis	3	Perennial grass
Lycium oxycarpum	2	Perennial shrub
Eragrostis jeffreysii	1	Perennial grass
Total cover	31	

7.1.1. Plot and soil profile descriptions

Fig. 108: Environmental aspect and site impression of profile 1526

The profile 1526 is located in the northern part of the study site (Fig. 107). According to the World Reference Base for Soil Resources, a main criterion to characterize this soil as Luvisol is fulfilled by the increased clay content with depth (Fig. 109 & Fig. 110). Thereby

it is irrelevant which pedogenic processes are responsible, whether it is clay migration or clay mineral weathering. However, the existing low pH-values favor the process of clay migration whereas clay mineral weathering begins only with much lower pH ranges. The overall soil texture is dominated by up to 70 % Sand subdivided into nearly even proportions of fine, medium and coarse sand subfractions. The homogenous reddish soil color indicates low organic matter content proved by laboratory analysis. The amount of rock fragments is increasing with depth to 40 % in the lowest horizon starting in 80 cm. 47 % of the overall root can be found in the upper 10 cm. Secondary biotic macropores build by termites and ants occur whereas no shrinkage or swelling dynamics are visible.

Profile 1526	Lat: -21,61126°	Long 16,870180°	1916 m h.s.l.	Loc.: Erichsfelde / Namibia
Topography: Plateau	**Slope:** 0°	**Exposition:** /	**Curvature:** plain	**Landscape unit:** /	**Land use unit:** Cattle farming	**Vegetation / Crop:** *Stipagrostis uniplumis, Acacia mellifera*
Remarks: ES				

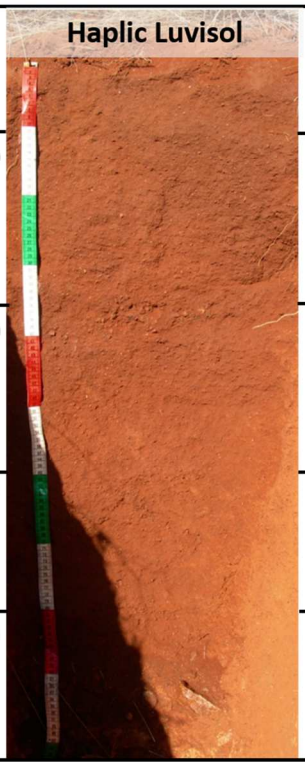

Ah	**Grain Size:** Medium loamy sand Sl3 (KA5)/SL (WRB); subangular structure; **Munsell Colour**: moist 5 YR 3/4, dry 5 YR 4/5; **Roots:** 40 roots dm^{-2}; 3 % rock fragments
10 cm Bw1	**Grain Size:** weak clayey sand St2 (KA5)/SL (WRB); subangular structure; **Munsell Colour**: moist 5 YR 3/4, dry 5 YR 4/5; **Roots:** 15 roots dm^{-2}; 5 % rock fragments
35 cm Bw2	**Grain Size:** medium clayey sand St3 (KA5)/SL (WRB); subangular structure; **Munsell Colour**: moist 2.5 YR 2.5/3, dry 5 YR 4/5; **Roots:** 20 roots dm^{-2}; 10 % rock fragments
60 cm Bw3	**Grain Size:** medium clayey sand St3 (KA5)/SL (WRB); subangular structure; **Munsell Colour**: moist 2.5 YR 2.5/3, dry 5 YR 4/5; **Roots:** 8 roots dm^{-2}; 8 % rock fragments
80 cm	**Grain Size:** medium clayey sand St3 (KA5)/SL (WRB); subangular structure; **Munsell Colour**: 5 YR 3/4, dry 5 YR 4/5; **Roots:** 3 roots dm^{-2}; 40 % rock fragments

Fig. 109: Description of profile 1526

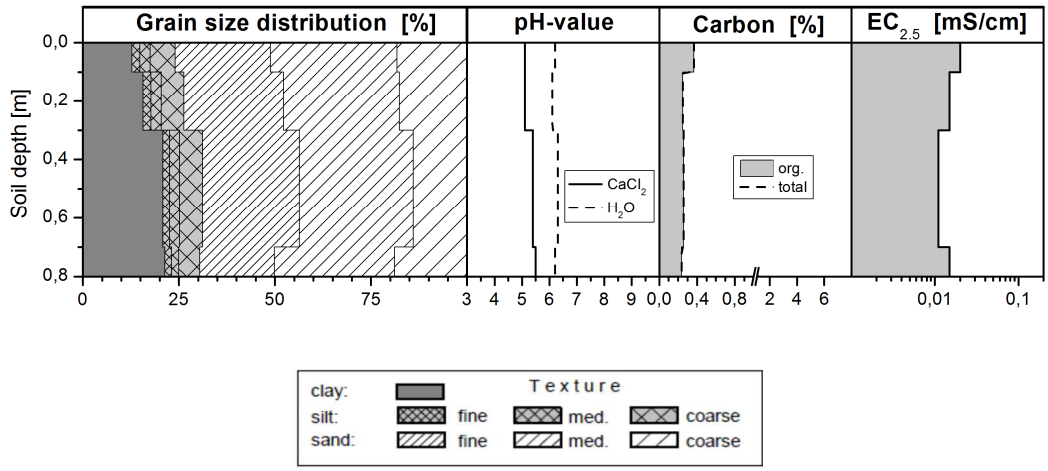

Fig. 110: Soil texture and chemical properties of profile 1526

Fig. 111: Environmental aspect and site impression of profile 1527

Plot 1527, as already mentioned above, is, regarding its soil properties (Fig. 112 & Fig. 113), comparable to plot 1526 but differs in vegetation structure. This difference can be realized not only by the aboveground vegetation structure but also by looking at the root distribution. 47 % of the all over root numbers are to be found in the second horizon between 10 cm and 35 cm which is an indication of the dominance of deeper rooting shrubs

and trees contrasting plot 1526.The microtopography is characterized by sinks and uplifted areas due to animal activities which leads to a heterogeneous surface structure consisting of undisturbed areas with topsoil capping and disturbed parts where capping is broke open. Therefore, small-scale lateral surface water redistribution because of not infiltrated precipitation can be a considerable dynamic. According to profile 1526 biotic macropores by termites and ants play a role in shortcutting infiltration processes to deeper soil horizons

Profile 1527	Lat: -21,65408°	Long 16,88562°	1916 m h.s.l.	Loc.: Erichsfelde / Namibia

Topography: Plateau	**Slope:** 0°	**Exposition:** /	**Curvature:** plain	**Landscape unit:** /	**Land use unit:** Cattle farming	**Vegetation / Crop:** *Acacia mellifera, Monechma genestifolium*

Remarks: EL

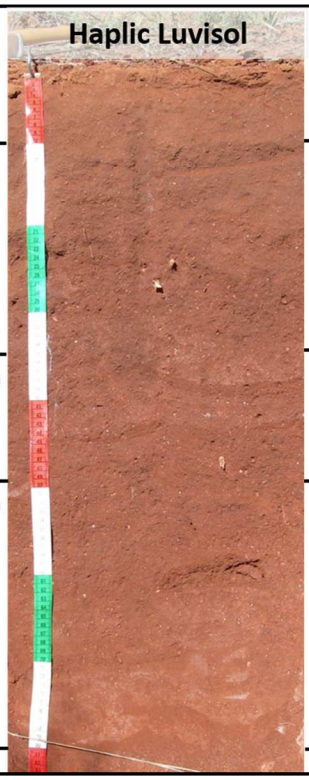

Ah	**Grain Size:** medium loamy sand Sl2 (KA5)/LS (WRB); subangular structure; **Munsell Colour**: moist 5 YR 3/4, dry 5 YR 4/5; **Roots:** 18 roots dm^{-2}; 2 % rock fragments
10 cm Bw1	**Grain Size:** weak clayey sand St2(KA5)/LS (WRB); subangular structure; **Munsell Colour**: moist 5 YR 3/4, dry 5 YR 4/5; **Roots:** 35 roots dm^{-2}; 6 % rock fragments
35 cm Bw2	**Grain Size:** medium clayey sand St3 (KA5)/LS (WRB); subangular structure; **Munsell Colour**: moist 2.5 YR 2.5/3, dry 5 YR 4/5; **Roots:** 14 roots dm^{-2}; 6 % rock fragments
60 cm Bw3	**Grain Size:** medium clayey sand St3 (KA5)/LS (WRB); subangular structure; **Munsell Colour**: moist 2.5 YR 2.5/3, dry 5 YR 3/4; **Roots:** 7 roots dm^{-2}; 5 % rock fragments
80 cm	

Fig. 112: Description of profile 1527

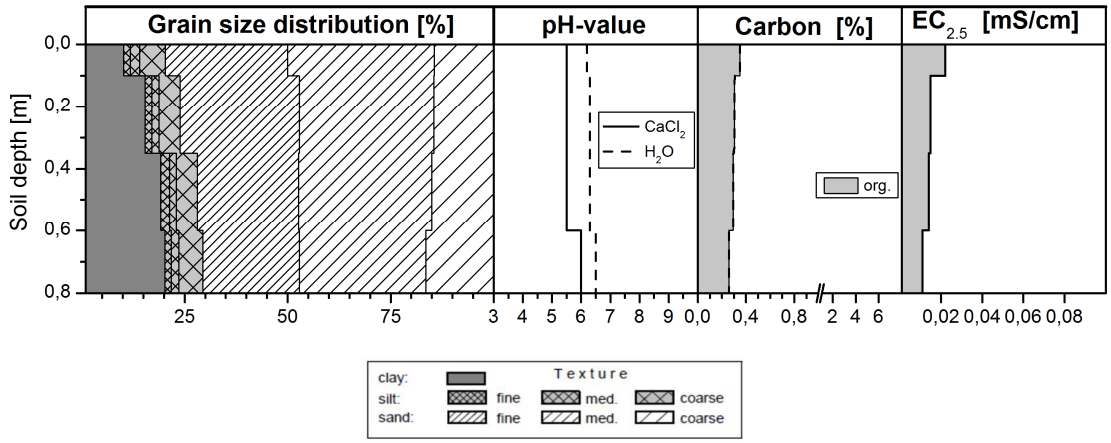

Fig. 113: Soil texture and chemical properties of profile 1527

7.1.2. Soil hydrological properties

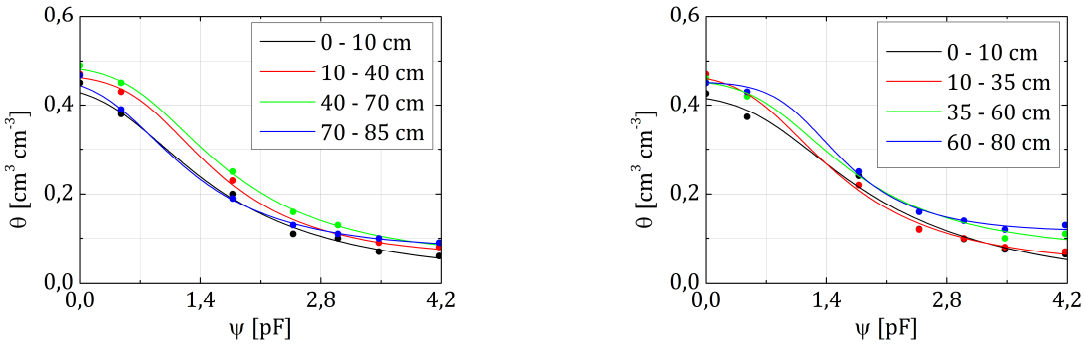

a) b)

Fig. 114: Water retention curves for profiles (a) 1526 and (b) 1527

The site selection for this case study was orientated on comparable soil properties but divergent vegetation composition to minimize external influences on the effect of vegetation on soil water dynamics. According to these preconditions, the soil hydraulic properties of the two selected profiles in Erichsfelde are in large parts identical (compare Fig. 114 and Tab. 24). Both show a depth-increasing PWP between 0.07 $cm^3\ cm^{-3}$ to 0.12 $cm^3\ cm^{-3}$ with θ_s ranging from 0.43 $cm^3\ cm^{-3}$ to 0.45 $cm^3\ cm^{-3}$ in the topsoil and 0.45 $cm^3\ cm^{-3}$ to 0.47 in 60 – 85 cm depth. The depth related variability, as well as the inter-site variability, shows only little differences with respect to the range of the PWP in profile 1527 where the range of the PWP is between 0.08 $cm^3\ cm^{-3}$ in the topsoil and 0.12 $cm^3\ cm^{-3}$ in the subsoil due to depth-increasing clay contents. Due to the high PWP water contents, the uFC is limited to under 0.20 $cm^3\ cm^{-3}$ showing minimum water contents of only 0.09

$cm^3\ cm^{-3}$ in the lowest sampled horizon of profile 1526 and a maximum of 0.17 $cm^3\ cm^{-3}$ in the topsoil of profile 1527.

Tab. 24: Soil hydrological characteristics of the studied horizons at the Erichsfelde site

Horizon	Upper [cm]	Lower [cm]	θ_s [$cm^3\ cm^{-3}$]	PWP [$cm^3\ cm^{-3}$]	FC [$cm^3\ cm^{-3}$]	uFC [$cm^3\ cm^{-3}$]
1526_1	0	10	0.45	0.07	0.20	0.13
1526_2	10	40	0.47	0.09	0.23	0.14
1526_3	40	70	0.49	0.10	0.25	0.15
1526_4	70	85	0.47	0.10	0.19	0.09
1527_1	0	10	0.43	0.07	0.24	0.17
1527_2	10	35	0.47	0.08	0.22	0.14
1527_3	35	60	0.46	0.10	0.25	0.15
1527_4	60	80	0.45	0.12	0.25	0.13

The van Genuchten-Mualem functions for retention and conductivity were fitted to the measured retention and conductivity values to obtain the relevant parameter as input for the SWAP model. As a result, these parameters are shown in Tab. 25.

Tab. 25: Derived van Genuchten-Mualem parameter for the Erichsfelde site

Layer	Upper [cm]	Lower [cm]	θ_s [$cm^3\ cm^{-3}$]	θ_r [$cm^3\ cm^{-3}$]	α	n	K_s [$cm\ d^{-1}$]	l
1	0	30	0.4330	0.0620	0.0571	1.479	356.20	0.089
2	30	300	0.4140	0.0890	0.0354	1.624	402.00	0.615

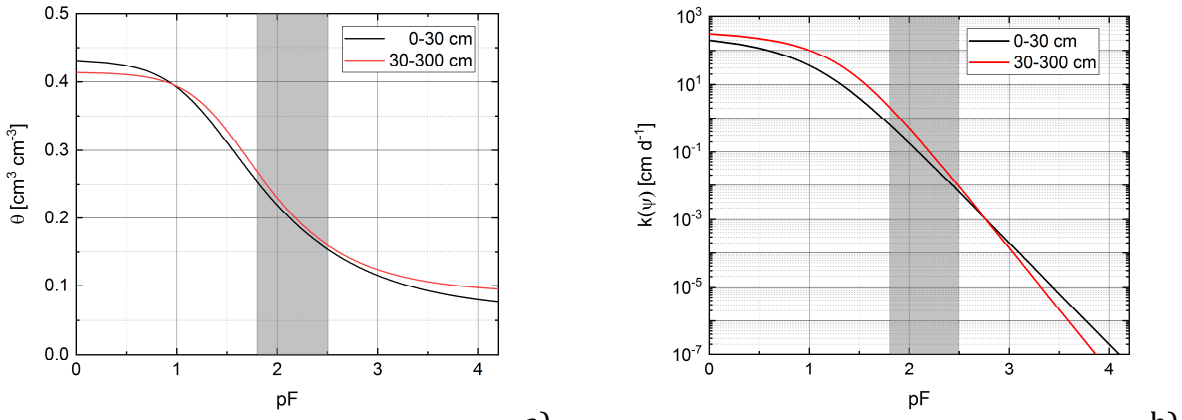

Fig. 115: Diagram of the resulting soil hydrological retention (a) and conductivity functions (b) according to the fitted van Genuchten-Mualem parameters for the topsoil parameter and the subsoil parameters for the Erichsfelde site

Only one parameter set was chosen to be defined as model input but contrary to the method of the other case studies, this time a vertically differentiated set of two layers is used to represent the luvic properties of the site's soil. Fig. 115a and Fig. 115b shows the retention and conductivity functions for both layers as parameterized for this case study

simulation. The retention, as well as the conductivity as a function of the soil water pressure head, do not differ significantly. The topsoil layer shows a little higher volume of total pore space and little less PWP volume which reflects the less clayey character of this layer in contrast to the subsoil layer with a little higher PWP and less total pore space due to its higher bulk density. The topsoil layer shows lower conductivities starting with 356.2 cm d^{-1} under saturated conditions and $7.57 \cdot 10^{-1}$ cm d^{-1} at pF 1.8. Compared to layer one layer two shows little higher conductivities with 402 cm d^{-1} under saturation and 2.52 cm d^{-1} at pF 1.5.

7.1.3. Soil hydrological measurements

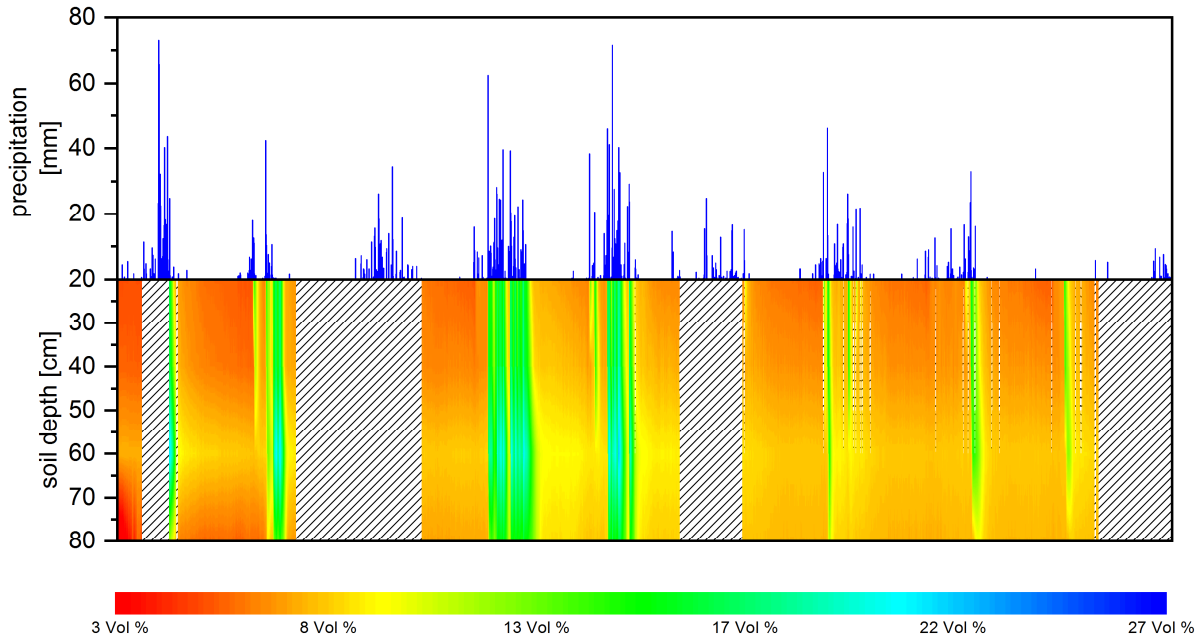

Fig. 116: Measured soil water contents of the canopy plot on site 1526

In this section, a condensed overview on the long-term soil water monitoring campaign, comprising canopy and intercanopy measurement profiles on to plots, gives indications of the effect of bush encroachment on soil water dynamics with respect to infiltration, percolation and evapotranspiration dynamics. The presented descriptions and evaluations base on an 8 year measurement period beginning with the rainy season 2007/2008 and ending with season 2014/2015 (unpublished data by *Gröngröft* et al. (2018)). The soil water measurements with a temporal resolution of eight hours refer to 20 cm equidistant depths from 20 cm to 80 cm. The plot specific incoming precipitation amounts were recorded by tipping bucket rain gauges to be able to quantify site-specific fluxes by applying soil hydrological balance methods. Since no hydrophysical information about

underlying bedrock formations is available the following considerations refer only to the 100 cm depths of the respective soil profiles.Fig. 116 and Fig. 117 show the seasonal course of the absolute soil water contents of the canopy and intercanopy influenced plot expressed in millimeter (residual water content corrected) throughout all measured profile depths as color matrix complemented with the profile sum for total water content indicated by the black line. Times with missing values are hatched. The incoming rains show a high inter-seasonal variability with a minimum of 184 mm in season 2012/2013 and maxima with 754 and 794 mm in two consecutive seasons from 2010/2011 to 2011/2012. Since rain events are mainly formed by convective dynamics, rainstorms occur with maximum measured intensities of 31.4 mm $0.5h^{-1}$. The first comparison between the canopy and intercanopy water dynamics reveals two main differences referring to infiltration and percolation dynamics and water buffer characteristics which support subsequent deep drainage and evapotranspiration fluxes. Seasons with high precipitations show a moistening of the measurement profile onto the maximum depth at both plots whereas in the season 2013/2014 with isolated rainfall events and medium to low intensities, the canopy plot shows a lower increase in bulk soil water contents compared to the intercanopy plot. At the end of the rainy season 2010/2011 and little less pronounced in season 2011/2012, the intercanopy plot is able to sustain higher water content over a certain period compared to the canopy plot where the available soil water is reduced rapidly.

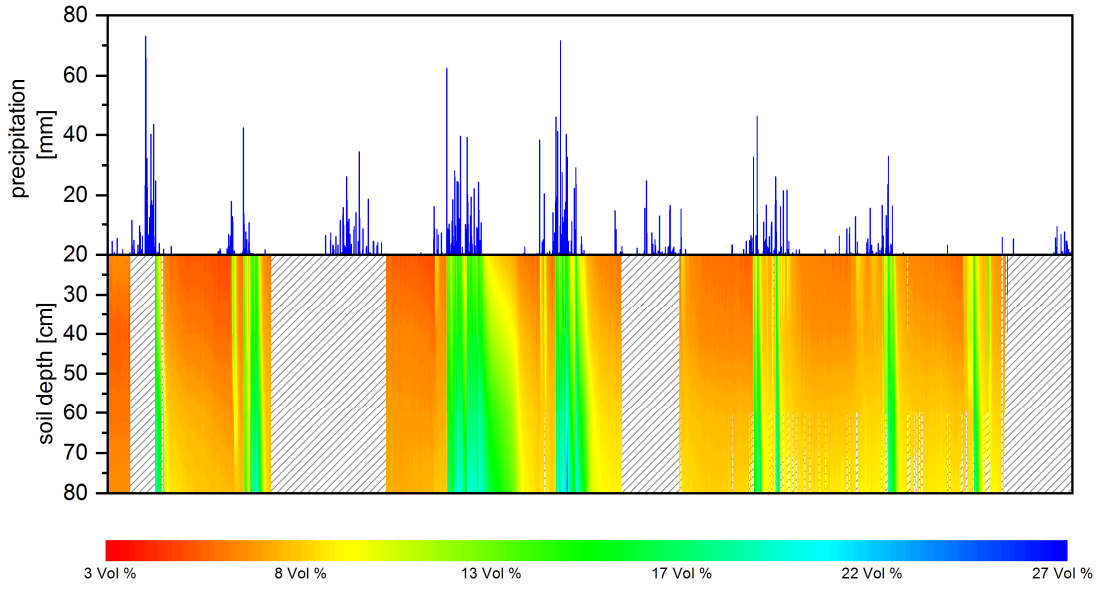

Fig. 117: Measured soil water contents of the intercanopy plot on site 1526

Looking at the measurements of site 1527 in Fig. 116 the analyses of the rain gauge readings show a minimum input of 198 mm again in season 2012/2013 and maximum amounts in the respective high input rainy seasons in 2010/2011 and 2011/2012 with 760 mm and 652 mm. The maximum rainfall intensities with 34.4 mm $0.5h^{-1}$ to 39.0 mm $0.5h^{-1}$ are 9% to 19% higher compared to site 1526, indicating the high spatiotemporal variability of the study site Erichsfelde. The combination of a higher encroacher density at site 1527 and different rainfall characteristics are reflected in the measured soil water contents. In season 2010/2011 at the canopy plot, only cumulated rainfall events in the middle of the rainy season are able to increase bulk soil water contents to a maximum of about 150 mm while isolated rain storms at the onset of the season rewet the profile only to a depth of 40 cm. The same input characteristic of the mentioned season leads to higher infiltration amounts and to a deeper relocation by percolation processes at the intercanopy plot. The season 2013/2014, with 65.2 mm more rainfall input compared to site 1526, and less isolated events at high intensities, increase the bulk soil water content at the canopy plot significantly correlated with two events with high intensities. Rain events with lower intensities show only little impact on soil water changes. The response of the development of soil water contents at the intercanopy plot shows a more pronounced dynamic where those rain events, that had no impact on soil water changes at the canopy site, infiltrate and increase soil water contents to a depth of 40 cm where it contributes to evapotranspiration. Comparing the soil water reduction dynamics at the end of the rainy season a similar pattern to 1526 is visible. The, in total, lower water contents at the canopy plot get depleted in short-term while the intercanopy shows a similar tailing of soil water reduction in deeper layers.

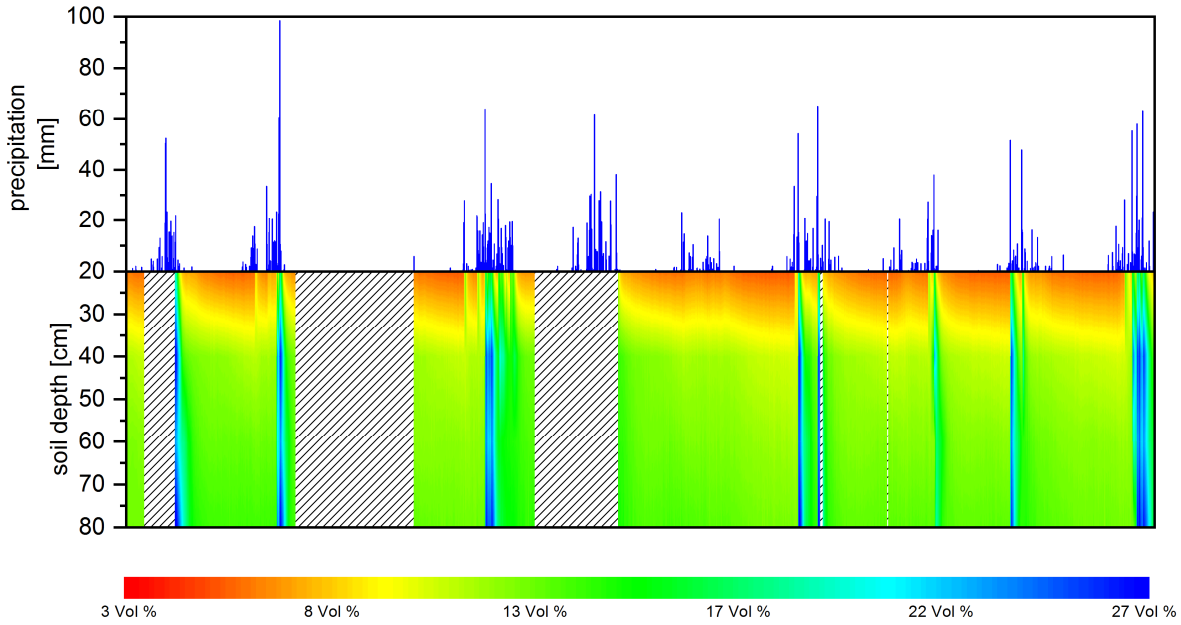

Fig. 118: Measured soil water contents of the canopy plot on site 1527

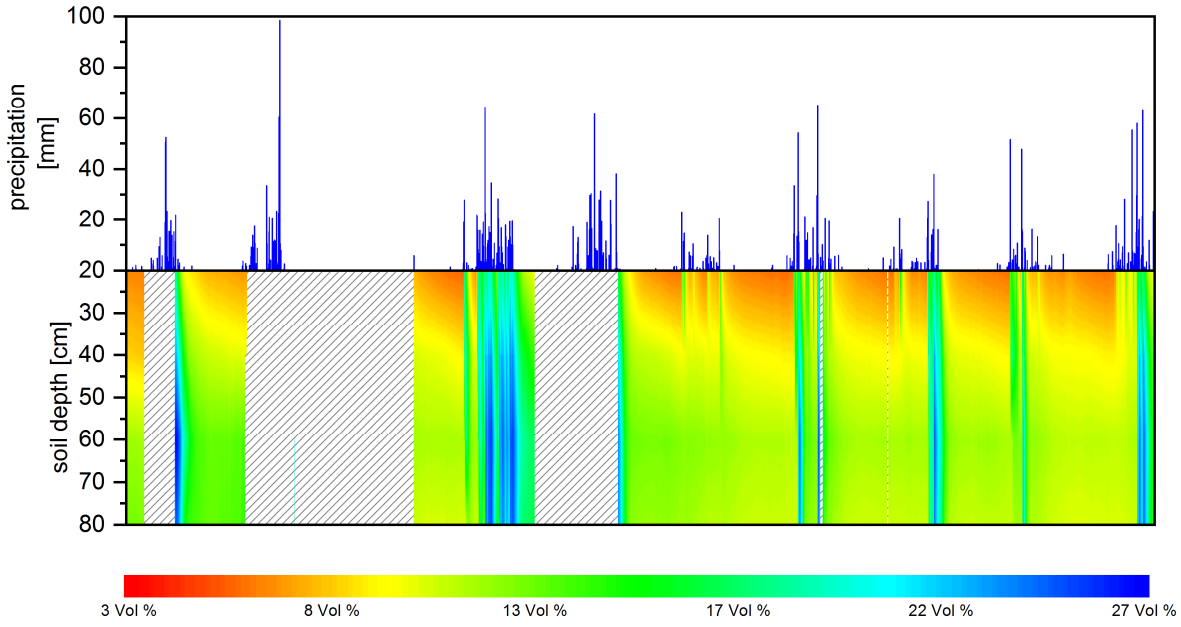

Fig. 119: Measured soil water contents of the intercanopy plot on site 1527

To distinguish whether the described differences in soil water dynamics are caused by vegetation induced input reduction, infiltration modification or influences on evapotranspiration fluxes the assessment also include analyses made by *Gröngröft* et al. (2018). A first analysis focusses on the recovery rate of daily precipitation amounts within the soil hydrological cycle. Therefore the cumulated daily precipitation is correlated with the cu-

mulated positive total soil water content changes for periods without data gaps. The resulting scatterplots pattern indicate the recovery relation between incoming precipitation and infiltration amounts as shown in Fig. 120 and Fig. 121.

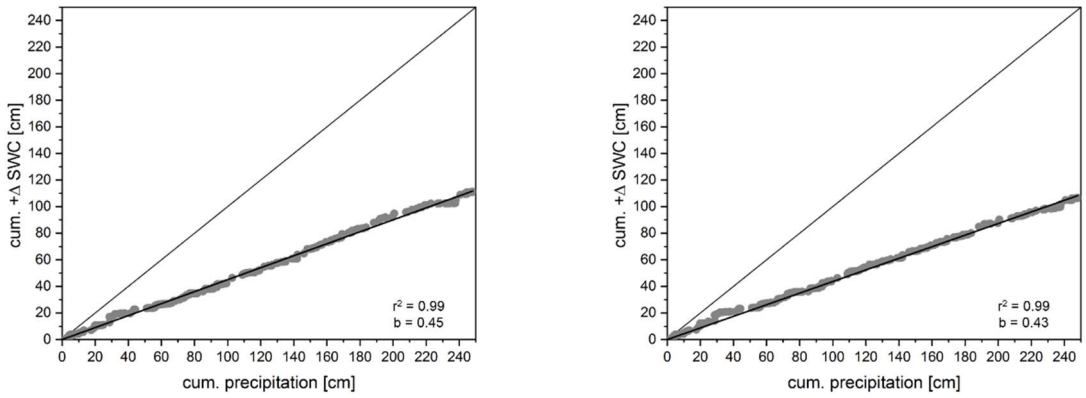

a) b)

Fig. 120: Scatterplots showing the relation between the cumulated precipitation input and the cumulated positive profile water content changes for profile 1526 a) canopy and b) intercanopy plot

At all examined sites the relations determination is highly linear with r^2 of 0.99. The slope of the linear regression as a measure of the recovery rate is site-specific and exhibit a certain inter- and intra-site variability. The recovery rate at profile 1526 with its low encroachment impact shows a rate of 0.45 at the intercanopy plot and 0.43 at the canopy plot whereas the plot 1527 with higher plant densities reveals a more pronounced intra-site variability with 0.52 recovery at the intercanopy plot and 0.32 at the canopy plot. The inter and intra site-specific differences can be explained by the higher vegetation heterogeneity of plot 1527 with a higher proportion of shrubs and trees whereas 1526 is more homogeneous with respect to the species composition as well as the spatial distribution (see Fig. 108 and Fig. 111).

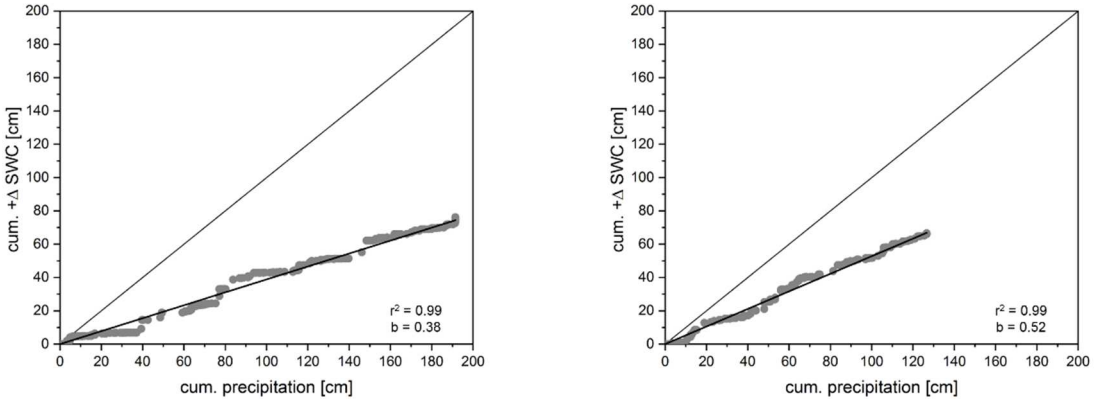

a) b)

Fig. 121: Scatterplots showing the relation between the cumulated precipitation input and the cumulated positive profile water content changes for profile 1527 a) canopy and b) intercanopy plot

Since no interception measurements are available the recovery rate of incoming precipitation within the bulk soil can be used as a measure for interception whereas the absolute values seem to overestimate interception losses which may result from the fact that the first TDR probe is installed in 20 cm depth and low-intensity rainfall events do not change the top soil water content in this depth before recycled to the atmosphere. In contrast *Gröngröft* et al. determined precipitation to infiltration dynamic by comparing rain events < 8 mm 8 h -1 with positive profile soil water changes. The analysis shows significant differences to the previous approach with recovery rates of 71 % for the canopy site and 87 % for the intercanopy site of profile 1526. On profile 1527 the recovery rates are 67 % under canopy and 108 % in intercanopy space. The rainfall exceeding soil water increases in the intercanopy space is explained by an infiltration surplus resulting in lateral surface water redistribution which is indicated by the correlation between high rainfall intensities and with exceeding positive soil water changes. Since the previous approach includes only a temporal subset of the available data the analysis are only valuable for this respective period whereas the approach by *Gröngröft* et al. relies on the total data population with a higher temporal resolution and are therefore more representative. Analysis regarding deep percolating water need to address soil hydraulic heads measurements in the soil layer at the bottom of the profile. A separation of phases in which the subsoil is below field capacity (≤ pF 1.8) is an appropriate approach to characterize times and events with possible downward oriented water movement. Respective analysis reveal that the intercanopy sites show in tendency more days (1526: 87 days / 1527: 102 days) within the

period of moist subsoil than the canopy sites (1526: 22 days / 1527: 40). This semi-quantitative results does not account for any hydraulic gradients which have a great influence on the velocity, and therefore, on the amount of water which possibly percolates. Nevertheless, it can be assumed, that in these periods gravitational soil water reallocation processes take place, which, in result, shows that the intercanopy spaces tend to higher percolation dynamics in times of moist soil profiles.

7.1.4. Weather forcing data

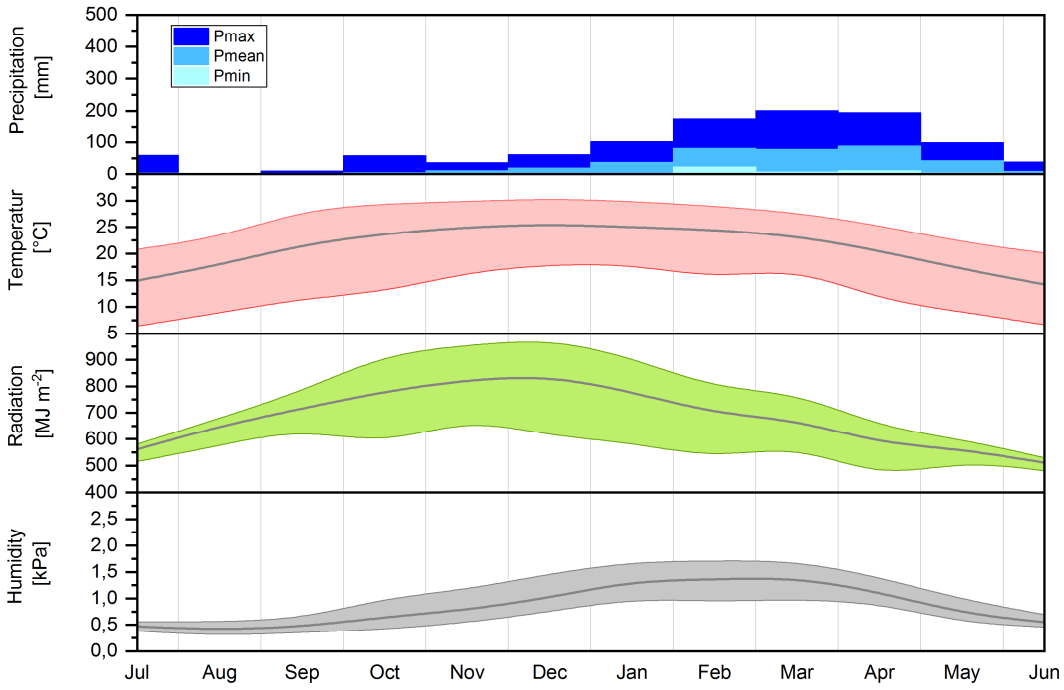

Fig. 122: Diagram showing the 30year ERA-INTERM Dataset for the study site Erichsfelde as monthly means for temperature and humidity as well as monthly sums for radiation and precipitation (with minimum and maximum). The grey lines represent mean values whereas the colored areas showing the span between minimum and maximum.

Fig. 122 shows the ERA-INTERIM weather input data for the Erichsfelde site as long year monthly sums for radiation and precipitation as well as monthly means for temperature and humidity. With 377.0 ± 86.8 mm annual precipitation and a mean annual potential evaporation of 2396.5 ± 54.2 mm the dataset shows an arid character through an aridity index of 0.16 and a climatic water deficit of -2019.5 mm. The rainfall variability, described by the relation between standard deviation and the 30 years mean, is 23 % and therefore the highest among all study sites.

7.2. Model results

7.2.1. Model evaluation with weather station data

To evaluate the model input parameterization a validation simulation with station weather data is performed for four consecutive rainy reasons between 2010 and 2014 and compared to measured soil water contents. In Fig. 123 and Fig. 124 the simulation results for depth related soil water dynamics and the profile sums are illustrated. The measured total profile water contents expressed in mm m^{-1} is plotted against the simulation result to explain the goodness of fit. The soil water dynamic time series is complemented with the flux components potential and actual transpiration and evaporation to illustrate the vegetation influence as parameterized.

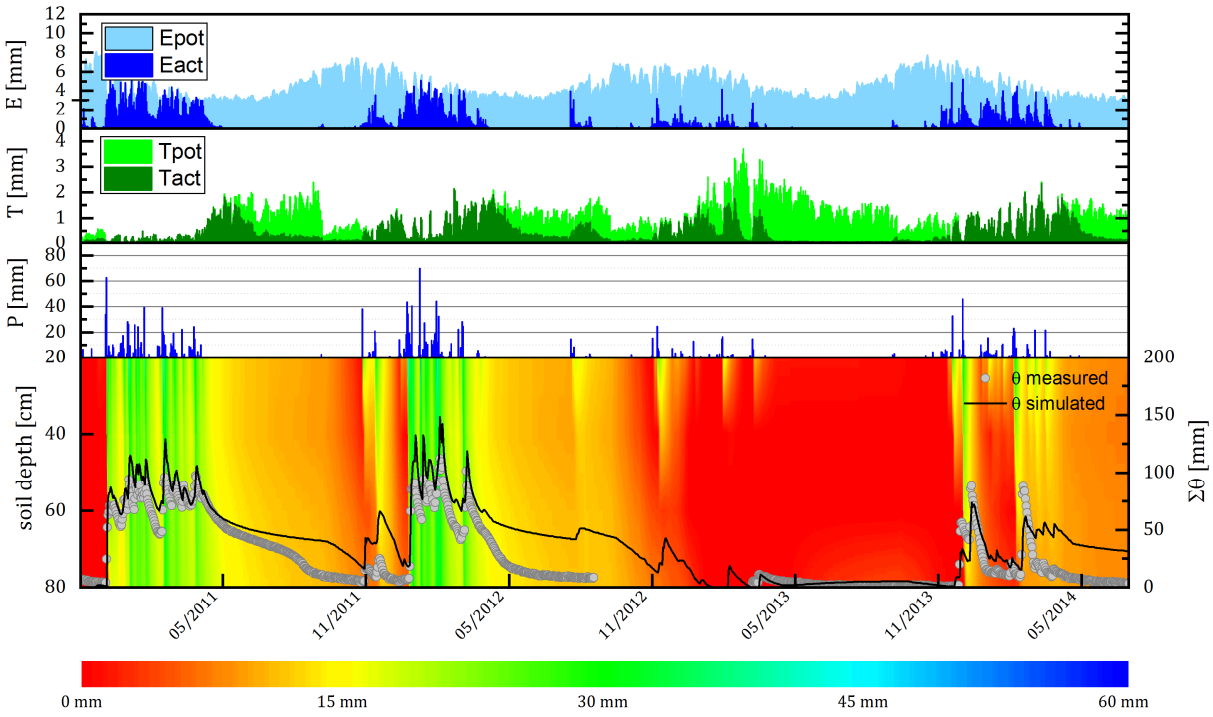

Fig. 123: Model output of the validation simulation for the intercanopy scenario.

For both simulations, the weather input data are derived from a climate station at the study site to be able to simulate under field conditions. These four years were chosen according to their high interannual variability with long years maximum rainfall amount of 648 mm in 2010/2011 and 813 mm in 2011/2012 followed by a below-average season with 218 mm and a season with average rainfall amounts. For the intercanopy scenario, the simulation results show a quick response to incoming rainfalls with increasing water contents up to 150 to 180 mm in total profile water. The infiltration and the following

percolation process rewets the subsoil within one day, which is also shown in the measurement data. At the middle of the first two rainy seasons, the water content shows sequences of short-term drying and wetting cycles without any deeper reaching drying front. Only at the end of these seasons, the soil water gets diminished significantly. Focusing on the drying out process the tailing in soil water reduction followed by an increase in reduction rate is visible in season one and less pronounced in season two. The slight reduction at the end of the rainy season can be explained by the reduced transpiration dynamic of the grass vegetation and the insufficient supply of water for soil evaporation processes. With the emergence of the vegetation at the onset of the following rainy season, the remaining soil water is depleted until additional rainfalls refill the soil buffer again. This process of tailing and increasing is also supported by the measurement data. The temporal shift between soil water reduction increase within the simulation and the measurements is due to the fixed vegetation cycle parameterized in the model, where the grass starts its phenological cycle in October. In the field, the start of the phenology is triggered by external influences such as day length, temperature sums or rainfall threshold. Referred to this case earlier reduction of buffered soil water may be due to an earlier start of the vegetation than as defined in the simulation. In the second season, the soil water reduction is less pronounced in the simulation compared to the measurements with nearly 60 mm less soil water decrease. The following two rainy seasons show only little impacts on soil water change mostly within the first 40 – 60 cm. Soil water supply to transpiration is still sufficient at the first half of the season to sustain actual transpiration rates on a level of their potential. After a complete depletion of the soil water at the end of this low input season the average input season show a rewetting of the profile to the bottom of the considered profile due to the low and more or less equally distributed rain events the soil water dynamic shows a distinct drying an rewetting but no lasting soil water concentration in lower profile areas. Looking on the drying cycle at the end of the model period, the reduced soil water fluxes in the simulation results appear again with about 30 mm less flux.

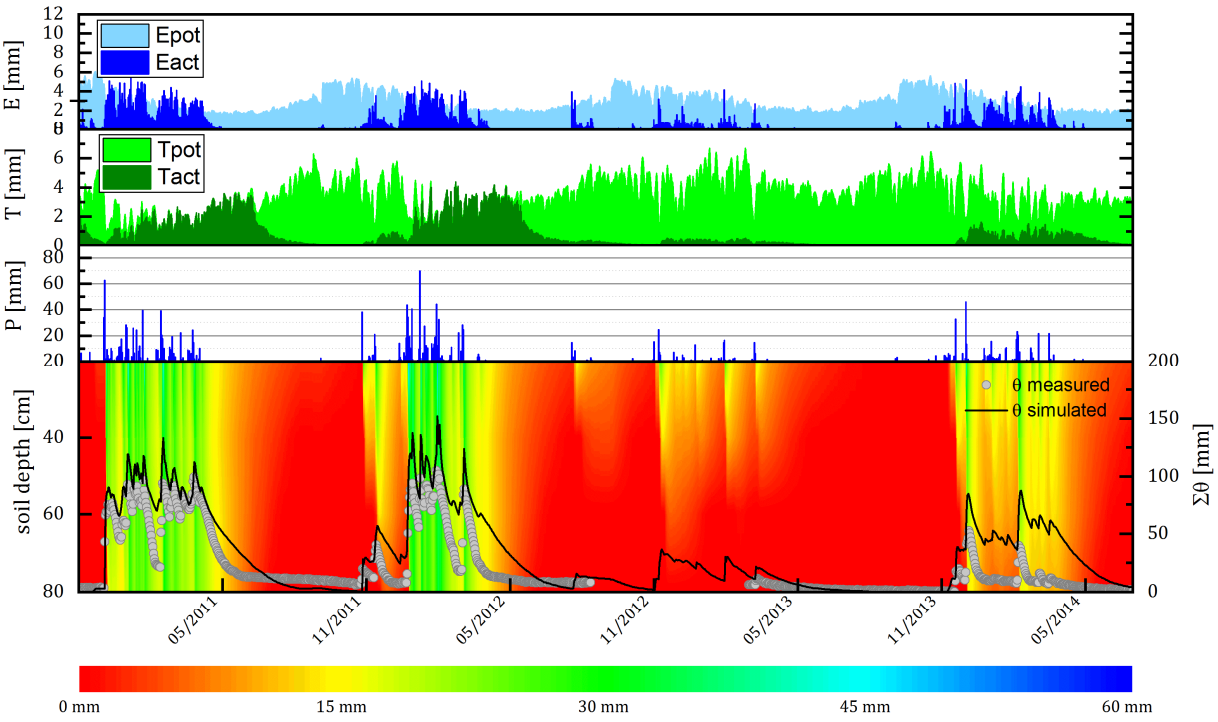

Fig. 124: Model output of the validation simulation for the canopy scenario.

Fig. 124 shows the same simulation setting with respect the weather data and soil but with differing vegetation settings. The canopy scenario based on the field observations by *Oldeland* (unpublished data 2009) shows a different impact on soil water reduction as the intercanopy scenario due to its long phenological cycle and the deeper rooting characteristics. Whereas the infiltration patterns do not differ significantly, the soil water depletion pattern misses the tailing sequence because of a complete utilization of available soil water at the end of the rainy season. As the time series of the transpiration rates reveal is the transpiration soil water flux directly linked to the plant available soil water and only in times with sufficient supply actual transpiration reaches potential rates. The deviations between simulation and measurement in drying periods are still visible but less pronounced due to the enhanced transpiration fluxes. A statistical model evaluation to quantify the quality of predictions is presented in the following section. To illustrate the deviation between simulation results and observed soil water contents for the respective simulation period, special diagrams that include several model performance parameter developed by *Taylor* (2001) are given in Fig. 125 to Fig. 127.

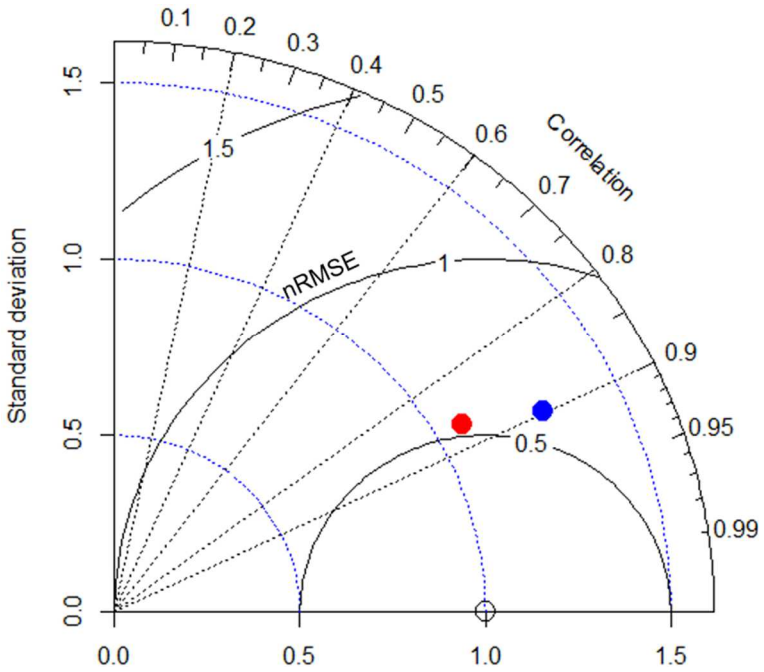

Fig. 125: Taylor diagram showing Pearson´s correlation coefficient, RMSE and standard deviation for the intercanopy (red) and canopy (blue) validation simulation in relation to the measurements (circle)

These diagrams showing the standard deviation normalized to the standard deviation of the observations, the correlation coefficient and the normalized root mean square error (nRMSE) of a given set of simulation and measurement values. The standard deviation is assigned to the x and y-axis, the correlation coefficient stretches as a function of the cosine between the x and y-axis and the nRMSE spreads concentric, centered to the observation point. The observation point is always located on the x-axis since it correlates with itself. The nearer the points tend to the observational reference the better is the model performance. Fig. 125 gives an example for the summed-up profile water contents of the intercanopy and the canopy simulation in relation to the field observations. Since these diagrams show standard deviation normalized values the respective absolute ranges are given in Tab. 26. Whereas the observations show a standard deviation of 28.3 mm and 26.2 mm, the intercanopy and canopy simulation having higher variabilities with 30.8 mm and 35.3 mm. The dynamic of the observations as represented by the model is correlated with 0.88 and 0.9 to the observed dynamic but with an absolute deviation of simulated water contents with RMSE values of 21.3 mm to 21.6 mm. Both simulations show a systematic overestimation of the profile water sums to 100 cm depth with coefficients of residual mass (CRM) of -0.59 and -0.68. Comparing both model performances, the intercanopy parameterization shows a slightly better fit to the observations as the canopy settings.

Whereas the overall dynamic representation is satisfactory, the water content deviation, especially within the dry seasons, reveals uncertainties in flux dynamic parameterizations.

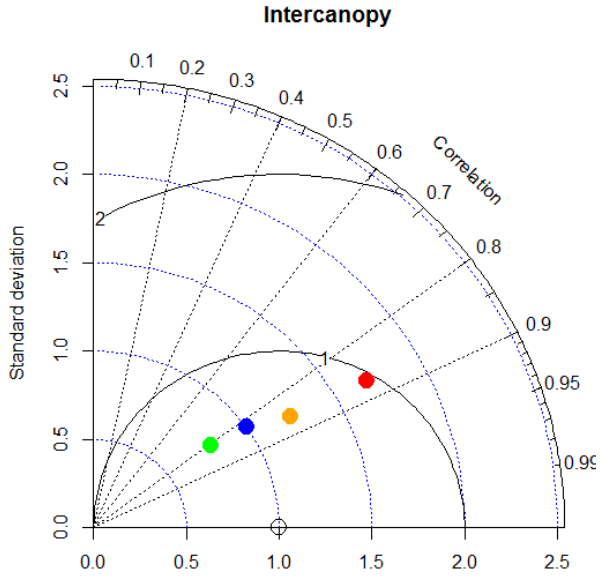

Fig. 126: Taylor diagram showing the goodness of fit for the intercanopy simulation in depth of 20 cm (red), 40 cm (orange), 60 cm (blue) and 80cm (green) with reference to field measurements (circle)

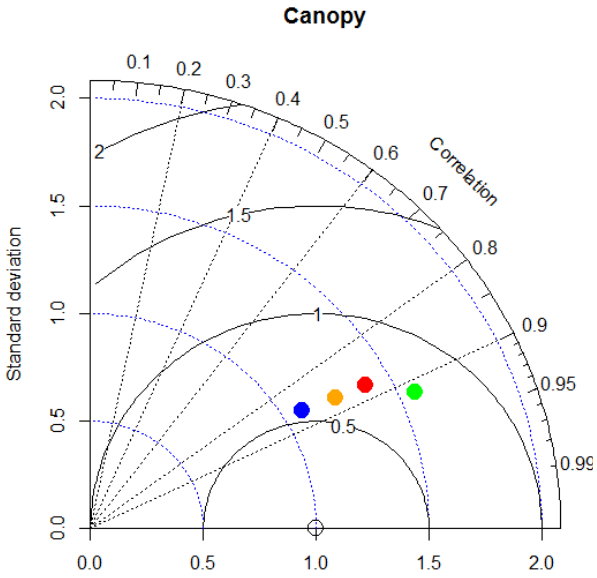

Fig. 127: Taylor diagram showing the goodness of fit for the canopy simulation in depth of 20 cm (red), 40 cm (orange), 60 cm (blue) and 80cm (green) with reference to field measurements (circle)

A depth related model evaluation for 20 cm equidistant soil layers from 20 cm to 80 cm reveals additions information about the origin of the all over model performance. For the intercanopy scenario, the evaluation shows an improved model performance with depth indicated by the relative distance of the model data points to the reference in Fig. 126 and the decreasing CRM and RMSE which comes at the cost of the dynamic representation with lower correlation coefficient. A look at the differences of the standard deviations between simulation and observational data indicates, that most of the model deviations occur in areas with high seasonal water dynamics driven by infiltration processes and evaporation fluxes. During the rainy season, the model overestimates infiltration amounts while in the dry season the surface evaporation flux is underestimated. Since evaporation fluxes show a long-term dynamic the standard deviation of soil water contents in the dry season is in a low range while the rainy seasons exhibit higher standard deviations. In consequence, the differences between predicted and observed standard deviations can

only be explained by overestimated dynamics within the rainy seasons. The depth improving model fit is shown by decreased standard deviation differences, reaching areas of the profile where percolating waters increase short-term dynamics only in times with high precipitation input. The underestimation of long-term fluxes driven by deep percolation and transpiration dynamics is indicated by the depth-related RMSE of about 5 mm in all subsoil layers. A special case in this context is shown by the 80 cm layer of the Canopy scenario. In contrast to the depth decrease of the CRM in the intercanopy scenario, the CRM increases again in the 80 cm layer indicating an increase in overestimation of water contents due to higher percolation rates into that area also indicated by a high standard deviation difference.

Tab. 26: Mean water contents and standard deviations for different evaluation levels together with parameters describing the goodness of fit between observations and simulation. The colors in the first column correspond to the labels in Fig. 125 to Fig. 127.

Data set	$\bar{x} \pm \sigma$ [mm]	CRM	r^2	RMSE [mm]
ES_I pred.	41.3 ± 30.8	-0.59	0.88	21.3
ES_I obs.	26.0 ± 28.3			
ES_C pred.	34.3 ± 35.3	-0.68	0.90	21.6
ES_C obs.	20.5 ± 26.2			
ES_I_20 pred.	11.5 ± 9.0	-1.13	0.87	8.00
ES_I_20 obs.	5.4 ± 5.1			
ES_I_40 pred.	9.6 ± 8.0	-0.56	0.86	5.37
ES_I_40 obs.	6.1 ± 6.3			
ES_I_60 pred.	9.8 ± 8.0	-0.34	0.82	5.30
ES_I_60 obs.	7.3 ± 7.8			
ES_I_80 pred.	10.4 ± 7.3	-0.29	0.81	5.86
ES_I_80 obs.	8.1 ± 9.1			
ES_C_20 pred.	11.4 ± 9.9	-0.93	0.88	7.54
ES_C_20 obs.	5.9 ± 6.7			
ES_C_40 pred.	8.6 ± 8.9	-0.65	0.87	5.59
ES_C_40 obs.	5.3 ± 6.7			
ES_C_60 pred.	7.6 ± 9	-0.37	0.86	4.98
ES_C_60 obs.	5.5 ± 8			
ES_C_80 pred.	6.6 ± 8.8	-0.55	0.92	5.02
ES_C_80 obs.	4.3 ± 5.4			

To summarize these findings, it needs to be noted that the model performs reasonably well under the assumed conditions with respect to the profile water sums. It represents the infiltration and percolation dynamics with good correlations to the observational data

with a tendency to overestimate soil water contents especially by looking at depth related volumes. These overestimations can be related to higher infiltration dynamics and lower evapotranspiration fluxes compared to the real-world situation. For a later assessment of the long-term model application, these key findings need to be considered.

7.2.2. 30-years intercanopy scenario simulation

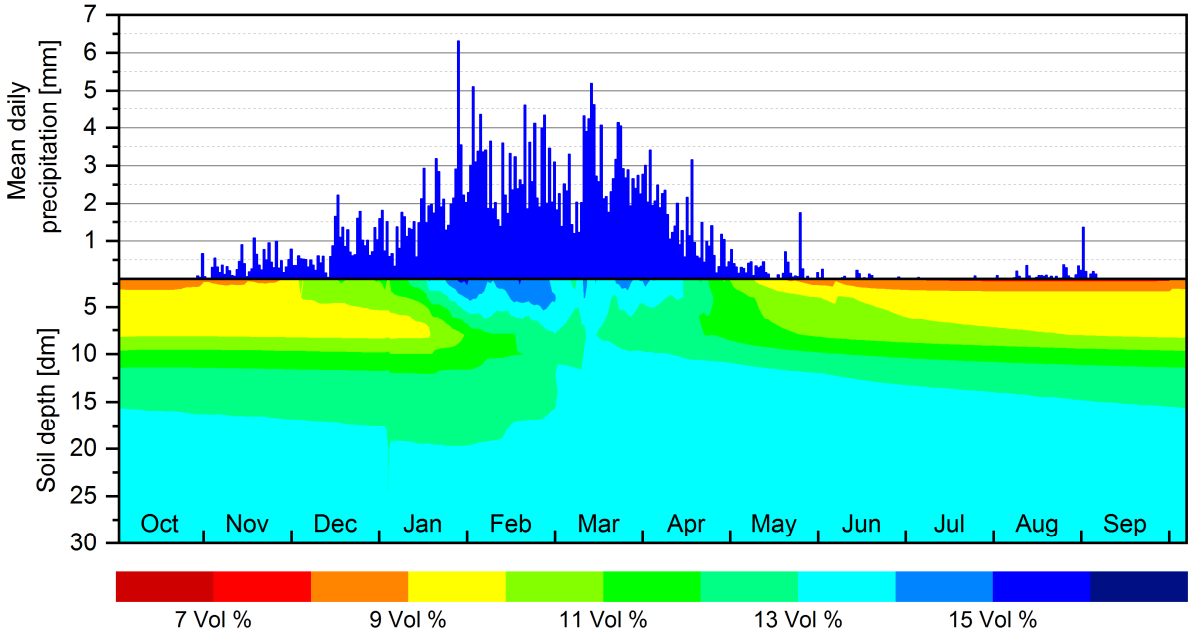

Fig. 128: Mean daily water content for a period from October to September based on a 30-year model run for intercanopy conditions at the study site of Erichsfelde

Fig. 128 illustrates the seasonal course of the modeled volumetric water contents as 30 year daily means for the intercanopy scenario together with the associated precipitation events. The soil was discretized according to the previous scenario onto a depth of 300 cm. On the basis of the validation simulation, all setting were adopted and the simulation was driven by ERA-INTERIM time series. The color matrix presented in Fig. 128 shows an average rainy season with 375.5 mm rain and 2396.5 mm potential evaporation as described in section 7.1.4. with a homogenous grass coverage at low density and shallow rooting properties. The phenological cycle covers the whole season with only low transpiration dynamic over the dry season. In context of these flanking assumptions, the soil water dynamics are governed by transpiration fluxes as well as a distinct proportion of bare soil evaporation over the dry season. Starting in October short before the onset of the rainy season, the vegetation is still in its initial state with low rooting depth and tran-

spiration rates. The soil profile shows a certain amount of plant-available soil water, remaining from the last rainy season, which supports transpiration demands at this early stage of the vegetation cycle. The grass vegetation utilizes this buffer which results in a depletion of the soil water contents down to the bottom of the rooting zone until cumulative rainfalls exceed the evapotranspiration amounts and infiltrating rainwater start to percolate into deeper horizons. The period of reduced water contents is compensated by percolation processes in the middle of the rainy season. The topsoil water content reaches its maximum in February with 16 Vol% to decrease again due to evaporation while the grass vegetation is at the end phase of its phenological cycle. From that point on only evaporative fluxes controls the soil water dynamics guided by the soil hydraulic properties to supply atmospheric demands. Based on the soil hydraulic functions the topsoil shows a hydraulic head of pF 3.1 with an unsaturated conductivity of $1.02 \cdot 10^{-4}$ cm d^{-1} and the subsoil with little higher water contents pF 2.8 and a conductivity of $6.65 \cdot 10^{-4}$ cm d^{-1}. The capillary supply of this individual soil is not sufficient enough to completely deplete even deep buffered soil water and a certain amount of water stays available until the following rainy season as transpiration source.

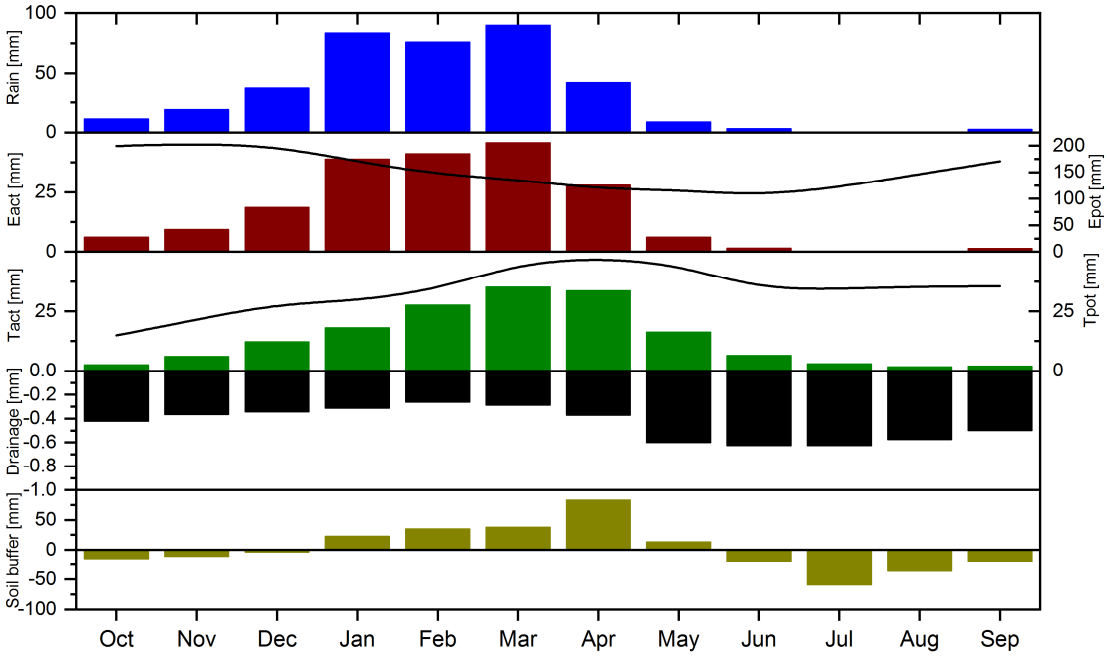

Fig. 129: Monthly mean soil water balance components for the intercanopy scenario at the Erichsfelde study site. The lines represent the monthly course of Epot and Tpot

Based on the soil water dynamics, the resulting balances as long year monthly means are shown in Fig. 129. The seasonal development of the atmospherical fluxes evaporation and

transpiration is following the precipitation course whereas the transpiration is guided by the phenological development and therefore shows a shifted peak. The evaporation reaches its maximum in March with 47 mm together with the precipitation maximum of 90 mm whereas the transpiration peaks in January at times of the mature state of the vegetation. At that time the soil water content within the root zone shows its minimum within the rainy season. The transpiration rates increase again while evaporation rates still increase due to reduced leaf shading effects and higher water contents in the topsoil supplying bare soil evaporation. In May the phenological cycle reaches its end and the remaining atmospherical fluxes are limited to evaporation with low rates of 11 mm in May to a mean dry season flux of 3 mm per month between June and September of the consecutive year. The bottom flux dynamic ranges on a low level between 0.43 and 0.96 mm per month. The seasonal water balance in Tab. 27 shows a dominant evaporative flux of 197.6 mm per year followed by transpiration withdrawals of 165.4 mm. The interception losses are low with 7.8 mm and the bottom fluxes show 5.3 mm per year which is compared to the other study sites in northern Namibia and Angola very low.

Tab. 27: Seasonal water soil water balance for the intercanopy scenario in Erichsfelde

Scenario	Input [mm]	Interception [mm a^{-1}]	Transpiration [mm a^{-1}]	Evaporation [mm a^{-1}]	Bottom flux [mm a^{-1}]
Intercanopy	375.5	7.8	165.4	197.6	5.3

7.2.3. 30-years canopy scenario simulation

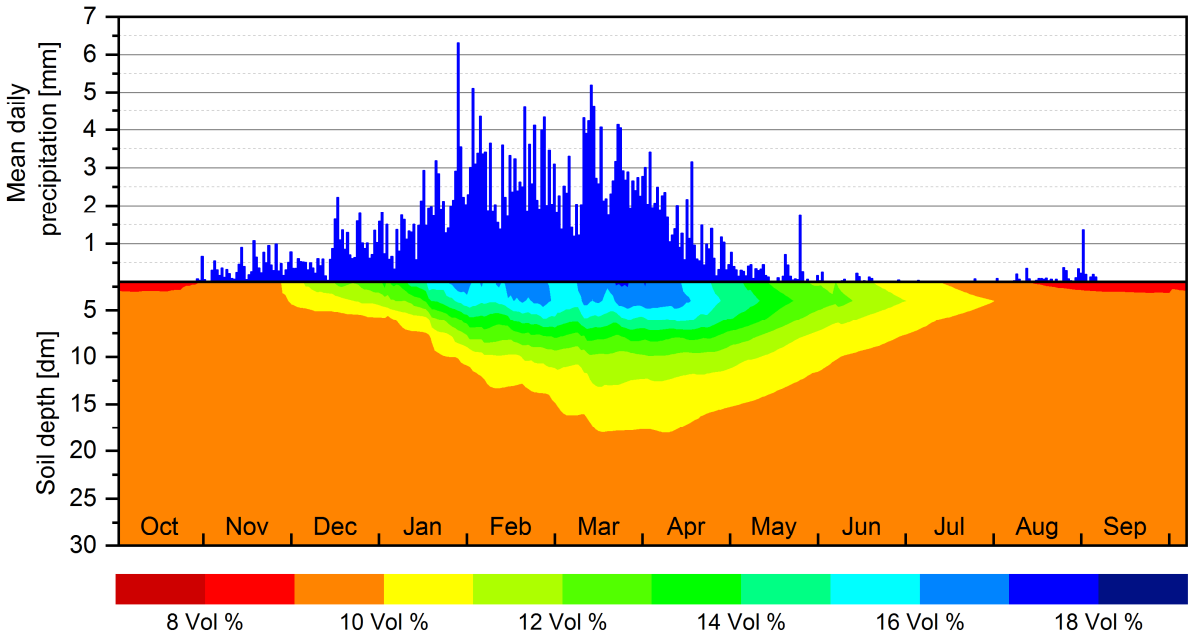

Fig. 130: Mean daily water content for a period from October to September based on a 30-year model run for the canopy scenario at the study site of Erichsfelde

The canopy scenario with its prolonged vegetation cycle and the deeper rooting properties down to the bottom of the profile reveals significant differences to the intercanopy scenario with respect to soil water dynamics and balances. A first overview shows the complete depletion of soil water contents at the end of the rainy season to the PWP and beyond in topsoil areas over the dry season. The hydrological year begins in October with a nearly complete dry soil profile only a residual amount of 9 Vol% to 10 Vol% is left of the previous rainy season. With the first rains, the profile shows a forming wetting front which moves slowly over time into depths of 160 cm in March with a maximum water content of 18 Vol% in the topsoil and 11 Vol% at the bottom boundary of the wetting front. There is no water content change visible under that boundary throughout the whole hydrological year. In April the profile starts to dry out again by evapotranspiration fluxes until July where the soil water contents over the total profile depth are at the initial state for the upcoming rainy season. In contrast to the intercanopy scenario, the infiltrated precipitation is turned over completely within a depth of 160 cm of the profile with no deep percolation to the bottom of pedon.

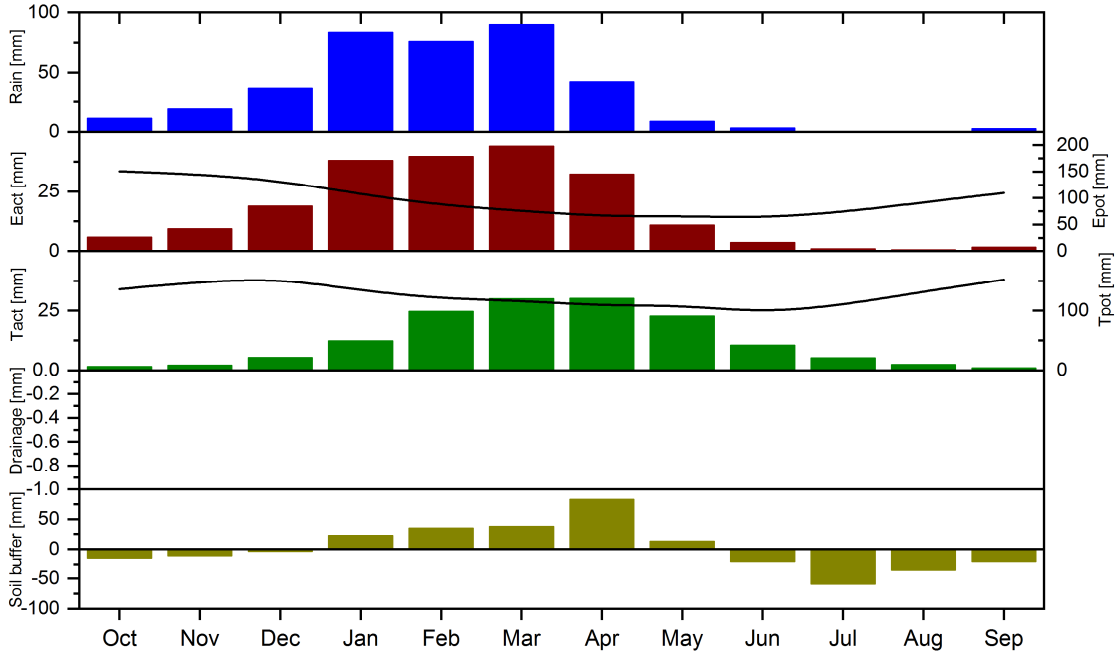

Fig. 131: Monthly mean soil water balance components for the canopy scenario at the Erichsfelde study site. The lines represent the monthly course of Epot and Tpot

In Fig. 130 no deep percolation occurs down to the bottom boundary of the assumed profile which is reflected in the absence of bottom fluxes in Fig. 131. Consequently, all precipitation input is returned to the atmosphere in varying proportions over the season by evaporation and transpiration. At the beginning of the rainy season, the transpiration fluxes are still on a low level with 4.5 mm because of the low content of plant available water and low phenological development. The evaporation rates range around 6.3 mm. With increasing rainfall input the rates increase whereas the slope steepness of the increase is higher for evaporation due the immediate return of rainfall inputs to the atmosphere whereas the vegetation needs a certain amount of infiltrated water to increase transpiration fluxes. With a completely formed canopy and root system, the transpiration withdrawals show the maximum rates in March and April together with the evaporation peak in March. Within the dry season, the relation is shifted towards higher proportions of transpiration due to water withdrawals from deeper soil water sources by root extraction.

Tab. 28: Seasonal water soil water balance for the canopy scenario in Erichsfelde

Scenario	Input [mm]	Interception [mm a^{-1}]	Transpiration [mm a^{-1}]	Evaporation [mm a^{-1}]	Bottom flux [mm a^{-1}]
Canopy	375.0	20.5	148.7	206.7	0.0

The seasonal soil water balance, as given in Tab. 28, show no bottom fluxes as long years mean and a high evaporation share with 206.7 mm. The transpiration fluxes account for 149 mm and therefore only little lower compared to the intercanopy scenario. In contrast, interception losses with 20.5 mm per season are 2.8 times higher compared to the intercanopy simulation.

7.3. Discussion

The following sections discuss the implementation of the previous field data and simulation output analysis with the focus on the impact of bush encroachment on groundwater recharge and on the consequences of these modifications for plant available soil water for grass production which is a primary determinant for livestock. These considerations include an assessment of the plausibility and constraints of the conclusions made which leads over to a general methodological oriented discussion in section 1.

7.3.1. Impact of bush encroachment on deep drainage dynamics as a proxy for potential groundwater recharge

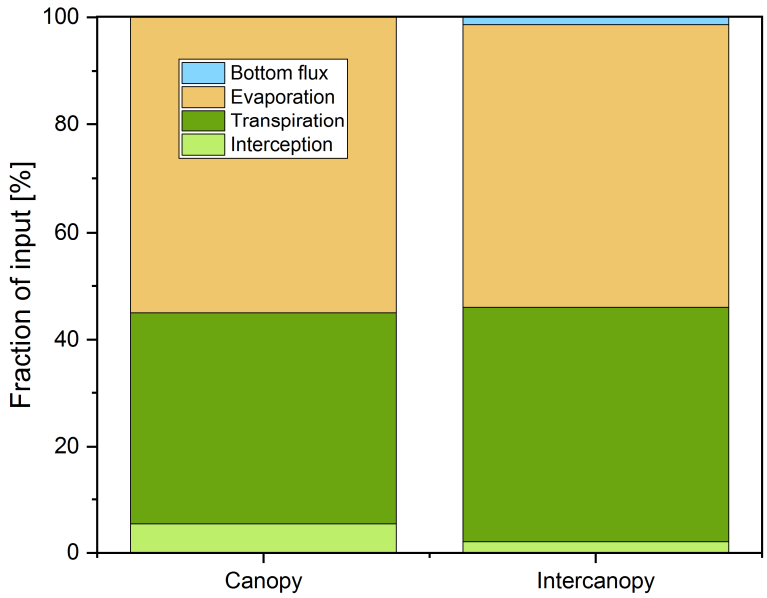

Fig. 132: Relative proportions of the soil water balances as fractions of the input for the Erichsfelde simulation sets

The application of a long-term simulation for bare soil conditions represents, due to the absence of plant-related transpiration and interception losses, the reference for an evaluation of the vegetation´s system impact. Based on the 30-year simulation the relation between bottom fluxes and evaporation losses is 1:3.4 reflecting the arid to semi-arid

character of the central Namibian Highlands on one side supported by the soil hydrological properties which prone to yield evapotranspiration fluxes by capillary rise on the other side. As a result, bare soil areas show a potential groundwater recharge, by taking bottom fluxes as a proxy, of mean 85 mm per season which is equal to 22.4 % of the mean precipitation input. By supplementing vegetation scenarios the additional fluxes need to be compensated by the reduction of evaporation or bottom fluxes which results in the relative balances for the canopy and intercanopy conditions shown in Fig. 132. The canopy scenario is fully compensating the additional transpiration losses by a complete depletion of potential deep percolation water by intercepting root water uptake in all profile areas. With 1.5 % of the input, the perennial grassland of the intercanopy scenario yields a low amount of bottom fluxes. Due to the shallow rooting characteristics, the percolation water interception by root extraction is limited to the first 100 cm of the profile. Net rainfall amounts exceeding actual evapotranspiration rates contribute to percolation processes below the rooting zone in the middle of the rainy season where it stays only little affected by capillary rise. This buffered soil water together with ongoing percolation processes above leads to the mean amount of bottom fluxes shown by the relative balances. The actual infiltration and the bottom flux generation are temporally decoupled because of the need of low soil hydraulic heads at the bottom of the profile. The topsoil water deficit established by evapotranspiration processes at the end of the rainy season has to be compensated by rainfall input before deep percolation processes can occur in the subsoil regions. Comparing the assumed vegetation parameter between the canopy and the intercanopy scenario the differences between the soil water balances can be explained by the phenology depending above ground LAI and the total rooting depth in combination with the root distribution as a function of soil depth. The pronounced LAI development of the canopy scenario with all over higher values compared to the intercanopy scenario results in higher interception losses which reduces the infiltrating water amounts to be turned over to the remaining balance components. Since higher LAI values normally result in higher transpiration rates but the actual modeled transpiration difference is little, the interactions between aboveground characteristics and rooting properties need to be addressed. The rooting density of the intercanopy shows a linear decrease from the soil surface to its maximum depth of 100 cm. Thus, root water extraction is highly effective within the first soil layers and infiltration water can be taken up immediately. This leads to reduced water contents in the topsoil which reduces evaporation rates. The higher

evaporation rates in the canopy scenario simulation show higher evaporation rates due to its bulbous shape with a main rooting horizon in 120 cm to 180 cm. The efficiency of root water uptake within the topsoil is therefore reduced and infiltrating water persist for a longer period held by capillarity and supplied to evaporation fluxes. Only when to on moving wetting reaches the depth of highest root density a sufficient water supply can be established. In consequence, the higher LAI is compensated by the different root density to depth function which is responsible for the lower transpiration fluxes due to lower soil water contents in the respective major rooting depths. In Tab. 29 the findings of the simulations are reduced to a qualitative description of the impact of the assumed vegetation properties on soil water balances. As described the root density distribution in combination with the LAI defines whether bottom flux occur or no deep percolation is simulated. A low LAI with high topsoil rooting yields a low bottom fluxes, where a high LAI with low topsoil rooting yield no bottom flux.

Tab. 29: Qualitative comparison of vegetation properties and the consequences for soil water balances for three different precipitation conditions

Rain	Scenario	LAI	Rooting depth	Topsoil rooting	Inter-ception	Transpi-ration	Evapo-ration	Bottom flux
Me-dium	Intercanopy	-	-	+	-	+	-	+
	Canopy	+	+	-	+	-	+	-
High	Intercanopy	-	-	+	-	-	=	+
	Canopy	+	+	-	+	+	=	-
Low	Intercanopy	-	-	+	-	+	-	+
	Canopy	+	+	-	+	-	+	-

Since these dynamics are driven not only by set vegetation conditions but also by the weather forcing Tab. 29 also includes high and low precipitation seasons. The low input season reveals no component relation shift but the high input scenario shows a change from lower to higher transpiration rates for the canopy scenario whereas the evaporation shifts to an equalized relation between the canopy and intercanopy fluxes. The high infiltration amounts are responsible for an increase in plant available water at the canopy site which results in a better transpiration performance whereas the high topsoil water contents compensate evaporation differences between the scenarios.

The comparison of empirical and simulated results show similarities with respect to deep drainage dynamics but with differing amounts. *Gröngröft* et al. (2018) calculated for both sites deep drainage rates between 47.6 % and 55.7 % of the precipitation for the

intercanopy sites and 14.5 % to 15,9 % for the canopy measurements reflecting the qualitative intercanopy to canopy relation of the simulations. The absolute value deviation between simulation and measurement analysis can be explained by the different reference layer to calculate bottom fluxes. The measurements refer to a depth of 80 cm whereas the bottom flux within the simulation refers to 300 cm. Fig. 128 and Fig. 130 show flux relevant water contents in a depth of 80 cm for both scenarios, which may result in similar findings compared to the field data evaluation. Other reference balances for savannah ecosystems are summarized in

Tab. 30 showing well comparable results for the balance components as they are calculated within this study. The differences in interception values are likely to occur because of the different savannah type examined by *Scholes* and *Walker* (1993) and *Whitmore* (1971) (in *Huntley* (1982)) referring to the broad-leafed type of the Nylsvley in South Africa. In addition, they take the ecosystem as a whole into account, whereas the present study focuses on individual vegetation type with the thornbush savannah ecosystem. For the set conditions with respect to weather, soil and vegetation parameters the simulation results showed values which comply with literature references. The effect of vegetation on groundwater recharge was examined with the result of a minimal potential for groundwater recharge under grass vegetation and no deep drainage under canopies as a function of interceptive root water uptake by the woody vegetation. These results can be seen as valid for Luvisols with a certain prone to evaporation fluxes. As described in section 4.4 the study site Erichsfelde shows a decent pedodiversity with different textures and related soil hydraulic properties which need to be evaluated separately to scale up from point related balances to the scale of the study site.

7.3.2. Modification of soil water dynamics under canopy and intercanopy spaces

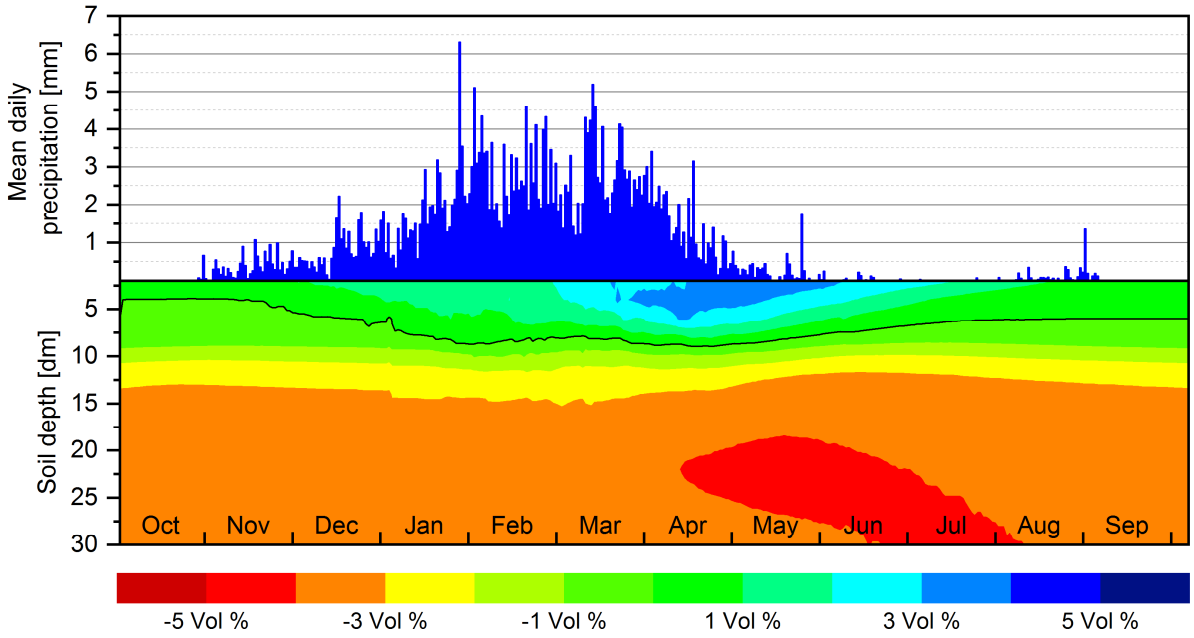

Fig. 133: Colour matrix showing the soil water differences in Vol% between the canopy and intercanopy simulation based on the long year daily means together with the mean daily precipitation.

Tab. 30: Literature references for savanna water balances compared to the simulation results

Precipitation [mm]	Runoff [% input]	Interception [% input]	Recharge [% input]	Evaporation [% input]	Transpiration [% input]	Reference
References						
630	6.0	11.6	2.8	32.8	47.8	*Huntley* (1982) after Whitmore (1971)
585	0.0	15.4	0.8	47.0	36.7	*Scholes* and *Walker* (1993)
Model results						
375	0.0	2.1	1.4	52.7	44.1	Intercanopy
375	0.0	5.5	0	55.1	39.7	Canopy
534	0.0	1.6	1.4	51.1	44.1	Intercanopy
534	0.0	4.2	0.0	49.1	49.8	Canopy

The color matrix, shown in Fig. 133, illustrates the 30 years mean daily water content deviation between the canopy and the intercanopy simulations. The black line indicates the soil depth in which no discrepancy between both simulation scenarios is identifiable. Below this line, the intercanopy results in higher soil water contents and above the canopy model shows wetter conditions in the long year trend. The shallow depth of the equilibrium line with 50 cm to 80 cm below surface and a major proportion of drier conditions

in the canopy simulation is also reflected in Fig. 134. The interceptive root water uptake by the woody vegetation effectively prevents any establishment of soil water sources in areas deeper than the main rooting zone which accounts for a concentration of soil water turnover dynamics only to a depth of 180 cm. Since no sustained storage in deeper areas takes place, the all over soil water contents over the long-term simulation period is lower in comparison to the intercanopy simulation. The intercanopy conditions reveal higher profile water contents as a consequence of the specific root distribution with its maximum in the topsoil area. As mentioned in the previous section evapotranspiration flux exceeding rainfalls are able to percolate below the main rooting zone where these soil waters stay relatively unaffected by transpiration due to lower root densities. The establishment of a high soil water gradient within the dry season additionally hampers capillary rise due to low conductivities even with high soil hydraulic head gradients. To evaluate which consequences an increase in bush encroachment has on potential biomass production with respect to soil water availability as a consequence of modified soil water dynamics, the focus for an assessment lies on the potential root zone for grasses assumed to be within the first 100 cm.

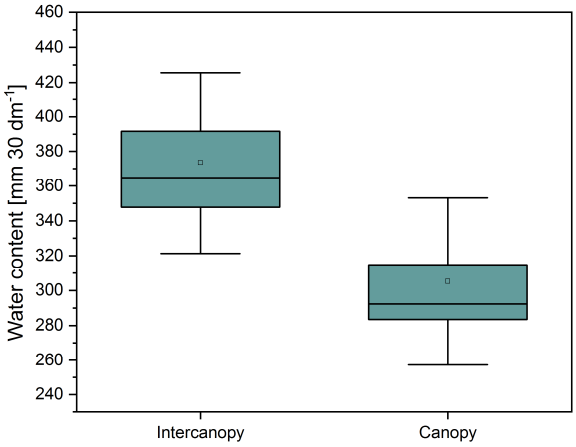

Fig. 134: Daily soil profile water contents over 30 year simulation period. The box indicates the 75 % and 25 % percentile with mean and median. The whiskers show the standard deviation.

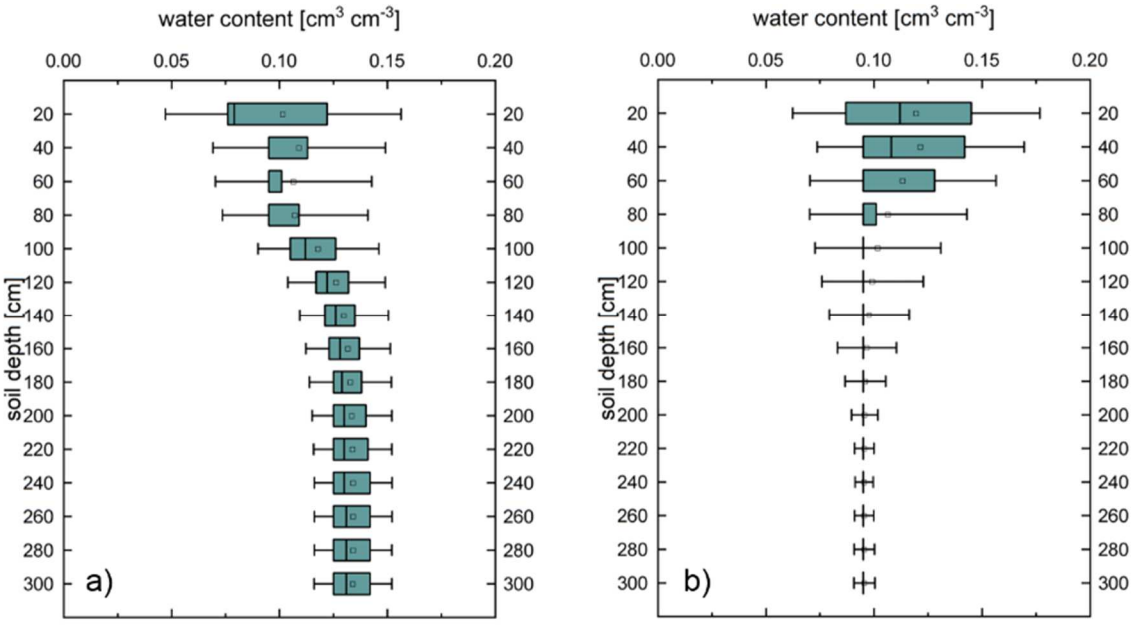

Fig. 135: Depth related daily soil water contents for the long-term simulations. The box indicates the 75 % and 25 % percentile with mean and median. The whiskers show the standard deviation. a) intercanopy b) canopy

Fig. 135 shows, that the highest daily soil water variability is concentrated to first 100 cm at both plots with little higher means at the canopy scenario, which reflects findings by *D'Odorico* et al. (2007), and as already described in subsoil regions for the intercanopy scenario whereas a medium variability on nearly the same level at the intercanopy site is visible with respect to soil depth from 120 cm to the bottom. The canopy scenario shows no significant soil water variability from a depth of 200 cm on downwards. The specific assumed root system of the woody vegetation provide little higher plant available water amounts in the topsoil region compared to the grassland vegetation which is likely to support transpiration withdrawals by a possible understory vegetation whereas the grassland scenario is limiting itself regarding topsoil water availability. On the other side, the conservative character of the soil water dynamics at the intercanopy site buffers soil water in depth of 80 cm to 300 cm.

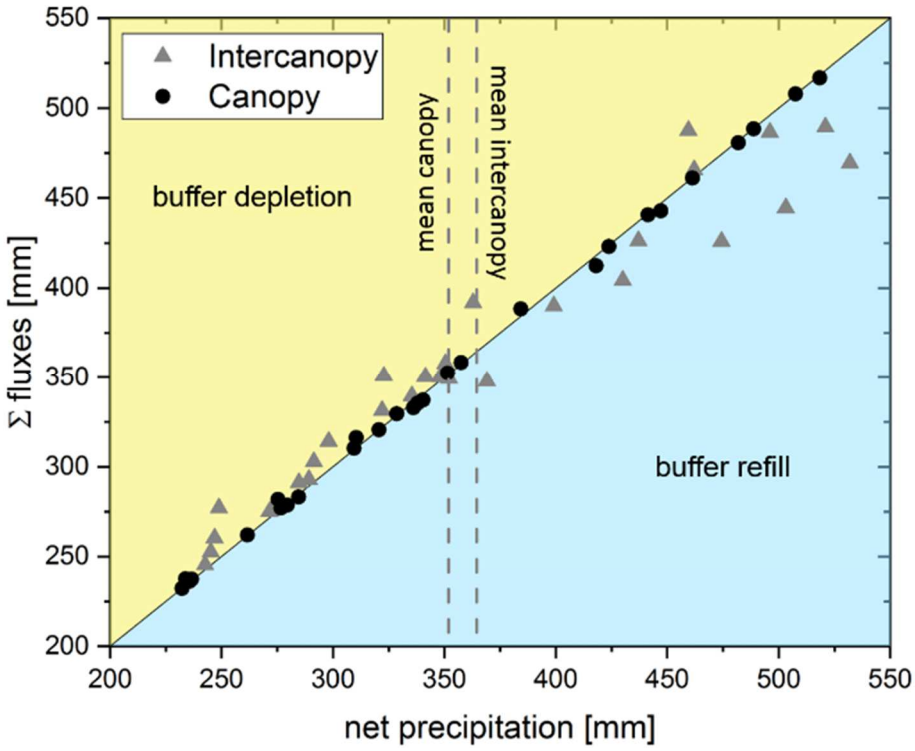

Fig. 136: Relation between net precipitation and total flux sums

In seasons with high precipitation sums, this buffer is filled to support transpiration in consecutive years with less rainfall, whereas the soil water turnover by the woody vegetation is nearly equal to one hydrological year, where the sums of fluxes are equal to the net precipitation (Fig. 136). In arid to semi-arid regions, soil water conservative interactions with established soil water buffers in deeper soil areas are likely to show a higher resilience against precipitation variabilities, whereas systems with short soil water turnover periods, like the canopy scenario, react sensitively on seasonal rainfall variations.

An increased bush encroachment, under loamy soil condition with certain proportions of medium to fine pores, is most likely to set pressure on soil water buffer resource established and sustained by intercanopy areas. Under the assumptions made, the competition for soil water do not refer to the same main rooting depth but the utilization of subsoil water buffers by encroacher species reduces an important source for grasses to sustain biomass production. In consequence, the ecosystem will suffer a decrease in resilience to overcome seasons with below-average rainfalls or intra-seasonal dry spells and is therefore predisposed to aridification. *Eldridge* et al. (2011) summarizes in a meta-study similar results but emphasizes the individual contexts of each study. Assuming more sandy soils with lower proportions of medium to fine pores and a tendency to percolate higher

volumes of infiltrating precipitation into deeper areas the resilience relation is more likely to be reversed. The main root system of the encroacher species has access to higher amounts of soil water even in depth below the main horizon whereas the grass vegetation needs to utilize the amount of water which remains after water percolation within its root zone without having access to possible ascending capillary water. These considerations coincide in parts with the findings by *Noy-Meir* (1973) and *Sala* et al. (1988) who refer to the inverse texture hypothesis. This implies that soils with high water-holding capacity lose higher proportions of infiltrated water by evaporation whereas sandy soils with lower capacities can conserve more water in deeper areas to be used for transpiration processes. The results of the simulations show that the transfer of this theory need to additionally address rooting characteristics since shallow rooting systems depend on sufficient amount of plant available water in the topsoil regions. In contrast, deeper rooting systems benefit from these percolated waters whereas higher water holding capacities, in this case, are not favorable, due to increased evaporation rates. The findings in this section show, that an increase of bush encroachment is likely to have consequences on the subsoil water buffering processes and ascending water supply to the grass root zone involved. This impact is particularly significant in years with below average precipitation.

8. Does the simulation results allow plausible conclusions?

Conclusions, based on simulation results, can only be as plausible, as the simulation input parameter and the process representation functions are. This section summarizes processes which are represented in the described simulations to identify possible uncertainties. The descriptions are more of a qualitative nature than based on a quantitative sensitivity analysis. For more detailed quantitative information of sensitivity and limitations, it is referred to *Wesseling* et al. (1998). Key findings concerning the model sensitivity are also summarized in *Kroes* et al. (1999) mentioning the importance of the boundary conditions as well as the role of the LAI for the calculation of soil and crop evaporation as well as interception losses.

This section is divided into three parts focusing on simulation forcing data provided by ERA-INTERIM/REMO datasets, the soil domain and its related processes as well as the vegetation domain describing relevant phenological parameter and its derivation. The chapter closes with a brief summary of the conclusions made in this study and their reflection amidst the described limitations and uncertainties mentioned in the section.

8.1. Weather forcing data

To predict the uncertainties of regional climate models, such as REMO, it is important to know the quality of the model forcing data which are usually itself model outputs, in this case, from ERA-INTERIM models. The uncertainties of the forcing data are adopted by the model which itself again has defined uncertainties which in consequence leads at best to a stable error propagation or to reinforcing effects (*Wu* et al. 2005). The quality of the used regional model data is summarized in the following, based on personal communication with *Dr. Torsten Weber* (Climate Service Center, Germany 2014).

8.1.1. 2m temperature

The annual mean 2m temperature of the ERA-INTERIM forcing data show a deviation of up to 4°C within the catchment area of the Okavango against the regionalized observation data of the Climatic Research Unit (CRU). The ERA-INTERIM forced REMO simulation consequently shows similar deviations with up to +3 °C in the middle and northern part of the catchment and negative deviations up to -2 °C in the southern part for the month of

the austral summer from December to February. In the austral winter time, the deviation is about 2 °C with a time variable uncertainty against observation data (Fig. 137).

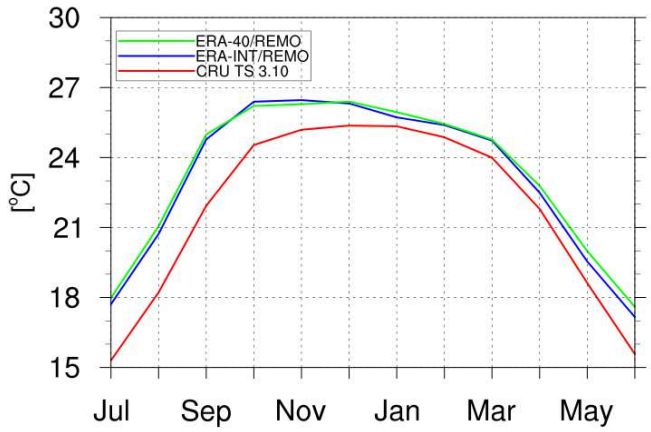

Fig. 137: Diurnal development of the mean 2m temperature of ERA-40 and ERA-INTERIM forced REMO simulation compared to CRU regionalized observation data for the climate model domain of southern Africa (personal communication *Weber* 2014; *Mitchell* and *Jones* 2005)

8.1.2. Mean daily precipitation

The mean daily precipitation amounts over the Okavango catchment show high uncertainties with deviations between -40 % to +40 % compared regionalized observation data by the Global Precipitation Climatology Center (GPCC). In some parts of southern Namibia the deviations are up to 100 % (Fig. 138). These uncertainties are likely to be based on inadequate simulated large-scale humidity transport dynamics into the catchment region as well as sea surface temperature developments not properly represented in the REMO forcing data.

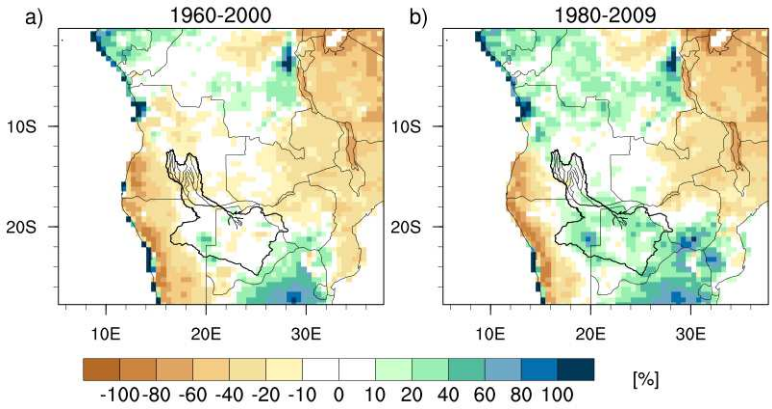

Fig. 138: Deviations of the mean daily precipitation [%] between December and February. a) ERA-40 minus GPCC regionalized observation data b) ERA-INTERIM minus GPCC observation data (personal communication Weber 2014;GPCC)

These considerations suggest that the uncertainties coming with the weather forcing data do have consequences for the simulation dynamics resulting in an overestimation of atmospheric demand due to the overestimated temperatures. Likewise, the rainfall input with its spatially variable uncertainties in areas with naturally high inter- and intra-seasonal rainfall variabilities makes it difficult to assume any tendency whether an over- or underestimation is to be expected from soil water balances and dynamic simulations without any further detailed insights to the climate model uncertainties. Nevertheless, since the aim of this study is to show balance patterns and long-term dynamics based on a 30-year model application the climate model uncertainties are likely to have small impacts on the mean long-term patterns observed in the previous sections, whereas they need to be considered. In general, station information, where available, are to be preferred since they provide more realistic, site-specific weather information.

8.2. Soil profile domain and related dynamics

The introduction addressed all relevant water fluxes to describe the soil-vegetation-atmosphere system in the context of the regional hydrological cycle. The representation of this system through a one-dimensional model needs simplified and conceptual assumptions for lateral processes like runoff and run on. Interflow processes cannot be simulated since adjacent pedons are not represented. Although integrated into SWAP, bypass flow through secondary macropores, which accounts in parts for a significant and quick reallocation of rainfall inputs without trespassing the soil matrix, can only be integrated appropriately when the macropore quantities, properties and distribution throughout the profile are known. In this section, these system processes and their representation and influence on the simulation results are discussed.

8.2.1. Soil hydraulic parameter derivation

Due to the application of Richard´s equation within the SWAP modeling scheme mass and energy preserved dynamics and balances are given as simulation results. Therefore, the physically based parameterization of the soil hydrological functions based on the van Genuchten-Mualem relations needs to be addressed as accurate as possible to guarantee plausible water flow representations. Whereas the determination of the water retention related parameters of the van Genuchten-Mualem function is relatively simple by fitting water retention characteristics resulting from pressure plate analysis, the derivation of

the conductivity parameter requires a more sophisticated method as described in section 3.2.4. Only with measurement-based parameters, the unsaturated water flow dynamics can be described realistically to distinguish between high and low conductivity properties while having nearly identical retention characteristics. As shown in the simulation results of this study, contrasting conductivity properties with similar retention characteristics lead to a divergent soil water dynamic and result in contrasting balances. Fig. 139 illustrates the analyzed soil water retentions for all mentioned study sites (dotted lines) against the retentions after the combined retention and conductivity parameter-fitting to derive model input parameters (red line). Nearly all retentions show sand-type shapes with steep slopes in the area of the field capacity. Only the Erichsfelde retentions reveal a less steep slope reflecting a higher amount of clay. The low amount of clay at the other sites is reflected by higher PWP values. The best agreement between measured and derived retentions is shown by the Mkda data, followed by Erichsfelde retentions. The total resulting effective saturation volume of the model input parameter set in Csu is, compared to the measurements, lower with a good shape representation whereas the shape representation of the remaining sites is, in comparison to the measurements, less well derived. In the case of the Cse data set, it is because of different samples used for the unsaturated conductivity measurements, reflecting the small-scale heterogeneity of the soil.

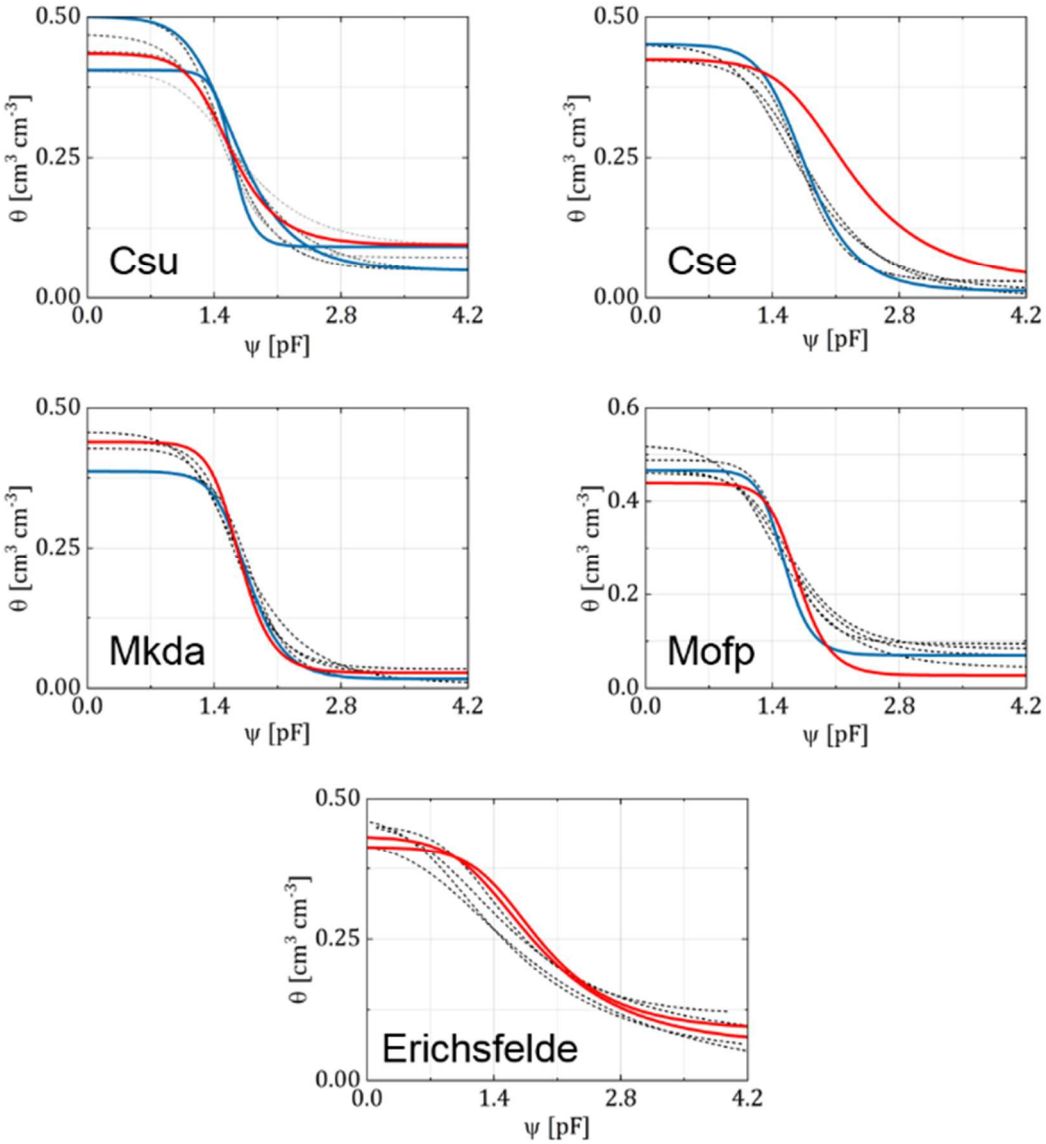

Fig. 139: Water retention curves for all five individual sites comparing pressure plate measurements (dotted lines) and resulting functions with derived van Genuchten-Mualem parameters (red lines). Blue lines represent data without or failed unsaturated conductivity measurements

In result, the deviations lead to higher water contents at field capacity in the simulation which, in combination the low unsaturated conductivities at field capacities lowers percolation dynamics, compared to expectable dynamics under real world conditions. In conclusion, there is a tendency to an underestimation of percolation resulting from the Cse data, whereas the Mofp and Csu simulations tend to slightly overestimate percolation with higher unsaturated conductivities.

8.2.2. Bypass flow dynamics

Besides the vertical water redistribution by the primary pore system of the bulk soil, a second, gravitation dominated water conduction, exist due to secondary macropores. The macropore system is established by plant roots, shrinking and swelling dynamics of clay enriched textures, as well as by faunal activity. The macropore system is a primary transport pathway which redistributes rapidly incoming rainfalls to greater depths of the profile through bypassing the soil matrix. At the bottom end of an assumed vertical macropore, the pore water infiltrates into the soil matrix when the saturation status of the surrounding area is unsaturated and a gradient occurs. In soil water measurements the appearance of macropore flow is indicated when a rapid soil water increase in greater depth occurs without corresponding soil water increases in lower depth. Especially in cohesive soils with a certain clay content and the presence of dominant soil fauna such as termites and ants a persistent macropore system is established. For the qualitative and quantitative description of a macropore system in a field survey, color tracer methods are effective means but require a considerable infrastructure especially in remote areas in southern Africa.

The parameterization of a macropore system is included in SWAP by defining the macropore geometry including the continuity of the pore system, its persistence and the horizontal distribution (*Kroes* et al. 2008). Since the approach of this study is to present a model setup including reliable measurements for parameter derivation and to minimize the degrees of freedom, the decision was to exclude macropore due to its rather conceptual approach. It is a valuable module if a macropore system can be described to be used for calibration purposes. In consequence, water infiltration and redistribution is modelled by bulk soil guided processes with soil hydrological function parameters based on lab analysis and fitted van Genuchten-Mualem functions. By neglecting macropore flow, the model results show an implicit tendency to underestimate infiltration and percolation dynamics connected with an overestimation of soil water contents. These considerations can be realized in section 7.2.1. For the resulting soil water balances, a possible overestimation of evaporation fluxes is expected because of higher top soil water contents due to reduced percolation dynamics by the missing bypass flow as well as a possible underestimation of bottom fluxes for the same reasons. For a quantification of the sensitivity and

the possible impact on simulation-observation deviation it is necessary to perform ensemble runs to find appropriate macropore parameter to optimize a fit of simulated results to observed values.

8.2.3. Lateral surface fluxes

Since SWAP is a one-dimensional model, lateral surface flow dynamics are represented in a conceptual bucket type way for runoff generation or need to be set as input values with respect to surface run on amounts as additional water input. Surface runoff dynamics are guided by a threshold-based function which sets the depth of a possible ponding before runoff will be calculated by applying a resistance function to estimate the runoff intensity. Ponding occurs under two different conditions. The rainfall excess defines rainfall intensities which exceed the infiltration capacity of a topsoil. The infiltration capacity of the topsoil is a function of the relative saturation (Se) and equal to the unsaturated conductivity at given Se for a certain time step, based on the van Genuchten-Mualem function. Is the rainfall excess less than the defined ponding depth it results in a possible amount of runoff which is included in the balance output. The second type of runoff generation occurs at topsoil saturation conditions, which is, in fact, comparable to the rainfall excess but with different initial conditions. Under saturated conditions, the infiltration capacity is the highest but due to hampered percolation processes by the saturated soil profile the infiltration capacity is zero and hence the rainfall excess is equal to the gross rainfall amount. Again, after exceeding the threshold, runoff is generated and assigned to the balance output. In all simulations, the threshold was set to a minimum of ponding with 1 mm of depth but no runoff was generated which is explained by the usage of the free outflow boundary condition. This condition causes a soil water withdrawal at the bottom of the soil domain as a function of the unsaturated conductivity compensated by occurring gradients in lower profile regions.

8.2.4. Irrigation design

The irrigation schedule of the respective simulations depends to a large extent on the threshold parameter for the onset of the irrigation and the depth of the reference point below the surface but also on the atmospheric demand. According to the selected combination of thresholds and reference depth, the amount of irrigation water differs significantly. A deeper reference depth needs more input to be set back to field capacity,

whereas a lower threshold increases the irrigation frequency due to a faster transgression of the threshold. Depending on soil hydraulic properties the irrigation schedule parameterization leads to different soil water balances and differing fluxes. For a prediction of consequences of different irrigation schedules on soil water balances, individual model runs need to be performed. In tendency, a deeper reference depth will most likely result in higher bottom fluxes due to higher input amounts and greater soil areas set to field capacity whereas lower thresholds tend to an increased recycling of irrigation water by evaporation because of lower infiltration depth caused by lower input intensities.

8.3. Vegetation parameterization and phenology implementation

Vegetation-induced fluxes and flux reductions depend on the development stage of the actual vegetation because of the increasing transpiration water demand in the mature state with high developed canopy and root system. There the plant physiological parameter which guides the transpiration calculation is assigned to the development stages as mentioned in section 3.4 (*Feddes* et al. 2001; *Kroes* et al. 2008). The final parameter set describes the time-related changes of plant physiognomy and serves for the dynamic calculation of transpiration fluxes, interception losses and evaporation reduction due to leaf shading effects. In the following, those parameters, mainly responsible for interactions between vegetation and soil water dynamics, are presented together with their possibilities and constraints. A more general consideration needs to focus on the 1-D model type immanent representation of the vegetation. Since no spatially distributed vegetation patterns can be addressed by the vegetation domain, microclimatic conditions, as they occur between components of heterogeneous surfaces, are not represented by SWAP. Likewise, the competition between different vegetation units, like the coexistence of grasses and trees in open savannahs and their different phenology and rooting characteristics, cannot be implemented. The presented dynamics and balances and the resulting conclusions are therefore valid but only for homogeneous surfaces with the given sets of vegetation parameters. To analyze interspecies competitions on a spatial basis, numerical models with the option to discretize two-dimensionally are appropriate.

8.3.1. Vegetation period and phenological cycle

The phenological cycle is defined vegetation specific with fixed start and end times and periods of phenological stages. The duration of the development from emerging to perish,

harvest or the transition into latent stages defines the potential amount of transpiration depending on rooting and leaf area or soil cover fraction. Since the vegetation development, as used in this study, is decoupled from the soil module, there are no water depending conditions fed back to the phenological development of the vegetation. It is important to determine the start and end days for each hydrological year individually because of the reaction of the vegetation on climatic parameters like rainfall, temperature sums or day length (*Joubert* et al. 2008; *Boke-Olén* et al. 2016; *Archibald* and *Scholes* 2007). Since an approximation of the start and end date for each year is not possible without field observations or remote sensing-based analysis this study assumed a vegetation period of 366 days with minimized dry season parameterization for perennial and evergreen pristine conditions. The integration of crop cycles based on the average phenological development after *Allen* et al. (1998) for Maize under dryland conditions.

8.3.2. Leaf area index

The information about the above ground vegetation characteristics is needed to distinguish between the share of evaporation and transpiration of partially covered soils. Since the aerodynamic term of the Penman-Monteith equation is neglected by SWAP, the effective radiation which reaches the soil surface is the only variable that control actual evaporation fluxes *(Kroes et al.* 1999*; Ritchie* 1972*; Belmans et al.* 1983*; Goudriaan* 1977). It only depends on the radiation interception by green leafs and decreases exponentially from top of the canopy to the soil surface. Therefore, it is important to predict the LAI and its phenological dependencies as good as possible to get plausible results for a division between soil evaporation and transpiration fluxes. As another parameter within the soil water balance, interception losses also depend on the LAI. Two different methods to derive this flux parameters are integrated into SWAP. For crops, the approach of *Hoyningen-Huene* (1981) and *Braden* (1985) integrates individual crop coefficients with precipitation intensities together with the LAI which forms an asymptotic function where interception losses decrease with the increased intensity of rain events. For closed forest canopies, the method of *Gash* et al.; *Gash* (1995; 1979) is integrated which accounts for the storage capacity of the canopy and the dependency of evaporation from the canopy surface as a function of the canopy saturation. For this study, the decision is only to refer to the simple assumptions of *Hoyningen-Huene* and *Braden* since the heterogeneity and the, in relation to temperate woodlands, open character of the appearing forests makes it

difficult to describe the necessary parameter after *Gash* et al. in an appropriate manner. In consequence, the estimate for interception losses by the woodland scenario are underestimated as realized in

Tab. 30 and are not compensated by referring to long year means of fluxes and dynamics.

The appropriate determination of the phenological dynamics throughout a vegetation period is another source of simulation uncertainties. Since the already mentioned dependency of the phenological development on external drivers (see also Fig. 45) a fixed start and end date for all considered season is likely to produce under- and overestimations of vegetation-related fluxes by to less or to highly developed vegetation independent from precipitation events. Nevertheless, it can be assumed, that an assessment based on 30 years mean values is likely to compensate that uncertainty to a certain degree, without the possibility to make any assumptions about the quantitative effects. Corrective measures base on the evaluation of long-term and simulation period covering remote sensing data to derive appropriately start and end dates for individual vegetation periods (*Schneibel* et al. 2013; *Ma* et al. 2013).

The model internal representation of the phenology and its depending vegetation parameter are derived by point measurements of the LAI of crops with different planting dates and thus at different development stages. These point measurements are combined and assigned to a mean phenological cycle period based on standard values according to *Allen* et al. (1998). Since it was not possible to have access to real-time series of phenological developments, this approximation is assumed to be sufficient for long-term simulation assessments. Since no coupled vegetation module is used to represent the soil-vegetation-atmosphere interactions and its phenology feedbacks, this approximation is likely to have less impact on the simulation results in relation to the neglected feedbacks. Nevertheless, an overestimation of transpiration fluxes can be assumed in dry spell periods where the calculated possible transpiration sets in immediately after the dry spell according to its development stage. Whereas, under real circumstances the transpiration rate will be lower because of the affected plant development (*Haverkort* and *Goudriaan* 1994). For pristine conditions, the phenological developments are derived by combining multiple LAI measurements of single individuals and different ages with literature references (*Scholes* and *Walker* 1993; *Chidumayo* 2001).

8.3.3. Rooting depth and density

The maximum rooting depth is parameterized as a function of the development stage. For annual crops and herbs, the rooting depth inclines throughout the vegetation period to reach its maximum within defined periods. For perennial vegetation, the root system is set to be established to its maximum over the complete phenological cycle. As shown in the different case studies, the maximum rooting depth has a significant impact on the soil water dynamics, since the root water uptake and therefore the subsequent transpiration is an important driver to shortcut the soil water transport to the atmosphere, even from greater depth where capillary rise under bare soil conditions is too slow to effectively redistribute water to the soil surface. The necessary field data for a realistic parameter derivation refer to the soil profile descriptions with the limitation that only the section of the profile is characterized which is surveyed. Therefore, not the complete rooting depth can be described based on field data. Nevertheless, to get approximations for the maximum rooting depth of the vegetation, this parameter is derived according to literature values. In case of the woodland, the maximum rooting depth is set to the maximum profile depth since even deeper rooting in profiles with no hampering barriers is possible but not included in the soil domain. One important consideration in this context is the role of the soil domain dimension. As larger as the soil domain is, as larger is the potential amount of accessible soil water for deep rooting vegetation. The limitation of the soil domain to 300 cm and the free outflow boundary condition at the bottom withdraws water potentially supplied to transpiration by deep rooting vegetation, which shows a certain trend to overestimate bottom fluxes and to underestimate transpiration losses. In addition, the rooting density to depth relation has an extensive impact on soil water dynamics. According to the shape of the distribution function, topsoil or subsoil dynamics get amplified or reduced. As shown in section 1, the deeper situated main root horizon of the woody vegetation generates higher top soil water contents and therefore higher evaporation rates by reduced transpiration in comparison to the topsoil rooting intercanopy vegetation. The assumptions made within the simulations with respect to root density of pristine vegetation fit to literature references and are therefore representative for grass and woodland scenarios (*Hipondoka* et al. 2003; *Hipondoka* and *Versfeld* 2006; *Scholes* and *Archer* 1997; *Accatino* et al. 2010)

8.3.4. Crop factor and vegetation height

SWAP optional provides two basic methods to calculate actual transpiration as a function of the plant available soil water (Fig. 140). One method refers to the calculation with actual crop information in combination with the application of the Penman-Monteith equation. This method needs information about the albedo, crop height and the canopy resistance of the actual crop to calculate the potential evapotranspiration. For crops, a more generalized, but widely accepted method is based on the FAO grass reference method in combination with phenology depending crop factors (*Allen* et al. 1998).

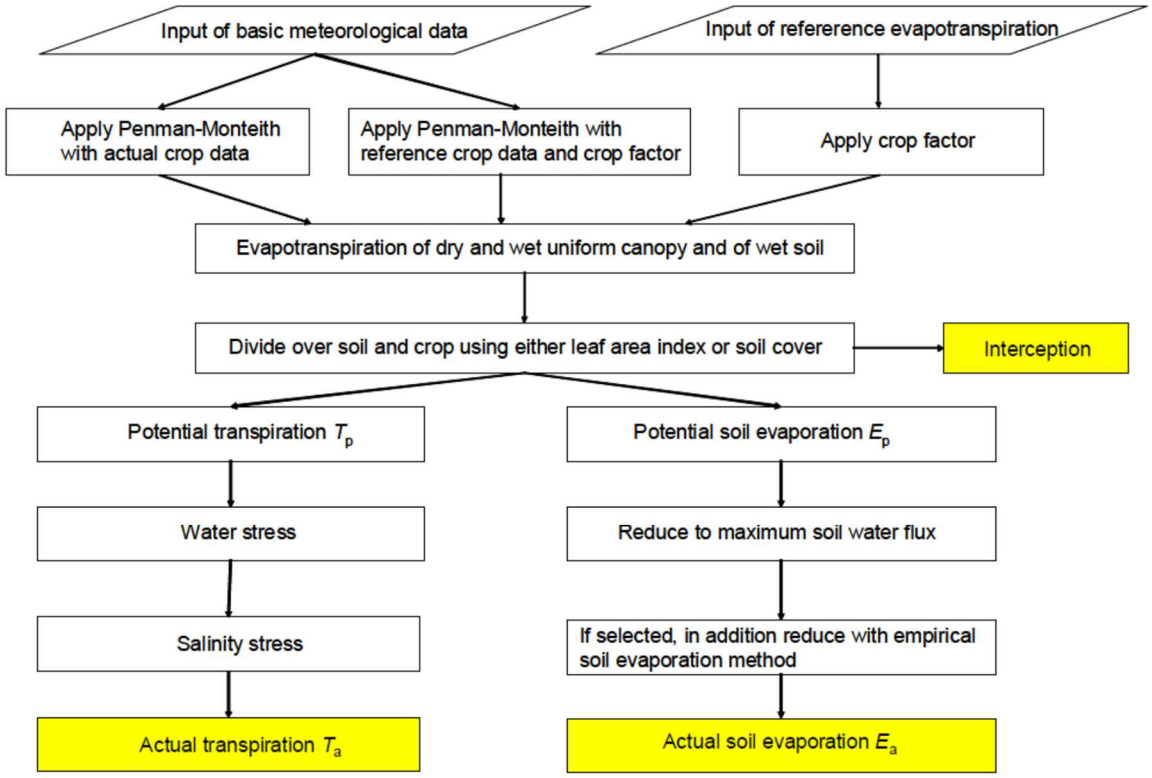

Fig. 140: Process flow chart representing the calculation method to derive actual soil evaporation and actual transpiration within SWAP (*Kroes* et al. 2008)

The crop factor describes the potential transpiration characteristics of an individual crop type in relation to the reference grass assumptions made by the FAO method. Standard values for most crops are published by the FAO and need to be adjusted to the actual climate conditions with respect to potential evaporation and rainfall characteristics. For pristine grass- and woodlands the Penman-Monteith equation was applied since available standard crop factors do not meet the needs for savannah type ecosystem parameterization. The actual height for the respective scenarios is derived in the field whereas albedo and canopy resistance are based on literature values (*Jarvis* 1976; *Houlton* et al. 2003). A

comparison between reference values for seasonal transpiration amounts and simulation results with *Ogola* et al. (2005) and *Scholes* and *Walker* (1993) showed satisfactory agreements so that the assumption of an appropriate transpiration representation within the SWAP environment can be concluded.

8.4. Boundary conditions

8.4.1. Soil surface evaporation functions

Beside the fact, that the bare soil evaporation dynamic within SWAP is governed by the atmospherical demand and modified by the intensity of soil coverage, the ability of the soil surface to supply soil water to evaporation processes needs be defined by the application of one out of three available functions. Whereas the application of the maximum Darcy fluxes leads to a maximized evaporation under high atmospheric demand, the functions of *Boesten* and *Stroosnijder* (1986) and *Black* et al. (1969) describe potential evaporation sum or time depending evaporation reductions. Through test simulations for the climatic conditions of southern Africa, it is indicated to use the *Boesten* and *Stroosnijder* function since a study by *Metzger* et al. (2014) determined the necessary parameter under field conditions by applying micro-lysimeter measurements.

8.4.2. Bottom boundary condition

SWAP provides several bottom boundary conditions to meet the needs of different simulation conditions. For this study, the bottom boundary for free outflow conditions is used to calculate deep percolation rates as a proxy for potential groundwater recharge. This decision is based on the assumption that a deep groundwater table has no capillary or drainage hampering influences on the water dynamics within the soil model domain. The occurrence of saturated conditions indicated by redoximorphic mottling in deeper parts of the surveyed soil profiles on Cusseque result rather from interflow dynamics than by a groundwater dynamic. With this boundary, a trade-off between evapotranspiration und deep percolation is possible in times with high subsoil saturation because of the immediate drainage of the soil water excess at the bottom. This dynamic withdraws soil water which cannot be involved in subsequent reallocation processes or root water extraction. For deep rooting vegetation this might have consequences if the soil water dynamics include the whole simulated profile of 300 cm. In this case, an underestimation of the transpiration is very likely.

9. Synthesis and outlook

The present study examined the impact of land use and land cover change on soil hydrological dynamics and connected downstream processes in the dry sub-humid to semi-arid catchment of the Okavango river system in southern Africa. Focused on scientific analyses of a combination of empirical and model-based data, case studies emphasizing different aspects of land use and vegetation dynamics provide the fundament for broader considerations. The integration of the individual case study results amidst the present interconnections and dependencies of the riparian states Angola, Namibia and Botswana, connected to each other via the waters of the Okavango, enables a final synthesis assessment of possible consequences on the catchment scale with respect to the water availability and future tendencies. This assessment follows the flow of the river water, starting in the headwater regions in Angola since changes to the soil hydrological system due to land use or land cover changes will result in consequences for the downstream regions. It could be shown, that a conversion of pristine ecosystems into dryland agricultural systems will increase the amount of bottom fluxes by about two times of the pristine state. Taking uncertainties into account and the fact, that bottom fluxes do not equate groundwater recharge or runoff, it still appears to be very likely that these additional waters will modify the Okavango hydrograph. Especially at the end of the rainy season, the runoff generation is prolonged with an expectable higher base flow over the dry season due to the water retention of the Cusseque sub-catchment. Along with the higher bottom fluxes impacts on water quality by leaching of solutes into the wetlands and related eutrophication processes are very likely and reported for dryland deforestations in Brazil and Australia (*Giménez* et al. 2016; *Peck* and *Williamson* 1987; *Allison* et al. 1990). Compensation measure based on the intensification of dryland agricultural practices with higher plant densities, which, from a soil hydrological point of view, are possible shown by the illustrated elasticity of the simulated soil-vegetation-atmosphere systems. Another measure focuses on extended fallow periods of existing fields with the subsequent establishment of secondary vegetation communities which can, as a positive side effect, restore soil fertility to a certain degree. Both measures are related to the bottom flux compensating effect of increased transpiration. Another way to control water balances is a planned functional ecosystem mimicry by landscape based vegetation management as a part of an agroforestry system (*Noorduijn* et al. 2010; *Hatton* and *Nulsen* 1999).

Going further downstream to the Namibian part of the Okavango catchment the impact of land clearance for agriculture results in similar dynamics as observed in the headwater regions but with more pronounced increases in bottom fluxes. The simulation results of the pristine conditions revealed low bottom fluxes indicating only little to nearly no groundwater recharge whereas after a conversion to dry land agriculture the bottom fluxes increase significantly to 15 % to 27 % of the annual precipitation input. Since the majority of the Okavango runoff is generated in the headwater regions in Angola within the rainy season and the influence of the base flow for the hydrograph is low (*Steudel* et al. 2013b; *Steudel* et al. 2013a), the contribution to runoff generation by increasing bottom fluxes will most likely affect the low flow hydrograph due to the retention function of the groundwater induced base flow. Nevertheless, a possible increase in groundwater recharge will positively affect livelihoods in the Kavango region by providing a source of water for direct human use in more remote areas of the region. Further research is needed if this more on groundwater can sustainably pumped and utilized to enable small-scale drip irrigation in the hinterland distant from river water to overcome times of dry spells (*Ngigi* 2008; *Rockström* and *Barron* 2007). A negative effect of the ecosystem conversion, the decrease in water use effectiveness, in combination with a high aridity index and a high rainfall variability could be mitigated by utilizing the additional groundwater in crucial crop development periods at the beginning of the cropping season. An upstream-downstream relation effect caused by an assumed increase in river discharge in low flow periods due to land clearance in the headwater regions is the provisioning of additional discharge for commercial irrigation purposes. Since most of the irrigation water is abstracted within the dry season and thus the impact of irrigation is the highest throughout the hydrological year (*Liebenberg* 2009), the additional low flow volumes may support a sustainable application of large-scale irrigation application. With the application of balance regulating measures in the upstream areas, this effect will be minimized and different irrigation measures are needed to sustain the regional water cycle. This study compared assumed impacts of planned commercial irrigation schemes, published by the OKACOM, with results of two simulations of irrigation scenarios on different textured soils. The outcome emphasizes the need for a soil hydrology related and simulation-based irrigation planning to minimize, on one hand, water abstractions and on the other side impact mitigation measures concerning regional water cycles with respect to bottom flux related effects. Even with a sustainable use of river water, with a minimal impact on water

availability for downstream regions, an inappropriate irrigation scheme bears the risk harmful consequences for the soil system, whether by over- or under-irrigation. An over-irrigation leads to high bottom fluxes and therefore unproductive water losses together with possible fertilizer additives into groundwater resources. An under-irrigation shows the effect of topsoil salinization with a simultaneous yield decline due to vegetation stress. An appropriate and sustainable irrigation scheduling needs to integrate and balance the three, in parts anticipating, components fresh water, yield and soil. A minimized water abstraction that is sufficient enough to guarantee high yields but is on the other side high enough to prevent salinization and low enough to minimize leaching is, therefore, the appropriate amount. This study showed in parts, that an assessment of the carrying capacity of a region with respect to irrigation application needs to consider integratively planned crop varieties, soil heterogeneities and characteristics, irrigation water sources in quantity and quality, groundwater quality and table depth as well as individual soil hydrological circumstances. Based on such an evaluation it is possible to set up irrigation schemes that are individually adjusted, from a hydrology point of view to a socio-ecological environment. On the dry end of the catchment, a dichotomy of this region with respect to human utilization can be illustrated. On one hand, conservational vegetation management is needed for flood control in river runoff generating landscapes. On the other hand, land clearance and the reestablishment of grass dominating savannah landscapes helps increasing deep drainage and restoration of soil water buffer or even groundwater recharge in a highly water-limited region. These measures can help to improve grass biomass production on a higher resilience level to cope with droughts with a simultaneously increased water use efficiency with a focus on fodder grass production for life stock.

This study presents the opportunities of an empiric-conceptional approach to illustrate and analyze site-specific combinations of soil hydrological conditions and land use characteristics. On the basis of case studies, which describe actual and possible land use conditions, it is possible to address questions emerging from the competitive utilization of the scarce resource water and related ecosystem services. The one-dimensionality of the used model neglects spatial lateral connections, which are, especially for the runoff-generating landscape, important to understand how lateral water dynamics, in the small scale, contribute to river discharge. In addition, a representative assessment on the regional scale needs to integrate the individual pedodiversity and the diversity of agricultural use based on the site-specific ecosystem diversity. This points the way to further

adoptions of the approach by addressing additional compartments like groundwater resources and a second dimension for lateral processes. Another improvement will be to derive the phenological development of crops and pristine ecosystems by remote sensing analysis for more realistic timing options in hindcast simulations. By referring to the introductory sections, this presented approach enables an increase in the understanding of hydropedological functioning under different land use and vegetation characteristics in drylands and thus emphasizes the meaning of a stronger integration of hydropedology into transdisciplinary projects for sustain or improve livelihoods.

References

Accatino, F., Michele, C. de, *Vezzoli, R., Donzelli, D., Scholes, R. J.* (2010): Tree-grass co-existence in savanna: Interactions of rain and fire. *Journal of theoretical biology* 267, 235–242.

Ad Hoc AG Boden (2005): Bodenkundliche Kartieranleitung.: 5. verbess. und erw. Auflage. Bundesanstalt für Geow. und Rohstoffe, Hannover.

Allen, R. G., Pereira, L. S., Raes, D., Smith, M. (Eds.) (1998): FAO Irrigation and Drainage Paper: Crop Crop Evapotranspiration. guidelines for computing crop water requirements, p. 326.

Allen, S. J., Grime, V. L. (1995): Measurements of transpiration from savannah shrubs using sap flow gauges. *Agricultural and Forest Meteorology* 75, 23–41.

Allison, G. B., Cook, P. G., Barnett, S. R., Walker, G. R., Jolly, I. D., Hughes, M. W. (1990): Land clearance and river salinisation in the western Murray Basin, Australia. *Journal of Hydrology* 119, 1–20.

Araya, T., Nyssen, J., Govaerts, B., Deckers, J., Cornelis, W. M. (2015): Impacts of conservation agriculture-based farming systems on optimizing seasonal rainfall partitioning and productivity on vertisols in the Ethiopian drylands. *Soil and Tillage Research* 148, 1–13.

Araya, T., NYSSEN, J. A.N., Govaerts, B., BAUDRON, F., CARPENTIER, L., BAUER, H., LANCKRIET, S. I.L., Deckers, J., CORNELIS, W. M.I.M. (2016): Resoring cropland productivity and profitability in northern Ethiopian drylands after nine years of resource-conserving agriculture. *Ex. Agric.* 52, 165–187.

Archibald, S., Scholes, R. J. (2007): Leaf green-up in a semi-arid African savanna -separating tree and grass responses to environmental cues. *Journal of Vegetation Science* 18, 583–594.

Bacon, M. (Ed.) (2009): Water Use Efficiency in Plant Biology. John Wiley & Sons, New York, NY, Online-Ressource.

Baiphethi, M. N., Jacobs, P. T. (2009): The contribution of subsistence farming to food security in South Africa. *Agrekon* 48, 459–482.

Bayala, J., Sileshi, G. W., Coe, R., Kalinganire, A., Tchoundjeu, Z., Sinclair, F., Garrity, D. (2012): Cereal yield response to conservation agriculture practices in drylands of West Africa: A quantitative synthesis. *Journal of Arid Environments* 78, 13–25.

Belmans, C., Wesseling, J. G., Feddes, R. A. (1983): Simulation model of the water balance of a cropped soil: SWATRE. *Journal of Hydrology* 63, 271–286.

Bennie, A.T.P., Hensley, M. (2001): Maximizing precipitation utilization in dryland agriculture in South Africa — a review. *Journal of Hydrology* 241, 124–139.

Bhark, E. W., Small, E. E. (2003): Association between Plant Canopies and the Spatial Patterns of Infiltration in Shrubland and Grassland of the Chihuahuan Desert, New Mexico. *Ecosystems* 6, 185–196.

Black, T. A., Gardner, W. R., Thurtell, G. W. (1969): The Prediction of Evaporation, Drainage, and Soil Water Storage for a Bare Soil1. *Soil Science Society of America Journal* 33, 655.

Bodart, C., Brink, A. B., Donnay, F., Lupi, A., Mayaux, P., Achard, F. (2013): Continental estimates of forest cover and forest cover changes in the dry ecosystems of Africa between 1990 and 2000. *Journal of biogeography* 40, 1036–1047.

Boesten, J. J. T.I., Stroosnijder, L. (1986): Simple model for daily evaporation from fallow tilled soil unde spring condition in a temperate climate. *NETHERLANDS JOURNAL OF AGRICULTURAL SCIENCE* 34, 75–90.

Boke-Olén, N., Lehsten, V., Ardö, J., Beringer, J., Eklundh, L., Holst, T., Veenendaal, E., Tagesson, T. (2016): Estimating and Analyzing Savannah Phenology with a Lagged Time Series Model. *PloS one* 11, e0154615.

Bouma, J., Montanarella, L. (2016): The soil and water Nexus for sustainable livelihoods., in Weigelt, J., Müller, A., Bekh, C., Töpfer, K.: Soils in the Nexus. A crucial resource for water, energy and food security. Oekom, München, pp. 85–103.

Braden, H. (1985): Ein Energiehaushalts- und Verdunstungsmodell for Wasser und Stoffhaushaltsuntersuchungen landwirtschaftlich genutzer Einzugsgebiete. *Mittelungen Deutsche Bodenkundliche Geselschaft,* 294–299.

Bulcock, H. H., Jewitt, G. P. W. (2012): Field data collection and analysis of canopy and litter interception in commercial forest plantations in the KwaZulu-Natal Midlands, South Africa. *Hydrol. Earth Syst. Sci.* 16, 3717–3728.

Cabral, A.I.R., Vasconcelos, M. J., Oom, D., Sardinha, R. (2011): Spatial dynamics and quantification of deforestation in the central-plateau woodlands of Angola (1990–2009). *Applied Geography* 31, 1185–1193.

Cavanaugh, M. L., Kurc, S. A., Scott, R. L. (2011): Evapotranspiration partitioning in semiarid shrubland ecosystems: A two-site evaluation of soil moisture control on transpiration. *Ecohydrol.* 4, 671–681.

Chidumayo, E. N. (2001): Climate and Phenology of Savanna Vegetation in Southern Africa. *Journal of Vegetation Science* 12, 347.

Chou, C., Neelin, J. D., Chen, C.-A., Tu, J.-Y. (2009): Evaluating the "Rich-Get-Richer" Mechanism in Tropical Precipitation Change under Global Warming. *J. Climate* 22, 1982–2005.

Collentine, D., Futter, M. N. (2018): Realising the potential of natural water retention measures in catchment flood management: Trade-offs and matching interests. *J Flood Risk Management* 11, 76–84.

Cosgrove, W. J., Rijsberman, F. R. (2000): Making water everybody's business. Earthscan; World Water Council, London, xvii, 108.

D'Odorico, P., Bhattachan, A., Davis, K. F., Ravi, S., Runyan, C. W. (2013): Global desertification: Drivers and feedbacks. *Advances in Water Resources* 51, 326–344.

Daamen, C. C., Simmonds, L. P., Wallace, J. S., Laryea, K. B., Sivakumar, M. V. K. (1993): Use of microlysimeters to measure evaporation from sandy soils. *Agricultural and Forest Meteorology* 65, 159–173.

Daryanto, S., Eldridge, D. J., Wang, L. (2013): Spatial patterns of infiltration vary with disturbance in a shrub-encroached woodland. *GEOMORPHOLOGY* 194, 57–64.

de Blécourt, M., Thomsen, S., Gröngröft, A., Eschenbach, A. (2017): When do Acacia mellifera trees use water? Response of sap velocity to soil water availability. vapour pressure deficit and global radiation. *Geophysical Research Abstracts*.

Deans, J. D., Munro, R. C. (2004): Comparative water use by dryland trees in Parklands in Senegal. *Agroforestry Systems* 60, 27–38.

Dee, D. P., Uppala, S. M., Simmons, A. J., Berrisford, P., Poli, P., Kobayashi, S., Andrae, U., Balmaseda, M. A., Balsamo, G., Bauer, P., Bechtold, P., Beljaars, A. C. M., van de Berg, L., Bidlot, J., Bormann, N., Delsol, C., Dragani, R., Fuentes, M., Geer, A. J., Haimberger, L., Healy, S. B., Hersbach, H., Hólm, E. V., Isaksen, L., Kållberg, P., Köhler, M., Matricardi, M., McNally, A. P., Monge-Sanz, B. M., Morcrette, J.-J., Park, B.-K., Peubey, C., Rosnay, P. de, *Tavolato, C., Thépaut, J.-N., Vitart, F.* (2011): The ERA-Interim reanalysis: Configuration and performance of the data assimilation system. *Q.J.R. Meteorol. Soc.* 137, 553–597.

D'Odorico, P., Caylor, K., Okin, G. S., Scanlon, T. M. (2007): On soil moisture-vegetation feedbacks and their possible effects on the dynamics of dryland ecosystems. *J. Geophys. Res.* 112, n/a-n/a.

Donaldson, C. H. (1969): Bush encroachment with special reference to the blackthorn problem of the Molopo area. Department of Agricultural Technical Services, Pretoria, p. 29.

Dovey, S. B., Du Toit, B., Clercq, W. P. de (2014): Nutrient leaching under zero tension in a subtropical clonal eucalypt plantation on a sandy soil in South Africa. *South African Journal of Plant and Soil* 31, 153–162.

Dunkerley, D. (2000): Hydrologic effects of dryland shrubs: Defining the spatial extent of modified soil water uptake rates at an Australian desert site. *Journal of Arid Environments* 45, 159–172.

Dunkerley, D. (2002a): Systematic variation of soil infiltration rates within and between the components of the vegetation mosaic in an Australian desert landscape. *Hydrol. Process.* 16, 119–131.

Dunkerley, D. L. (2002b): Infiltration rates and soil moisture in a groved mulga community near Alice Springs, arid central Australia: Evidence for complex internal rainwater redistribution in a runoff–runon landscape. *Journal of Arid Environments* 51, 199–219.

Dzikiti, S., Jovanovic, N. Z., Bugan, R., Israel, S., Le Maitre, D. C. (2014): Measurement and modelling of evapotranspiration in three fynbos vegetation types. *WSA* 40, 189.

Eldridge, D. J., Bowker, M. A., Maestre, F. T., Roger, E., Reynolds, J. F., Whitford, W. G. (2011): Impacts of shrub encroachment on ecosystem structure and functioning: Towards a global synthesis. *Ecology letters* 14, 709–722.

Eldridge, D. J., Soliveres, S. (2014): Are shrubs really a sign of declining ecosystem function?: Disentangling the myths and truths of woody encroachment in Australia. *Aust. J. Bot.* 62, 594.

Eldridge, D. J., Wang, L., Ruiz-Colmenero, M. (2015): Shrub encroachment alters the spatial patterns of infiltration. *Ecohydrol.* 8, 83–93.

Enfors, E. I., Gordon, L. J. (2008): Dealing with drought: The challenge of using water system technologies to break dryland poverty traps. *Global Environmental Change* 18, 607–616.

Erenstein, O., Sayre, K., Wall, P., Hellin, J., Dixon, J. (2012): Conservation Agriculture in Maize- and Wheat-Based Systems in the (Sub)tropics: Lessons from Adaptation Initiatives in South Asia, Mexico, and Southern Africa. *Journal of Sustainable Agriculture* 36, 180–206.

Feddes, R. A., Hoff, H., Bruen, M., Dawson, T., Rosnay, P. de, *Dirmeyer, P., Jackson, R. B., Kabat, P., Kleidon, A., Lilly, A., Pitman, A. J.* (2001): Modeling Root Water Uptake in Hydrological and Climate Models. *Bull. Amer. Meteor. Soc.* 82, 2797–2809.

Food and Agriculture Organization of the United Nations (2006): World reference base for soil resources, 2006: A framework for international classification, correlation, and communication. Food and Agriculture Organization of the United Nations, Rome, p. 145.

Food and Agriculture Organization of the United Nations (2015): World reference base for soil resources 2014: A framework for international classification, correlation, and communication. Food and Agriculture Organization of the United Nations, Rome, p. 203.

Gash, J. H. C. (1979): An analytical model of rainfall interception by forests. *Q.J Royal Met. Soc.* 105, 43–55.

Gash, J.H.C., Lloyd, C. R., Lachaud, G. (1995): Estimating sparse forest rainfall interception with an analytical model. *Journal of Hydrology* 170, 79–86.

German Institute for Standardization (1997): Soil quality - Determination of the specific electrical conductivity: 11265. Beuth, Berlin.

German Institute for Standardization (2002): Soil quality - Determination of particle size distribution in mineral soil material - Method by sieving and sedimentation: 11277. Beuth, Berlin.

German Institute for Standardization (2005): Soil quality - Determination of pH: 10390. Beuth, Berlin.

German Institute for Standardization (2012): Soil quality - Determination of the water retention characteristics - Laboratory methods: 11274. Beuth, Berlin.

German Institute for Standardization (2014a): Soil quality - Determination of dry bulk density: 11272. Beuth, Berlin.

German Institute for Standardization (2014b): Soil quality - Determination of unsaturated hydraulic conductivity and water-retention characteristic - Wind's evaporation method: 11275. Beuth, Berlin.

Giménez, R., Mercau, J., Nosetto, M., Páez, R., Jobbágy, E. (2016): The ecohydrological imprint of deforestation in the semiarid Chaco: Insights from the last forest remnants of a highly cultivated landscape. *Hydrol. Process.* 30, 2603–2616.

Glenn, E. P., Huete, A. R., Nagler, P. L., Hirschboeck, K. K., Brown, P. (2007): Integrating Remote Sensing and Ground Methods to Estimate Evapotranspiration. *Critical Reviews in Plant Sciences* 26, 139–168.

Goudriaan, J. (1977): Crop micrometeorology: a simulation study. Pudoc, Center for Agricultural Pub. and Documentation, Wageningen.

Gröngröft, A., de Blécourt, M., Classen, N., Landschreiber, L., Eschenbach, A. (2018): Impacts of bush encroachment on groundwater recharge – Evidence from 9 years of soil hydrological monitoring in a Namibian thornbush Savanna: unpublished report to GIZ Office Namibia, Hamburg.

Gröngröft, A., Luther-Mosebach, J., Landschreiber, L., Eschenbach, A. (2013a): Cusseque - Soils, in Oldeland, J., Erb, C., Finckh, M., Jürgens, N.: Environmental Assessments in the Okavango Region. Biodiversity & Ecology 5, Hamburg, pp. 51–54.

Gröngröft, A., Luther-Mosebach, J., Landschreiber, L., Eschenbach, A. (2013b): Mashare - Soils, in Oldeland, J., Erb, C., Finckh, M., Jürgens, N.: Environmental Assessments in the Okavango Region. Biodiversity & Ecology 5, Hamburg, pp. 105–108.

Gröngröft, A., Luther-Mosebach, J., Landschreiber, L., Kowalski, B. (2013c): A method for yield assessment on rainfed dryland agricultural fields, in Oldeland, J., Erb, C., Finckh, M., Jürgens, N.: Environmental Assessments in the Okavango Region. Biodiversity & Ecology 5, Hamburg, pp. 279–286.

Gröngröft, A., Luther-Mosebach, J., Landschreiber, L., Revermann, R., Finckh, M., Eschenbach, A. (2013d): Mashare - Landscape, in Oldeland, J., Erb, C., Finckh, M., Jürgens, N.: Environmental Assessments in the Okavango Region. Biodiversity & Ecology 5, Hamburg, pp. 101–102.

Hamerlynck, E. P., Scott, R. L., Susan Moran, M., Schwander, A. M., Connor, E., Huxman, T. E. (2011): Inter- and under-canopy soil water, leaf-level and whole-plant gas exchange dynamics of a semi-arid perennial C4 grass. *Oecologia* 165, 17–29.

Hatton, T. J., Nulsen, R. A. (1999): Towards achieving functional ecosystem mimicry with respect to water cycling in southern Australian agriculture. *Agroforestry Systems* 45, 203–214.

Haverkort, A. J., Goudriaan, J. (1994): Perspectives of improved tolerance of drought in crops. *Aspects of Applied Biology,* 79–92.

Hillel, D. (2009): Environmental soil physics. Academic Press, Amsterdam, XXVII, 771 Seiten.

Hipondoka, M.H.T., Aranibar, J.N., Chirara, C., Lihavha, M., Macko, S.A. (2003): Vertical distribution of grass and tree roots in arid ecosystems of Southern Africa: Niche differentiation or competition? *Journal of Arid Environments* 54, 319–325.

Hipondoka, M.H.T., Versfeld, W.D. (2006): Root system of Terminalia sericea shrubs across rainfall gradient in a semi-arid environment of Etosha National Park, Namibia. *Ecological Indicators* 6, 516–524.

Honda, E. A., Durigan, G. (2016): Woody encroachment and its consequences on hydrological processes in the savannah. *Philosophical transactions of the Royal Society of London. Series B, Biological sciences* 371.

Hough, J. (1986): Management Alternatives for Increasing Dry Season Base Flow in the Miombo Woodlandsof Southern Africa. *AMBIO* 15, 341–346.

Houlton, J. R., Curry, J. A. C., Pyle, J. A. (Eds.) (2003): Encyclopedia of atmospheric sciences. Academic Press, Amsterdam, S. 919-1405.

Hoyningen-Huene, J. v. (1981): Die Interzeption des Niederschlags in landwirtschaftlichen Pflanzenbeständen. Arbeitsbericht Deutscher Verband für Wasserwirtschaft und Kulturbau DVWK, Braunschweig, p. 66.

Huang, J., Li, Y., Fu, C., Chen, F., Fu, Q., Dai, A., Shinoda, M., Ma, Z., Guo, W., Li, Z., Zhang, L., Liu, Y., Yu, H., He, Y., Xie, Y., Guan, X., Ji, M., Lin, L., Wang, S., Yan, H., Wang, G. (2017): Dryland climate change: Recent progress and challenges. *Rev. Geophys.* 55, 719–778.

Huntley, B. J. (Ed.) (1982): Ecology of tropical savannas. Ecological studies 42. Springer, New York u.a., XI, 669 S.

Jarvis, P. G. (1976): The Interpretation of the Variations in Leaf Water Potential and Stomatal Conductance Found in Canopies in the Field. *Philosophical Transactions of the Royal Society B: Biological Sciences* 273, 593–610.

John Wood, Nick Webb, Chris Nicholl (2014): SunScan user Manual, Winster, p. 82.

Johnson, M. S., Lehmann, J. (2016): Double-funneling of trees: Stemflow and root-induced preferential flow. *Écoscience* 13, 324–333.

Jokisch, A., Urban, W., Kluge, T. (2016): Small Scale Rain- and Floodwater Harvesting for Horticulture in Central-Northern Namibia for Livelihood Improvement and as an Adaptation Strategy to Climate Change, in Leal Filho, W.: Implementing climate change adaptation in cities and communities: Integrating strategies and educational approaches. Climate change management. Springer International, [Cham], pp. 39–52.

Joubert, D. F., Rothauge, A., Smit, G. N. (2008): A conceptual model of vegetation dynamics in the semiarid Highland savanna of Namibia, with particular reference to bush thickening by Acacia mellifera. *Journal of Arid Environments* 72, 2201–2210.

Judd, M. J., Raupach, Finnigan, J. J. (1996): A wind tunnel study of turbulent flow around single and multiple windbreaks .1. Velocity fields. *BOUNDARY-LAYER METEOROLOGY* 80, 127–165.

Jürgens, N., Haarmeyer, D., Luther-Mosebach, J., Dengler, J., Finckh, M., Schmiedel, U. (2010): Biodiversity in Southern Africa: Volume 1: Patterns at local scale – the BIOTA Observatories. Klaus Hess Publishers, Göttingen, Windhoek Namibia, XX-801.

Kahinda, J.-m. M., Rockström, J., Taigbenu, A. E., Dimes, J. (2007): Rainwater harvesting to enhance water productivity of rainfed agriculture in the semi-arid Zimbabwe. *Physics and Chemistry of the Earth, Parts A/B/C* 32, 1068–1073.

Klerk, J. N. de (2004): Bush encroachment in Namibia: Report on phase 1 of the Bush Encroachment Research, Monitoring, and Management Project. Ministry of Environment and Tourism Directorate of Environmental Affairs, Windhoek Namibia, xvi, 255.

Kpadonou, R. A. B., Owiyo, T., Barbier, B., Denton, F., Rutabingwa, F., Kiema, A. (2017): Advancing climate-smart-agriculture in developing drylands: Joint analysis of the adoption of multiple on-farm soil and water conservation technologies in West African Sahel. *Land use policy* 61, 196–207.

Kroes, J. G., van Dam, J. C., Groenendijk, P., Hendriks, R. F., Jacobs, C. M. (2008): SWAP version 3.2: Theory description and user manual. Alterra, Wageningen, p. 266.

Kroes, J. G., van Dam, J. C., Huygen, J., Vervoort, R. W. (1999): User´s guide of SWAP version 2.0: Simulation of water flow, solute transport and plant growth in the Soil-Water-Atmosphere-Plant environment. DLO Winand Staring Centre, Wageningen.

Lal, R. (1997): Deforestation effects on soil degradation and rehabilitation in western Nigeria. IV. Hydrology and water quality. *Land Degrad. Dev.* 8, 95–126.

Landschreiber, L. (2010): Modellierung des Bodenwasserhaushaltes zweier Standorte in der Dornbuschsavanne Namibias. Diploma Thesis, Hamburg, p. 120.

Leduc, C., Favreau, G., Schroeter, P. (2001): Long-term rise in a Sahelian water-table: The Continental Terminal in South-West Niger. *Journal of Hydrology* 243, 43–54.

Leenders, J. K., van Boxel, J. H., Sterk, G. (2007): The effect of single vegetation elements on wind speed and sediment transport in the Sahelian zone of Burkina Faso. *Earth Surf. Process. Landforms* 32, 1454–1474.

Liebenberg, P. J. (2009): Technical report on irrigation development in the Namibia section of the Okavanago river basin, Windhoek Namibia.

Llorens, P., Poch, R., Latron, J., Gallart, F. (1997): Rainfall interception by a Pinus sylvestris forest patch overgrown in a Mediterranean mountainous abandoned area I. Monitoring design and results down to the event scale. *Journal of Hydrology* 199, 331–345.

Ma, X., Huete, A., Yu, Q., Coupe, N. R., Davies, K., Broich, M., Ratana, P., Beringer, J., Hutley, L. B., Cleverly, J., Boulain, N., Eamus, D. (2013): Spatial patterns and temporal dynamics in savanna vegetation phenology across the North Australian Tropical Transect. *Remote Sensing of Environment* 139, 97–115.

Maestre, F. T., Salguero-Gómez, R., Quero, J. L. (2012): It is getting hotter in here: Determining and projecting the impacts of global environmental change on drylands. *Philosophical transactions of the Royal Society of London. Series B, Biological sciences* 367, 3062–3075.

Mainguet, M. (1999): Aridity: Droughts and Human Development. Springer Berlin Heidelberg, Berlin, Heidelberg, 1 online resource (ix, 302.

Mendelsohn, J. (2009): Atlas of Namibia: A portrait of the land and its people. Sunbird Publ, Cape Town, p. 200.

Metzger, J. C., Landschreiber, L., Gröngröft, A., Eschenbach, A. (2014): Soil evaporation under different types of land use in southern African savanna ecosystems. *J. Plant Nutr. Soil Sci.* 177, 468–475.

Mitchell, T. D., Jones, P. D. (2005): An improved method of constructing a database of monthly climate observations and associated high-resolution grids. *Int. J. Climatol.* 25, 693–712.

Monteith, J. L. (1965): Evaporation and environment. *Symposia of the Society for Experimental Biology* 19, 205–234.

Moran, M. S., Scott, R. L., Keefer, T. O., Emmerich, W. E., Hernandez, M., Nearing, G. S., Paige, G. B., Cosh, M. H., O'Neill, P. E. (2009): Partitioning evapotranspiration in semiarid grassland and shrubland ecosystems using time series of soil surface temperature. *Agricultural and Forest Meteorology* 149, 59–72.

Ngigi, S. N. (2008): Technical evaluation and development of low-head drip irrigation systems in Kenya. *Irrig. and Drain.* 57, 450–462.

Noorduijn, S. L., Ghadouani, A., Vogwill, R., Smettem, K. R. J., Legendre, P. (2010): Water table response to an experimental alley farming trial: Dissecting the spatial and temporal structure of the data. *Ecological Applications* 20, 1704–1720.

Noy-Meir, I. (1973): Desert Ecosystems: Environment and Producers. *Annual Review of Ecology and Systematics* 4, 25–51.

O'Connor, T. G., Puttick, J. R., Hoffman, M. T. (2014): Bush encroachment in southern Africa: Changes and causes. *African Journal of Range & Forage Science* 31, 67–88.

Ogola, J. B.O., Wheeler, T. R., Harris, P. M. (2005): Water use of maize in response to planting density and irrigation. *South African Journal of Plant and Soil* 22, 116–121.

Oldeland, J., Erb, C., Finckh, M., Jürgens, N. (Eds.) (2013): Environmental Assessments in the Okavango Region. Biodiversity & Ecology 5, Hamburg.

Oweis, T., Hachum, A. (2006): Water harvesting and supplemental irrigation for improved water productivity of dry farming systems in West Asia and North Africa. *Agricultural Water Management* 80, 57–73.

Peck, A. J., Williamson, D. R. (1987): Effects of forest clearing on groundwater. *Journal of Hydrology* 94, 47–65.

Penman, H. L. (1948): Natural Evaporation from Open Water, Bare Soil and Grass. *Proceedings of the Royal Society A: Mathematical, Physical and Engineering Sciences* 193, 120–145.

Petersen, A. (2008): Pedodiversity of southern African drylands. Dissertation, Hamburg.

Pretty, J., Toulmin, C., Williams, S. (2011): Sustainable intensification in African agriculture. *International Journal of Agricultural Sustainability* 9, 5–24.

Raz-Yaseef, N., Rotenberg, E., Yakir, D. (2010): Effects of spatial variations in soil evaporation caused by tree shading on water flux partitioning in a semi-arid pine forest. *Agricultural and Forest Meteorology* 150, 454–462.

Raz-Yaseef, N., Yakir, D., Schiller, G., Cohen, S. (2012): Dynamics of evapotranspiration partitioning in a semi-arid forest as affected by temporal rainfall patterns. *Agricultural and Forest Meteorology* 157, 77–85.

Renger, M., Bohne, K., Wessolek, G. (2014): Bodenphysikalische Kennwerte und Berechnungsverfahren für die Praxis. Techn. Univ., Selbstverl., Berlin, 41 S.

Ritchie, J. T. (1972): Model for predicting evaporation from a row crop with incomplete cover. *Water Resour. Res.* 8, 1204–1213.

Rockström, J., Barron, J. (2007): Water productivity in rainfed systems: Overview of challenges and analysis of opportunities in water scarcity prone savannahs. *Irrig Sci* 25, 299–311.

Rockström, J., Falkenmark, M. (2010): Semiarid Crop Production from a Hydrological Perspective: Gap between Potential and Actual Yields. *Critical Reviews in Plant Sciences* 19, 319–346.

Röder, A., Schneibel, A., Stellmes, M., Frantz, D. (2013): Mashare - Earth Observation, in Oldeland, J., Erb, C., Finckh, M., Jürgens, N.: Environmental Assessments in the Okavango Region. Biodiversity & Ecology 5, Hamburg, pp. 113–115.

Sala, O. E., Parton, W. J., Joyce, L. A., Lauenroth, W. K. (1988): Primary Production of the Central Grassland Region of the United States. *ECOLOGY* 69, 40–45.

Scanlon, B. R., Keese, K. E., Flint, A. L., Flint, L. E., Gaye, C. B., Edmunds, W. M., Simmers, I. (2006a): Global synthesis of groundwater recharge in semiarid and arid regions. *Hydrol. Process.* 20, 3335–3370.

Scanlon, B. R., Keese, K. E., Flint, A. L., Flint, L. E., Gaye, C. B., Edmunds, W. M., Simmers, I. (2006b): Global synthesis of groundwater recharge in semiarid and arid regions. *Hydrol. Process.* 20, 3335–3370.

Scanlon, B. R., Reedy, R. C., Stonestrom, D. A., Prudic, D. E., Dennehy, K. F. (2005): Impact of land use and land cover change on groundwater recharge and quality in the southwestern US. *Global Change Biol* 11, 1577–1593.

Schindler, U. (1980): Ein Schnellverfahren zur Messung der Wasserleitfähigkeit im teilgesättigten Boden an Stechzylinderproben. *Arch. Acker-u. Pflanzenbau u. Bodenkd.* 24, 1–7.

Schindler, U., Müller, L. (2006): Simplifying the evaporation method for quantifying soil hydraulic properties. *J. Plant Nutr. Soil Sci.* 169, 623–629.

Schneibel, A., Stellmes, M., Frantz, D., Finckh, M., Revermann, R. (2013): Cusseque - Earth Observation, in Oldeland, J., Erb, C., Finckh, M., Jürgens, N.: Environmental Assessments in the Okavango Region. Biodiversity & Ecology 5, Hamburg, pp. 55–57.

Schneibel, A., Stellmes, M., Röder, A., Frantz, D., Kowalski, B., Haß, E., Hill, J. (2017): Assessment of spatio-temporal changes of smallholder cultivation patterns in the Angolan Miombo belt using segmentation of Landsat time series. *Remote Sensing of Environment* 195, 118–129.

Scholes, R. J., Archer, S. R. (1997): Tree-grass interactions in savannas, in Annual Review of Ecology and Systematics. Annual Review of Ecology and Systematics 28, pp. 517–544.

Scholes, R. J., Walker, B. H. (1993): An African savanna: Synthesis of the Nylsvley study. Cambridge Univ. Press, Cambridge u.a., XII, 306 S.

Schwilch, G., Liniger, H. P., Hurni, H. (2014): Sustainable land management (SLM) practices in drylands: How do they address desertification threats? *Environmental management* 54, 983–1004.

Scott, R. (2003): The understory and overstory partitioning of energy and water fluxes in an open canopy, semiarid woodland. *Agricultural and Forest Meteorology* 114, 127–139.

Segal, M., Avissar, R., McCumber, M. C., Pielke, R. A. (1988): Evaluation of Vegetation Effects on the Generation and Modification of Mesoscale Circulations. *Journal of Atmosperic Science* 45, 2268–2293.

Smit, G. N., Rethman, N.F.G. (2000): The influence of tree thinning on the soil water in a semi-arid savanna of southern Africa. *Journal of Arid Environments* 44, 41–59.

Spaans, E. J. A., Baker, J. M. (1992): Calibration of Watermark soil moisture sensors for soil matric potential and temperature. *Plant Soil* 143, 213–217.

Starr, M., Alam, S. A. (2015): Water balance of the Sudanese savannah woodland region. *Hydrological Sciences Journal* 60, 706–722.

Stellmes, M., Frantz, D., Finckh, M., Revermann, R. (2013): Okavango Basin - Earth Observation, in Oldeland, J., Erb, C., Finckh, M., Jürgens, N.: Environmental Assessments in the Okavango Region. Biodiversity & Ecology 5, Hamburg, pp. 23–27.

Steudel, T., Göhmann, H., Flügel, W.-A., Helmschrot, J. (2013a): Assessment of hydrological dynamics in the upper Okavango River Basins, in Oldeland, J., Erb, C., Finckh, M., Jürgens, N.: Environmental Assessments in the Okavango Region. Biodiversity & Ecology 5, Hamburg, pp. 247–261.

Steudel, T., Göhmann, H., Mosimanyana, E., Quintino, M., Flügel, W.-A., Helmschrot, J. (2013b): Okavango Basin - Hydrology, in Oldeland, J., Erb, C., Finckh, M., Jürgens, N.: Environmental Assessments in the Okavango Region. Biodiversity & Ecology 5, Hamburg, pp. 19–22.

Stroosnijder, L., Moore, D., Alharbi, A., Argaman, E., Biazin, B., van den Elsen, E. (2012): Improving water use efficiency in drylands. *Current Opinion in Environmental Sustainability* 4, 497–506.

Sturm, M., Zimmermann, M., Schütz, K., Urban, W., Hartung, H. (2009): Rainwater harvesting as an alternative water resource in rural sites in central northern Namibia. *Physics and Chemistry of the Earth, Parts A/B/C* 34, 776–785.

Taylor, K. E. (2001): Summarizing multiple aspects of model performance in a single diagram. *J. Geophys. Res.* 106, 7183–7192.

Thierfelder, C., Wall, P. C. (2010): Investigating Conservation Agriculture (CA) Systems in Zambia and Zimbabwe to Mitigate Future Effects of Climate Change. *Journal of Crop Improvement* 24, 113–121.

Thomson, S. J., Armstrong, C. F. (1987): Calibration of the Watermark Model 200 Soil Moisture Sensor. *Applied Engineering in Agriculture* 3, 186–189.

Trabucco, A., Zomer, R. J. (2009): Global Aridity Index (Global-Aridity) and Global Potential Evapotranspiration (Global-PET) Geospatial Database, http://www.csi.cgiar.org.

van Genuchten, M. T. (1980): A Closed-form Equation for Predicting the Hydraulic Conductivity of Unsaturated Soils. *Soil Science Society of America Journal* 44, 892.

Vereecken, H., Huisman, J. A., Bogena, H., Vanderborght, J., Vrugt, J. A., Hopmans, J. W. (2008): On the value of soil moisture measurements in vadose zone hydrology: A review. *Water Resour. Res.* 44, 1879.

Vereecken, H., Schnepf, A., Hopmans, J. W., Javaux, M., Or, D., Roose, T., Vanderborght, J., Young, M. H., Amelung, W., Aitkenhead, M., Allison, S. D., Assouline, S., Baveye, P., Berli, M., Brüggemann, N., Finke, P., Flury, M., Gaiser, T., Govers, G., Ghezzehei, T., Hallett, P., Hendricks Franssen, H. J., Heppell, J., Horn, R., Huisman, J. A., Jacques, D., Jonard, F., Kollet, S., Lafolie, F., Lamorski, K., Leitner, D., McBratney, A., Minasny, B., Montzka, C., Nowak, W., Pachepsky, Y., Padarian, J., Romano, N., Roth, K., Rothfuss, Y., Rowe, E. C., Schwen, A., Šimůnek, J., Tiktak, A., van Dam, J., van der Zee, S.E.A.T.M., Vogel, H. J., Vrugt, J. A., Wöhling, T., Young, I. M. (2016): Modeling Soil Processes: Review, Key Challenges, and New Perspectives. *Vadose Zone Journal* 15.

Walker, G. R., Zhang, L., Ellis, T. W., Hatton, T. J., Petheram, C. (2002): Estimating impacts of changed land use on recharge: Review of modelling and other approaches appropriate for management of dryland salinity. *Hydrogeology Journal* 10, 68–90.

Wallenfang, J., Finckh, M., Oldeland, J., Revermann, R. (2015): Impact of Shifting Cultivation on Dense Tropical Woodlands in Southeast Angola. *Tropical Conservation Science* 8, 863–892.

Walter, H. (1939): Grasland, Savanne und Busch der arideren Teile Afrikas in ihrer ökologischen Bedingtheit, S. 750-860.

Wang, X.-P., Berndtsson, R., Li, X.-R., Kang, E.-S. (2004): Water balance change for a re-vegetated xerophyte shrub area/Changement du bilan hydrique d'une zone replantée d'arbustes xérophiles. *Hydrological Sciences Journal* 49, 267.

Warburton, M. L., Schulze, R. E., Jewitt, G. P.W. (2012): Hydrological impacts of land use change in three diverse South African catchments. *Journal of Hydrology* 414-415, 118–135.

Ward, D., Wiegand, K., Getzin, S. (2013): Walter's two-layer hypothesis revisited: Back to the roots! *Oecologia* 172, 617–630.

Weber, T. (2013a): Cusseque - Climate, in Oldeland, J., Erb, C., Finckh, M., Jürgens, N.: Environmental Assessments in the Okavango Region. Biodiversity & Ecology 5, Hamburg, pp. 45–46.

Weber, T. (2013b): Mashare - Climate, in Oldeland, J., Erb, C., Finckh, M., Jürgens, N.: Environmental Assessments in the Okavango Region. Biodiversity & Ecology 5, Hamburg, pp. 103–104.

Weber, T. (2013c): Okavango Basin - Climate, in Oldeland, J., Erb, C., Finckh, M., Jürgens, N.: Environmental Assessments in the Okavango Region. Biodiversity & Ecology 5, Hamburg, pp. 15–17.

Weber, T., Helmschrot, J., Berndt, R., Jacob, D. (2014): Bewertung der Klimadynamik in der Okavango-Region unter Verwendung von hochauflösenden ERA-40 Reanalyse-Daten. *zgp1* 2014, 171–187.

Wendroth, O., Ehlers, W., Kage, H., Hopmans, J. W., Halbertsma, J., Wösten, J. H. M. (1993): Reevaluation of the Evaporation Method for Determining Hydraulic Functions in Unsaturated Soils. *Soil Science Society of America Journal* 57, 1436.

Wesseling, J. G., Kroes, J. G., Metselaar, K. (1998): Global sensitivity analysis of the Soil-Water-Atmosphere- Plant (Swap) model. DLO Winand Staring Centre, Wageningen.

Whitford, W. G., Anderson, J., Rice, P. M. (1997): Stemflow contribution to the 'fertile island' effect in creosotebush,Larrea tridentata. *Journal of Arid Environments* 35, 451–457.

Wilcox, B. P., Breshears, D. D., Turin, H. J. (2003): Hydraulic conductivity in a pinon-juniper woodland: Influence of vegetation. *Soil Science Society of America Journal* 67, 1243–1249.

Wind, G. P. (1969): Capillary conductivity data estimated by a simple method. *Water in the unsaturated zone ; Symp. 1966, Proc. UNESCO/IASH* 80.

World Meteorological Organization (2011): Technical regulations: Basic documents no. 2, Volume I: General Meteorological Standards and Recommended Practices. World Meteorological Organization, Geneva, 1 online resource .

Wu, W., Lynch, A. H., Rivers, A. (2005): Estimating the Uncertainty in a Regional Climate Model Related to Initial and Lateral Boundary Conditions. *J. Climate* 18, 917–933.

Abstract

The catchment of the Okavango River extends over three countries and two hydro-climatic zones in Southern Africa, from the dry sub-humid headwaters in the central highlands of Angola over the semi-arid Kavango region in northern Namibia to its semi-arid inland delta region in Botswana. For flora, fauna and not the least the human population, the river system is a reliable source of livelihood in an environment otherwise characterized by very limited water supply. An increasing population growth exerts direct pressure on this resource by abstraction for human consumption, irrigation purposes or livestock farming, whereas indirect pressure effects due to change of land use cause modifications of the hydrological cycle. The change-related reactions and consequences for soil-water balances and dynamics are analyzed based on three overarching questions:

1.) How does agricultural land use expansion change soil water balances in a dry sub-humid landscape in Angola?

2.) How is the influence of different vegetation and agricultural land use characteristics on soil water balances in northern Namibia?

3.) How does bush encroachment alter soil water dynamics and potential groundwater recharge in the semi-arid highlands of central Namibia?

Three regional case studies along the hydro-climatic gradient of the catchment describe 1.) pristine conditions with grassland and woodlands as well as 2.) scenarios characterized by smallholder dryland agriculture and commercialized agriculture under irrigation. Methodically, a detailed pedological survey comprising static soil-hydrological parameters, time series of soil-water contents and potentials as well as vegetation analysis are combined with a long-term soil-hydrological simulation based on land-use scenarios. General findings show an increase in deep drainage by an additional 29 % of the precipitation input for the study sites in Angola and northern Namibia with conversion from pristine conditions to subsistence agriculture. For the irrigation scenarios, the key finding is that application of integrated soil-hydrology irrigation management will lead to a 30 % to 60 % lower water abstraction in contrast to the evapotranspiration demand calculations. An increasing bush encroachment leads to complete suppression of bottom fluxes in the central Namibian highlands. The soil-hydrological elasticity of the pristine ecosystems in Angola and northern Namibia are able

to support medium-to-high crop densities provided there is sufficient nutrient supply. On the other hand, the ecosystem drought resilience of the thornbush savannah in central Namibia decreases with increasing bush encroachment caused by diminished soil water buffers. The hydrological effects of land-use changes have multiple impacts on upstream/downstream relations, where the higher drainage rates in the headwater regions lead to improved water supply in downstream regions over the dry season. Increasing bottom fluxes are concomitant with an increased nutrient leaching, and mitigation measures - e.g. vegetation management in an agroforestry system in headwater regions - decrease the formerly positive effects of downstream hydrograph changes. In contrast to flood and leaching control by conservational vegetation management in areas generating river run-off, debushing measures in parts of the catchment affected by dry spells can support groundwater recharge and increase the ecohydrological resilience by restoring soil water buffers. This study illustrates the possibilities of how a combined empiric-conceptional based approach can contribute to an in-depth knowledge of fundamentals and consequences of land use and land cover change in an area of tension between contrasting soil water utilization in drylands and subsequent hydrological processes. Especially in regions with limited data, this approach is able to support measures for a sustainable land use and ecosystem management.

Zusammenfassung

Das Einzugsgebiet des Okavango erstreckt sich über drei Länder und zwei hydroklimatische Zonen im südlichen Afrika, ausgehend von den trocken-subhumiden Gebieten des Oberlaufs im zentralen Hochland Angolas über die semiaride Kavangoregion in Nordnamibia bis zu den semiariden Bereichen des Inlanddeltas in Botswana. Für Flora, Fauna und nicht zuletzt für die menschliche Bevölkerung stellt dieses Flusssystem eine zuverlässige Quelle der Existenzsicherung in einer sonst wasserlimitierten Umgebung dar. Ein zunehmendes Bevölkerungswachstum übt einen direkten Nutzungsdruck auf diese Ressource aus, sei es durch Wasserentnahme für den direkten menschlichen Konsum, zur Bewässerung landwirtschaftlicher Nutzflächen oder für die Viehhaltung. Hinzu kommt die indirekte Beeinflussung des hydrologischen Kreislaufs durch einen zunehmenden Landnutzungswandel. Die, durch den Wandel bedingten Auswirkungen auf Bodenwasserdynamiken und den damit verbundenen Konsequenzen für Wasserbilanzen werden anhand von drei übergeordneten Fragestellungen analysiert:

1. Wie verändert eine Expansion landwirtschaftlicher Nutzflächen die Bodenwasserbilanzen einer trocken sub-humiden Landschaft in Angola?

2. Wie ist der Einfluss verschiedener Vegetations- und Landnutzungscharakteristika auf Bodenwasserbilanzen in Nordnamibia?

3. Wie verändert eine Verbuschung Bodenwasserdynamiken und welche Konsequenzen hat dies für eine potentielle Grundwasserneubildung im zentralen Hochland von Namibia?

Drei regionale Fallbeispiele, entlang des hydroklimatischen Gradienten des Einzugsgebietes des Okavango, beschreiben dazu 1.) natürliche und naturnahe Bedingungen von Gras- und Waldgebieten sowie 2.) Nutzungsszenarien des kleinbäuerlich-extensiven Regenfeldbaus im Kontrast zu kommerziell-intensivem Bewässerungsanbau. Methodisch werden dafür detaillierte statische wie zeitlich dynamische bodenhydrologische Messungen und Vegetationsanalysen mit Langzeitsimulationen des Bodenwasserhaushaltes verbunden. Im Ergebnis zeigen sich Zunahmen der Tiefendrainage um zusätzlich 29 % des erwartbaren Niederschlages in den Untersuchungsgebieten in Angola und Nordnamibia durch eine Umwandlung naturnaher Flächen in kleinbäuerliche Nutzungssysteme. Unter der Berück-

sichtigung bodenhydrologischer Eigenschaften und Dynamiken innerhalb eines modellbasierten Bewässerungsmanagements, ergeben sich mögliche Verringerungen der Wasserentnahme um 30 % bis 60 % im Vergleich zu Berechnungen basierend auf der Wassernachfrage der aktuellen Evapotranspiration. Die Auswirkungen zunehmender Verbuschung im zentralen Hochland Namibias zeigen eine komplette Reduktion von in offeneren Landschaftsteilen gering auftretenden Tiefenversickerungen bei gleichzeitiger Abnahme der bodenhydrologischen Resilienz durch verringerte Mengen an zwischengespeichertem Bodenwasser. Die abgeleitete ökohydrologische Elastizität der naturnahen Systeme in Angola und Nordnamibia zeigt dagegen die Möglichkeit höher Pflanzdichten im Trockenfeldbau unter der Voraussetzung einer ausreichenden Verfügbarkeit von Nährstoffen. Die hydrologischen Effekte des Landnutzungswandels haben vielfache Auswirkungen auf die Oberlauf-Unterlaufbeziehungen der betreffenden Regionen der Anrainerstaaten. Eine zunehmende Tiefenversickerung in Oberlaufregionen verbessert die Wasserverfügbarkeit zu Trockenzeiten in Regionen am Mittellauf. Die erhöhte Bodenwasserdynamik ist gleichzeitig verbunden mit Nährstoffauswaschungen und Kompensationsmaßnahmen durch ein Vegetationsmanagement schwächen die positiven Effekte erhöhter Trockenabflussmengen im Unterlauf wiederum ab. Im Gegensatz zu konservierendem Ökosystemmanagement in abflussgenerierenden Regionen, Entbuschungsmaßnahmen in Bereichen des Einzugsgebietes, welche besonders anfällig gegenüber Trockenzeiten sind, können sich positiv auf die Tiefenversickerung und damit auf die Grundwasserneubildung auswirken. Gleichzeitig kommt es zu einer Steigerung der ökohydrologischen Resilienz gegenüber Dürreperioden durch die Erhöhung zwischengespeicherter Bodenwassermengen. Diese Studie zeigt auf, wie ein empirisch-konzeptioneller Ansatz dazu beitragen kann, ein vertieftes Systemverständnis von Auswirkungen des Landnutzungswandels im Spannungsfeld unterschiedlicher Bodenwassernutzungen in Trockengebieten zu entwickeln. Speziell in Regionen mit eingeschränkter Datenverfügbarkeit ist ein solcher Ansatz in der Lage ein nachhaltiges Landnutzungs- und Ökosystemmanagement zu unterstützen

List of figures

List of tables

List of abbreviations

a.s.l. ..... *Above sea level*
AI ..... *Aridity Index*
BA ..... *Bottom to atmospherical water flux ratio*
CGIAR ..... *Consultative Group on International Agricultural Research*
CRM ..... *Coefficient of residual mass*
CRU ..... *Climatic Research Unit*
CseB ..... *Cusseque, eastern slope, bare soil scenario*
CseGr ..... *Cusseque, eastern slop, grassland scenario*
CseMa ..... *Cusseque, eastern slope, dryland agr. scenario with Maize*
CsuB ..... *Cusseque, summit, bare soil scenario*
CsuMa ..... *Cusseque, summit, dryland agr. scneario with Maize*
CsuWd ..... *Cusseque, summit, dense woodland scenario*
CV ..... *Coefficient of variation*
EC ..... *Electrical conductivity*
Epot ..... *Potential evaporation*
ES_C ..... *Erichfelde canopy scenario*
ES_I ..... *Erichsfelde intercanopy scenario*
ETp ..... *Potential evapotranspiration*
EVI ..... *Enhanced vegetation index*
FAO ..... *Food and Agriculture Organization of the United Nations*
FC ..... *Field capacity*
GB ..... *Green to blue water ratio*
GPCC ..... *Global Precipitation Climatology Center*
k(ψ) ..... *Unsaturated conductivity af funtion of the soil water pressure head*
K_s ..... *Saturated conductivity*
ku ..... *Unsaturated conductivity*
l ..... *Van Genuchten-Mualem shape parameter describing tortuosity*
LAI ..... *Leaf area index*
LSU ..... *Landscape unit*
MAP ..... *Mean annual precipitation*
MHz ..... *Megahertz*
Mkda ..... *Mashare Kalahari dune area*
MkdaB ..... *Mashare Kalahari dune area, bare soil*
MkdaGr ..... *Mashare Kalahari dune area, grassland conditions*
MkdaMa ..... *Mashare Kalahari dune area, dryland agr. conditions with Maize*
MkdaMaWi ..... *Mashare Kalahari dune area, irrigation condition with crop rotation*
MkdaWd ..... *Mashare Kalahari dune area, dense woodland conditions*
MkdaWo ..... *Mashare Kalahari dune area, open woodland conditions*
MODIS ..... *Moderate-resolution Imaging Spectroradiometer*
Mofp ..... *Mashare old floodplains*
MofpB ..... *Mashare old floodplains, bare soil conditions*
MofpGr ..... *Mashare old floodplains, grassland conditions*
MofpMa ..... *Mashare old floodplains, dryland agr. conditions with Maize*

MofpMaWi ..... *Mashare old floodplains, irrigation conditions with crop rotation*
MofpWd ..... *Mashare old floodplains, dense woodland conditions*
MofpWo ..... *Mashare old floodplains, open woodland conditions*
n ..... *Van Genuchten-Mualem shape parameter*
nRMSE ..... *Normalized root mean square error*
OKACOM ..... *The Permanent Okavango River Basin Water Commission*
PAR ..... *photosynthetically active radiation*
PWP ..... *Permanent wilting point*
rSWI ..... *Relative soil water index*
Se ..... *Effective saturation*
SWAP ..... *Soil-Water-Atmosphere-Plant Model*
SWC ..... *Soil water content*
TBA ..... *Tree basal area*
TDR ..... *Time domain reflectometry*
TM ..... *Thematic Mapper*
Tpot ..... *Potential transpiration*
uFC ..... *Utilizable field capacity*
WMO ..... *World Meteorological Organization*
$\bar{x}$ ..... *Mean*
α ..... *Inverse of the air entry point*
θ_r ..... *Residual water content*
θ_s ..... *Total porosity*
σ ..... *Standard deviation*

Acknowledgments

The long journey, leading to this very end of this thesis, began in 2008 with my first field trip to Namibia where I was allowed to get to know the most beautiful country with astonishing landscapes and ecosystems and not least dear people to become colleagues and friends. Those people, who introduced me to the culture and nature of southern Africa and the fantastic field of soil hydrology, I would like to thank with these view lines, without forgetting those who supported my attempt to understand a little more of how this world works.

At first, sincere thanks go to Annette Eschenbach and Alexander Gröngröft for the supervision of the field- and laboratory work as well as for their advisory support to finally bring these results in its present form. Additionally, I would like to sincerely thank Eva-Maria Pfeiffer for the review of my thesis.

A good company under field conditions cannot be overestimated and therefore I am very grateful to had two persons on my side with whom the, in parts and literally spoken, dry work was always pleasant. With Jona Luther-Mosebach work could be done effectively without many words but a lot of fun often found in small things. Together with the analytic view and the open-hearted nature of Alexander Gröngröft, the field trips will be in lovely memories. Thank you for (incomplete list follows) evaporative cooled Windhoek Lager, dancing in the savannah, "why is that like that" discussions, roadside Skat, the colourful world of birds and the most important thing: that I had the opportunity to learn and understand. Our core team was extended from time to time and thus I would like to thank Annette, Johanna and Kira for our impressing and memorable time together. Thanks to all colleagues from the TFO project, but especially to Rasmus, Johannes, Manfred, Michael, Laura, Robin, Felix, Björn and Hendrik for your dear company and our fruitful exchange. Without the great support of the paraecologists Robert, Meshak and Miguel, the work together with the people of the Kavanago, in Seronga and Cusseque would have been inconceivable. Enoc and Israel deserve a thank you as well, for their great field assistance and their hard work in Cusseque. Rudi and Roswitha from Erichsfelde, without the possibility to work on their farm and their kind hospitality, a large part of this study would not have been written.

A lot of people supported direct and indirect my work at the home base in the Institute of Soil Science in Hamburg. First and foremost, thanks to all my room- and housemates Inga,

Julia, Christoph, Simon, Marleen, Volker and Katja for their patience and supportive discussions and, very important, for the breaks when I needed them. For the support in the laboratory, I would like to thank Monika, Angela, Deborah and Birgit, who handled half a ton of dust, twice a year.

I would like to thank my dear wife Nadine for her forbearance and endurance in supporting me and my, not always straight-lined, way. Good to have you with me. And the last but not least grateful thanks go to my parents and my sister who always believed in me. Thank you all for encouraging me to bring this work to a successful end.

This study was created within the project “The Future Okavango” funded by the German Federal Ministry of Education and Research (01LL0912xx)